



**Projection radiography in obese populations:
how can image quality be improved?**

Volume 1 of 1

Submitted by Saeed Jaber M. Alqahtani to the University of Exeter as a thesis
for the degree of Doctor of Philosophy in Medicine In March 2019

This thesis is available for Library use on the understanding that it is copyright
material and that no quotation from the thesis may be published without proper
acknowledgement.

I certify that all material in this thesis which is not my own work has been
identified and that no material has previously been submitted and approved for
the award of a degree by this or any other University.

Signature:

A handwritten signature in black ink, appearing to be "S. Alqahtani".

Acknowledgements

Undertaking this PhD has been a truly life-changing experience for me and it would not have been possible to do without the support and guidance that I received from many people. I would like to first say a very big thank you to my supervisor Prof. Karen Knapp, Dr Jude Meakin and Dr Rachel Palfrey for all the support and encouragement they gave me during my PhD journey. Without their guidance and constant feedback this PhD would not have been achievable.

I gratefully acknowledge the funding received towards my PhD from Najran University, Saudi Arabia. I am also grateful to the University of Exeter for facilitating all resources I needed to accomplish my PhD. I also would like to thank the Medical Imaging Department team at Exeter University for being my family during my time at the university.

I would also like to say a heartfelt thank you to the sole of my father and to the white heart of my Mum for always believing in me and encouraging me to follow my dreams. I am so grateful to my brothers and sisters and all my friends for supporting me in all aspect during this journey.

And lastly, I am so grateful to my little family, my wife, two little princess and my little sun for being next to me during the hard days as well as good days. Thanks to everyone who supported me during this adventurous journey.

Abstract:

Introduction

The prevalence of obesity is increasing globally; this, in turn, has impacted negatively on health service delivery, especially in radiology. The high radiation dose is one of the main challenges as the literature suggested.

Objectives

This thesis aimed to; identify the most challenging procedures in projection radiography, quantify the FM and FFM in these areas in order to build obese phantoms, to build multiple phantoms, which then were used to investigate dose optimisation in obese patients.

Materials and methods

Radiation dose delivered to this group of patients in the UK was assessed using DAP. Based on the result of that, the FM and FFM of the most challenging areas were then quantified based on DXA scans of 264 female participants. The phantoms were then built using PMC 121/30 dry with other additives(CaCo₃, phenolic microspheres) Density, HU and attenuation coefficient were used to validate the phantoms materials. Dose optimisation was then carried out using factorial design.

Results

Abdominal and lumbar spine radiographs were the most challenging body parts with over 600% increase in DAP compared to the UK NDRL. The DXA scans show an increase in FFM along with FM and prediction models were produced to predict FFM and FM in these areas. The phantoms were built, and all validations steps show agreement with the ICRU 44 report. kVp and filtration were the most beneficial factors in dose optimisation in this thesis. kVp and filtration were the most influential factors in dose optimisation. mAs prediction model was also developed.

Conclusions

High doses are delivered to obese patients primarily in the lumbar and abdominal radiograph. Subsequently, high chance of induced cancer is expected. The DXA data shows a big gap in the literature where previously constructed phantoms are considering FM only and ignoring the FFM. The prediction models produced will help standardised construction of obese computational and physical phantoms. The phantoms built show a promising pathway in producing obese phantom with different BMI to tackle the dose and image quality issues. Low kVp with high filtration is recommended when imaging this group of patients. mAs prediction model can be used and the tube limit should be known to act accordingly.

List of contents:

Acknowledgments	2
Abstract.....	3
List of contents.....	4
List of figures.....	12
List of tables.....	15
List of equations.....	17
List of appendices.....	18
List of Publications.....	19
List of Abbreviations.....	21
1. Chapter 1: Introduction	22
1.1. Background	22
1.2. Statement of the problem:.....	23
1.3. Rationale for the study	24
1.4. Research question	24
1.5. Thesis aims	24
1.6. Thesis objectives.....	25
2 Chapter 2: Literature review.....	26
2.1 Introduction	26
2.2 Ionising radiation and interaction with matter:	26
2.2.1 Photoelectric effect	26
2.2.2 Compton scattering.....	28
2.3 Ionising radiation biological effects:.....	28
2.3.1 Deterministic effects:	28
2.3.2 Stochastic effects:.....	29
2.4 Radiation protection principle	32
2.4.1 Justification	32
2.4.2 Optimisation.....	32
2.4.3 Diagnostic reference level (DRL)	33

2.5	Obesity	34
2.6	The obesity challenge in radiology	35
2.7	Previous studies of exposure factors prediction models.....	39
3	Chapter 3: Radiation dose Audit	48
3.1	Introduction:	48
3.1.1	Overall aim:.....	48
3.1.2	Objectives:.....	48
3.2	Radiation dosimetry in projection radiography	49
3.2.1	Absorbed dose (D):.....	49
3.2.2	Equivalent dose (H):	49
3.2.3	Effective dose (E):	50
3.2.4	Effective risk (R):	52
3.3	Dose monitoring quantity:.....	53
3.3.1	Entrance surface dose (ESD):	53
3.3.2	Dose area product (DAP):	54
3.3.3	Diagnostic reference level (DRL)	54
3.4	Dose modelling:	54
3.5	Radiation dose of obese patients in projection radiography.....	55
3.6	Methods:	57
3.6.1	Patient Recruitment:	57
3.6.2	Ethical considerations:.....	58
3.6.3	Data access:.....	59
3.6.4	Patients:.....	59
3.6.5	Inclusion and exclusion criteria:.....	60
3.6.6	Obtaining the data	61
3.6.7	Final statistical analysis:	62
3.6.8	Dose modelling:.....	63

3.6.9	Lifetime cancer risk estimation:.....	70
3.7	Results	72
3.7.1	Included and excluded files and procedures.....	73
3.7.2	Patients' characteristics:.....	75
3.7.3	Radiation dose (DAP):.....	76
3.7.4	Patients' dose (DAP) compared to the NDRL:.....	77
3.7.5	Correlations between patients' size and received doses:	78
3.7.6	Absorbed dose:.....	79
3.7.7	Effective dose:	83
3.8	Discussion:.....	86
3.9	Conclusion:	92
4	Chapter 4: Body composition quantification.....	94
4.1	Introduction:	94
4.1.1	Aims:.....	94
4.1.2	Objectives:.....	94
4.2	Body composition:.....	96
4.3	The importance of body composition:.....	96
4.4	Body composition models:	98
4.5	Body composition measurement methods:	100
4.5.1	Indirect methods:	100
4.5.1.1	Body Mass Index (BMI):	100
4.5.1.2	Anthropometrics:	100
4.5.1.3	Bioelectrical Impedance analysis (BIA):	101
4.5.1.4	Skin fold thickness (SFT).....	101
4.5.2	Direct methods:.....	102
4.5.2.1	Total body water (TBW):.....	102
4.5.2.2	Total body potassium (TBP):.....	102

4.5.3	Criterion methods:	103
4.5.3.1	Body density:.....	103
4.5.3.2	Dual-energy X-ray absorptiometry (DXA):.....	103
4.5.3.3	Magnetic resonance imaging (MRI):.....	105
4.6	Method:	107
4.6.1	Data nature and study population:.....	107
4.6.2	DXA data:	107
4.6.2.1	Ethical approval:.....	107
4.6.2.2	Recruitment:.....	107
4.6.2.3	Measurements:.....	108
4.6.2.4	Statistical analysis:	111
4.6.3	MRI data:	113
4.6.3.1	Participant:	113
4.6.3.2	Scan protocol:	113
4.6.3.3	Image segmentation:.....	113
4.6.3.4	Statistical analysis:	116
4.7	DXA results:	117
4.7.1	Objective one:.....	117
4.7.2	Objective two:	120
4.7.3	Objective three.....	126
4.8	Discussion:.....	135
4.8.1	Limitations:	137
4.9	Conclusion:	138
5	Chapter 5: Phantom construction	139
5.1	Introduction:	139
5.1.1	Overall aim	139
5.1.2	Objectives.....	139

5.2	Background to phantoms	139
5.2.1	Types of phantom uses in radiology (Ionising radiation):.....	140
5.2.1.1	Radiation dosimetry phantom:.....	140
5.2.1.2	Quality control phantoms:.....	141
5.2.1.3	Imaging phantoms:.....	142
5.2.2	Phantoms used in similar studies:	143
5.2.3	Phantom requirements	149
5.3	Methods and materials:.....	151
5.3.1	Tissue equivalent substitutes trial fabrication:	151
5.3.1.1	Lean-tissue equivalent substitutes (LTES):.....	151
5.3.1.2	Fat Tissue Equivalent Substitute (FTES):.....	152
5.3.2	Trial sample moulds:.....	152
5.3.3	Health and safety and pre fabrication process:.....	153
5.3.4	Mixing process:.....	153
5.3.5	Validation process:	155
5.3.5.1	Density:	155
5.3.5.2	Attenuation coefficient:	156
5.4	Validation results:.....	157
5.4.1	Physical density:.....	158
5.4.2	Attenuation coefficient:	159
5.4.3	Hounsfield Unit (HU):.....	162
5.5	Final phantom construction:	164
5.5.1.1	Calculation stage:.....	164
5.5.1.2	Mould design and laser cutting:.....	165
5.5.1.3	Mould assembly and sealing:	170
5.5.1.4	Mixing stage:	174
5.5.1.4.1	FTES:.....	174

5.5.1.4.2	LTES:	175
5.5.1.5	Improved mould design:	175
5.5.1.5.1	Mixing and final construction stage using new and improved FTES and LTES mould designs:	176
5.5.1.6	Validation:.....	180
5.5.2	Validation result of the final FTES and LTES:.....	182
5.6	Discussion:.....	185
5.7	Conclusion:	188
6	Chapter 6: Dose optimisation study	189
6.1	Introduction:	189
6.1.1	Overall aim	189
6.1.2	Objectives.....	189
6.2	Rationale for dose optimisation of Lumbar spine:	190
6.2.1	Operational radiographic acquisition factors:.....	191
6.2.1.1	Tube potential (kVp):.....	191
6.2.1.2	Tube current and tube current-exposure time (mA & mAs)	193
6.2.1.3	Angle of anode target:	193
6.2.1.4	Focal spot size:	195
6.2.1.5	Anode heel effect:	196
6.2.1.6	Tube filtration:.....	197
6.2.1.7	Collimation:.....	198
6.2.1.8	Source to image distance (SID).....	199
6.2.1.9	Anteroposterior and posteroanterior projection:	199
6.2.2	Object-to-image distance (OID)	200
6.2.2.1	Anti scatter grid:	201
6.2.2.2	Automatic exposure control (AEC)	202
6.2.3	Image quality assessment:	204
6.2.3.1	Physical assessment (objective):	205

6.2.3.1.1 SNR.....	206
6.2.3.1.2 CNR	206
6.2.4 Visual measurement:.....	207
6.2.4.1 Fulfilment of image criteria (IC)	207
6.2.4.2 Visual Grading Analysis (VGA):.....	208
6.3 Methods and materials:.....	209
6.3.1 Overview:.....	209
6.3.2 Imaging equipment:	210
6.3.2.1 X-ray unit:.....	211
6.3.2.2 Image receptor:	211
6.3.2.3 Phantom:.....	211
6.3.2.4 Display monitors and lighting:.....	215
6.3.3 Imaging technique:	215
6.3.3.1 Study design:.....	216
6.3.3.2 Radiation dose:	218
6.3.4 Image assessment:.....	219
6.3.4.1 Visual assessment of image quality:	221
6.3.4.1.1 Image quality criteria:	221
6.3.4.1.2 Observers:.....	222
6.3.4.1.3 Image display:	225
6.3.4.2 Physical assessment of image quality:.....	225
6.3.5 Optimisation score (Figure Of Merit, FOM_{VGAS}):	234
6.3.6 Statistical analysis:	234
6.4 Results:.....	236
6.4.1 Inter-observer agreement:	237
6.4.2 Descriptive analysis	239
6.4.3 Main and interaction effects of kVp, SID and filtration on DAP and VGAS	244

6.4.3.1 Phantom (1).....	245
6.4.3.2 Phantom (2).....	250
6.4.3.3 Phantom (3).....	255
6.4.3.4 Phantom (4).....	260
6.4.3.5 Phantom (5).....	265
6.4.4 Optimal optimisation factors	270
6.4.5 Correlation between physical and visual aseessment of image quality 274	
6.5 Discussion:.....	275
6.5.1 Inter and intra-observer agreement for visual assessment:.....	275
6.5.2 Effects on DAP:	276
6.5.3 Effects on VGAS:.....	280
6.5.4 Correlation between VGAS and CNR	282
6.6 Conclusion	283
7. Chapter 7: Conclusion	284
7.1. The story of the thesis:.....	284
7.2. Research achievement:.....	285
7.3. Strengths of this research:	286
7.4. Limitations:.....	287
7.5. Overall conclusion of the thesis:.....	287
7.6. Research impacts:.....	289
7.7. Recommendations for further studies:.....	289
8. Appendices:.....	291
9. References:	344

List of figures:

Figure 1 Photoelectric absorption and Compton scattering.....	27
Figure 2 Examination data window in PCXMC.....	65
Figure 3 x-ray spectrum in compute doses window in PCXMC.....	67
Figure 4 patients dose input window in PCXMC.....	69
Figure 5 Number of files included and excluded based on files screening.....	73
Figure 6 Number of included and excluded radiographic investigations.....	74
Figure 7 Body composition level adapted from Wang et al. (1992).....	99
Figure 8 DXA scan showing body subdivision regions considered for FM and LBM measurement.....	110
Figure 9 MRI region of interests (ROIs) across subcutaneous and visceral fat.....	115
Figure 10 Segmented subcutaneous fat (SF) and visceral fat (VF) of one slice across L4-L5 level.....	116
Figure 11 Cross scatter plot of fat % against BMI.....	122
Figure 12 Two-way scatter plot of total FM and LBM across BMI.....	125
Figure 13 Two way scatter plot shows the linear relationship between total (A), abdominal (B), trunk (C) FM and BMI.....	127
Figure 14 Post estimation test and Sharipo-Wilk to investigate the residual normal distribution.....	128
Figure 15 Two ways scatter plot shows the linear relationship between total (A), abdominal (B), trunk (C) LBM and FM in the same region.....	132
Figure 16 Post estimation test and Shapiro-Wilk to investigate the residual normal distribution.....	133
Figure 17 Scatter plot of total pixel area segmented fat in MRI and android FM measured by DXA.....	134
Figure 18 FTES (A) and LTES (B) trial sample and the physical density of each sample.....	158
Figure 19 FTES attenuation compared to lard (mGy).....	159
Figure 20 LTES attenuation compared to Perspex (mGy).....	160
Figure 21 CT scan image for lard, LTES, FTES and Perspex.....	162
Figure 22 Mould's design cross cut (A) for LTES (B) and FTES (C) prior to laser cutting.....	168
Figure 23 Diameters of FTES and LTES final layers.....	169

Figure 24 FTES sealed mould.....	171
Figure 25 LTES sealed moulds	173
Figure 26 Improved FTES (A), and LTES (B) moulds with fabricated materials	179
Figure 27 CT scan of all FTES and LTES layers wrapped around the KYOTO phantom	181
Figure 28 FTES final layers HU.....	182
Figure 29 LTES final layers HU	183
Figure 30 First (A) and second (B) LTES showing the improvement in the final product	184
Figure 31 Anode angle	195
Figure 32 X-ray beam intensity difference between the cathode and anode..	196
Figure 33 Automatic Exposure Control (AEC) ionisation chambers orientation in digital radiography detector	203
Figure 34 phantoms used in dose optimisation study.....	213
Figure 35 Flowchart of the image quality assessment methods applied in this study.....	220
Figure 36 small and large ROIs used to calculate SNR and CNR.....	228
Figure 37 Feature extraction used in the plugin	230
Figure 38 Image with ROIs without alignment.....	232
Figure 39 Images with ROIs after alignment	232
Figure 40 Plot file for image stack before (A) and after alignment (B) plugins	233
Figure 41 VGAS values for each phantom	240
Figure 42 CNR values for each phantom	241
Figure 43 mAs changes across phantoms	242
Figure 44 DAP changes with the phantom size.....	243
Figure 45 Main effect (A) and interaction effect (B) of kVp, SID and filtration on DAP for phantom 1 (BMI: 18.3 kg/m ²)	245
Figure 46 Main effect (A) and interaction effect (B) of kVp, SID and filtration on VGAS for phantom 1 (BMI: 18.3 kg/m ²).....	247
Figure 47 Acquisition factor combination (kVp, SID * filtration) that led to image with similar VGAS to the reference image or above including DAP, VGAS and FOM _{VGAS} for each combination (phantom 1, BMI: 18.3 kg/m ²)	249

Figure 48 Main effect (A) and interaction effect (B) of kVp, SID and filtration on DAP for phantom 2 (BMI: 29 kg/m ²)	250
Figure 49 Main effect (A) and interaction effect (B) of kVp, SID and filtration on VGAS for phantom 2 (BMI: 29 kg/m ²).....	252
Figure 50 Acquisition factor combination (kVp, SID * filtration) that led to image with similar VGAS to the reference image or above including DAP, VGAS and FOM _{VGAS} for each combination (phantom 2, BMI: 29 kg/m ²).....	254
Figure 51 Main effect (A) and interaction effect (B) of kVp, SID and filtration on DAP for phantom 3 (BMI: 38 kg/m ²)	255
Figure 52 Main effect (A) and interaction effect (B) of kVp, SID and filtration on VGAS for phantom 3 (BMI: 38 kg/m ²).....	257
Figure 53 Acquisition factor combination (kVp, SID * filtration) that led to image with similar VGAS to the reference image or above including DAP, VGAS and FOM _{VGAS} for each combination (phantom 3, BMI: 38 kg/m ²).....	259
Figure 54 Main effect (A) and interaction effect (B) of kVp, SID and filtration on DAP for phantom 4 (BMI: 42 kg/m ²)	260
Figure 55 Main effect (A) and interaction effect (B) of kVp, SID and filtration on VGAS for phantom 4 (BMI: 42 kg/m ²).....	262
Figure 56 Acquisition factor combination (kVp, SID * filtration) that led to image with similar VGAS to the reference image or above including DAP, VGAS and FOM _{VGAS} for each combination (phantom 4, BMI: 42 kg/m ²)	264
Figure 57 Main effect (A) and interaction effect (B) of kVp, SID and filtration on DAP for phantom 5 (BMI: 46 kg/m ²)	265
Figure 58 Main effect (A) and interaction effect (B) of kVp, SID and filtration on VGAS for phantom 5 (BMI: 46 kg/m ²).....	267
Figure 59 Acquisition factor combination (kVp, SID * filtration) that led to image with similar VGAS to the reference image or above including DAP, VGAS and FOM _{VGAS} for each combination (phantom 5, BMI: 46 kg/m ²)	269
Figure 60 Contour plot of VGAS, DAP of each phantom (1, 2, 3 and 4) constrained by VGAS equal and above reference image and the 1st quartile of DAP	272
Figure 61 Quadratic (A), and linear prediction model (B) of mAs with kVp of 75, SID of 125 cm and filtration of 0.3 mm Cu.....	273

List of tables:

Table 1 Brief comparison between radiation stochastic and deterministic effects	31
Table 2 List of terms used in database search	39
Table 3 literature review results.....	41
Table 4 Tissue weighting factors (ICRP, 1977, ICRP, 1991, ICRP, 2007).	51
Table 5 PCXMC exposure details for both groups	66
Table 6 Lifetime cancer risk incidence by organ, age and sex for a composite Euro-American population (% per mGy).....	71
Table 7 Patients' characteristics	75
Table 8 Patient dose (DAP).....	76
Table 9 patient dose (DAP) compared to the NDRL.....	77
Table 10 Spearman correlation between DAP and patients' anthropometrics .	78
Table 11 Estimated absorbed dose (mGy) for normal weight adult group.....	80
Table 12 Estimated absorbed dose (mGy) for patients with obesity.....	81
Table 13 Effective dose for all procedures in both groups of patients	83
Table 14 Radiation-related lifetime cancer risk incidence for both obese and non-obese groups of patients (per 10 ⁶)	84
Table 15 Summary of data resources and measurement tools	108
Table 16 Descriptive characteristics of the participants anthropometry and body composition values.....	117
Table 17 Descriptive characteristics of participant body composition (Mean & SD) based on BMI & fat % groups.....	118
Table 18 Pearson correlation between LBM and FM across different body parts based on BMI and fat% subdivision groups.	120
Table 19 One-Way Analysis of Variance (ANOVA) of age by fat percentage	121
Table 20 Pearson correlation between FM and anthropometrics across different body parts and based on total cohort and BMI subdivision groups	123
Table 21 Pearson correlation between LBM and age, height and FM across different body regions and based on the cohort and BMI subdivision groups	124
Table 22 Summary of regression analysis for BMI (kg/m ²) predicting FM (kg) of different regions in the whole cohort.....	126
Table 23 Summary of regression analysis for height (m) and total FM (kg) predicting total LBM (kg)	129

Table 24 Regression analysis for height (m) and FM (kg), of different regions, predicting abdominal LBM (kg) in obese group.	130
Table 25 Regression analysis for height (m) and FM (kg), of different regions, predicting trunk LBM (kg) in obese group.....	131
Table 26 List of examples of previous studies and the approaches used to fabricate obese phantoms.	144
Table 27 Comparison of attenuation coefficient (mGy) difference percentage for LTES compared to Perspex, and FTES compared to lard across various kVp levels.	161
Table 28 Hounsfield Unit (HU) results for fabricated and bench marking materials.....	163
Table 29 Final mixing quantity for each mould	178
Table 30 Lumbar spine (AP & LAT) absorbed dose adopted and recalculated form Chaparian et al., 2014	191
Table 31 phantom characteristics.....	214
Table 32 Images of each phantom if all technical factors were considered in the factorial design	218
Table 33 Lumbar spine CEC modified image quality criteria.....	222
Table 34 Definitions of the degree of visibility for anatomical structures in the image	223
Table 35 Anatomical details included and the image criteria used in this study	224
Table 36 Intra-Class Correlation (ICC) of observer agreement on visual image quality scores for all phantoms	237
Table 37 Intra-class Correlation Coefficient (ICC) of observer consistency in individual phantom set and for all phantoms	238
Table 38 Descriptive analysis of DAP, VGAS and FOM_{VGAS} for images that match the reference image VGAS score or above for each phantom	271
Table 39 Spearman correlation between VGAS and CNR based on two different size ROIs (Significance level: $P<0.001$)	274

List of equations:

Equation 1	49
Equation 2	50
Equation 3	50
Equation 4	53
Equation 5	126
Equation 6	126
Equation 7	126
Equation 8	129
Equation 9	130
Equation 10	131
Equation 11	155
Equation 12	221
Equation 13	226
Equation 14	226
Equation 15	273

List of appendices:

Appendix 1 Invitation letter for engagement in the study 291

Appendix 2 Draft of the study protocol 292

Appendix 3 Follow up justification of the study protocol 293

Appendix 4 Permission to conduct the study..... 295

Appendix 5 Radiation related lifetime cancer risk of organs for both groups, normal weight and obese, for all reported procedures 296

Appendix 6 COSHH form for the fabrication of trial samples..... 310

Appendix 7 Interval plots of DAP, VGAS and FOM_{VGAS} of experimental images that match VGAS of reference image and above for phantom (1)..... 340

Appendix 8 Interval plots of DAP, VGAS and FOM_{VGAS} of experimental images that match VGAS of reference image and above for phantom (2)..... 341

Appendix 9 Interval plots of DAP, VGAS and FOM_{VGAS} of experimental images that match VGAS of reference image and above for phantom (3) 342

Appendix 10 Interval plots of DAP, VGAS and FOM_{VGAS} of experimental images that match VGAS of reference image and above for phantom (4) 343

List of abbreviations:

2AFC	2 Alternative Forced Choice
AEC	Automatic Exposure Control
ALARA	As Low As Reasonably Achievable
AP	Anteroposterior
BIA	Bioelectrical Impedance Analysis
BMI	Body Mass Index
CAD	Computer Aided Design
CEC	Commission of European Communities
CNR	Contrast to Noise Ratio
COSHH	Control Of Substances Hazardous to Health
CR	Computed Radiography
CT	Computed Tomography
Cu	Copper
<i>D</i>	Absorbed dose
DAP	Dose Area Product
DDR	Direct Digital Radiography
DI	Deviation Index
DQE	Detective Quantum Efficiency
DR	Digital Radiography
DRL	Diagnostic Reference Level
DXA	Dual-energy X-ray Absorptiometry
E	Energy beam
<i>E</i>	Effective dose
EI	Exposure Index
ESAK	Entrance Surface Air Kerma
ESD	Entrance Surface Dose
FFM	Fat-Free Mass
FID	Film to Image Distance
FM	Fat mass
FOM	Figure Of Merit
FSD	Focal to Skin Distance
FTA	Foot towards Anod
FTC	Foot towards Cathod

FTER	Fat Tissue Equivalent Ring
FTES	Fat-tissue Equivalent Substitutes
Gy	Gray
<i>H</i>	Equivalent dose
HPA	Health Protection Agency
HU	Hounsfield Unit
IAEA	International Atomic Energy Agency
ICRP	International Commission on Radiological Protection
ICRU	International Commission on Radiation Units and measurements
ICS	Image Criteria Score
IPA	Interpretative Phenomenological Analysis
IR(ME)R	Ionising Radiation (Medical Exposure) Regulations
J/Kg	Joules per kilogram
KAP	Kerma Area Product
kV	Kilovolt
kVp	Peak Kilovoltage
LBM	Lean Body Mass
LNT	Linear No Threshold
LSS	Life Span Study
LTES	Lean-tissue Equivalent Substitutes
mA	Milliamp
mAs	Milliamp per second
MRI	Magnetic Resonance Imaging
MSDS	Material Safety Data sheet
MTF	Modulation Transfer Function
NDRL	National Diagnostic Reference Level
NHS	National Health Service
NRPB	National Radiological Protection Board
OID	Object to Image Distance
OSCC	Oxford Survey of Childhood Cancers
PA	Posteroanterior
PACS	Picture Archiving and Communication System
PMMA	Poly(methyl methacrylate)
PVA	Poly(vinyl acetate)

QA	Quality assurance
QC	Quality control
<i>R</i>	Effective risk
RCR	Royal College of Radiologists
RIS	Radiology Information System
ROI	Region of interest
SF	Subcutaneous fat
SFT	Skin Fold Thickness
SID	Source to Image Distance
SNR	Signal to Noise Ratio
STER	Soft Tissue Equivalent Ring
TBP	Total Body Potassium
TBW	Total Body Water
TLD	Thermoluminescent dosimeter
TPA	Total Pixel Area
VF	Visceral fat
VGA	Visual Grading Analysis
VGAS	Visual Grading Analysis Score
WHO	World Health Organisation
Z	Atomic number

1. Chapter 1: Introduction

1.1. Background

Medical imaging plays an integral part in the monitoring and diagnosis of a wide variety of diseases. Since the first onset of x-ray discovery by the scientist Wilhelm Röntgen in 1895, it was implemented in medicine. The advantages of x-rays were quickly realised, but it took radiation scientists much longer to understand the harmful effects of ionising radiation. Initially, it was assumed X-rays passed from side to side of the skin as harmlessly as light. However, within several years of the x-ray utilization in medicine, reports of burns and skin damage, as a result of exposure to x-rays were becoming more widespread. In 1904, Thomas Edison's assistant, Clarence Dally, who had worked extensively with X-rays in developing fluoroscopy, died of skin cancer (Matanoski et al., 2001). This was due to the fact that the x-rays used in medical imaging are a form of ionising radiation, that have sufficient energy when interacting with human tissues to result in ionisation and or excitation (Bushberg and Boone, 2011, Linet et al., 2012). This has the potential to cause damage to the exposed tissue and result in cell mutation or apoptosis. Since then, there has been a developing theoretical and clinical understanding of the harmfulness of ionising radiation to human tissue (Johnston et al., 2011). This has led to the practice of radiation protection in medicine which is based on the As Low As Reasonably Achievable (ALARA) principle.

Nowadays, improvements have been made in ionising radiation based technologies including the transformation from analogue to digital radiography. This has impacted positively on the quality of the medical imaging services through advanced acquisition, post processing options, storage and advanced and flexible viewing. On the other hand, more reliance on medical imaging assessment in health services has been noted since the introduction of digital systems leading to an increase in the number of radiographic investigations. Hence, Medical imaging is by far the largest man-made source of ionising radiation delivered to the general population (Sinnott et al., 2010). It accounts for 15% of the radiation dose from both natural and artificial sources, and 90% of the artificial source alone (Hart et al., 2012). In England, approximately 40.7 million radiographic procedures were carried out in the year between March

2015 and March 2016, of projected population of 54.4 million (England, 2016, Rutherford, 2012). More than half (22.6 million) were projection radiography examinations.

1.2. Statement of the problem:

In recent years, the prevalence of obesity has increased globally and nationally leading to new challenges in health services generally and in radiology practice specifically. Obesity is commonly defined using the Body Mass Index (BMI) which is calculated as weight (kg) divided by the squared height (m) and has the unit of kg/m^2 (WHO, 1995). BMI is commonly categorised to four main categories; underweight ($\leq 18.5 \text{ kg/m}^2$), normal weight ($>18.5 \text{ \& \leq } 24.99 \text{ kg/m}^2$), overweight ($\geq 25 \text{ \& \leq } 29.99 \text{ kg/m}^2$) and obese ($\geq 30 \text{ kg/m}^2$). In 2016, around two billion adults were overweight, of these 650 million were obese with a BMI $\geq 30 \text{ kg/m}^2$ (WHO, 2016).

Literature has emerged recently reporting the challenges facing radiology departments managing patients with obesity. In the context of radiation protection, patients with obesity are receiving high doses as a result of computed tomography (CT) and interventional procedures (Wang et al., 2013, Hsi et al., 2013, Cushman et al., 2016, Smuck et al., 2013). However, in projection radiography, the dose to patients with obesity in clinical practice has yet to be reported. At the time of this project commencement, a sole study has modelled the radiation dose to obese patients in projection radiography based on simulation (Yanch et al., 2009). Other studies have reported a steady increase in radiology reports that were limited due to body habitus (Abo et al., 2011, Baliyan et al., 2018, Fu et al., 2016). For instance, Uppot and colleagues investigated five million radiology reports over fifteen years period of time, between 1989 and 2003, and they found a linear increase of 0.01% per year of reports that were limited due to body habitus (Uppot et al., 2006).

In the UK context, a very recent study investigated the challenge facing CT radiographers in 86 NHS Trusts in the UK (Wiles et al., 2017). Fourteen respondents stated that they are considering utilising local veterinary centres' equipment to scan those obese patients who cannot fit into the scanners

available in the trust. With regard to radiation dose reduction protocol, only 3% of respondents reported a formal protocol in place for scanning obese patients.

1.3. Rationale for the study

The best practice in radiography is to select the most appropriate exposure factors based on the patient's size and condition while adhering to the ALARA principle (Alexander, 2016). With this in mind, different patient-based radiographic exposure factor selection models have been developed over the years, yet they are based on an analogue x-ray system and might not be suitable to use in a digital era due to the different latitudes between the two systems (Ching et al., 2014).

With the high prevalence of obesity and the amount of radiographic exposures conducted annually as discussed earlier, it is of high importance to explore the actual dose delivered to obese patients during projection radiography and to work upon the most challenging body parts in order to develop radiographic exposure factors selection to aid radiographers when imaging this group of patients.

1.4. Research question

The current thesis intended to answer the following question:

“Are there opportunities to optimise the image quality of patient with obesity in projection radiography or are we working at the limit of the available technology?”

1.5. Thesis aims

1. To identify current practice in projection radiography with specific regards to radiation dose delivered to patients with obesity
2. To quantify body composition based on the most challenging body part to underpin obese phantoms construction
3. To construct obese phantom for dose optimisation purposes
4. To conduct dose optimisation experiments in order to improve image quality in patients with obesity

1.6. Thesis objectives

1. To evaluate the radiation dose delivered to patients with obesity in projection radiography based on clinical data
2. To investigate the relationship between patients' sizes and received dose in order to demonstrate possible dose variation
3. To estimate the radiation-related lifetime-cancer risk of patients with obesity based on the reported dose in comparison with normal weight patients.
4. To quantify body composition with specific regards to fat and lean tissues in total and regional basis, especially the most challenging body parts.
5. To produce fat and lean prediction models using anthropometric measures in order to facilitate phantom construction
6. To fabricate and validate fat and lean tissue-equivalent substitutes that can be used to build reusable obese phantoms
7. To construct obese phantoms that account for fat and lean changes in order to mimic different body size
8. To investigate the impact of different exposure factors on radiation dose and image quality on the most challenging body part, identified earlier
9. To evaluate the change in the effect of these exposure factors when the phantom size increases
10. To produce a preliminary exposure factors prediction model that can aid radiographers selecting the most appropriate exposure factors based on the patient's size in lumbar spine radiographs.

2 Chapter 2: Literature review

2.1 Introduction

This chapter will introduce the reader to the topic through a brief description of x-ray interaction with matter. This is to facilitate the idea of Compton scattering which causes image quality deterioration in cases of patients with obesity. Additionally, the biological effects of radiation will be explained to appreciate the importance of radiation protection practice in medical imaging, which then will follow. The challenges that have risen as a result of obesity in medical imaging will then be introduced with special focus on radiation dose and image quality matters. Previous studies that have been reported in the literature in an attempt to tackle the issue of non-diagnostic image quality with regards to obese patients will be discussed in order to define the gap in the literature, which this project is trying to address accordingly.

Due to the distinctive nature of all topics that will be covered in this thesis, each study had its own literature review, method, results, discussion and conclusion. Hence, the reader can expect to see more literature reviewed in each study specific chapter.

2.2 Ionising radiation and interaction with matter:

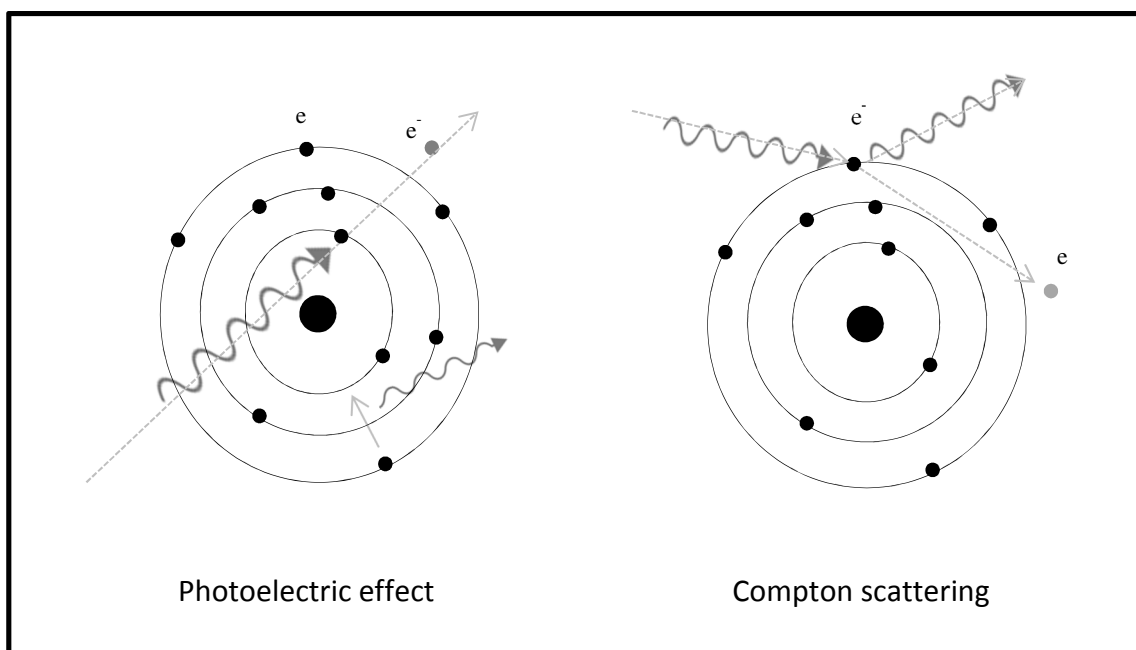
When a beam of x-rays passes through a matter, three main different scenarios of interactions between the x-ray's photon and the orbiting electrons of the material's atom will occur, the photon either loses some of its energy (*scattering*), all of its energy (*absorption*), or pass through with no loss of energy (Graham et al., 2012). In diagnostic radiography, two types of interaction are the most predominant; photoelectric absorption and Compton scattering.

2.2.1 Photoelectric effect

This process of attenuation is crucial in the photon energies of diagnostic radiography procedures. In this process, the x-ray photon energy is absorbed totally due to the collision with an electron of an atom of the absorber, Figure 1 illustrates the process (Graham et al., 2012). The probability of this interaction depends on the binding energy of both the electrons of the absorber and the photon energy. If the photon energy is less than the electron binding energy,

then the probability of photoelectric absorption is zero (Graham et al., 2012). Once the collision occurs, the photon will give all of its energy to the absorber electron and disappear while the electron is ejected from its orbit. Due to the created vacancy in the orbit, a new electron will fill the place of the emitted electron resulting in emission of characteristic radiation (Bushberg and Boone, 2011). The energy of the characteristic radiation is equal to the electron energy difference before and after the jump. In the case where the photoelectric effects occur in human tissue, the energy difference is within the infrared part of the electromagnetic spectrum (1.2×10^{-2} eV and 1.8×10^{-2} eV) (Dendy and Heaton, 2011, Bushberg and Boone, 2011). This process of interaction is related to the beam energy (E) and the atomic number (Z) of the absorber. In diagnostic energy spectrum, usually less than 150 keV, the mass attenuation coefficient of photoelectric effect is proportion to the Z^3 and inversely related to the beam energy (E^3) (Bushberg and Boone, 2011). With this in mind, the photoelectric effect is more likely to occur in bone as it has double the atomic number of the soft tissue (13.8) and linear attenuation coefficient for photoelectric absorption is 16 times that of soft tissue (Graham et al., 2012). For this reason, bone appears white on the radiographic image due to the low radiation dose received by the image detector (Graham et al., 2012).

Figure 1 Photoelectric absorption and Compton scattering



2.2.2 Compton scattering

In this process, the conditions for Compton scattering to occur are different compared to the photoelectric effect. If the binding energy of the electron is very small compared to the energy beam, then the electron could be considered as a free electron and the interaction between the free electron and x-ray photon is known as Compton scattering (Bushberg and Boone, 2011). Since the interaction in Compton scattering is between x-ray photon and electron density, hence, the electron density of the medium is important. The x-ray photon gives some of its energy to the free electron and the remaining energy is scattered as shown in Figure 1.

The mass attenuation and absorption coefficients resulting from Compton scattering are proportional to the electron density and inversely proportional to the energy beam (E) (Graham et al., 2012). It is known for materials with a Z number below 11, the incident x-ray beam is mainly scattered and poorly absorbed (Almeida et al., 2019). Hence, more Compton scattering is more likely to be produced when imaging obese patients where more soft tissues and adipose is present.

2.3 Ionising radiation biological effects:

Based on the discussion above, it is clear that when x-ray photons pass through the human body energy is imparted to the absorbing medium through photoelectric absorption and Compton scattering. This in turn will result in radiobiological effects that can be categorised into two categories; deterministic and stochastic effects.

2.3.1 Deterministic effects:

This category of radio-biological effect is also called “tissue reaction effect” and results in cell death which in turns impacts on the function of tissue or organ (Stewart et al., 2012). This is due to the failure of the cell to repair the damage caused by the passage of ionising radiation through the organ. This type of radiobiological effects occurs only when the absorbed dose by a tissue or organ exceeds a deterministic threshold dose of that tissue or organs (Linnet et al., 2012). Effects include skin erythema, necrosis, cataract and reduced fertility

(Kalender, 2014). The threshold is reported to be around 2 Gy for acute exposure and 4 Gy for fractionated radiation doses, while higher levels are also reported for long-term exposure (ICRP, 2008). However, an even lower dose (0.5 Gy) has been suggested by recent human and mechanistic studies (Ainsbury et al., 2009).

Since the organ doses from a single projection radiographic procedure (0.1 – 1.5 mGy) is far below the lowest suggested deterministic threshold (0.5 Gy), deterministic effects are rarely seen in radiographic procedures (Mettler Jr et al., 2008). In other modalities, such as CT scanning and angiography, this category of effects may become an issue where high dose and multiple scans are required (Mahesh, 2001, Mayo, 2008). For instance, temporary hair loss has been reported for patients who had CT brain perfusion investigations demonstrating the high dose delivered in such modalities (Huda et al., 2008). However, in projection radiography the dose is far below the dose delivered during by CT procedures, therefore, deterministic effects are not of concern when conducting such procedures.

2.3.2 Stochastic effects:

In diagnostic imaging, where the dose is not considered excessive, the primary relevant effect is stochastic. This happens when radiation induces DNA damage, but does not kill the cell which survives but with mutation in its DNA (Sykes, 2016). The stochastic effects are not categorised by their severity as in deterministic effects, indeed their incidence is what categorises them. Despite the fact that this category of radiation effects has no threshold, the effect increases as the radiation dose increases (Zanzonico et al., 2016). This is based on the Linear No Threshold model (LNT) which is recognised by different radiation protection bodies and organisations and is the basis for radiation protection principles in medical imaging (Linnet et al., 2012). This model has been implemented in radiation protection for more than seven decades (Siegel et al., 2017). It is based on the assumption that no safe limit of radiation dose exists, but rather the cancer risk increases linearly as the dose increases (Samei et al., 2018).

Different studies have investigated the association between radiographic procedures and subsequent cancer risk resulted from stochastic effects. Back in the forties and sixties, an abdominal radiograph was a commonly requested procedure by obstetricians to evaluate pregnancy related medical issues (Linnet et al., 2012). Within the same period, Stewart and colleagues investigated the likelihood of cancer among children by conducting a large scale survey, Oxford Survey of Childhood Cancers (OSCC) (Stewart et al., 1956). They observed a 2-fold statistically significantly higher risk of total paediatric cancer mortality in the offspring of women who had undergone x-ray procedures during pregnancy compared with risk in the offspring of women who had not (Stewart et al., 1956). With regards to adults, two large retrospective studies investigated the relationship between radiation dose and cancers in patients who had repeated fluoroscopic investigations as a result of tuberculosis monitoring (Boice Jr et al., 1991, Howe and McLaughlin, 1996). Their findings demonstrated significant dose-response relationships for breast cancer (RR, 1.29; 95% CI, 1.1-1.5) but no evidence of increased lung cancer risk. In terms of diagnostic x-rays exposure and link with cancers, a large case-control study reported small, but non-significant, increases in myeloma (Boice et al., 1991). Similarly, a cumulative number of x-ray procedures, retrieved from medical records, was not found to be linked with thyroid cancer (Inskip et al., 1995).

Based on the discussion above, it is apparent that inconsistent findings and limited numbers of relevant epidemiological studies complicate drawing a clear and definite conclusion about radiography procedures and the risk of cancer. Therefore, a conservative approach on practicing radiation protection to protect patient should always be employed. Mechanistic approaches along with epidemiological studies may provide more insights into the link between low dose radiographic procedures and cancers. Table 1 illustrates the difference between the radiobiological effects.

Table 1 Brief comparison between radiation stochastic and deterministic effects

Caused by	Sub-fatal DNA damage	Cell death
Radiation dose threshold	No There is no safe dose, effects can be caused by any radiation dose	Yes Effects occur in organ when the threshold of the specific organ exceeded
Severity of clinical effects and dose	The clinical effects severity is independent of dose, all or none response, individual either manifests or does not	Severity of clinical effects is proportional to the dose
Radiation dose and effect relationship	Frequency of effect proportional to the dose, the higher the dose the more risk of manifesting the effects	Probability of effects independent on dose, once threshold exceeded, individual will manifest effect
Caused by radiation dose in diagnostic imaging	Yes	Usually No, but cases have been reported as a result of long interventional radiology procedures
Examples	Cancer Heritable effects	Cataract Skin burn Sterility

DNA: Deoxyribonucleic acid

2.4 Radiation protection principle

With the deterministic effects being more related to high radiation dose (>0.5-4 Gy), stochastic effects are the source of risk in low dose procedures such as projection radiography.

2.4.1 Justification

This is the first measure that should be considered in order to prevent unnecessary radiation dose to patients. It means that no practice can be conducted in diagnostic imaging unless it provides positive net benefits to the patients more than imposed risks (Musolino et al., 2008). This principle is implemented in medical imaging at three different levels according to the International Commission on Radiological Protection (ICRP, 2008). Firstly, is the use of ionising radiation in medicine and this is internationally granted as justified and accepted. The second level of justification principle is the justification of a defined radiological procedure. This level aims to evaluate if a radiological procedure will improve the diagnosis or provide a basic management information in favour of the patient (Malone et al., 2012). The third level considers the justification of each radiographic exposure on an individual level.

With regards to projection radiography, the role of justification usually lies within the duties of the radiographers. It's one of the duties of the practitioner under the Ionising Radiation (Medical Exposure) Regulations and radiographers are practitioners under this legislation (IR(ME)R, 2000).

2.4.2 Optimisation

This principle is more focused on the technical aspects of radiation protection measures. It aims to maintain the radiation dose delivered to the irradiated patient at as low a level as possible. Out of three basic radiation protection principles; justification, optimisation and dose limit, optimisation can be considered to be the most crucial element and should always be practiced efficiently (ICRP, 1991, IAEA, 2002). It acts in favour of maximising the benefits over the harm of the radiological procedure. In order to achieve this,

optimisation follow the ALARA principle as suggested by the ICRP in the seventies (ICRP, 1977).

According to the ICRP, part of the optimisation process is the identification of all possible protective measures to keep the exposure as low as reasonably achievable based on each patient individually (ICRP, 2006). One of these measures that are used and recommended by the ICRP and the IR(ME)R 2000, is the Diagnostic Reference Level (DRL) (ICRP, 1996, IR(ME)R, 2000).

2.4.3 Diagnostic reference level (DRL)

Back in 1980s, the National Radiological Protection Board (NRPB), now known as the Health Protection Agency (HPA), conducted a national survey in order to evaluate the entrance-surface exposure, this was either in DAP or ESD (Shrimpton et al., 1986). A similar survey was conducted in the USA in 1970 (Burkhart, 1984). These surveys promoted the recommendation for the DRL in radiographic technique due to the reported variations in radiation dose delivered for the same radiographic procedures (ICRP, 2017).

In the UK, where this study is based, the Royal College of Radiologists (RCR) and the NRPB have introduced the concept of reference dose (RCR, NRPB, 1990) in their publication titled "Patient dose reduction in diagnostic radiology". It is based on the third quartile values of distribution of doses reported for a specific radiological investigation from a representative sample of patients at each hospital participating in the national patient dose survey in mid 1980s. This was adopted by the ICRP to introduce the terms DRL in 1996 officially and to determine its rules and how to be established (ICRP, 1996). The ICRP defined the DRL as an investigation level utilized for optimising the practice of radiation protection in the medical exposure of patients (ICRP, 2017). In the UK, under IR(ME)R 2000, the hospital employer is required by law to set a DRL and ensure it is followed and adhered to (IR(ME)R, 2000). On a national level, each five years the NDRL is reviewed and updated. In the 2010 DRL survey, the reference doses were 10 % less than the previous survey in 2005, but also less than half of the reference doses reported in the 1980s (Hart et al., 2012). This could be attributed to the application and updating the DRL, but also to new technologies, i.e. digital radiography.

However, as this project concerns patients with obesity, the NDRL are based on average weight patients, where the average weight patient per x-ray room is 70 ± 5 kg. This indicates that radiation dose delivered to obese patients is not reported, or in another word the NDRL is valid for the normal weight populations.

2.5 Obesity

Obesity is one of the major global health issues today. It is now recognised by the World Health Organisation (WHO) as a global noncommunicable disease (Kontis et al., 2014).

The high prevalence of obesity, as discussed in section 1.2, is attributed to multiple different factors. These include; physical inactivity and reduced energy expenditure, calories rich food and high energy intake, genetic susceptibility and heritability and other socio-economic factors (Stenholm et al., 2016, Eaton and Eaton, 2017, Thasanasuwan et al., 2016). These factors are believed to contribute to high prevalence of obesity which in turn has impacted on obese patients health. This includes the cause of insulin resistance type II Diabetes mellitus, cardiovascular disease, elevated blood pressure and other diseases including rarer types of cancer, bladder cancer for instance (Hartstra et al., 2015, Sun et al., 2015, Ortega et al., 2016). The causes and effects of obesity mechanisms are beyond the scope of this thesis, however, this is just to give the reader a glance on the danger of obesity. Due to the recognised obesity comorbidities (Hartemink et al., 2006, Guh et al., 2009, Publishing, 2010, Renehan et al., 2008), patients with obesity are more likely to present for health assessment than their normal weight peers.

Due to the limitations incurred by physical size and body composition variation compared to adult patients with normal weight, obesity poses a challenge in patient assessment and management in hospital (Beechy et al., 2012). The ability to achieve an adequate clinical examination is compromised in this population (Padilla et al., 2005). Likewise, it becomes difficult to listen to heart sounds, lung respiration, and bowel sounds (Padilla et al., 2005). Additionally, the capability to palpate the abdomen, perform a clinical pelvic examination, and evaluate for masses is compromised in clinical practise (Padilla et al., 2005). These in turn have increased reliance on other healthcare assessments,

including medical imaging, for this substantial group of people (Padilla et al., 2005).

2.6 The obesity challenge in radiology

Different studies have reported the challenges of managing obese patients in healthcare. In this section, studies that have reported challenges that have adverse impact directly or indirectly on the radiation dose and or image quality in obese patients will be discussed. Le and colleagues investigated radiographers' learning experiences in imaging obese patients (Le et al., 2015b). Using a semi structured focus group, diagnostic radiography students from Sydney University were recruited through email invitation to participate. A total of 31 students took part in the study. Students have expressed lack of confidence and need for more help when imaging obese patients as they believe that technique amendments are needed. They also stated the lack of resources that aid the radiographers to adjust the exposure factors based on the patient's size. The most challenging aspect of imaging obese patients was selecting the appropriate exposure factors. Despite the fact that this study was based on students' experiences during clinical placement, which does not necessarily reflect the experience of experienced radiographers, nevertheless it provides evidence of the difficulty in imaging obese patients and the lack of resources to aid selecting exposure factors. Some students have reported their own technique to avoid repetition through using high exposure factors on purpose. This phenomenon has already been reported in the literature even when imaging patients of normal weight in order to avoid underexposure which is not favourable to radiologists, and it is known as dose creep (Ma et al., 2013, Seeram et al., 2013). A similar study was conducted in Australia but with the focus on experienced diagnostic radiographers and those working as designated clinical educators (Aweidah et al., 2016). Using an interview approach with 37 diagnostic radiographers from different hospitals and with an average experience of 12 years, the study found that one of the main themes was "image-focussed" where participants expressed blame and frustration when imaging obese patients due to the lack of skills among peers which in turns result in low diagnostic image quality.

Researchers investigated the experience of radiographers when imaging obese patients in the UK (Woods et al., 2016). Using interpretative Phenomenological Analysis (IPA), the researcher used semi-structured interviews with eight radiographers (experience ranged from 5 – 35 years). One of the reported themes of challenges that impact on image quality was the difficulty of positioning the patients and to locate bony landmarks in order to centre x-ray beam accurately. This issue has been reported in another study highlighting the impact of malpositioning obese patients and its impact on the image quality and radiation dose (Carucci, 2013). For example, in abdominal radiographs, the centring point of the beam is recommended to be by the level of iliac crest in the midline (Bontrager and Lampignano, 2013). When the upper part of the abdomen needs to be assessed, the central ray (CR) should be centred 5cm (2 inches) above the iliac crest level (Bontrager and Lampignano, 2013). Accurate centring is crucial to avoid misalignment of examined part and of high importance when Automatic Exposure Control (AEC) is used, this is to eliminate image distortion especially in joint imaging. With a thick layer of adipose tissue subcutaneously, the process of locating the iliac crest becomes difficult and hence the centring of the beam might be compromised by estimation. As doctors are more skilled in palpation for anatomical landmarks than allied health professionals, such as radiographers, it has been reported that they face a difficulty in finding anatomical landmarks, such as iliac crest, in obese patients (Kam and Taylor, 2010). As an alternative, Carucci (2013) have suggested using the elbow level as an alternative but there is no research evidence in support of this suggestion.

Other studies have reported the challenges encountered when imaging obese patients based on opinions rather than evidence. This includes the difficulty to cover the body dimension of the obese patient presented to radiography exam (Buckley et al., 2009, Uppot, 2007, Carucci, 2013, Reynolds, 2011, Yanch et al., 2009). Such issue is more common when imaging chest, abdomen and pelvis in obese patient and can be exacerbated if the patient is morbidly obese. Several studies recommend the use of multiple cassettes to cover the patient body dimension (Buckley et al., 2009, Reynolds, 2011, Carucci, 2013, Uppot, 2007). However, none of these studies have produced guidelines to follow in terms of

cassette orientation or central ray location according to patient size. Using multiple cassettes in a nonstandard fashion will indubitably increase the patient dose since the patient will have multiple exposures in the overlapped regions and might have some repeated exposures in cases where the image quality was not optimal. In terms of staff safety, using multiple cassette will require the radiographer to move the patient and fit the cassette under the patient multiple times and this will increase the risk of musculoskeletal injuries to the radiographer, which is a documented issue among health carers in general and radiographers specifically (Lorusso et al., 2007). In addition, where the system is a cassette-less DR system, this can result in procedure cancellation or conducting the procedure with mobile x-ray machine. So, the idea of using multiple cassettes seems to be a valuable solution but needs to be conducted in a standardised way; so far the literature is lacking such standards.

Body thickness is an important factor in x-ray attenuation. With high diameter of soft-tissue thickness, the x-ray beam needs to travel longer distances through different tissue of different densities, this will lead to the x-ray energy being attenuated and scattered more than when travelling through standard soft-tissue thicknesses due to low photon penetration. The penetrating power of the beam is known as the quality of beam, which is related to its average photon energy and practically termed the kVp (Graham et al., 2012). The issue of poor photon penetration is a well-recognised issue in imaging the obese patient (Buckley et al., 2009). It results in low receptor signals due to the high amount of x-ray photons being attenuated and scattered. Several studies, (Buckley et al., 2009, Uppot, 2007, Carucci, 2013), have suggested multiple solutions to overcome this issue. The given solutions in the literature included increasing the exposure factors, kVp and mAs, and using a secondary grid. However, increasing these factors will inevitably increase the patient dose. The process of x-ray attenuation is a result of the absorption and scattering effects (Fetterly and Schueler, 2007). The Compton process is more relevant when imaging the obese patient since it tends to occur in areas with a high concentration of electrons per unit of mass, fat for instance (Fetterly and Schueler, 2007). With the Compton process being the reason behind the need for increasing kVp in cases of obese patients (Aichinger et al., 2011), it is of value to consider the

negative impact of high kVp on image contrast besides scattered radiation. The suggestion of Buckley et al. (2009) is to increase the exposure time to compensate the attenuated photons by adipose tissues. However, others have pointed out the high chance of motion artefact as a resultant of high tube current (Uppot, 2007, Yanch et al., 2009). In cases where AEC ionisation chambers are used, previous studies have recommended an extra precaution to prevent exposure cut-off due to overheating of the anode before a satisfactory image density has been reached.

In terms of scattered radiation, some researchers have suggested the use of a secondary grid placed between the image receptor and the patient to eliminate unwanted scattered radiation which would otherwise cause deterioration of the signal to noise ratio of the image (Uppot, 2007). It has been shown that a secondary grid has the ability to absorb 80-95% of scattered radiation but also 40-50% of the primary beam photons (Williams et al., 2007). For this reason, the main compromises include an increased radiation dose and the likelihood of motion artefact due to a longer exposure time. Additionally, the author suggested this technique did not provide any guidance on how to change the kVp and mAs in order to compensate for the absorbed main beam. The use of proper beam collimation can reduce scattered radiation (Modica et al., 2011). This technique is applicable when the patient is not morbidly obese or in imaging the extremities. However, in case of abdomen and pelvis radiography, beam collimation will not added any value to saving patient dose as obese patient's diameter tends to be more than light beam diaphragm.

However, all the technical solutions, which have been discussed above, are lacking in support from the evidence base. Studies in the current literature have treated each parameter in isolation and are limited in reliability (Le et al., 2015a).

From the discussion above, it is very clear how challenging it is to select exposure factors based on the patient's size. Hence, a narrative literature review was conducted to identify any literature that has discussed exposure factors selection based on patient's size in digital systems.

2.7 Previous studies of exposure factors prediction models

The literature search was conducted using various data bases and peer reviewed journals that were available to the researcher. Data bases searched included CINHALL complete, Medline (EBSCO) and Medline Ovid with abstract. Keywords used in the search are illustrated in ge of the relevant literature.

Table 2. These terms were adopted from a similar review conducted by Ching and colleagues but with additional terms (Ching et al., 2014). A different search was conducted with manipulation of the search terms in order to maximise the results of relevant studies. Other peer reviewed journals were searched including; Radiography, European Journal of Radiology, European Radiology, Radiology, Radiologic Technology, Journal of Medical Radiation Science, Radiographics, Medica Physica, Current problems in diagnostic radiology, Journal of Radiation Protection Dosimetry and the British Journal of Radiology. Terms used in searching these journals include; “obese”, “obesity” and “exposure factor selection”. Studies that have been conducted using digital radiography (DR) systems were included while those using analogue systems were excluded. Reference and citations of relevant studies were also reviewed in order to ensure a full coverage of the relevant literature.

Table 2 List of terms used in database search

Population	Intervention	Outcomes
"exposure determination" OR "point system" OR "exposure adaptation" OR "exposure modification" OR "exposure parameter" OR "exposure factor" OR "exposure selection" OR "exposure adjustment" OR "exposure decision" OR "exposure alteration" OR "exposure correction" OR "exposure variation" OR "exposure technique" OR "exposure calculation" OR "exposure setting" OR "exposure approach" OR "technique chart" OR "fixed	Thickness OR size OR body thickness OR body part thickness OR obese OR non-standard OR overweight OR morbidly obese OR size specific	radiography OR general radiography OR projection radiography OR digital radiography OR DR or computed radiography OR CR OR x-ray OR radiograph

kvp" OR "fixed tube potential" OR "fixed kilovoltage" OR "fixed kv" OR "fixed peak kilovoltage" OR "variable kvp" OR "variable tube potential" OR "variable kilovoltage" OR "variable kv" OR "variable peak kilovoltage" OR "system of exposure adaption" OR "bit system" OR "Siemens point system" OR "25% rule" OR "15% rule" OR "exposure chart" OR "guiding equation"		
---------------------------------------------------------------------------------------------------------------------------------------------------------------------------------------------------------------------------------------------------------------------------------------------------------------------------------------------------------------------------	--	--

Table 3 literature review results

Study	x-ray system	Body part	Phantom	Image quality assessment	Brief description of the study	Results	Limitations
1- (Ching et al., 2015b)	DDR Carestream	Pelvis (sacral area)	Kyoto abdomen - pelvis + 3 cm pork belly. Max thickness (21.5 cm)	EI: $1500 \pm 2\%$	Using 5 kVp levels and 6 SID levels, along with two different body thickness, the mAs was established on 70 kVp through AEC. Using DuPont system, each exposure was assigned a bit value with a total of 38 bit value, which is equal to the initial bit value of the first exposure using AEC.	Out of 60 produced images, 16 achieved the target bit value and EI. Amendments were applied to the kVp, this increased the number of images that met the target bit and EI to 38. A new system was established called DigiBit system.	<ul style="list-style-type: none"> • Use of EI for image quality assessment • Small thickness (21.5 cm) • Initial exposure factors based on conventional radiography system (DuPont) which has not been stated in the literature ((Ching et al., 2014) • Pork belly, added to one orientation, anteriorly.
2- (Ching et al., 2015a)	DDR Carestream	pelvis	KYOTO abdomen-pelvis + pork belly added anteriorly. Max	EI: $1500 \pm 2\%$	60 radiographs were taken for each phantom thickness. using 5 levels of kVp (60 – 100 kVp)	The 25% rule accurately predict 53% of mAs when thickness	<ul style="list-style-type: none"> • Similar to the above.

			thickness (21.5 cm)		and 6 SID levels (80 -130 cm). for each exposure the mAs was adjusted until EI target achieved. Different exposure factors prediction systems (DuPont – DigiBit and 25% rule) were tested to identify the most accurate system that accurately predict mAs when thickness increased. DuPont, DigBit and 15% kVp rule also were tested to identify the best predictor when kVp change.	increased. The DigiBit was the most accurate mAs predictor when kVp changed.	
3- (Zheng et al., 2017)	-	-	-	-	Based on mathematical modelling assuming the image quality is a function of radiation dose	For a constant patient thickness, mAs should be increased 3.35 times the kVp. For a constant kVp,	<ul style="list-style-type: none"> The technique chart that underpins the new prediction models was based on CR and the author did not have control over how the

						the mAs need to be increased by 7.8 % for every 1 cm of patient thickness increase.	chart was derived
4- (Zheng, 2018)	-	-	Two Perspex CT dose phantoms with 16 and 32 cm diameter	-	Based on pure mathematical modelling, new equations to predict mAs, kVp based on patient size.	-	<ul style="list-style-type: none"> Based on experiments conducted to measure the dose output using water phantom which does not accurately represent human.
5- (Allen et al., 2013)	CR (Agfa system)	Chest (PA)	Anthropometric chest phantom (unknown resource)	Visual assessment (5 observers) using CEC image quality criteria.	10 kVp rule (where increasing the tube potential by 10 kVp while reducing the mAs by 50%) was applied on 391 match pairs of chest (PA) for anthropometric chest phantom	The 10 Kvp rule show a promising results in producing a consistent contrast in chest x-ray but break down in high mAs.	<ul style="list-style-type: none"> The 10 Kvp was applied for the same size phantom The experiment restricted to chest x-ray only

6- (Steward et al., 2018)	Direct Digital radiography system (GE Optima XR656)	Lumbar spine	Anthropometric phantom (unknown)	EI deviation index (DI) was used along with 10 radiologists who assessed the image contrast.	To test the effect of mAs and the 15% and 10kVp rules while keeping the mAs constant. Additionally, the 15% kVp rule was tested while halving the mAs as the kVp increased.	Images produced using 10 mAs and 320 mAs were of diagnostic quality. Various opinions presented with regards to kVp that produced the best image contrast.	<ul style="list-style-type: none"> • One size anthropometric phantom • The assessment of image quality was vague • The final images were manipulated in terms of windowing before presented to the radiologist
---------------------------	-----------------------------------------------------	--------------	----------------------------------	----------------------------------------------------------------------------------------------	-----------------------------------------------------------------------------------------------------------------------------------------------------------------------------	------------------------------------------------------------------------------------------------------------------------------------------------------------	-------------------------------------------------------------------------------------------------------------------------------------------------------------------------------------------------------------------------------------------------

Table 3 demonstrates these studies that have been found and a discussion of all these studies will follow. In the first study, (Ching et al., 2015a), the researcher extended a pelvis phantom with 18.5 cm thickness into 21.5 cm by adding a pork belly sourced from a local butcher. However, no validation studies have been conducted in order to investigate the suitability of pork belly to represent fat tissue. This is due to the fact that pork belly density will change as it dries out over time. Moreover, the Hounsfield Unit (HU) of pork belly might change over time and affected by the room temperature during experiment (Alzyoud et al., 2019). Since the researcher did not provide any information regarding pork belly density and HU, this jeopardise the reliability of pork belly to mimic human fat tissue with regards to radiological properties. Additionally, the pork belly was added to the front aspect of the phantom only. However, Yanch and colleagues have demonstrated, through a Monte Carlo simulation study using a stylized phantom with five different orientations of added fat, difference in radiation dose and tube current needed to achieve a diagnostic image between all different fat orientations (Yanch et al., 2009). This will impact on the applicability of their results when transferred into a clinical practice as obese patients tend to have different fat orientation. Moreover, the maximum thickness achieved in Ching and colleagues' study, 21.5 cm, considered to be of a normal to overweight rather than obese patients (Qurashi et al., 2018). This in turn will restrict the result of the study to a maximum thickness of 21.5 cm.

With regards to the image quality assessment, Ching and colleagues focused on exposure index (EI) only in determining the suitability of the image quality. However, the EI aims to safeguard against overexposure and is only an indirect indication of image quality (Seibert and Morin, 2011, Peters and Brennan, 2002). Additionally, the EI is energy dependant and the value of EI will change as a result of changes in collimation, exposure factor manipulation and patient size (Butler et al., 2010).

In the second study listed in Table 3, (Ching et al., 2015b), the researcher used similar methods in terms of phantom extension to represent obese patients and image quality assessment, however, the researcher compared different exposure factors prediction models in order to investigate the best model to predict kVp and mAs based on phantom thickness. Three models for predicting

exposure factors namely; 25 % rule, DuPont™ and the DigiBit system, were compared to investigate which of these three models predict the mAs accurately as the patient size increases. Additionally, the 15 % rule and DuPont™ were compared to test the best predictor of kVp change as the phantom size increased. However, the quality of the produced images was assessed based on EI only, which does not reflect the clinical assessment in practice, i.e visual assessment by the radiologists. Additionally, the results showed only moderate success of the prediction systems to predict exposure factors. For example, 53% of mAs change was correctly predicted when using 25% rule and 33% when using DigiBit to predict mAs when the kVp was changed.

In the third and fourth study, shown in Table 3, the researcher based his exposure factors equations on pure mathematical modelling assuming that the image quality is a function of the radiation dose (Zheng, 2018). However, in the third study, Zheng based the modelling on a techniques chart reported in the literature for a computed radiography (CR) system, over which the author had no control. In the fourth study by the same author Zheng, the modelling was based on a Perspex phantom which does not represent human heterogeneous structures. Additionally, the author assumed in both studies, three and four, that image quality is linearly proportioned with radiation dose. This may be true in analogue systems but in digital systems the story is different where the detector can accommodate large doses while producing the same image quality, i.e producing an image quality in low dose that is similar to image produced with high dose (Mraity, 2015).

In the studies number five and six, the authors investigated the applicability of different exposure factors selection models that have been used in analogue systems but only on normal weight phantom. Despite the promising results of these studies in normal weight patients, it is not clear if these models will be applicable in case of patients with obesity.

An additional systematic review was conducted by Ching and colleagues in order to identify patient-based radiographic exposure factor selection (Ching et al., 2014). Twenty eight studies were identified but all were used in analogue system and most of these models have not been reported in literature.

From the literature review, it is very clear that radiographers are facing challenges when imaging obese patients, especially in selecting the appropriate exposure factors. Such challenges are not based on actual data reflecting the actual practice in terms of radiation dose delivered to obese patients. With regards to the available exposure factors selection models, few studies are existed with it limitations that making their implementation in clinical practice possible only if validated more and improved. According to that, it is of value to explore the challenge in imaging obese patients in clinical practice in order to conduct dose optimisation research according to the needs.

Hence, the next chapter will investigate the practice of imaging obese patients in terms of radiation dose delivered to obese patients in order to explore the most challenging areas and act accordingly.

3 Chapter 3: Radiation dose Audit

3.1 Introduction:

Based on what has been discussed in the previous chapter regarding the high prevalence of obesity in the UK, where 26 % of UK adult population are obese based on a BMI ≥ 30 kg/m². Additionally, the obesity comorbidities that cause a high influx of patients with obesity to hospitals compared to their normal-weight peers, and the high radiation dose already reported to this group of patients in other modalities. It is apparent that investigating the radiation dose delivered to this group of patients in projection radiography is of great value. This is even more significant with the large number of radiographic procedures (>22 million) conducted in England, as discussed in the literature review. Hence, this chapter explores the radiation dose delivered to patients with obesity in projection radiography.

In this chapter, the reader will be introduced to the main dose quantities used in projection radiography including the monitoring dose quantities. Additionally, the concept of dose modelling will be discussed. Previous studies that have reported the radiation dose delivered to patients with obesity will also be explored and discussed.

The method will then be presented in detail followed by the results and the discussion.

3.1.1 Overall aim:

To identify current practice in projection radiography with specific regard to radiation dose delivered to patients defined as obese.

3.1.2 Objectives:

11. To evaluate the radiation dose delivered to obese patients in projection radiography based on clinical data
12. To investigate the relationship between patients' sizes and received dose in order to demonstrate possible dose variation
13. To estimate the radiation-related lifetime-cancer risk of patients with obesity based on the reported dose in comparison with normal weight patients.

3.2 Radiation dosimetry in projection radiography

3.2.1 Absorbed dose (D):

When ionising radiation interacts with matter, part of the radiation energy is deposited in the matter as a result. The deposited radiation quantity is called absorbed dose and is defined as the amount of energy absorbed ($d\varepsilon$) per unit mass of irradiated matter (dm)(ICRP, 2007).

$$D = \frac{d\varepsilon}{dm} \quad \text{Equation 1}$$

Where D is the absorbed dose

$d\varepsilon$ is the absorbed energy

dm is the unit mass of the irradiated area

The unit of the absorbed dose is joules per kg (J/kg) while the SI unit is the Gray. Based on the amount of radiation of energy, i.e. kilovolt or megavolt, the absorbed dose commonly reported in mili-Gray or micro-Gray. Absorbed dose applies to any type of ionising radiation and absorbing medium and it is considered to be the most important unit of radiation dose (Tootell et al., 2014).

3.2.2 Equivalent dose (H):

Since the aim of radiation dosimetry is to monitor the radiation dose in order to reduce the risk of organ damage due to radiation exposure, hence, the absorbed dose cannot determine the risk of damage alone, as the type of radiation has to be considered. Equivalent dose (H) was developed by the ICRP to serve the purpose of determining limits of radiation exposure (ICRP, 2007). The product of the mean absorbed dose of tissue (T) and the radiation weighting factor (R) yields the equivalent dose. The radiation weighting factor defines the biological damage ratio resulting from direct and indirect ionising radiation. Since this project is looking at diagnostic projection radiography, where the photon is the radiation particle, the radiation weighting factor is of unity (ICRP, 2007). Equation 2 demonstrates the calculation of equivalent dose.

$$H_T = W_R \cdot D_{T,R} \quad \text{Equation 2}$$

Where H_T is the equivalent dose of tissue T

W_R is the radiation weighting factor

$D_{T,R}$ is the absorbed dose of tissue (T) by radiation type (R)

The equivalent dose unit is Joules/kg, and the SI unit is Sievert. For example, if the absorbed dose in a tissue is 0.5 mGy, then the equivalent dose for that organ is $0.5 \text{ mGy } (D_{T,R}) \times 1 (W_R) = 0.5 \text{ mSv}$.

The reason equivalent dose is discussed is that it is crucial in order to calculate the next dose quantity, which is the effective dose.

3.2.3 Effective dose (E):

Different tissues have different sensitivity to radiation; for this reason, effective dose is used. This takes into account the irradiated tissues and the amount of radiation deposited into the body in total. The ICRP has recommended the effective dose to be used for dose assessment in planning and optimisation and for demonstration of compliance with dose limits (ICRP, 2007). This includes the comparison of risk between various imaging techniques or modalities (Tootell et al., 2014). In practice, the effective dose can be calculated as the sum product of the equivalent doses of body organs and tissues (H_T) and the weighting factors of those tissues/organs (W_T). The Effective dose (E) can be calculated using Equation 3

$$E = \sum_T W_T \cdot H_T \quad \text{Equation 3}$$

Where E is the effective dose to the whole body

W_T is the tissue weighting factor of tissue (T) as reported by the ICRP

H_T is the equivalent dose absorbed by tissue/organ (T)

The Tissue weighting factor is defined as the quantity stating the contribution of a specific tissue or organ to the total body detriment from stochastic effect

(ICRP, 2007). This can be calculated based on the evidence and data that emerge from different studies such as; the Life Span Study (LSS) and studies from radiation workers. Hence, these factors have been updated multiple times by the ICRP, as Table 4 shows.

Table 4 Tissue weighting factors (ICRP, 1977, ICRP, 1991, ICRP, 2007).

	ICRP 26 (1977)	ICRP 60 (1991)	ICRP 103 (2007)
Gonads	0.25	0.20	0.08
Red bone marrow	0.12	0.12	0.12
Colon	-	0.12	0.12
Lung	0.12	0.12	0.12
Stomach	-	0.12	0.12
Breasts	0.15	0.05	0.12
Bladder	-	0.05	0.04
Liver	-	0.05	0.04
Thyroid	0.03	0.05	0.04
Skin	-	0.01	0.01
Bone surface	0.03	0.01	0.01
Salivary glands	-	-	0.01
Brain	-	-	0.01
Remainder*	0.03	0.05	0.12
Total	1.00	1.00	1.00

*Remainder tissues: Adrenals, Extrathoracic (ET) region, Gall bladder, Heart, Kidneys, Lymphatic nodes, Muscle, Oral mucosa, Pancreas, Prostate (♂), Small intestine, Spleen, Thymus, Uterus/Cervix (♀)

The effective dose is the most commonly used measure in radiology as it facilitates a comparison of the risks anticipated as a result of different imaging techniques (Brenner, 2008). For instance, in the Journal of Radiation Protection Dosimetry, between 2005 and 2008, 60 % of the publications have reported the effective dose (Martin, 2007b). However, more recently, a new debate sparked around the limitation of effective dose in estimating the biological risk resulting from exposure to ionising radiation. The problematic issues of effective dose to be used as a risk indicator for individuals have been summarised by Brenner (Brenner, 2008) in three main points:

- Firstly, the tissue weighting factors affecting the effective dose calculation are determined by the committee subjectively to achieve a balance between: various cancer mortality, stochastic endpoints of cancer incidence, heritability risk and life shortening. These factors have been updated based on the latest scientific evidence available of the radiation exposure physics and biology, Table 4.
- The second argued issue by Brenner is the fact that effective dose is defined independently of age while the available literature suggests that the attributable radiation risks are age dependant (Preston et al., 2007).
- The third matter is a practical one where this dose quantity is misused and sometimes confused. This is due to the fact that both equivalent dose and effective dose have the same unit, i.e. Sieverts, but measuring different quantity. Hence, some studies in the literature have used equivalent, effective and even absorbed dose confusingly, (Brenner, 2008).

For these reasons, Brennan suggested that a new calculation should be used instead of using the tissue weighting factor (Brenner, 2012), he suggests that the new quantity be called “*effective risk*”.

3.2.4 Effective risk (R):

Brennan suggested this new dose quantity in 2008, where he proposed a similar equation used in effective dose (Equation 3) but with a new factor replacing the tissue weighting factor (W_T), called “organ-specific radiation induced cancer risk” (Brenner, 2008). To simplify this, Brennan recommended

that instead of multiplying the absorbed dose by committee-devised numbers, the best-available, organ specific lifetime cancer risk should be used instead. Hence, the effective risk can be calculated using Equation 4.

$$R = \sum_T r_T \cdot H_T \quad \text{Equation 4}$$

Where R is effective risk

r_T is the lifetime radiation-attributable tissue-specific cancer risks (per unit equivalent dose to tissue/organ (T))

H_T is the equivalent dose absorbed by tissue/organ (T)

The Nuclear and Radiation Studies Board, known as BEIR VII, has published organ-specific radiation-induced cancer risk that can be used to calculate the effective risk (National Research Council, 2006). A very recent report prepared by Wall and colleagues from the HPA also reported the organ specific risk (Wall et al., 2011).

3.3 Dose monitoring quantity:

3.3.1 Entrance surface dose (ESD):

From its name, the ESD is defined as the absorbed dose in air at the point at which the x-ray beam intersects with the patient surface, including the backscatter radiation (IPSM, 1992). If the backscatter radiation is excluded, this quantity can be referred to entrance surface air kerma (ESAK) (Wambersie et al., 2005).

In order to measure the ESD, two types of dosimeters can be used, namely thermoluminescent dosimeters (TLDs) and ionisation chambers. This means, in order to report the patient's dose in ESD quantity, the study has to be conducted prospectively. However, the current study was conducted retrospectively, hence it was not possible to use this dose quantity as it is not a common practice to measure ESD, but rather the dose area product (DAP) was used.

3.3.2 Dose area product (DAP):

The DAP can be defined as the product of radiation absorbed dose in air over the area of x-ray beam in a perpendicular plane to the integral beam axis (Lee et al., 2016). The unit of the DAP as its name suggested is Grays per centimetre squared ($Gycm^2$). This quantity is the one most commonly used and which most radiographers are familiar with (Tootell et al., 2014). This quantity is not a patient dose and also it is independent of the focal to patient distance. Usually DAP is measured by a DAP meter that is attached to the x-ray tube in front of the collimator. In order to calculate the patient dose based on the DAP quantity, the focal to skin distance (FSD), field size and the irradiated area are required (Moores, 2005).

3.3.3 Diagnostic reference level (DRL)

In current day, the DRL is an important measure used in medical imaging in order to investigate the level of radiation dose for a specific radiographic investigation on an average patients cohort (ICRP, 2007, Han et al., 2011) . When practiced as recommended by the ICRP, DRL allows the identification of any elevated radiation doses in a specific radiographic procedure and act accordingly in order to specify the source of error and rectify it (ICRP, 2007, Hart et al., 2012). To avoid repetition, more details have been discussed in the literature review regarding the DRL.

3.4 Dose modelling:

The ESD and DAP are the quantities that can be quantified in clinical practice. In order to calculate the absorbed, equivalent or effective dose, dose modelling has to be conducted. The easiest and timely efficient modelling method is through the use of commercially available Monte Carlo simulation software (Tootell et al., 2014). Monte Carlo PCXMC 2.0 (STUK-Radiation and Nuclear Safety Authority, Helsinki, Finland) is a software program that is commonly used to mathematically model the dose. It is a computer program for calculating patients' organ doses and the effective dose in radiology examinations. It provides a flexible stylized phantom to freely adjust for the x-ray projection and other examination conditions of projection radiography and fluoroscopy. The anatomical data of the phantom are based on the mathematical hermaphrodite

phantom models of Cristy and Eckerman, with some modifications and user-adjustable phantom sizes (Tapiovaara and Siiskonen, 2008, Cristy and Eckerman, 1987).

3.5 Radiation dose of obese patients in projection radiography

Different studies have investigated the radiation dose delivered to patients with obesity in different modalities such as CT, interventional radiology and fluoroscopy (Hsi et al., 2013, Wang et al., 2013, Cushman et al., 2016, Smuck et al., 2013). However, the current study is focused on projection radiography and hence relevant studies will be discussed.

The most cited article that reported effective dose to patients with obesity is a study conducted in the USA by Yanch and his colleagues (Yanch et al., 2009). In their study, an advanced Monte Carlo simulation software (MCNPX) was used along with a modified stylized phantom. Computational fat layers were added to the phantom in different orientations, and the effective dose was calculated with and without the fat layers. However, the study was based on the assumption that the image quality of all phantoms produced by the simulation is equal. This excluded the issue of compromised image quality in this group of patients, which is the main concern currently (Le et al., 2015a). Additionally, the dose reported in Yanch's study did not base simulation on the dose reported in the clinical practice, but rather they speculated that exposure factors and other factors such as use of grid and the projection used were relevant. This in turn impacts on the reliability of the study to represent what is happening in clinical practice.

Two further studies estimated the effective dose and absorbed dose in chest radiography (Kim et al., 2012, Tung et al., 2008). Tung and colleagues based their study on 293 patients who had chest radiography. The ESDs were measured using TLD-100H and the effective doses were modelled using WinODS organ dose calculation software. However, their study was constrained to chest (PA) radiography. Additionally, the highest BMI of patients included in their study was 26 kg/m², which is at the lower boarder of the overweight category. Hence, their study did not reflect the challenge of radiation dose increase in patients with obesity.

In Kim and colleagues study, the sample size was large, 899 patients, who had had chest (PA) radiographs using three levels of kVp; 100, 120 and 140 kVp (Kim et al., 2012). The radiation dose (ESD) was used to estimate the effective dose using PCXMC for all patients. However, it was not clear how the ESD was estimated as the author claimed that the ESD was reported from the Dicom header of each radiograph that was included in the study. Additionally, the researcher did not have the data of image width and height, which is necessary if the FSD will be calculated using the PCXMC. This will eventually impact on the radiation dose received as the simulated field size will be smaller than the actual field size used in clinical practice. Additionally, photons used in PCXMC are recommended to be at least 20,000 photons or more (Tapiovaara and Siiskonen, 2008), however, in Kim's and colleagues study the photons used were 12,000 for 100kVp simulation, 14,000 photons for 120 kVp and 20,000 photons for 140 kVp simulation. This in turn will increase the errors in the lower kVp compared to the high kVp simulation, resulting in unbalanced report of absorbed doses. Similarly, Terlizzi and colleagues investigated the relationship between radiation dose and size of patients who had chest x-rays across two different DR systems (Terlizzi et al., 2011). Using the ESD, calculated based on the output of the x-ray system, patients were grouped based on their BMI (Underweight, normal weight and obese) and the average dose to each group was averaged and correlated with the patients size. Despite the reported increase in radiation dose along with the BMI in their study, this is only to be expected as more radiation is required in order to penetrate a thicker body part (Hart and Hillier, 2007). However, their study did not include any obese patients and the reported dose was limited to chest radiography.

A recent study, published after the current study was conducted, reported the radiation dose delivered to 1869 patients with obesity as a result of projection radiography procedures (Metaxas et al., 2018). The study was conducted prospectively yielding the advantages of reporting more patients' anthropometrics such as height, weight, thickness as well as technical parameters of the procedures such as film to image distance (FID), tube current (mA) and tube potential (kV). The BMI reported in their study ranged between 18.6 and 38.5 kg/m² for most procedures (lumbar spine AP + LAT, abdomen

AP, pelvis AP and KUB AP) and up 44.5 kg/m² for chest PA and lateral. Their findings illustrate that dose (kerma area product KAP) received by patients with obesity reach up to 300 % compared to normal weight, especially in lumbar spine and abdomen radiographs.

Based on the studies discussed above, it is of high value to understand the situation of radiation dose delivered to obese patients in the UK, as one of the countries reporting the highest rates of obesity (Baker, 2017). Additionally, understanding the situation of imaging obese patients in clinical practice is important in order to conduct the suitable research which will have a direct impact on patient care. Subsequently, this will impact on the radiation-related cancer risk resulted from medical ionising radiation.

3.6 Methods:

3.6.1 Patient Recruitment:

The study aimed to explore the radiation dose delivered to patients with obesity; hence, the largest bariatric centre in the South West was the main targeted site. This centre has been running since 2003 and it is the first centre, outside the USA, to be awarded Centre of Excellence status by the Surgical Review Board. Around 300 operations were conducted in the centre in 2009/10. This promotes a high influx of patients with obesity to receive treatment in the centre. For this reason it was considered to be the best choice to access a high volume of patients with obesity records. In order to maximise the number of obese patients to be included in the study, and to cover a broad range of BMI groups, i.e. overweight, obese and morbidly obese, a request to engage in the study was prepared in order to be sent to health professionals who work closely and mainly with obese patients in the same hospital, see Appendix (1).

A list containing seventeen medical and allied health professionals, who work in the bariatric centre and dealing mainly with patients with obesity, was suggested by a senior radiographer working in the centre. The list includes bariatric surgeons, nutritionists and nurses working in diabetic clinic and weight management clinic. The letter was sent by email to all health personnel. A

bariatric surgeon was the only respondent and was happy to engage in the study.

A meeting was then set with the bariatric surgeon in order to discuss the nature of the study and to clarify the study proposal and the anticipated outcomes of the study. An agreement was granted by the bariatric surgeon to provide a list of patients with obesity, who visited the bariatric surgery clinic, after the required ethical approval is in place.

3.6.2 Ethical considerations:

In order to save time, a proposal of the study was sent to the research manager in the hospital seeking their opinion of which ethical committee the study should go through (Appendix 2). The research manager assured the researcher that the study will not need R&D approval but would need to go through the clinical audit department first. Due to the dilemma around the patients' data anonymity as the patients' hospital numbers need to be shared with the researcher in order to be able to access the patient's data, the study proposal was sent to the Caldicott Guardian for consideration. To overcome this issue, the researcher suggested the data could be collected by a member of the radiology department, who has the right to access patients' data, and receives a payment from the researcher fund allocated for such purposes. This was passed into the clinical audit department and the Caldicott Guardian. A number of questions that needed further clarification were sent back to the researcher. This included:

- The quantity of records it is proposed to access (1000). There seems no clear justification for the need for this volume
- The intention to pass the data (anonymised according to the description) onto the research team at Exeter University – there is a degree of uncertainty about what happens to the information from that point onwards
- The proposed inclusion of the hospital number within the information provided by our clinical team, thus potentially jeopardising true anonymization.

- As an associated issue there is no stated engagement between student and Radiology team. Their critique and approval of this would appear important prior to any data collection.

These were responded to, see Appendix 3, and the response sent back to the researcher manager, who was the link between the researcher and the hospital authority. Based on the proposal and the requested response to the further clarification, the permission was granted, (Appendix 4), and the study was considered by the clinical audit department as a service evaluation.

A New challenge rose when the radiology team at the hospital contacted the researcher apologising that there was insufficient capacity to perform the task as required. The solution suggested by the research manager at the hospital is for the researcher to sign an honorary contract with the hospital in order to be granted access to the patients' data.

A Disclosure and Barring Service (DBS)_check was first conducted, when successfully returned, the researcher agreed to sign the staff code of confidentiality, protection & use of patient information, model declaration form, data protection and confidentiality policy. Once all papers were in place and the contract was signed, the researcher was given a username and a password to access the patients' files under the supervision of a senior radiographer from the radiology department.

3.6.3 Data access:

An induction to the Radiology Information System (RIS) and the Picture Archiving and Communication System (PACS) was given to the researcher by the appointed supervisor. This includes how to access both systems and where to find the required data including the DAP and its unit, and the number of images.

3.6.4 Patients:

A list of 1964 obese patients, with a BMI equal to, or over, 30 kg/m², was provided from the bariatric surgeon. All patients had visited the bariatric surgery clinic and undergone a bariatric surgery procedure. The list contained the

patients' hospital number, height (m), weight (kg), BMI (kg/m²) and ethnicity. All anthropometric measures were completed prior to the patient undergoing bariatric surgery. The age of the patients at the time of their radiography examination was determined from their date of birth subtracted from the date of the radiography exam.

3.6.5 Inclusion and exclusion criteria:

All patient data provided by the bariatric surgeon were for obese patients, with a BMI ≥ 30 kg/m², hence, they were eligible for the study.

During the initial screening of patients' files, files were excluded if:

- The file number was in a different format to the standard hospital number. This could mean these patients have undergone a bariatric surgery procedure by the bariatric surgeon but in different hospital, such as a private one.
- The file showed more than one name for the hospital number. As the list provided by the surgeon did not include the patient's name. Hence, these files were excluded.
- The file number showed no patients name at all. This could be attributed to a mistake in typing the patient's file number in the list.

The eligible files were then screened for a projection radiography history. All projection radiography procedures were of interest, however, since the study aimed to evaluate the radiation dose delivered to obese patients in a comparison to the normal-weight adult's doses, the DAP was the only possible dose quantity to be collected as it is recorded in the RIS system. ESD was not possible due to the nature of the study being conducted retrospectively. All radiography procedures that has a comparator in the NDRL were included, i.e. the procedures that has a DAP value in the NDRL. This includes;

- Abdomen AP
- Chest PA
- Cervical spine AP + LAT
- Lumbar spine AP + LAT
- Thoracic spine AP + LAT

- Pelvis.

These are the main procedures that have been focused on since they have a comparator in the NDRL with DAPs value.

With these in mind, files were screened and any projection radiography procedure was included unless:

- The DAP or its unit was missing
- The procedure did not match the NDRL criteria in terms of the number and types of projections for a comparison purposes
- The DAP readings were recorded once for multiple exams of different body regions

In the abdomen (AP) radiograph, as noted in the PACS, radiographers usually perform abdominal x-ray using two images, and three images in certain occasions, but one DAP reading was recorded in the RIS. This is justifiable by the fact that the largest image receptor, which is 35 cm x 43 cm, cannot accommodate the whole abdomen. For this reason, whether the patient had two or three images to cover the abdominal area, it was considered as an AP view, and hence analysed and compared to the NDRL.

3.6.6 Obtaining the data

The process of data retrieving started in March 2016 and took three months. For every patient, the patient's hospital number entered into the RIS; (Carestream Vue RIS, Version 11.0.12.51) in order to open the radiology file of the patient. If the patient's file and the conducted procedure were eligible for the study, then the following information was recorded in an external Excel spreadsheet:

- Patient gender
- Date of birth
- Type of exam and projections
- Date of exposure
- kVp and mAs used (for each image – from RIS or PACS if not provided in the RIS)

- The DAP reading and its unit as entered by the radiographer in the RIS
- Number of rejection and the reason for rejection.

Along with this information, other data were extracted from the initial list provided by the surgeon and recorded in the excel sheet, this includes:

- Patient's hospital number
- Type of exam and views
- Date of birth
- Body mass index (kg/m²)
- Height (m)
- Weight (kg)

If the patient had had a certain exam on a different date, these also were recorded under the same patient.

In order to reduce the human errors during the data recording, several rules had to be followed during the data transition. To confirm the file belonged to the right patient, the researcher had two checks. First, the hospital number which is supplied in the initial list. Secondly, the researcher had to calculate the patient age based on the patient's date of birth, appeared in the RIS, and match the calculated age with the listed age. The DAP unit for each entry was recorded as it appears in the RIS, and then converted to Gy.cm² prior to the analysis. To check the procedure matches the DRL criteria in terms of number and type of view, PACS (VUE PACS version 12.0.0.8902) was used to access the images and confirm the eligibility of each procedure. The data were recorded in separate excel sheet for each examination.

3.6.7 Final statistical analysis:

Every examination was analysed separately. The mean, median, standard deviation, minimum and maximum were calculated for age, height, weight, BMI and dose (DAP) in each exposure set. Any extreme values were investigated and errors were corrected after checking patient details again before the final analysis. A double check of the DAP readings were conducted for random files (20 files in total including extreme high DAP values) by a medical physicist working in the hospital. The statistical analysis was performed using STATA 14.

In order to testify a possible correlation between the DAP and patient's anthropometrics, the data distribution had to be tested using histogram and Shapiro-Wilk test,(Altman, 1991), in order to use the suitable correlation statistical test.

In addition, the kVp and mAs were descriptively analysed in order to be used in the dose modelling.

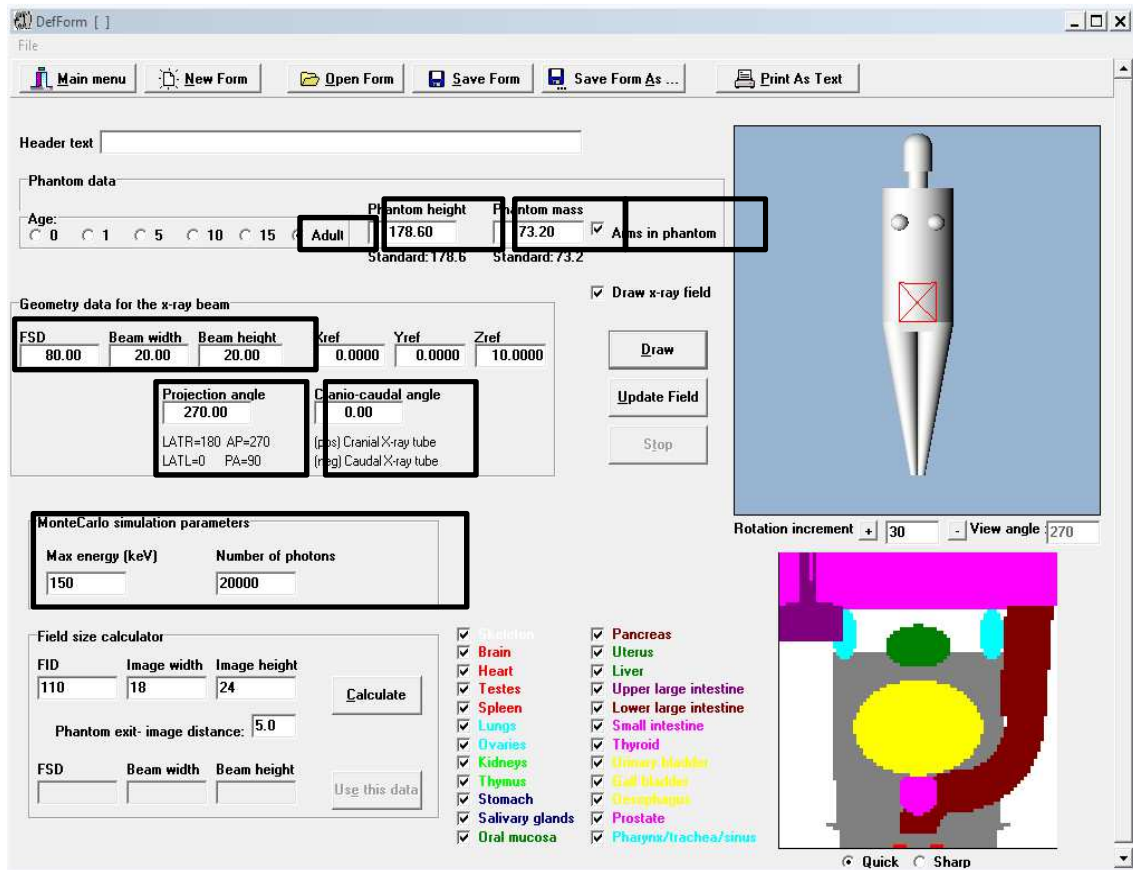
3.6.8 Dose modelling:

As the DAP reading is not a patient dose, it was essential to estimate the absorbed dose for each examination based on the reported DAP in order to be used in effective risk estimation as per Equation 4. The Monte Carlo PCXMC 2.0.1.4 (STUK-Radiation and Nuclear Safety Authority, Helsinki, Finland) was used to model the mean organ absorbed doses. The software was installed in PC run by Windows 7 Enterprise version and has a processor with 3.60 GHz. All simulations were set and run by the researcher.

In the first step of simulation, "*examination data*" Figure 2, the user is provided with a flexible interface to change different parameters including; the patient's height and weight, the type of patient, i.e. paediatric or adult, the beam width and height, projection angle, cranio-caudal angle, projection i.e. AP, LAT or PA, and the number of photons. Therefore, for both groups, the type of phantom chosen was an adult phantom as the study considers this age group only. The phantom height (cm), weight (kg), was set based on the median reported in this study due to data skewness. For the normal- weight group, these two parameters were set based on the mean value, the only reported value in the NDRL report. The type of view was selected based on the reported values in both groups, median value. The cranio-caudal angle was kept zero for all procedures except for cervical spine it was set to 15°. The max energy and the number of photons were both kept to the max values, 150 Kev and 1 million photons. This is to reduce the estimation errors in organ dose estimation. FSD was set to the standard figure for each procedure as described by Bontrager and Lampignano (Bontrager and Lampignano, 2013). However, the PCXMC uses the FSD, this was calculated by using the phantom width measured by the beam width tool then subtract the result from the FID, 100cm. The reason for

not using the calculator provided by the PCXMC, at the lower left corner, is because it requires the operator to have the actual data of the actual image height and width data, Figure 2. This type of data was neither collected in this study nor in the NDRL review. Number of photons was set to one million to minimise the errors.

Figure 2 Examination data window in PCXMC



In this window, the end user has the chance to amend different patient and projection related values. All these parameters have been rectified according to data in Table 5, which is based on data reported in this study and in the NDRL 2010 review (Hart et al., 2012).

Table 5 PCXMC exposure details for both groups

		Weight	FSD	Tube voltage	Filtration	x-ray beam width	x-ray beam height	Arms in phantom	Dose value (Gy.cm ²)	
Abdomen (AP)	DRL	71	82	77	3.1	34	43	no	1.8	
	Obese	Upper	141.55	75	80	3.1	46	30	no	4.445
		lower	141.55	75	80	3.1	45	28	no	4.445
Chest (PA)	DRL	70	160	90	3.1	34	28	no	0.08	
	Obese	125	153	120	3.1	48	30	no	0.156	
Pelvis (AP)	DRL	71	80	75	3.1	34	32	no	1.7	
	Obese	125	76	75	3.1	44	33	no	3.46	
Lumbar spine (AP)	DRL	71	80	79	3.1	16	35	no	1.2	
	Obese	126.25	75	80	3.1	18	35	no	3.9	
Lumbar spine (LAT)	DRL	71	70	88	3.1	15	25	no	1.9	
	Obese	126.25	54	94	3.1	18	25	no	6.5	
Cervical spine (AP)*	DRL	71	90	68	3	14	20	yes	0.1	
	Obese	119	87	65	3	15	20	yes	0.145	
Cervical spine (LAT)	DRL	71	177	72	3	13	24	yes	0.1	
	Obese	119	172	72	3	15	26	yes	0.145	

PCXMC: A PC program for X-ray Monte Carlo simulation software

FSD: Focus to skin distance

NDRL: National diagnostic reference level

kVp: Peak kilovoltage

AP: Anteroposterior

PA: Posteroanterior

LAT: Lateral

The x-ray beam projection, size and collimation were freely adjusted. The researcher used his experience as a radiographer and as recommended in the radiography textbook,(Bontrager and Lampignano, 2013), in order to set the centring point and the collimation for each procedure.

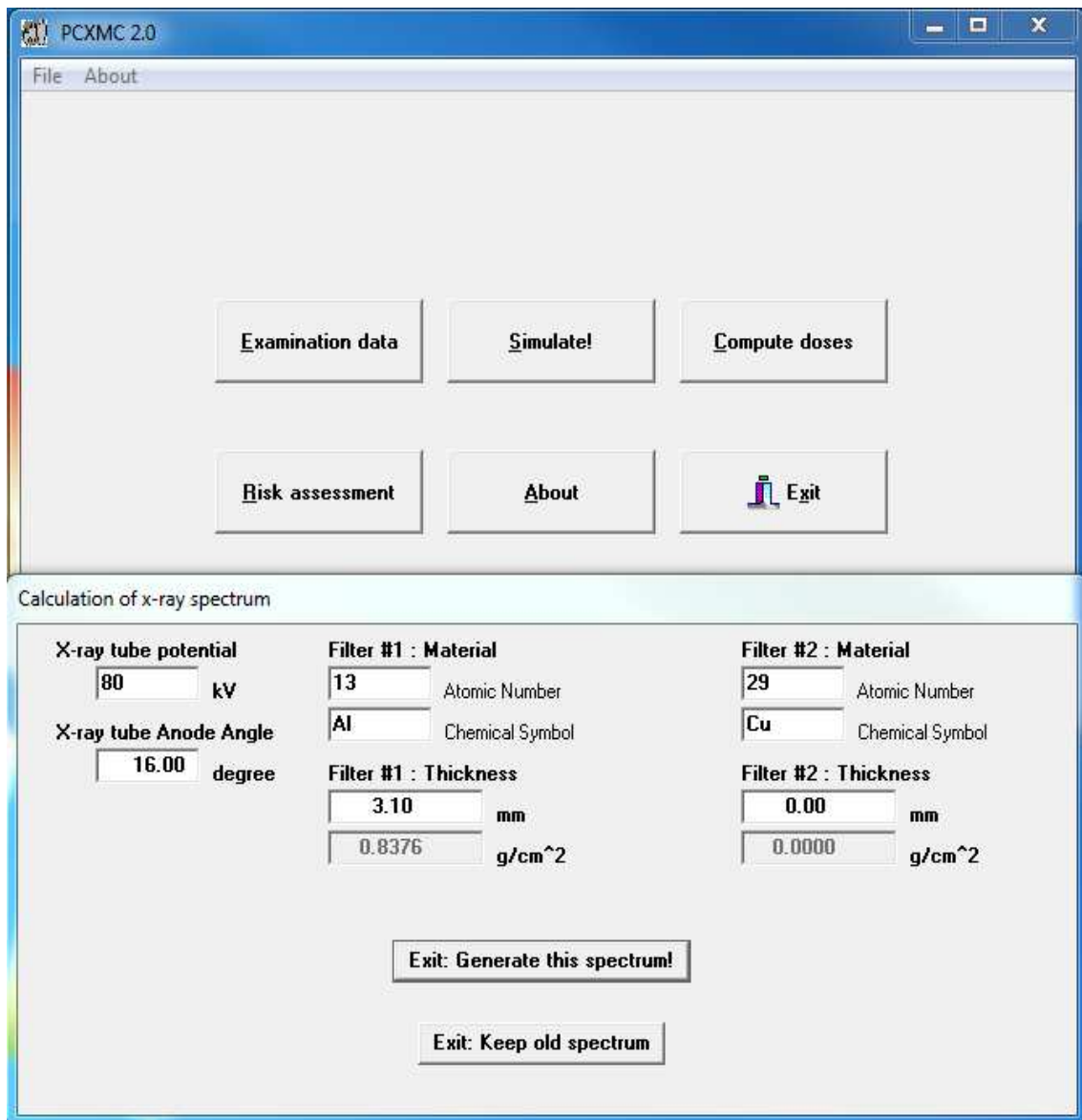
For both cervical spine and lumbar spine, both left and right lateral views were conducted. The abdominal AP for patients with obesity group was conducted twice, i.e. upper abdomen and lower abdomen, this is justified by the fact that during the data collection the images on PACS indicates that the most predominant practice in this group of patients is two images for the upper and lower abdomen.

The second step was the “*simulation*”. This was run for each projection and procedure for both groups of patients. The simulation for each projection took about 4 minutes. This is due to the high number of photons, which means the

simulation was repeated for each set of kVp range ten times before averaging the results.

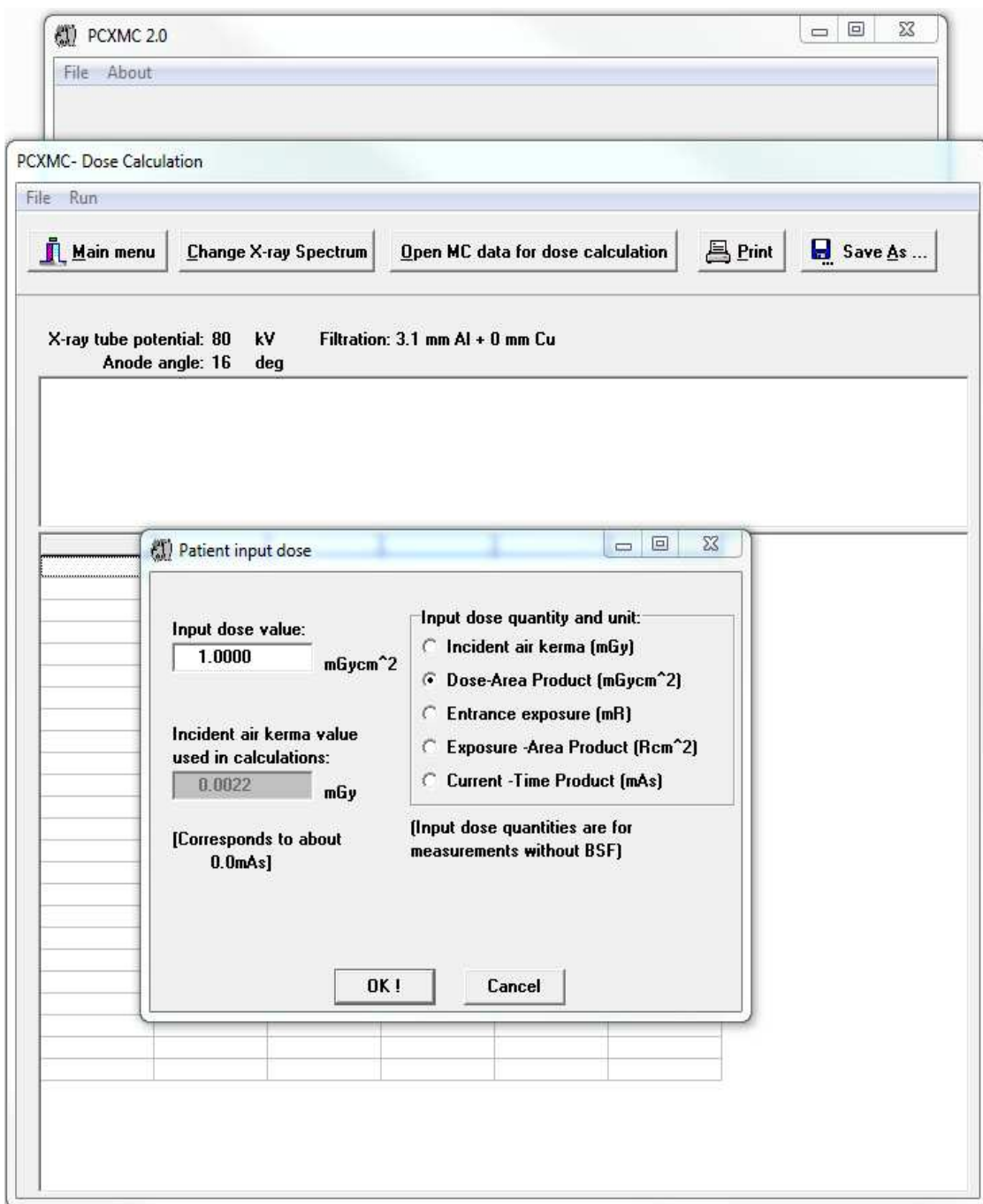
In the third step “*compute doses*”, the researcher input the x-ray spectrum, i.e. kVp, anode angle and the filtration as per values in Table 5 for each projection in each group of patients.

Figure 3 x-ray spectrum in compute doses window in PCXMC



In order to calculate the absorbed dose, the PCXMC allows the end user to enter the patient dose in different values. In this study, the DAP was the measured value, hence, for consistency purpose and in order to make the two sets of data comparable, the calculation of the absorbed dose and effective dose by PCXMC utilised the median DAP (mGy.cm²) value as reported in the 2010 review (Hart et al., 2012), and in this study for each type of radiographic examination, Table 5. However, the DAPs for cervical and lumbar spine in the obese group were extracted from the RIS as one number for both views, AP and LAT. Hence, the combined DAP of lumbar spine AP and LAT, from the 2010 review, was used as a benchmark to determine the percentage of DAP for each projection separately. As a result, the AP lumbar spine represents 37.5% while the LAT view represents 62.5% of the total DAP. For the cervical spine, the AP and lateral views represent 50% each, of the median combined DAP value. The DAP value for each procedure in both groups of patients, obese and normal weight, was converted into mGy/cm² and input into PCXMC as shown in Figure 4. The organ absorbed doses were estimated for the radiographic examination reported in this study and their comparator from the diagnostic reference level 2010 review (Hart et al., 2012). For the abdominal AP in the obese patients group, the sum of the absorbed dose for both upper and lower abdomen was reported as the final absorbed dose. The final absorbed dose for the lateral view in both lumbar and cervical spine for both groups of patient was the average of the right and left lateral for each procedure.

Figure 4 patients dose input window in PCXMC



3.6.9 Lifetime cancer risk estimation:

The risks of cancer were calculated using Equation 4 (see page 53) as described by Brenner, (Brenner, 2014).

In this study, the age and sex specific lifetime cancer risk figures reported by Wall et al. (Wall et al., 2011) was used in effective risk calculation after conversion into mGy, Table 6. The sum of the product of the estimated organ dose (mGy) and the lifetime risk of cancer incidence for that organ (percentage per mGy) gave the effective risk. The age was set from 20 years and above, as our data shows very few patients under the age of 20 years and thus this group of age was not included in the effective risk estimation.

Table 6 Lifetime cancer risk incidence by organ, age and sex for a composite

organ	Age at exposure (Y)						
	20-29	30-39	40-49	50-59	60-69	70-79	80-89
Males							
Lung	0.00073	0.00078	0.0008	0.00076	0.00061	0.00038	0.00015
Stomach	0.00057	0.00043	0.00031	0.0002	0.00012	0.00006	0.00002
Colon	0.00098	0.00079	0.0006	0.00043	0.00025	0.00012	0.00003
RBM	0.00077	0.00076	0.00078	0.00065	0.00049	0.00033	0.00017
Bladder	0.00065	0.00055	0.00046	0.00035	0.00023	0.00012	0.00004
Liver	0.00034	0.00026	0.00018	0.00012	0.00007	0.00003	0.00001
Thyroid	0.00005	0.00003	0.00001	0.00001	0	0	0
Oesophagus	0.00011	0.00011	0.00012	0.00014	0.00015	0.00015	0.0001
Other	0.00202	0.00142	0.00096	0.0006	0.00031	0.00012	0.00003
All cancers	0.00622	0.00513	0.00422	0.00326	0.00223	0.00131	0.00055
Females							
Breast	0.00221	0.00144	0.00084	0.00045	0.00021	0.00008	0.00002
Lung	0.00158	0.0017	0.00178	0.00172	0.00139	0.00082	0.00029
Stomach	0.00088	0.00067	0.00048	0.00033	0.0002	0.0001	0.00003
Colon	0.00048	0.00038	0.00029	0.00021	0.00014	0.00007	0.00002
RBM	0.0005	0.00045	0.00077	0.00049	0.00029	0.00015	0.00006
Bladder	0.00052	0.00045	0.00039	0.00032	0.00024	0.00014	0.00005
Liver	0.00015	0.00011	0.00008	0.00006	0.00003	0.00002	0
Thyroid	0.00026	0.00013	0.00006	0.00002	0.00001	0	0
Oesophagus	0.0001	0.00012	0.00015	0.00021	0.00028	0.0003	0.00019
Ovary	0.00031	0.00024	0.00017	0.00011	0.00006	0.00002	0.00001
Other	0.00156	0.00111	0.00075	0.00048	0.00027	0.00013	0.00004
All cancers	0.00855	0.0068	0.00576	0.0044	0.00312	0.00183	0.00071

Euro-American population (% per mGy)

Other: includes all remainder tissues: Extrathoracic (ET) region, Gall bladder, Heart, Kidneys, Lymphatic nodes, Muscle, Oral mucosa, Pancreas, Prostate (♂), Small intestine, Spleen, Thymus, Uterus/Cervix (♀)

3.7 Results

Of 1964 obese patients' files, 1225 were not eligible for the study. The remaining 739 files were screened and 630 of them showed a history of projection radiography while 109 showed no history.

In Figure 5, included and excluded files are listed with the justification of the decision. From 630 files that met the inclusion criteria, the investigations that have been accessed through RIS are listed in Figure 6 with the justification of the inclusion and exclusion.

3.7.1 Included and excluded files and procedures

Figure 5 Number of files included and excluded based on files screening

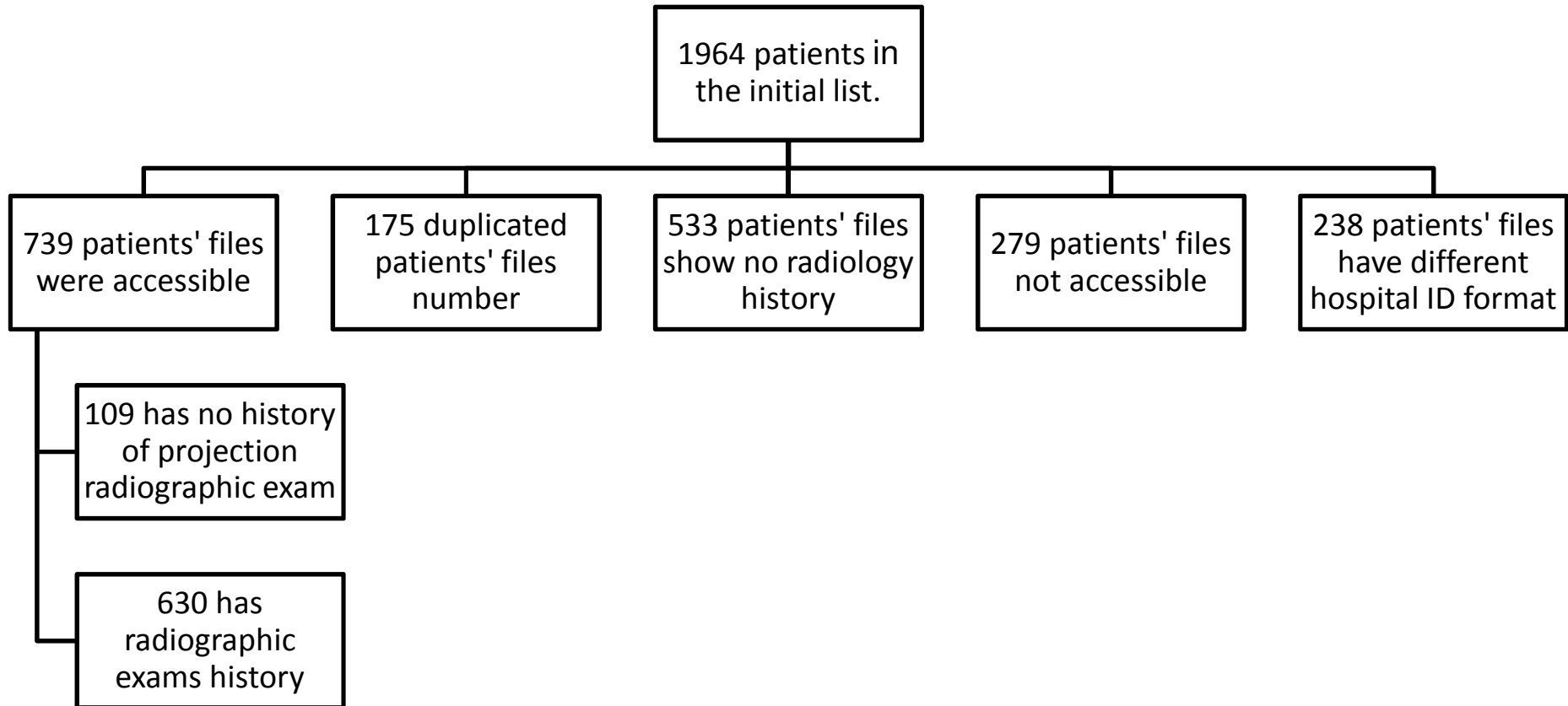
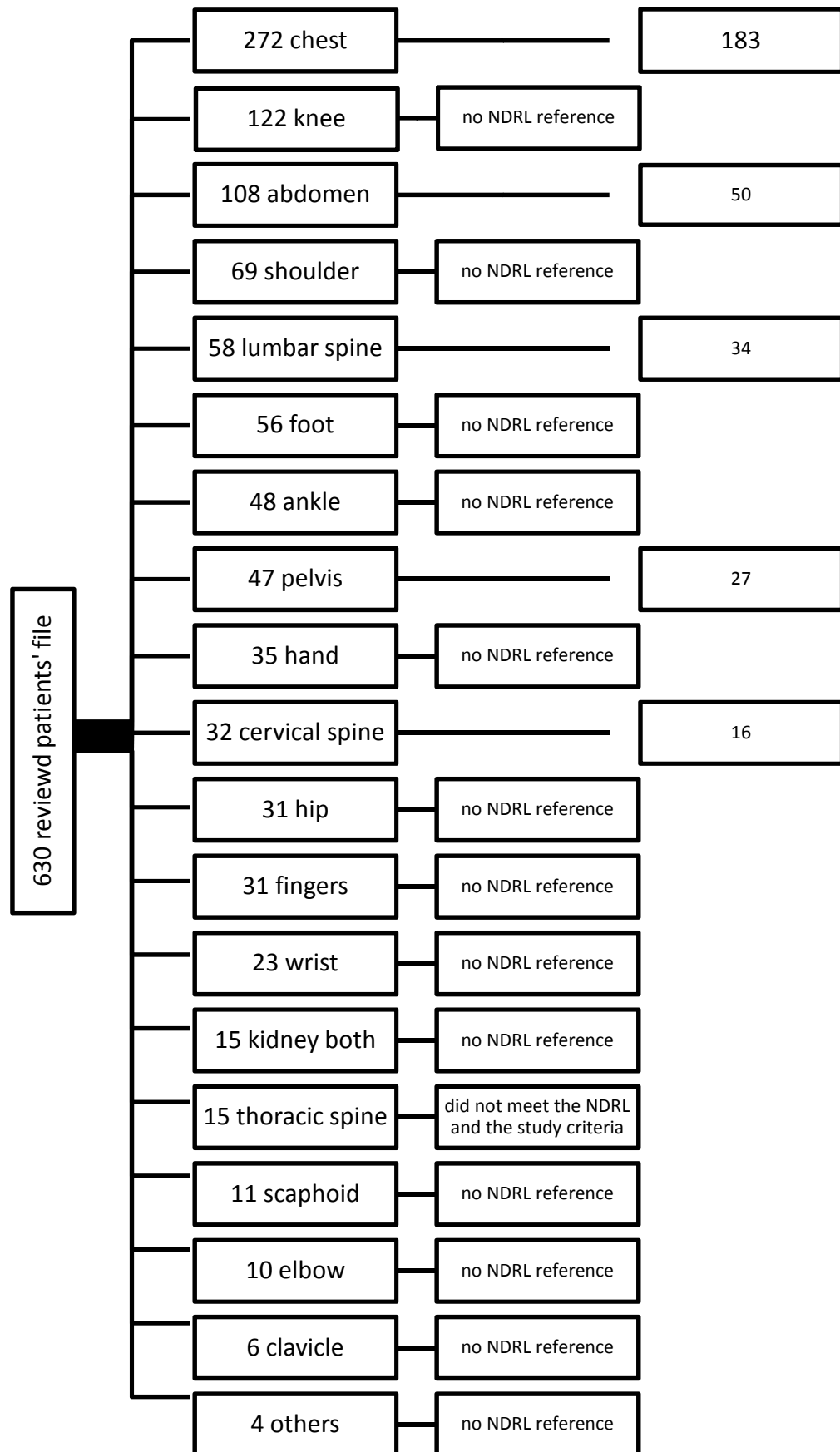


Figure 6 Number of included and excluded radiographic investigations



3.7.2 Patients' characteristics:

Table 7 Patients' characteristics

	Number		Age (year)	Height (m)	Weight (kg)	BMI (kg/m ²)
Abdomen (AP)	50	Mean ± SD	48 ± 12.5	1.66 ± 0.1	142.39 ± 29.19	50.71 ± 8.36
		Median	47.57	1.66	141	50.25
		(min – max)	(19.7 – 75.2)	(1.4 – 1.93)	(81.4 – 222)	(32.6 – 69.7)
Chest (PA)	183	Mean ± SD	47.98 ± 10.78	1.67 ± 0.09	140.16 ± 30.57	49.86 ± 8.94
		Median	48.46	1.65	136	48.8
		(min – max)	(18 – 70.2)	(1.48 – 1.96)	(81.4 – 301.6)	(34.5 – 98.5)
Pelvis (AP)	27	Mean ± SD	55.22 ± 8.34	1.67 ± 0.08	130.09 ± 25.30	46.02 ± 6.65
		Median	55.70	1.68	125	45.2
		(min – max)	(43.2 – 83.13)	(1.52 – 1.84)	(91.6 – 199)	(35.8 – 59.4)
Lumbar spine (AP & Lt)	34	Mean ± SD	47.43 ± 12.58	1.68 ± 0.11	129.33 ± 27	45.57 ± 7.37
		Median	46.30	1.68	126.2	44
		(min – max)	(19.37 – 83.20)	(1.48 – 1.98)	(78.5 – 186)	(30.7 – 61)
Cervical spine (AP & Lt)	16	Mean ± SD	53.24 ± 10.88	1.64 ± 0.08	124.95 ± 26.39	45.77 ± 7.68
		Median	55.15	1.65	118.8	44.4
		(min – max)	(27.27 – 70.18)	(1.5 – 1.83)	(85.7 – 177.8)	(35.8 – 59.4)

Table 7 summarises the characteristics of patients' anthropometry for each procedure. This included patients who met the criteria of the NDRL for each procedure in terms of number and types of projection. From Table 7 it can be seen that among the obese patients in our sample are young patients, less than 20 years of age. Additionally, of these patients, who underwent projection radiography and managed by radiographers, are patients with body weight up to 300 kg and a BMI of 98.2 kg/m².

3.7.3 Radiation dose (DAP):

Table 8 Patient dose (DAP)

	DAP (Gy.cm ³)						
	Number	Mean	Min.	Max.	1 st quartile	Median	3 rd quartile
Abdomen (AP)	50	21.09	0.13	431.12	3.59	8.89	17.6
Chest (PA)	183	0.33	0.007	6.81	0.08	0.15	0.32
Pelvis (AP)	27	5.1	0.078	21.48	1.12	3.46	5.69
Lumbar spine (AP & Lt)	34	26.57	0.43	181	3.70	10.40	30.31
Cervical spine (AP & Lt)	16	0.80	0.02	6.73	0.08	0.2	0.9

Table 8 summarises the radiation dose (DAP) received by obese patients of both genders for each procedure. In the abdomen AP exam, the recorded DAP reached a maximum of 431 Gy.cm². This was considered at the beginning to be an outlier, since the next figure below was 174 Gy.cm². However, this value was double checked specifically by the medical physicist for typographical error but was found to be correctly entered. The analysis was done without this figure but the descriptive DAP analysis shows similar high median and 3rd quartile values, 8.75 and 17.3 Gy.cm², respectively. It can be seen the 3rd quartile DAP for lumbar spine (AP + LAT) and abdominal (AP) are the highest while the chest (PA) is the lowest.

3.7.4 Patients' dose (DAP) compared to the NDRL:

Table 9 patient dose (DAP) compared to the NDRL

	3 rd quartile (Gy.cm ²)	DAP NDRL (Gy.cm ²)	DAP Increase %
Abdomen AP	17.6	2.5	604
Chest PA	0.32	0.15	133
L. spine (AP + LAT)	30.3	4	657
C. spine (AP + LAT)	0.9	0.3	200
Pelvis AP	5.69	2.2	158.6

Table 9 shows the 3rd quartile of the DAP reported in this study compared to the NDRL values. The DAP value in the NDRL for lumbar spine AP and LAT were combined in order to be comparable with the current study results. The same applied to the cervical spine. As shown in Table 9, the patient dose (DAP) for lumbar spine and abdominal examination are the highest, more than 600% higher, compared to the NDRL values.

3.7.5 Correlations between patients' size and received doses:

Table 10 Spearman correlation between DAP and patients' anthropometrics

DAP (Gy.cm ²)	Age (year)			Height (m)			Weight (kg)			BMI (Gy.cm ²)		
	n	r	P	n	r	P	n	r	P	n	r	P
Abdomen	50	-0.07	0.61	50	0.38	0.006	50	0.52	0.0001	50	0.42	0.002
Chest	183	-0.05	0.42	183	0.15	0.035	183	0.25	0.0005	183	0.20	0.005
Pelvis	27	-0.17	0.37	27	0.06	0.74	27	0.10	0.60	27	-0.15	0.44
Lumbar spine	34	-0.01	0.93	34	0.22	0.2	34	0.14	0.41	34	-0.02	0.90
Cervical spine	18	-0.05	0.84	18	0.05	0.83	18	0.13	0.59	18	0.16	0.51

n= Number of patients included in the analysis

r= correlation coefficient

P= significant level

Since the dose in normal weight patients is dependent on the patient size (Hart et al. 2009), the relationship between the DAP and the patients' anthropometrics was tested. Histograms of the anthropometric measures demonstrated the data were not normally distributed. For this reason, Spearman's correlation was conducted to investigate the relation between the DAP in each procedure and the participants' age, height, weight and BMI. As shown in Table 10, weak to moderate correlations were found between dose in chest and abdomen with patient's size.

3.7.6 Absorbed dose:

Both Table 11 and Table 12 summarise the estimated body organs absorbed dose that has a tissue weighting factor values in the ICRP as mentioned earlier in Table 4 for both groups, normal weight and obese.

Table 11 Estimated absorbed dose (mGy) for normal weight adult group

	Abdomen AP	Chest PA	Lumbar spine AP	Lumbar spine LAT	Cervical spine AP	Cervical spine LAT	Pelvis AP
Active bone marrow	0.108693	0.016209	0.071944	0.212476	0.007607	0.0079235	0.079894
Adrenals	0.109176	0.016684	0.112605	0.158413	0.000078	0.000076	0.002529
Brain	0.00002	0.000204	0.000002	1.65E-05	0.001408	0.013466	0
Breasts	0.018911	0.011107	0.007462	0.004307	0.00117	0.0003255	0.001525
Colon (Large intestine)	0.516864	0.000137	0.568795	0.445779	0.000003	0.000001	0.450814
Extra thoracic airways	0	0.001702	0	0	0.129275	0.0965375	0
Gall bladder	0.621758	0.001284	0.86362	0.333645	0.00002	0.0000125	0.046708
Heart	0.097638	0.017297	0.031475	0.01902	0.001156	0.000428	0.000676
Kidneys	0.110651	0.001775	0.131187	0.64617	0.000022	0.00002	0.015505
Liver	0.524419	0.008401	0.247497	0.551324	0.000149	0.0000805	0.012646
Lungs	0.075691	0.049341	0.016052	0.019784	0.005584	0.0027555	0.000465
Lymph nodes	0.279524	0.007259	0.350861	0.211796	0.040548	0.033522	0.14491
Muscle	0.22197	0.0084	0.181478	0.213189	0.008214	0.0065825	0.223765
Oesophagus	0.093113	0.021656	0.064925	0.034929	0.007698	0.003931	0.001266
Oral mucosa	0	0.000636	0	0	0.043731	0.0719815	0
Ovaries	0.3796	0.000003	0.519549	0.418014	0	0	0.427441
Pancreas	0.31732	0.005834	0.393251	0.291252	0.000084	0.0000585	0.008109
Prostate	0.521442	0	0.657472	0.033067	0	0	0.748688
Salivary glands	0.000046	0.001221	0.000038	0.00002	0.104901	0.1432115	0
Skeleton	0.135787	0.027961	0.076982	0.177099	0.023929	0.034724	0.136799
Small intestine	0.487214	0.000159	0.667478	0.44225	0.000002	0.000002	0.444676
Spleen	0.189677	0.00836	0.141632	0.750045	0.000108	0.000073	0.007019
Stomach	0.747396	0.003772	0.811369	0.327241	0.000059	0.000043	0.023392
Testicles	0.180483	0	0.07389	0.005865	0	0	1.709212
Thymus	0.007655	0.008789	0.002753	0.002679	0.015235	0.0013315	0
Thyroid	0.000173	0.004263	0.000017	0.000014	0.281831	0.172378	0
Urinary bladder	0.804832	0.000003	1.269072	0.084356	0	0	1.036563
Uterus	0.48837	0.000022	0.775065	0.234694	0	0	0.574929

Table 12 Estimated absorbed dose (mGy) for patients with obesity

	Abdomen PA	Chest PA	Lumbar AP	Lumbar LAT	Cervical spine AP	Cervical spine LAT	Pelvis AP
Active bone marrow	0.215588	0.022015	0.085017	0.398479	0.007554	0.007744	0.062619
Adrenals	0.11805	0.040371	0.134804	0.286962	0.000169	0.000224	0.003298
Brain	0.000155	0.000809	0.000044	0.000157	0.002334	0.018313	0
Breasts	0.08901	0.008903	0.024472	0.013796	0.001888	0.0004685	0.003829
Colon (Large intestine)	1.527316	0.000595	0.801672	0.825316	0.000007	0.000007	0.443185
Extra thoracic airways	0.000776	0.004668	0.000219	0.000681	0.119913	0.0755965	0
Gall bladder	1.560365	0.003206	1.714574	0.445695	0.000068	0.000055	0.066478
Heart	0.263725	0.016744	0.098051	0.053221	0.002856	0.00074	0.001287
Kidneys	0.147443	0.0065	0.12215	1.006011	0.000049	0.000059	0.014376
Liver	1.101965	0.014416	0.620903	1.373744	0.000276	0.0002135	0.019104
Lungs	0.174816	0.056435	0.039569	0.083668	0.004819	0.0040075	0.000988
Lymph nodes	0.716022	0.010316	0.567227	0.357315	0.03526	0.0303865	0.151667
Muscle	0.676348	0.010952	0.364005	0.51779	0.007796	0.0065885	0.281335
Oesophagus	0.136343	0.026266	0.131944	0.084659	0.004874	0.00403	0.001934
Oral mucosa	0.000937	0.001696	0.00002	0.000536	0.064456	0.05685	0
Ovaries	0.938332	0.000245	0.720481	0.635418	0	0	0.373365
Pancreas	0.492233	0.012342	0.498785	0.566744	0.000173	0.000149	0.011939
Prostate	1.050915	0.000014	1.523294	0.085477	0	0	0.800879
Salivary glands	0.000965	0.003196	0.000077	0.00073	0.085168	0.149172	0
Skeleton	0.273477	0.034262	0.112848	0.337881	0.023272	0.035131	0.126609
Small intestine	1.454548	0.000736	1.055025	0.685665	0.000008	0.000008	0.42345
Spleen	0.256834	0.020904	0.066189	1.783312	0.000187	0.0001865	0.009561
Stomach	1.718967	0.006389	0.749021	0.647911	0.000138	0.0001105	0.034845
Testicles	1.112807	0.000003	0.593803	0.01827	0	0	2.39224
Thymus	0.033636	0.007086	0.013869	0.011178	0.073776	0.0016355	0.000006
Thyroid	0.002174	0.010324	0.000536	0.002635	0.233857	0.1518775	0
Urinary bladder	2.215332	0.000057	2.811318	0.161473	0	0	1.22662
Uterus	1.399839	0.000199	1.390383	0.275324	0	0.0000005	0.55856

Table 11 demonstrates the organ absorbed radiation dose (mGy) for the normal weight group based on exposure parameters illustrated earlier in table 5. In table 12 the absorbed radiation dose (mGy) values are for the obese patients based on exposure parameters illustrated in table 5. These values are based on the average value generated by PCXMC simulation software with errors less than 10% due to the one million photons used to run the simulations.

3.7.7 Effective dose:

Table 13 Effective dose for all procedures in both groups of patients

E: Effective dose

NDRL: National Diagnostic Reference Level

	Non obese (NDRL)		Obese group		Δ	Δ %
	<i>E</i> (mSv)	Error %	<i>E</i> (mSv)	Error %		
Abdomen (AP)	0.285	0.2	0.741	0.3	0.456	160
Pelvis (AP)	0.212	0.2	0.245	0.2	0.033	15.56
Chest (PA)	0.012	0.1	0.015	0.1	0.003	25
Lumbar spine (AP)	0.299	0.1	0.459	0.1	0.16	53.51
Lumbar spine (LAT)	0.198	0.2	0.389	0.2	0.191	96.46
Cervical spine (AP)	0.016	0.3	0.015	0.3	-0.001	-6.25
Cervical spine (LAT)	0.012	0.3	0.011	0.3	-0.001	-8.33
Lumbar spine (AP + LAT)	0.497	0.3	0.848	0.3	0.351	70.62
Cervical spine (AP +LAT)	0.028	0.6	0.026	0.6	-0.002	-7.14

mSv: millisievert

AP: Anteroposterior

PA: Posteroanterior

LAT: Lateral

Δ : difference

Table 13 shows the effective dose received by each group in all reported procedures. The highest difference between the two groups is in abdominal AP and lumbar spine AP and LAT. In the cervical spine the difference between the two groups is of a negative value.

Table 14 Radiation-related lifetime cancer risk incidence for both obese and non-obese groups of patients (per 10⁶)

Age		Abdomen AP		Chest PA		Pelvis (AP)		Lumbar spine (AP)		Lumbar spine (LAT)		Lumbar spine (AP+LAT)		Cervical spine (AP)		Cervical spine (LAT)		Cervical spine (AP+LAT)	
		Male	Female	Male	Female	Male	Female	Male	Female	Male	Female	Male	Female	Male	Female	Male	Female	Male	Female
20-29	DRL	21.8	20.5	0.7	1.3	14.2	11.1	24.8	23.1	14.7	12.5	39.4	35.6	0.7	1.3	0.7	0.9	1.4	2.2
	Obese	55.1	51.9	0.9	1.5	15.4	12.0	41.9	36.2	29.1	24.5	71.0	60.7	0.7	1.2	0.6	0.9	1.4	2.0
	Δ %	152.6	153.1	33.7	16.6	9.1	8.3	69.0	56.8	98.5	95.5	80.0	70.4	4.4	-5.9	-5.7	-6.4	-0.5	-6.1
30-39	DRL	17.4	16.4	0.6	1.2	11.6	9.1	19.7	18.3	11.6	9.7	31.3	28.0	0.5	0.8	0.5	0.6	1.0	1.4
	Obese	44.1	41.4	0.8	1.4	12.6	9.8	33.6	29.2	23.0	19.2	56.6	48.3	0.5	0.7	0.5	0.6	1.0	1.3
	Δ %	153.1	152.4	29.9	16.7	9.0	8.7	70.4	59.2	99.1	97.5	81.0	72.5	4.2	-4.2	-4.7	-4.0	-0.1	-4.1
40-49	DRL	13.5	13.2	0.6	1.2	9.2	7.6	15.2	14.4	8.9	8.1	24.2	22.5	0.4	0.5	0.3	0.4	0.7	0.9
	Obese	34.2	33.1	0.8	1.4	10.1	8.2	26.3	23.4	17.8	16.1	44.0	39.5	0.4	0.5	0.3	0.4	0.7	0.9
	Δ %	153.2	149.9	26.9	17.8	8.9	8.1	72.3	62.4	99.4	99.6	82.3	75.7	4.4	-3.2	-3.0	-0.8	0.8	-2.2
50-59	DRL	9.8	9.9	0.6	1.1	6.8	5.7	10.9	10.6	6.3	5.6	17.3	16.2	0.3	0.3	0.2	0.2	0.5	0.6
	Obese	24.7	24.7	0.7	1.3	7.4	6.2	19.0	17.7	12.7	11.5	31.8	29.2	0.3	0.3	0.2	0.3	0.5	0.6
	Δ %	153.2	149.1	24.5	17.3	8.9	9.3	74.6	66.9	100.4	104.4	84.1	79.9	1.6	-3.2	-1.7	3.6	0.0	-0.2
60-69	DRL	6.2	6.7	0.4	0.8	4.3	3.9	6.8	7.1	3.9	3.5	10.7	10.6	0.2	0.2	0.1	0.2	0.3	0.4
	Obese	15.5	16.7	0.5	1.0	4.7	4.3	11.9	12.3	8.0	7.3	19.9	19.6	0.2	0.2	0.1	0.2	0.3	0.4
	Δ %	151.5	148.0	22.6	17.0	8.9	10.5	76.4	72.2	102.0	109.0	85.8	84.3	0.5	-6.2	1.1	6.8	0.8	-0.7
70-79	DRL	3.2	3.7	0.3	0.5	2.2	2.1	3.4	3.9	2.1	1.8	5.5	5.7	0.1	0.1	0.1	0.1	0.2	0.2
	Obese	8.0	9.2	0.3	0.6	2.4	2.4	6.1	6.9	4.2	3.9	10.3	10.8	0.1	0.1	0.1	0.1	0.2	0.2
	Δ %	148.1	144.1	21.7	17.2	8.3	11.7	76.9	77.2	102.9	114.7	56.6	89.2	-4	-9.0	3.1	10.4	-0.8	-1.0
80-89	DRL	1.1	1.3	0.1	0.2	0.7	0.7	1.1	1.4	0.8	0.6	1.9	2.0	0.0	0.0	0.0	0.0	0.1	0.1
	Obese	2.7	3.1	0.2	0.2	0.8	0.8	2.0	2.4	1.6	1.3	3.6	3.8	0.0	0.0	0.0	0.0	0.1	0.1
	Δ %	138.9	138.3	21.8	17.5	7.0	11.5	77.5	80.3	104.0	114.0	88.2	90.8	-8.6	-13.8	4.0	10.1	-3.0	-4.2

DRL= Diagnostic Reference Level.

AP: Anteroposterior.

PA: Posteroanterior.

LAT: Lateral.

Δ %: difference percentage

As Table 14 shows, radiation-related lifetime cancer risks are highest in lumbar spine, abdomen and pelvis radiographs for both normal-weight and obese patients. However, the differences between the two groups reach up to 153 % higher in patients with obesity when undergoing abdominal radiograph. In lumbar spine, the gap in radiation-related lifetime cancer risk is high, 70 %. However, a small negative trend of cancer risk is observed as a result of cervical spine in patients with obesity compared to normal-weight patients.

3.8 Discussion:

This study is the first study to report the radiation dose (DAP) delivered to obese patients and estimated the cancer risk induced as a result in the UK. For the five procedures reported in this study, obese patients are receiving higher doses than normal weight adults, as shown in Table 9. This result is in line with other studies conducted in other modalities (Wang et al., 2013, Hsi et al., 2013, Cushman et al., 2016, Smuck et al., 2013). In projection radiography, the current results broadly align with what has been reported in the literature (Terlizzi et al., 2011, Kim et al., 2012, Tung et al., 2008). With regard to the percentage of radiation dose (DAP) increase between NDRL and patients with obesity (Table 9) the current study agrees with what has been reported by Metaxas et al, where the radiation dose in lumbar spine and abdomen reach up to 375 % more than normal weight patient dose (Metaxas et al., 2018). The difference percentage reported in the current study is almost double the figure reported by Metaxas and colleagues, which is attributed to the difference in BMI reported in both studies. In the current study the average BMI was 48 kg/m², while in Metaxas et al, the average BMI is was 32 kg/m². Additionally, the DRLs in both studies are different.

In the current study, the patient dose (DAP) was significantly high compared to the NDRL values, Table 9. The highest difference between patients with obesity dose (DAP) and the NDRL was in lumbar spine (AP & LAT) and abdominal (AP) radiographs. These two examinations are expected to be the most challenging in imaging and it could reasonably be speculated that higher exposures would be needed. These high doses are of concern as these two examinations comprise 3.81% and 2.53% of the x-ray examinations conducted in the UK out of 231 examinations (Hart et al., 2010). Additionally, these two examinations involve irradiation to the reproductive organs and this will increase the occurrence of heritable effects. Moreover, the more sensitive organs such as colon and stomach are in the direct beam of radiation in these two procedures, while the remaining sensitive tissue such as lungs and breast are in the near field of scattered radiation.

It could be argued that these two examinations are less requested these days due to the availability of advance modalities such as CT. However, it should be pointed out that the challenge of fitting patients with obesity into the CT scan bore is increasing, due to gantry width and table weight limits (Carucci, 2013). In a very recent study in the UK considering the challenges in imaging patients with obesity and preparedness of UK radiography departments to meet these challenges, 14 out of 86 trusts in the country were already considering utilising their local veterinarian's scanner for patients with obesity (Wiles et al., 2017). Therefore, lumbar spine and abdominal radiographs for patients with obesity are still requested and in some cases as the only available option.

In the abdominal AP radiograph, this issue could be exacerbated as the predominant practice in this group of patients is to undertake two images or even more due to the constraint of the size of image receptors (Carucci, 2013). With the absence of guidelines in managing this group of patients, (Le et al., 2015a), the overlapping between the two images could be larger than what is required in order to avoid missing a part of the examined area. This could explain the result of high patient dose (DAP) in this study compared to the NDRL.

In the remaining procedures; chest and cervical spine, the patient dose is higher than the NDRL but in an expected range. For the pelvis AP, the reason for the comparable patient dose to the NDRL could be due to the low number of patients in the current study, 27 patients respectively.

In terms of the estimated effective dose for both groups of patients based on the reported dose (DAP) in the current study and in the NDRL (Hart et al., 2012), the results of this study agreed broadly with the reported results in the literature (Yanch et al., 2009, Tung et al., 2008). For the purpose of comparison with the NDRL group, the current study's results agree with a similar study reported for the same group of patients in the UK (Wall et al., 2011). Minor differences can be attributed to the fact that in Wall and colleagues study, the effective dose was based on two simulations based on the ESD and the DAP. Additionally; the field size, anode angle and FSD might be different to the values set in the current study, as they were not reported in their paper.

In Yanch and colleagues' study, the reported effective dose varied based on the fat orientation (Yanch et al., 2009). The body type, in Yanch et al's study, where the result could be comparable to the current result is the body type 5, where the subcutaneous fat is distributed equally on each side of the patients. Even though, the effective dose reported by Yanch and colleagues is much higher than the effective dose in the current study. The reasons could be attributed to the fact that different Monte Carlo simulations software was used; PCXMC in the current study and MCNPX in Yanch's et al's study. Additionally, the modification of the stylized phantom in their study to represent obese patients was different as layers of subcutaneous fat were added, while in the current study, PCXMC increases the mass of organs rather than adding fat layers.

Despite the differences between the two studies, the effective dose is higher in patients with obesity which indicates higher risk of induced cancer as a result (Table 13). The absorbed doses estimated again are higher in patients with obesity. As Table 11 and Table 9 show, the most sensitive organs, i.e. organs that have high tissue weighting factor such as; colon and stomach, are receiving the highest dose in abdomen AP and lumbar spine AP & LAT.

However, these results contradict the result reported by (Tung et al., 2008, Kim et al., 2012). In Tung and colleagues study, the reason could be attributed to the use of different Monte Carlo software, WinODS, which is no longer available; this work could be repeated using different software to explore any differences. Although, the absorbed dose to the stomach was reported to relate inversely with the BMI in Tung's study, the effective dose reported in their study shows a proportionate relation with the BMI. In Kim and colleagues study, the same value of patient dose was used, i.e. the ESD (Kim et al., 2012). This could be attributed to the fact that the estimation of effective dose based on ESD agreed less with the value measured directly with TLD in a phantom study (Theocharopoulos et al., 2002).

This in turn creates a debate around whether the fat works as cushion to protect the organs inside the abdomen and chest. This could be true as Yanch and colleagues suggested in their study (Yanch et al., 2009). Their phantom consists of a layer of subcutaneous fat and they noticed decrease in the

absorbed dose to the organs that are located deep in the abdomen. This is anticipated as most of the photons will be attenuated before penetrating into the deeper tissues. In the current study, no fat was added as it was not possible; hence, it was not possible to test this hypothesis using PCXMC.

However, fat distribution is different between individuals i.e. some people have more visceral fat while other have more subcutaneous. The visceral fat was not taken into account in either of the Yanch and Kim studies (Yanch et al., 2009, Kim et al., 2012) where the organ dose was reported to be lower than in lean phantoms. It is very difficult to incorporate visceral fat in any stylised, mathematical or physical phantom. The reason is that no study described the deformation or movement of internal organs in response to visceral fat (Ding et al., 2012). Also in physical phantoms, there is no phantom that represents obese patients. So, this could explain the discrepancies between the results of current study and previous studies. Until standard phantoms that represent obese patients of various BMI are constructed, it is difficult to prove whether deeper organs absorbed less energy when both visceral and subcutaneous fat are considered.

From Table 11 and Table 9, it can be noted that the absorbed dose in cervical spine AP and LAT radiographs is less in certain organs in the patient with obesity group compared to the NDRL patient. This could be attributed to the fact that the difference in patient dose (DAP) used in the simulation for the two groups was very low, $0.04 \text{ Gy}\cdot\text{cm}^2$, (Table 5). In a previous study conducted by Kim and colleagues, absorbed dose in high BMI compared to low BMI groups is similar if the patient dose (DAP) was similar (Kim et al., 2012). This is due to the excess fat layers in patients with obesity that absorbed radiation dose and protects internal organs.

The weak to fairly moderate correlations between the DAP and patient's size in abdomen and chest procedures indicate that high DAPs are delivered to lower BMI patients within the cohort and vice versa. This could be attributed to the absence of clear guidelines in the literature to help achieve an optimal image with the lowest practicable dose (Le et al., 2015a). Such variation has already been reported in selection of exposure factors, which impact directly on DAP,

for patients with obesity (Darcy et al., 2015). However, the local DRL, in the hospital where the study was carried out, for the reported investigations in this study is lower by 32% on average than NDRL. This indicates that there are good protocols already in place to ensure adherence with the ALARA principle. As a result, the reported DAPs for patients with obesity could be at the lower band of radiation dose (DAP) to this group of patients as the local DRLs evidence the good practice in place. Additionally, as a bariatric centre, the radiographers are highly trained to x-ray patients with obesity.

In terms of lifetime cancer risk to the patients with obesity group in comparison with the NDRL group, the highest difference was in lumbar spine and abdominal radiographs. The increase in the radiation-related lifetime cancer risk incidence is an indication of new challenges in the health management of patients with obesity. Due to the semi-identical median DAP for both groups in cervical spine AP & LAT projections, the absorbed dose in the obese group was less than NDRL group. This eventually impacts on the cancer risk estimation which shows a decrease in radiation-related lifetime cancer risk in the obese group compared to the DRL group. This could be explained by the fact that the absorbed dose in patients with obesity is less than the normal-weight adult when receiving identical DAPs, due to the extra fat which acts as a protection layer for the internal organs.

The reported radiation-related lifetime cancer risk in this study is a projected risk and did not take into account any other factors or background cancer rates. Additionally, it did not consider the issue that obese patients may receive more diagnostic radiography procedures but rather considered the single exposure reported in this study. This is due to the uncertainty in the model used to calculate the risk. Although, obesity is already reported to increase the risk of different types of rare cancers (Renehan et al., 2008), the projected radiation-related lifetime cancer risk reported in this study is applied only on this cohort group based on the reported DAP of the specific radiographic investigations. Hence, the radiation-related lifetime cancer risk to the obese population as a whole has not been considered as the data were collected from one centre. Likewise, the same applies to the normal-weight group, as the projected radiation-related lifetime cancer risk is for the patients who received identical

DAP dose reported in the NDRL, which doesn't necessarily apply to all patients with normal weight due to the variation of local DRLs across the country. More data of radiation-related lifetime cancer risk is provided in Appendix 5.

Radiographers are facing tremendous challenges when imaging obese patients as the data show the weight of obese patients can reach up to 300 kg. The weak to fairly moderate correlations between the dose and patient's size in abdomen and chest procedures indicate that high doses are delivered to lower BMI patients within the cohort and vice versa. This could be attributed to the absence of clear guidelines in the literature to help with achieving an optimal image with the lowest practicable dose (Le et al., 2015a). The increase in life time cancer risk incidence is an indication of new challenge in the health management of obese patients as more cancers can be seen as a result of radiation exposure.

The current study should be interpreted in the context of its limitations. One of the study limitations is the fact that it was conducted retrospectively. This imposes extra restrictions in inclusion criteria. For example, DAP readings are usually entered by radiographers for multiple views or even multiple examinations, if conducted at the same time. As a result, inclusion of such patients was not possible as the DAP was not representative of the view and examination of interest. This means the dose could be higher than the reported dose in the study. The opposite is also possible, as the DAP readings are at risk of typographical errors when entered by the radiographers at the time of the examination.

Another limitation of the study is the use of PCXMC 2.0 to estimate mean organ absorbed dose. This is due to the fact that the stylised phantom used is not a true representation of the human organs. Furthermore, it does not take into account the amount of fat that increases along with the BMI, which contributes to high rate of scattered radiation, but instead increases the mass of the organ in proportion to the whole phantom mass. Due to the semi-identical median DAP for both groups in cervical spine, AP & LAT view, absorbed dose in the obese group was less than DRL group. This eventually impacts on the cancer risk estimation which shows a decrease in lifetime cancer risk in the obese

group compared to the DRL group. This problem is explained by the fact that when high BMI patients exposed to same radiation as normal weight using PCXMC, they absorbed less radiation in their organs than normal weight group (Kim et al., 2012). Also the difference between the DAPs, obese and DRL, readings is 45 mGy, while the difference in body mass is 47kg for the whole body. However, to date there is no accessible voxel phantom with high BMI similar to the mean BMI of the participants in the current study in order to use other Monte Carlo as an alternative.

The study shows a new potential challenge in obese patients' management in the radiology department with serious implications for the health service. Dose variations demonstrate the need for clear and accessible guidelines for the management of radiation dose to obese patients in radiology departments. Additionally, the study highlights the estimated increase in cancers likely to be seen among obese patients who undergo such investigations. Despite the high doses reported in this study, radiographers in the main centre of the study are highly trained to deal with obese patients and this could mean the reported dose is at the lower range compared to other hospitals where less training is provided for the radiographers. Therefore, further research into dose optimisation is required and more guidelines are needed to guide the radiographers in imaging these patients. These guidelines should contain a thickness-based exposure factor predictor that can be used by radiographers when selecting the exposure factors to reduce radiation dose variation received by patients with obesity.

The study's scale is small compared to the number of obese patients in the UK, this means similar studies are needed to investigate if the case in this study is similar in other parts of the country. Our study also considers obese patients, but the BMI range was 40 kg/m² and over, so the obese patients ranged from 30 to 40 kg/m² need to be evaluated to determine whether the same dose figures are true. Further studies could also determine the factors that impact on dose such as radiographer's experience and type of x-ray machine.

3.9 Conclusion:

The findings of the current study may have implications for clinician, radiographer, policy makers and health economists. Clinicians considering the

correct investigation before writing the x-ray request especially for obese patients should be aware of the increased risks compared to normal weight patients, in particular whether projection radiography will affect the diagnosis or whether alternative radiology investigations should be considered. Radiographers should take extra effort to evaluate the dose to obese patients periodically. Policy makers considering improving the quality of health services could take this result into account and negotiate it with health technology manufacturers to find ways to tackle the high dose delivered to obese patients. Additionally, this means research is needed in dose optimisation for obese patients in order to establish exposure guidelines in such patient groups. For health economists, this could be taken into account when estimating the economic burden as a result of obesity.

4 Chapter 4: Body composition quantification

4.1 Introduction:

Based on the conclusion of the previous chapter, abdomen and lumbar spine radiographs are the most challenging body parts in projection radiography. The body composition in this region has to be quantified in order to build obese phantoms that reflect that of obese patients.

This chapter will introduce the reader to the topic of “body composition” and aims to illustrate the changes in body composition within obese populations. The reader will first be introduced to the definition and rationale for the use of body composition in the formation of the radiographic image and the justification of including such a study in this project. The reader then will be briefly introduced to the models and methods used to measure body composition. More details will be contained in the body composition measurement methods used in this study. The method will follow along with a statistical analysis. The results will be presented in forms of tables and figures, and then a discussion will follow. The conclusion will then be drawn with a brief link of this study to the subsequent chapter.

4.1.1 Aims:

The aim of this study was to demonstrate the changes in body composition of obese populations, on total and regional basis of the body, compared to normal weight populations in order to underpin the construction of obese phantoms.

4.1.2 Objectives:

- 1- To measure body composition, FM and LBM, across a cohort of participants with a wide range of BMI. The purpose was to observe how the FM and LBM across different body regions changes along with BMI and fat percentage group. This was achieved by categorising the participants into subcategories based on BMI and fat % to fully visualise the trend of FM and LBM across different body parts.
- 2- To investigate the relationship between FM and LBM compared to the participants' anthropometrics.

3- To produce prediction equations models for FM and LBM on regional basis. The total body was also included to aid in standardizing FM and LBM quantity in areas of research where researchers modify normal weight computerised phantoms into obese phantoms. The abdominal and trunk regions were selected as they pose challenges in medical imaging as the first study illustrated. The prediction models aimed to facilitate the planning of transforming any normal-weight phantom into obese representative phantoms. This was accomplished through linear and multiple regression analysis.

4.2 Body composition:

Body composition is defined as the amount of lean and fat tissue in the human body (Prado and Heymsfield, 2014). The study of body composition is a well discussed topic which has been in existence since 440 BC when Hippocrates proposed that our bodies consist of blood, yellow bile, black bile and phlegm (Wang et al., 1992). As a result of developments in various science subjects, such as anatomy, histology, chemistry etc., body composition understanding has impacted positively since that time (Wang et al., 1992).

As obesity is becoming a global epidemic, the interest in the study of body composition is increasing in order to better understand and monitor obesity and its comorbidities (Mattsson and Thomas, 2006).

4.3 The importance of body composition:

The ICRP recognised the importance of body composition in measuring radiation dose. In its publication titled; "*Reference Man: Anatomical, Physiological and Metabolic Characteristics*", in 1975, emphasis is put on the importance of characterising body composition when the ionising radiation dosimetry is of focus (ICRP., 1975). If the measured ionising radiation dose was from an internal source, a nuclear medicine procedure for instance, more biological properties of the exposed individual are needed to estimate the radiation dose accurately. This includes daily air and water intake, breathing rate, excretion data and other sophisticated anatomical and physiological information (ICRP., 1975). However, this is not the case in this project as the ionising radiation source is external. The ICRP committee suggested that individual body composition, mass and dimensions are sufficient to achieve a good estimation of the radiation dose. Hence, the committee produced the report number 23 (ICRP., 1975), which contains extensive details for physicist to compare their results with the lowest rate of uncertainty (ICRP., 1975). The "*reference man*" as called by the ICRP, was then defined as Caucasian with the customs and habitat of a Western European or North American individual. However, in this project, the individuals of interest are obese, which means the "*reference man*" reference data cannot be used.

In projection radiography, the human body consists of a 3-compartments model of tissues (fat, lean and bone) each of which attenuates ionising radiation differently. This forms the basis for the process of formulating a radiograph in digital and all radiographic imaging. It provides a representation of the spatial distribution of the examined area's tissue components in a form of different signal on the image (Martin, 2007a). Additionally, the International Commission on Radiation Units and measurements (ICRU) state very clearly that muscle, fat and bone should be accounted for when building a phantom used in radiation dosimetry studies (White et al., 1989).

In terms of x-ray attenuation, fat and lean tissue attenuate x-ray photons differently especially in the low kVp range and these soft tissues attenuation merge as the kVp increases resulting in a reduction in the difference of contrast between fat and lean (Bushberg and Boone, 2011). This is due to the different density between these two tissues, with fat ranging between 0.91 – 0.95 g/cm³, while lean tissue ranges between 1.04-1.05 g/cm³ (ICRU, 1989, Berger, 2005). The same weight of fat or lean will also affect the thickness of the body part, as x kg of lean tissue will have a smaller volume than the same mass of fat tissue.

Therefore, it is crucial to take the individual characteristics; mass, dimensions and composition, when constructing an obese phantom. Different representative physical obese phantoms (Wang et al., 2013, Meinel et al., 2014, Schindera et al., 2007, Shin et al., 2016) and computerized phantoms (Ding et al., 2012, Cassola et al., 2011, Broggio et al., 2011) have been constructed in an attempt to conduct research on dosimetry in patients with obesity. However, these studies have paid attention to the thickness, mass and focused on fat mass only.

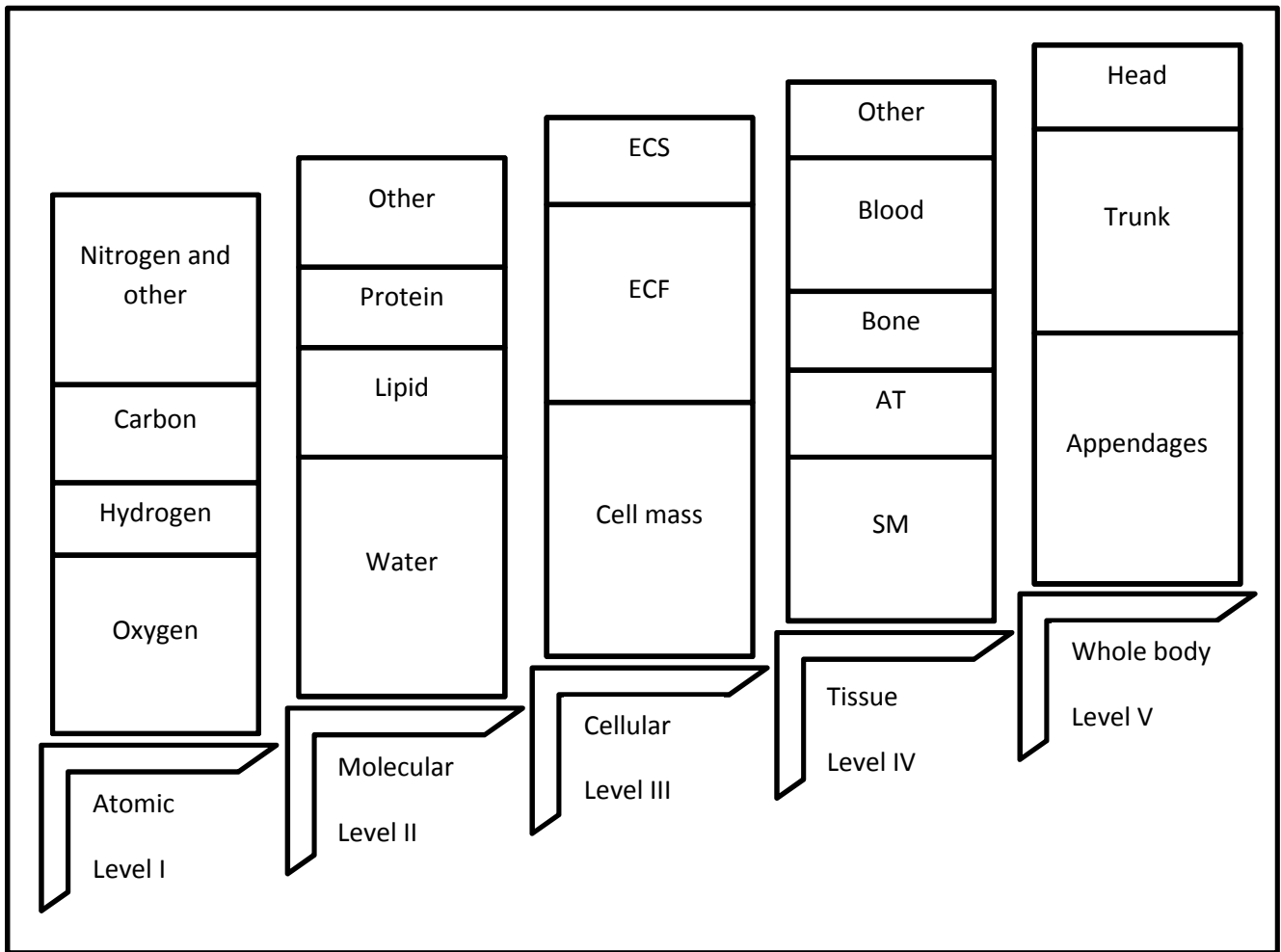
However, it has been known for long time that the fat mass (FM) and fat free mass (FFM) tend to change together (Keys and Brožek, 1953, Gray and Bauer, 1991, Forbes, 1987). Increases in FM typically lead to increases in other body components that are engaged in the nourishment, support and mobility of the increasing body mass (Keys et al., 1955, Pitts, 1962, Mingrone et al., 2001). This change includes increases in the mass of the kidneys, pancreas, heart, liver (Naeye and Roode, 1970) blood and extracellular fluid (Keyes et al., 1955,

Pitts, 1962, Messerli, 1982), but more largely to the skeletal muscle (Janssen and Ross, 1999, Rice et al., 1999). This could be attributed to the need for extra muscle to support the extra FM in obesity. For these reasons, understanding the change in body composition of patients with obesity is a crucial step before building a representative phantom.

4.4 Body composition models:

In order to fully appreciate the body composition science and to understand the underlying philosophy of the body composition assessment methods, one should first understand the body composition models (Heyward and Wagner, 2004). The Constructed body composition model is related to the utilized number of components. The first and most basic of all models is the body weight, representing the sum of the mass of each of the body components. According to Wang and colleagues, body composition can be divided into five levels; atomic, molecular, cellular, tissue and whole body, Figure 7, (Wang et al., 1992).

Figure 7 Body composition level adapted from Wang et al. (1992)



ECS: Extracellular solids
 ECF: extracellular fluids
 AT: adipose tissue
 SM: skeletal muscle

4.5 Body composition measurement methods:

In the literature, three different ways of measuring body composition have been reported; direct, indirect and criterion methods (Duren et al., 2008).

4.5.1 Indirect methods:

4.5.1.1 Body Mass Index (BMI):

The BMI is the most widely used measure of obesity, and has been used extensively in the literature (Romero-Corral et al., 2008). In obesity, where BMI is ≥ 30 kg/m², the WHO has classified the obesity into three subcategories; Class I 30-34.9 (kg/m²), Class II 35-39.9 (kg/m²) and Class III ≥ 40 (kg/m²) (WHO, 2000). As a body-composition marker, the accuracy of BMI is still a questionable tool due to the fact that obesity is defined as an excessive accumulation of fat mass that imposes health risks (Vanderwall et al., 2017, Wong et al., 2016). Hence $\geq 25\%$ of fat in men and $\geq 30\%$ of women is considered as obesity (Frankenfield et al., 2001). However, in obesity, fat percentage and BMI do not correlate strongly, and BMI missed identifying more than 50 % of obese individuals based on the fat percentage (Romero-Corral et al., 2008, Okorodudu et al., 2010). Along with the limitation of BMI to identify the distribution of fat (Akpinar et al., 2007), the BMI can still be used as a tool for screening and tracking obesity, but not to assess body composition (Beechy et al., 2012).

4.5.1.2 Anthropometrics:

Different anthropometric measures have been used in the literature in attempts to simplify body composition including: size; fatness and shape assessment. Different measurements and body sites have been used to estimate the body composition. This includes height, weight, waist and hip circumferences, abdomen sagittal and transverse diameters and waist-hip-ratio (Heymsfield et al., 2005). Despite the simplicity and ease of these techniques, they pose challenges when it comes to patients with obesity. This is attributed to their dependence on the skill of the staff taking the measurements, the difficulty in identifying the correct waistline and the interference between hip measurement and the abdominal dropped fat (Das, 2005, Andreoli et al., 2016).

4.5.1.3 Bioelectrical Impedance analysis (BIA):

This technique measures the resistance to electrical current passing through the body by connecting electrodes to the arms, the legs or one arm and one leg. The theory is based on the fact that most of the human body is water, which contains ions that can conduct electrical current at different rates (Dehghan and Merchant, 2008). There are two sites where the water is localised in the cell, either intracellular or extracellular, with the water being considered as a good conductor of electricity. Other tissues can act as a resistor, fat cells, due to their low concentration of water (Dehghan and Merchant, 2008). Based on these two facts, and depending on the type of BIA technique used, i.e single frequency BIA, multi-frequency BIA or bioelectrical spectroscopy, different equations can be used to predict the total body water (TBW), conductor, and FM as a resistor. FFM can then be calculated by subtracting the FM from TBW (Kyle et al., 2004). Despite the fact that this technique is non-invasive, inexpensive, less laborious and safe for frequent measurements (Shafer et al., 2009, Strain et al., 2008), the assumption behind this technique, that the hydration status of FFM is constant at 73.2%, is not accurate in case of obese individuals where hydration is greater at 77.5% (Das, 2005, Alvarez et al., 2007). This makes the accuracy of this technique (BIA) debatable. Fat % has been overestimated in overweight and obese groups, while the FM has been underestimated significantly in normal weight women (Shafer et al., 2009, Neovius et al., 2006). Other sources of errors are arm positioning, fat asymmetry, temperature and bladder status (Andreoli et al., 2016).

4.5.1.4 Skin fold thickness (SFT)

As the name indicates, this technique for the indirect measurement of body composition relies on measuring the subcutaneous fat thickness in specific body parts including the bicep, triceps, subscapular and supra-iliac muscles (Pietrobelli and Heymsfield, 2002, Heymsfield, 2009).

However, this technique has limitations such as; observer variability, fat and skin elasticity, which varies with age and race for instance, and further, pose some discomfort for participants (Kuczmarski et al., 1987). These limitations encountered in patients with obesity in addition to the fact that fat thickness in

this group of patients makes it hard to raise the required amount of fat to yield an accurate measurement (Gray et al., 1990). Additionally, the size of the calliper used in this group of patients cause extra errors as well as the variation in compressibility of the fat from one area to another (Kuczmarski et al., 1987, Chumlea, 2006).

4.5.2 Direct methods:

4.5.2.1 Total body water (TBW):

This technique is based on the assumption that hydration status in FFM is 73%. As so, deuterium labelled water ($^2\text{H}_2\text{O}$), for example, is used to measure the TBW (De Lorenzo et al., 1999). Based on the dilution space of the isotope, the TBW can be converted into kilograms using the water density (0.99336 kg/m^3) as the conversion factor (De Lorenzo et al., 1999). However, since the hydration rate is larger, at 77.3%, in patients with obesity, than the assumption hydration rate of 73%, which underpinned the principle of this technique, this results in overestimation of FM and underestimation of FFM in obesity (Das, 2005).

4.5.2.2 Total body potassium (TBP):

Cells are the most metabolically active portion of the body, with potassium considered as the most abundant intracellular ion. Based on these two facts, the cell mass can be quantified using the naturally radioactive potassium (^{40}K) through a whole body counter (De Lorenzo et al., 2003). FFM then can be calculated using equations based on gender (De Lorenzo et al., 2003). Despite the promising accuracy of this technique in monitoring of patients with obesity (De Lorenzo et al., 2003), the hydration status might affect the potassium content within the cells in this group of patients (Das, 2005). Additionally, there are only a limited number of detectors used in this technique that are available worldwide, which limits the availability of this as a feasible method (Duren et al., 2008).

4.5.3 Criterion methods:

4.5.3.1 Body density:

Hydrostatic weighing, also known as hydro-densitometry, is one method that uses this technique of body composition measurement. The participant is required to submerge completely in a water tank in order to estimate the body composition by combining body weight, body volume and the residual lung volume (Beechy et al., 2012). A new technique is able to exclude the head (De Lorenzo et al., 2003), making it more acceptable to patients.

However, this technique is not popular in clinical practice for several reasons; it is considered impracticable, time consuming, laborious, highly dependent on participants' performance and their adherence to the preparation instructions before and during the procedure, and finally the discomfort it causes to participants (Heath et al., 1998, Das, 2005, Chumlea, 2006, Petroni et al., 2003, Horie et al., 2008).

Another technique similar to hydro-densitometry is the air displacement plethysmography (ADP). This technique utilizes a unit of two chambers: a testing chamber for participants to sit in and a reference chamber to hold the breathing circuit, electronics and pressure transducers (Shafer et al., 2009, Beechy et al., 2012). Despite its non-invasive nature, the time it requires and its validity in patients with obesity is prohibitive (Ginde et al., 2005, Le Carvenec et al., 2007). Furthermore the participant must wear tight fitting swimming clothes with a cap and this in turn may constrain its application in patients with obesity (Beechy et al., 2012).

4.5.3.2 Dual-energy X-ray absorptiometry (DXA):

Since the introduction of DXA into clinical use in the 1980s, its main function and use was to measure bone mineral density and aid in the detection and assessment of osteoporosis (Toombs et al., 2012). However, a second and non-negligible application of DXA is the study of body composition which started in the late 1980s (Kehayias et al., 1993).

Until now, five vendors are producing DXA scanners worldwide; Hologic, Lunar, Norland, Stratos and Korean scanner (Chin, 2017). In both applications and across all different vendors, the principle of DXA is the photon attenuation as a function of tissue composition (Plank, 2005). DXA uses x-ray photon energy at two different ranges, low (40 - 60 kV) and high (70-100 kV). When the x-ray source generates the x-ray beams, high and low energy beams, the photons will attenuate, absorbed by the tissues, differently as passing through the body part, based on the density and thickness (Toombs et al., 2012). The absorption can then be expressed as a ratio (R) of the attenuation at the lower energy relative to the higher energy (Heyward and Wagner, 2004).

The DXA technique sometimes refers to the three compartment model (Heyward and Wagner, 2004), and sometimes the two compartment (Toombs et al., 2012). However, rather than producing three independent measures, it comprises two sets of 2-compartment model equations (Ginde et al., 2005). The first set is bone mineral and soft tissue, including fat and fat free mass. In order to calculate these two compartments, the x-ray beam is passed through the body part, the beam attenuation decreases with its energy and the density of the compartment, bone attenuates more while soft tissues attenuate less photons (Pietrobelli et al., 1996). The R can then be calculated to differentiate bone from soft tissue. The second 2-compartment is the fat and fat free mass. To differentiate between these two components, the DXA measures R in areas that does not contain bone, the attenuation of the two photons energy is related to the percentage of fat in soft tissue (Laskey, 1996).

4.5.3.3 Magnetic resonance imaging (MRI):

The MRI is one of the methods used in body composition quantification with the benefit of being a non-invasive and safe procedure. It is based on the fact that atomic nuclei, which consists of protons and neutrons, can behave like a magnet (Lukaski, 1987) but in a very weak way, such as the strength of the earth's magnetic field (Ellis, 2000). However, placing a human body in a strong magnetic field, greater than earth's magnetic field, will result in the magnetisation vector of nucleons such as the proton to align with or against that magnetic field (Despres, 1996). The Hydrogen protein (^1H) specifically is more likely to align with the magnetic field (Ellis, 2000). Other atoms, such as Carbon (^{13}C), Fluorine (^{19}F), Sodium (^{23}Na) and Potassium (^{39}K), behave in the same manner as the Hydrogen protein does under strong magnetic fields, but at a significantly lower response rate (Ellis, 2000). Despite the fact that only a small percentage of Hydrogen nuclei will align, the abundance of hydrogen protons in the human body is enough to detect any changes in the proton magnetisation vector orientations when a radio-frequency pulse is applied or the magnetic field altered.

Based on this theory, MRI utilizes a combination of a strong magnetic field of 1.5 to 3 Tesla (~30,000 – 60,000 times the earth's magnetic field), and pulses of radio waves to produce the required image of the examined body part (Lukaski, 1987). The MRI system typically consists of a primary magnetic field, gradient coils and radiofrequency coils (RF), all inside a specially designed room with walls lined with a copper Faraday cage to eliminate electrical noise and interference.

Inside the human cells, when a strong external magnetic field is introduced, the protons will start aligning parallel or antiparallel to the external magnetic field. The RF coil functions as a transmitter of the radiofrequency to and from the examined tissue. It pushes the protons against their normal alignment axis, thus, once the RF pulse turned off, the protons will realign with the magnetic field. This will produce a signal which is then sent to a computer processor that runs sophisticated mathematical processes in order to produce an image out of the received signal. Different tissues will give different signals, which makes it

possible to differentiate between the different tissues (Dale et al., 2015). There are two types of time needed for the proton to relax completely. This measured in T1, which is the time needed for the longitudinal component of the magnetisation vector to return to its relaxing state, and T2, which is the time needed for a transverse component of the magnetisation vector to return to its equilibrium state (Dale et al., 2015).

Different molecules have different relaxation times; this makes it possible to distinguish between tissues based on its molecules contents. For example, hydrogen bound to a lipid molecule will relax slowly producing low efficacy in T1, while free water will relax quickly in T1 relaxation. This relaxation time is closer to the Larmor frequency, which is defined as the number of times proton precesses per second. These differences can be distinguished by the “repetition time TR” and the “echo time TE”, representing how quickly the RF pulse and how quickly listening to the returned signal. These will eventually produce different signals from the proton in T1 and T2, i.e. each molecule will look different in T1 and T2. This helps to analyse and segment different body tissues, of which are the fat and muscle, for instance.

MRI is used widely in the study of body composition as it has the advantages of studying the FM and LBM on a region basis and the ability to visualise the distribution of the fat (Prado and Heymsfield, 2014). It has been used in the study of body composition in different groups; obesity, sarcopenia, child obesity, haemodialysis and human immunodeficiency virus (Neeland et al., 2013, Manini et al., 2013, Zoico et al., 2013, Karlsson et al., 2013, Molino et al., 2013, Shah et al., 2012). The MRI overcomes the assumption of hydration status that underpins most of the body composition techniques discussed earlier, making it more reliable in obesity where the hydration changes. However, still MRI has its own limitations such as difficulty to accommodate morbidly obese patients, the cost, time and the expertise needed to conduct the scan and to run the segmentation process afterwards (Prado and Heymsfield, 2014). This makes it impracticable in a routine clinical setting or in epidemiological studies, and hence DXA can be used instead, which has shown a good agreement with MRI derived body composition values.

4.6 Method:

4.6.1 Data nature and study population:

The data used in this study were sourced from four studies conducted previously with different primary outcomes. Participants in these studies were all female healthy participants and not on any medications which might affect their FM and LBM. Two types of data were used in this study: DXA and MRI based data.

This section will cover the main aspects of ethical approval, participant recruitment, anthropometric measurements and DXA and MRI protocols used in all studies.

4.6.2 DXA data:

4.6.2.1 Ethical approval:

All studies had ethical approvals before commencement. The researcher had to sign an agreement with the principle investigator of each study before having access to the data in order to comply with the ethical requirement of reusing the data for other purposes.

4.6.2.2 Recruitment:

Forty five subjects participated in a study conducted by Hopkins and colleagues (Hopkins et al., 2016). The recruitment was carried out through leaflet and poster distributed around Exeter university campuses and other public gyms and health clubs around Exeter. A talk was also given to selected groups, who were interested in osteoporosis and leaflets distributed to anyone desiring to participate. In this study participants were postmenopausal women as the main aim was to compare osteoporosis between healthy and other post fracture and post knee replacement groups.

Forty one subjects participated in a study conducted by (Connolly et al., 2014). The recruitment was conducted through an advertisement campaign in the local newspaper, local radio station and community venues. All participants in this study were premenopausal women.

One hundred and two participants were recruited from the general public through posters and advertisements into a study conducted by (Knapp et al., 2012).

The remaining eighty subjects participated were recruited using the same method used in Connolly and colleagues study as described earlier (Bowtell et al., 2016, Connolly et al., 2014).

4.6.2.3 Measurements:

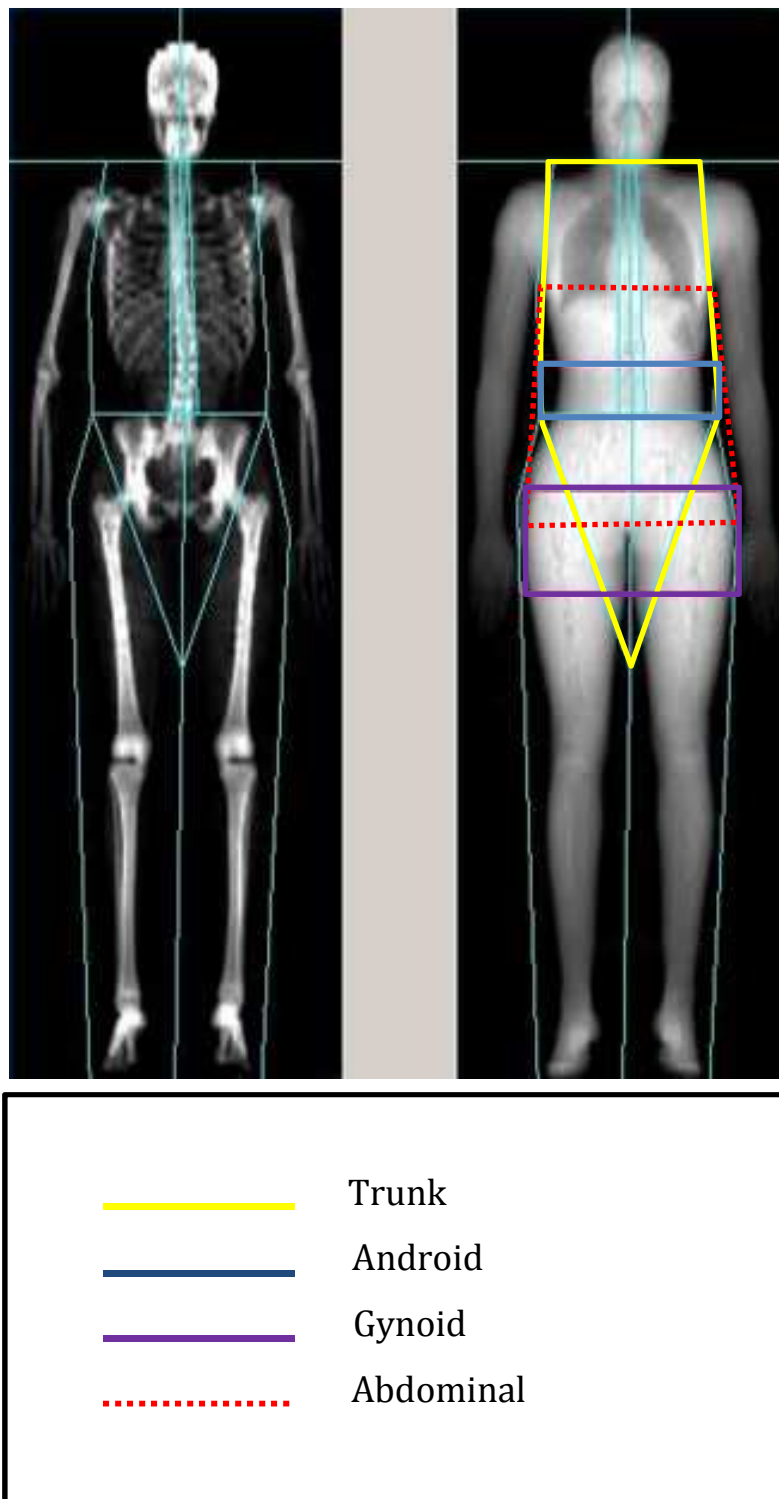
Table 15 summarises the number of participants in each study and the tools used to measure height and weight for participants. In all studies, this was accomplished before conducting the DXA scan. The height was measured to the nearest 0.01m, and the mass to the nearest 0.1kg. All tools had quality control check before use as indicated in studies listed in table 15.

Table 15 Summary of data resources and measurement tools

Study	Number	Measurement tool	
		Height	Mass
(Hopkins et al., 2016)	45	Seca stadiometer SEC-225; Seca, Hamburg, Germany	(Seca 877, Germany)
(Connolly et al., 2014)	41	Seca stadiometer SEC-225; Seca, Hamburg, Germany	(Seca 877, Germany)
(Knapp et al., 2012)	102	Stadiometer (Holtain, Crymych, Dyfed, UK)	Beam balance scale (Avery, Birmingham, UK)
(Connolly et al., 2014), (Bowtell et al., 2016)	80	Seca stadiometer SEC-225; Seca, Hamburg, Germany	(Seca 877, Germany)

All participants were scanned in a GE Lunar Prodigy DXA scanner (GE Healthcare, Bedford, UK). This scanner utilizes the narrow angle fan beam technology and accommodates individuals up to 159 kg. The scan mode used, standard or thick, was selected automatically by the scanner software depending on the patient size. The GE Lunar Encore 2005 software, version 9.30.044 (GE Healthcare, Little Chalfont, UK) was used for scan analysis. Figure 8 illustrates the body regions assessed for FM and LBM. The trunk region includes the neck, chest, abdominal and pelvic regions. It is defined between the inferior edge of the chin and the lower borders intersect the femoral necks in the middle without touching the pelvic rim (Stults-Kolehmainen et al., 2013). The android region is defined as the region from the pelvic cut (lower boundary) to above the pelvic cut by 20% of the distance between neck cut line (upper boundary) and the pelvic cut line (Kang et al., 2011). The gynoid region defined as 1.5 x android height below the pelvic cut, and comprises double the android area (Kang et al., 2011). The total, trunk, android and gynoid regions were auto-demarcated by the computer, for the abdominal regional, the region of interest (ROI) was drawn manually between the pubic symphysis and two centimetre above the xiphoid process. Figure 8 demonstrates these regions as demarcated on the DXA image. The regions demarcated by the computer were checked manually by the researcher and manual adjustments made where needed. The total, trunk, gynoid and android region were exported directly from the DXA scanner into an Excel sheet ready for analysis. The abdominal region data, demarcated manually, was entered manually into the Excel sheet by the researcher.

Figure 8 DXA scan showing body subdivision regions considered for FM and LBM measurement



4.6.2.4 Statistical analysis:

All data analysis was performed using STATA software (STATA 12). The data was stored in an excel spreadsheet ready to import into STATA . Data from the Knapp et al, study (Knapp et al., 2012) contained two DXA for each participant with ten minutes gap between the two scans. The average values of body composition of the two scans was calculated and used in the analysis. The first visit scan data from Hopkins and colleague's study (Hopkins et al., 2016) were used as the gap between each scan was more than six months, therefore it was inappropriate to take the average value. Data were screened for any unusual values in anthropometrics, FM and LBM values. This was achieved through generating a detailed summary of each variable to visualise the highest and lowest values.

The normality of the data distribution was checked using histograms. However, the normality assumption should not cause major issues when the sample size is above 30 or 40, and can be ignored when the sample consists of hundreds of subjects, as in this study (Altman, 1991, Ghasemi et al., 2012).

Descriptive statistics, including mean and standard deviations, were calculated for all anthropometric and outcomes measurement including: participant's age (year), weight (kg), height (m), BMI (kg/m^2), fat percentage (%) and body composition, FM and LBM (kg), in total and regional basis.

Participants were grouped based on BMI into; normal ($18.3 - 24.99 \text{ kg}/\text{m}^2$), overweight ($25 - 29.99 \text{ kg}/\text{m}^2$) and obese ($\geq 30 \text{ kg}/\text{m}^2$) to demonstrate the difference in body composition between the different BMI groups. Descriptive statistics for each group were determined. To illustrate the limitation of BMI in differentiating between FM and LBM, the two variables were plotted against each other to demonstrate BMI limitation. And to investigate the relationship between LBM and FM, correlations between FM and LBM across different body regions were conducted and one-way ANOVA was used to test any significant difference in age between each fat percentage groups.

In order to investigate the association between FM, LBM and the anthropometrics, a Pearson correlation was used as the data are continuous

and normally distributed. For the FM, the correlations were conducted with age and BMI. The reasons for choosing these two variables are:

- There is a curvilinear correlation between age and FM (Mott et al., 1999). The peak of the FM was found in middle age (50-60 years) but then decreases. For this reason, it was essential to investigate if this relation is a factor in the FM or not.
- The use of BMI attributed to the simplicity of its calculation and the fact that two variables are already incorporated in its value.

The correlation was conducted across the whole cohort and BMI subdivision groups. The reason is to establish the best correlation in order produce the regression model.

For the LBM, the correlations were conducted with age, height and FM.

Linear regression and multiple regression equations were used to predict FM and LBM in different regions. To predict the FM, FM was used as the dependant variable, and the BMI as independent variable. For the LBM, the LBM was used as the dependent variable, while the FM and height were used as independent variables.

Scatter plots were used to demonstrate the shape of relationship between the dependant dependent and independent variables. The probability plot as well as the Shapiro-Wilk test was used to test the distribution of the residual for each model.

Both multiple regressions were conducted for the whole cohort and for the BMI subdivision groups to produce the best equation. Three levels of significance reported as * if $p < 0.05$, ** if $p < 0.01$, *** if $p < 0.001$ across all tests.

4.6.3 MRI data:

4.6.3.1 Participant:

A subset of 49 healthy females who participated in one of the DXA studies, (Hopkins et al., 2016), underwent an abdominal MRI scan. The subset data analysed in this section were used to test the agreement between DXA and MRI, as MRI is considered being the gold standard (Yip et al., 2015, Denton and Karpe, 2016).

4.6.3.2 Scan protocol:

The region of interest was the abdomen, the image acquisition was performed on a 1.5 Tesla superconducting MR scanner (GyroScan Intera; Philips, The Netherland) using a spoiled T1- weighted gradient-echo sequence with repetition time (TR) = 201 ms and echo time (TE) = 1.96 ms. Axial slices were acquired in two phases, pelvic and lower abdomen in one phase, and upper abdomen in the second phase due to the limitations of the coil size.

4.6.3.3 Image segmentation:

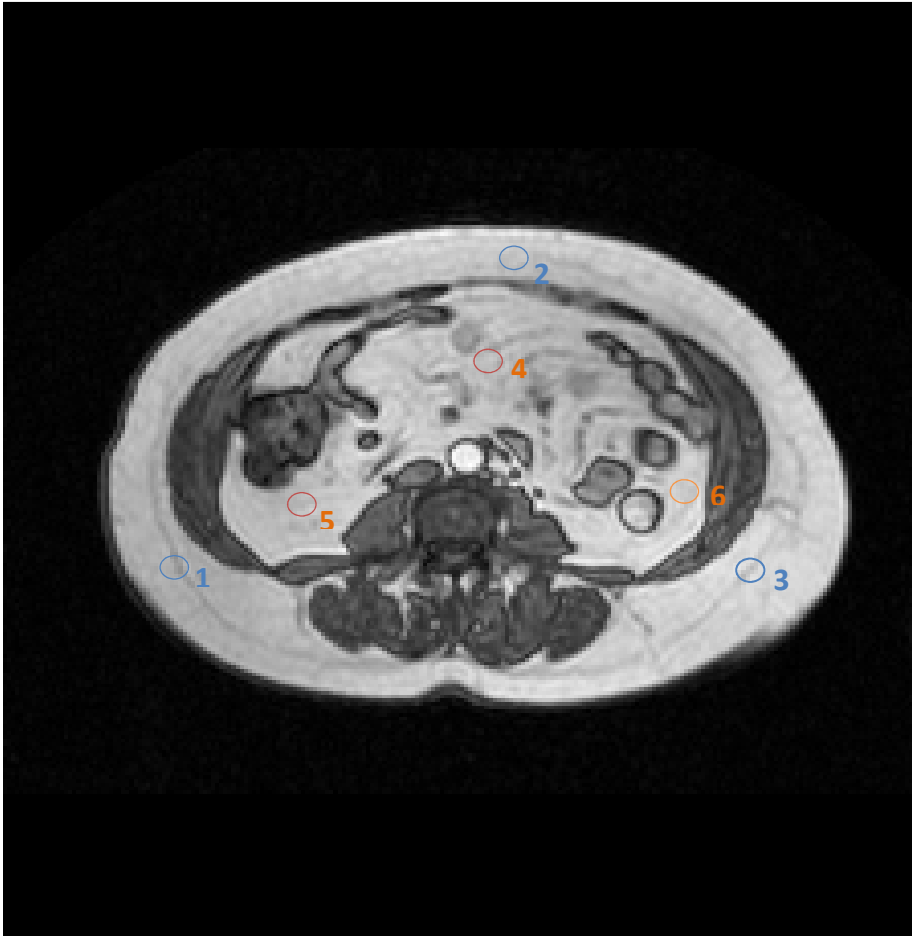
The segmentation of subcutaneous fat (SF) and visceral fat (VF) was performed manually by the researcher. A single slice, at the L4-L5 level, from each participant was used for segmentation. Different studies have reported the strong correlation between one slice FM at L4-L5 level and the total abdominal FM (Shen et al., 2016, Schaudinn et al., 2015, Hu et al., 2016).

For each image, three regions of interest (ROIs) were drawn manually in different locations in SF and VF regions, Figure 9. The minimum and maximum pixel intensity values for each fat region, i.e SF or VF, were averaged and used in the automatic ROI dialog box to segment the fat in the image. As the intensity of both SF and VF were similar, the automatic ROI drawer covers both regions. The researcher had to amend the segmented areas in two steps:

- The SF first separated from the visceral fat and the final total pixel areas were recorded.

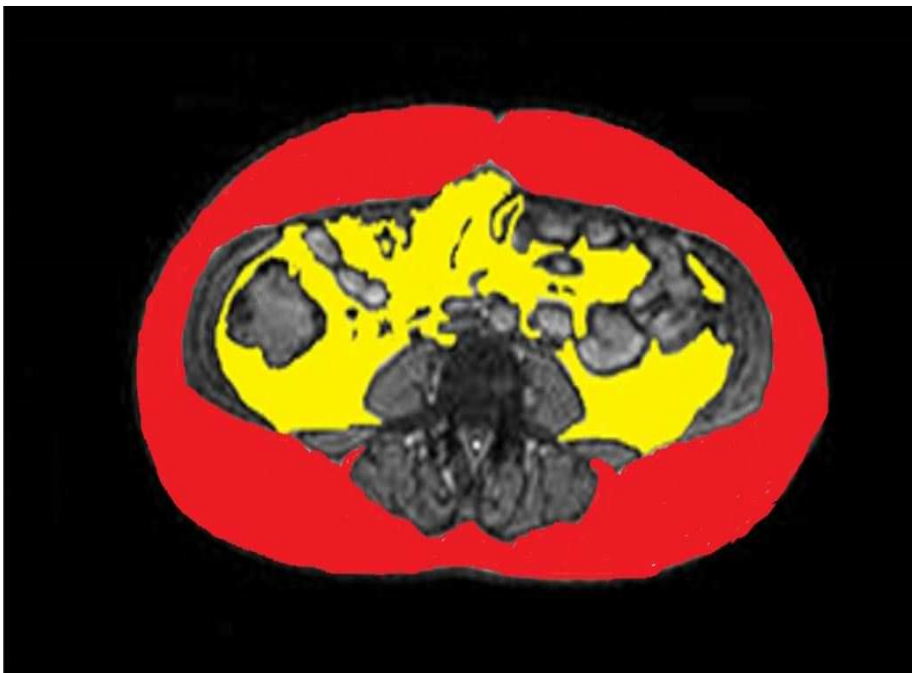
- The segmented VF was then amended to exclude lean tissue and residual faeces in the intestine which had similar pixel intensity to the VF. In areas where there was a dilemma of whether the pixel intensity was representing VF or faeces, the researcher in this case would scroll up and down to adjacent images to track the texture and identify the nature of the pixels. In occasions where decision was hard to take, help was sought from the MRI operator, John Fulford, who has more than 20 years of experience in MRI segmentation.

Figure 9 MRI region of interests (ROIs) across subcutaneous and visceral fat



1, 2 and 3 ROI: subcutaneous fat
4, 5 and 6 ROI: Visceral fat

Figure 10 Segmented subcutaneous fat (SF) and visceral fat (VF) of one slice across L4-L5 level



4.6.3.4 Statistical analysis:

All data, total pixel areas (TPA) of VF and SF were entered into the excel sheet in preparation for analysis. The data were checked for any abnormal values using box plot to visualise outliers and investigate them before the analysis.

The data were checked for normality, TPA of FM in one slide, L4-L5, and the android FM measured by DXA. Since the data was not normally distributed, the Spearman correlation was used to test the strength of the relationship between these two values.

4.7 DXA results:

4.7.1 Objective one:

Table 16 Descriptive characteristics of the participants anthropometry and body composition values

Characteristics	Mean \pm SD	Range	
		Min	Max
Age (Years)	44.4 \pm 15.2	18	85
Height (cm)	1.65 \pm 0.06	1.46	1.84
Weight (kg)	70.95 \pm 14.83	42.5	130
BMI (kg/m ²)	25.98 \pm 5.07	18.35	45.93
Total fat mass (kg)	26.52 \pm 11.07	4.86	67.61
Trunk fat mass (kg)	13.81 \pm 6.72	1.68	38.99
Abdominal fat mass (kg)	10.64 \pm 5.08	1.12	27.58
Android fat mass (kg)	2.33 \pm 1.29	0.16	6.72
Gynoid fat mass (kg)	5.15 \pm 1.77	1.66	13.29
Total Lean mass (kg)	40.60 \pm 5.03	28.63	59.90
Trunk lean mass (kg)	20.06 \pm 2.88	13.19	31.51
Abdominal lean mass (kg)	14.17 \pm 2.02	9.20	22.42
Android lean mass (kg)	2.84 \pm 0.47	1.73	4.70
Gynoid lean mass (kg)	5.96 \pm 0.85	4.21	8.77

SD = Standard deviation

Min = minimum value

Max = maximum value

Table 17 Descriptive characteristics of participant body composition (Mean & SD) based on BMI & fat % groups.

Group	BMI Groups			Fat % Groups			
	Normal	Overweight	Obese	<30%	30-39.9%	40-44.9%	>=45%
Number	126	86	52	61	106	53	44
Age(years)	41.9 ± 16.34	47.19 ± 14.4	46.11 ± 12.67	37.37 ± 16.10	46.38 ± 14.57	47.35 ± 14.50	46.29 ± 13.62
Height (cm)	1.65 ± 0.05	1.64 ± 0.06	1.64 ± 0.06	1.65 ± 0.05	1.64 ± 0.06	1.66 ± 0.06	1.64 ± 0.06
Weight (kg)	60.36 ± 6.54	73.40 ± 6.69	92.57 ± 13.86	57.18 ± 5.51	67.02 ± 7.34	77.76 ± 11.56	91.32 ± 14.88
BMI (kg/m ²)	22.02 ± 1.79	26.93 ± 1.30	34.00 ± 3.99	20.90 ± 1.61	24.61 ± 2.18	28.11 ± 3.16	33.73 ± 4.65
Total fat (kg)	18.15 ± 5.44	29.02 ± 4.84	42.67 ± 8.40	13.67 ± 3.5	23.75 ± 3.57	32.63 ± 5.39	43.65 ± 8.13
Android fat (kg)	1.42 ± 0.67	2.55 ± 0.61	4.20 ± 1.08	0.97 ± 0.61	2.00 ± 0.48	2.93 ± 0.70	4.31 ± 1.08
Abdominal fat (kg)	6.79 ± 2.53	11.75 ± 2.26	18.11 ± 3.65	4.77 ± 1.65	9.46 ± 1.87	13.32 ± 2.84	18.39 ± 3.60
Gynoid fat (kg)	3.98 ± 0.98	5.47 ± 1.00	7.45 ± 1.79	3.36 ± 0.77	4.73 ± 0.78	5.93 ± 1.08	7.71 ± 1.73
Trunk fat (kg)	8.78 ± 3.17	15.15 ± 3.11	23.80 ± 4.99	6.19 ± 1.89	12.11 ± 2.53	17.38 ± 3.51	24.18 ± 5.07
Total lean (kg)	38.75 ± 4.01	40.52 ± 3.57	45.19 ± 6.34	39.98 ± 4.07	39.55 ± 3.85	41.10 ± 5.94	43.35 ± 6.44
Trunk lean (kg)	18.96 ± 2.04	19.93 ± 1.95	22.92 ± 3.86	19.51 ± 2.01	19.47 ± 2.06	20.17 ± 3.15	22.09 ± 4.16
Abdominal lean (kg)	13.61 ± 1.55	13.93 ± 1.50	15.91 ± 2.73	14.12 ± 1.38	13.70 ± 1.57	14.31 ± 2.42	15.18 ± 2.77
Android lean (kg)	2.61 ± 0.30	2.84 ± 0.33	3.38 ± 0.56	2.66 ± 0.28	2.72 ± 0.35	2.92 ± 0.52	3.27 ± 0.59
Gynoid lean (kg)	5.64 ± 0.72	5.94 ± 0.61	6.78 ± 0.93	5.79 ± 0.76	5.77 ± 0.69	6.04 ± 0.94	6.57 ± 0.92
Fat %	30.1 ± 6.99	39.99 ± 4.08	46.80 ± 3.83	24.31 ± 4.95	35.93 ± 2.52	42.54 ± 1.60	48.44 ± 2.63

Table 16 shows the descriptive characteristics of participants and the FM and LBM in different regions. The cohort contained a wide range of participants' age (18 – 85 year), BMI (18.5 – 45.6 kg/m²) and mean height (1.65 m) that is similar to the mean height of women (Social and Neave, 2017). The total FM ranged between 4.8 and 67.6 kg with a mean of 26.5 kg. Similarly, the total LBM ranged between 28.6 and 59.9 kg with an average of 40.6 kg.

Table 17 illustrates the participants' anthropometrics, FM and LBM across different regions based on BMI and fat percentage subdivision groups. The increase in FM and LBM across different regions is clear across the subdivision fat percentage groups as well as BMI subgroups. With regards to LBM, the increase across all regions is very clear on fat percentage subdivision groups.

4.7.2 Objective two:

Table 18 Pearson correlation between LBM and FM across different body parts based on BMI and fat% subdivision groups.

Body regions	BMI groups			Fat % groups			
	Normal (n=126)	Overweight (n=86)	Obese (n=52)	<30% (n=61)	30-39.9% (n=106)	40-44.9% (n=53)	≥45% (n=44)
Total body	-0.14	0.18	0.61***	-0.01	0.68***	0.91***	0.80***
Trunk	-0.11	0.20	0.72***	-0.03	0.61***	0.85***	0.84***
Abdominal	-0.12	0.24*	0.63***	-0.11	0.56***	0.84***	0.81***

n: Number of participants

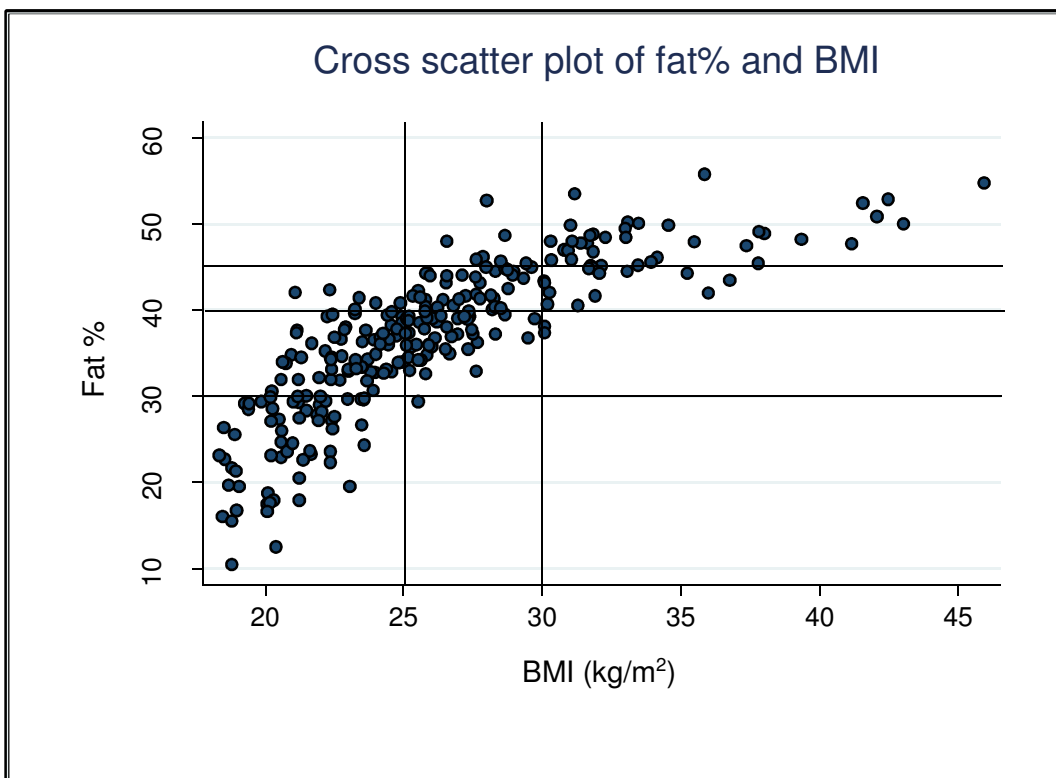
Since BMI is based on height and weight only, it is limited in distinguishing between fat and lean masses (Wells and Fewtrell, 2006). Therefore, participants were grouped depending on their fat percentage into four groups, Table 18. This is to demonstrate that the increase in LBM is a result of FM increase in the cohort and to eliminate the misrepresentation FM by the BMI. In this approach, subjects in a high fat percentage group are not necessarily in a high BMI group and vice versa.

Table 19 One-Way Analysis of Variance (ANOVA) of age by fat percentage

	Sum of Squares (SS)	df	Mean square	F	Sig
Between groups	4047.122	3	1349.040	6.18	0.0005
Within groups	56776.817	260	218.372		
Total	60823.817	263	231.372		

A Tukey post-hoc test revealed the age was statistically significant lower in the first group (fat% < 30) compared to the second group (fat% = 30-39.9%) ($\Delta=9.0 \pm 2.37$ SE years, $P= 0.001$), and ($\Delta=9.9 \pm 2.77$ SE years, $P= 0.002$) compared to the third group (fat % = 40-44.9%) and ($\Delta=8.91 \pm 2.92$ years, $P= 0.013$) compared to the fourth group (fat% = $\geq 45\%$). However, there were no statistically significant differences between the second group (fat% = 30-39.9%) and the third group (fat% = 40-49.9%) ($\Delta=0.97 \pm 2.48$ SE years, $P=0.98$), the second group and the fourth group ($\Delta=-0.09 \pm 2.65$ SE years, $P= 1.0$), the third group and the fifth group ($\Delta=-1.06 \pm 3.01$ SE years, $P= 0.98$). This indicates that the strong correlation between LBM and FM, Table 18, is not affected by age.

Figure 11 Cross scatter plot of fat % against BMI



As can be seen in Figure 11, there are patients who are obese based on fat % (>30 %) and yet they are grouped as overweight and even normal weight based on BMI classification.

Table 20 Pearson correlation between FM and anthropometrics across different body parts and based on total cohort and BMI subdivision groups

	Normal			Overweight			obese			Non-normal (BMI>=25)			Whole group		
	trunk	abdomen	total	trunk	abdomen	total	trunk	abdomen	total	trunk	abdomen	total	trunk	abdomen	total
age	0.25**	0.26**	0.21*	0.07	0.12	-0.06	-0.16	-0.22	-0.32*	-0.04	-0.05	-0.15	0.15*	0.16**	0.10
Height	0.18*	0.21*	0.22*	0.39***	0.44***	0.52***	0.36**	0.39**	0.45***	0.24**	0.26**	0.31***	0.12	0.13*	0.16**
Weight	0.71***	0.73***	0.74***	0.65***	0.72***	0.77***	0.85***	0.87***	0.92***	0.89***	0.90***	0.93***	0.92***	0.93***	0.94***
BMI	0.77**	0.78***	0.77***	0.59***	0.64***	0.60***	0.84***	0.85***	0.87***	0.89***	0.90***	0.90***	0.93***	0.93***	0.94***

Table 20 demonstrated, weight and BMI had strong correlations with FM in all subdivision groups. The highest correlation observed for the whole cohort, i.e no subdivision. The height also had a strong correlation with FM across the whole cohort and subdivision groups.

Table 21 Pearson correlation between LBM and age, height and FM across different body regions and based on the cohort and BMI subdivision groups

	Normal			Overweight			obese			Non-normal (BMI>=25)			Whole group		
	trunk	abdomen	total	trunk	abdomen	total	trunk	abdomen	total	trunk	abdomen	total	trunk	abdomen	total
age	-0.04	-0.00	-0.13	0.24*	0.25*	0.03	-0.13	-0.14	-0.26	0.02	0.03	-0.10	0.05	0.05	-0.05
Height	0.59***	0.59***	0.65***	0.54***	0.50***	0.72***	0.54***	0.51***	0.68***	0.45***	0.43***	0.61***	0.44***	0.46***	0.56***
Fat (regional)	-0.11	-0.12	-0.14	0.20	0.24*	0.18	0.72***	0.63***	0.61***	0.66***	0.61***	0.60***	0.56***	0.46***	0.50***

Table 21 illustrates the strong correlation between FM and LBM and height especially in obese and overweight subdivision groups. Age had weak correlation with LBM across total, abdominal and trunk regions. Apart from that, there is no significant correlation between age and LBM. It can be concluded that the relationship between LBM, height and FM is when BMI restricted to 30 kg/m² or above. This can be seen clearly in Figure 12.

Figure 12 Two-way scatter plot of total FM and LBM across BMI

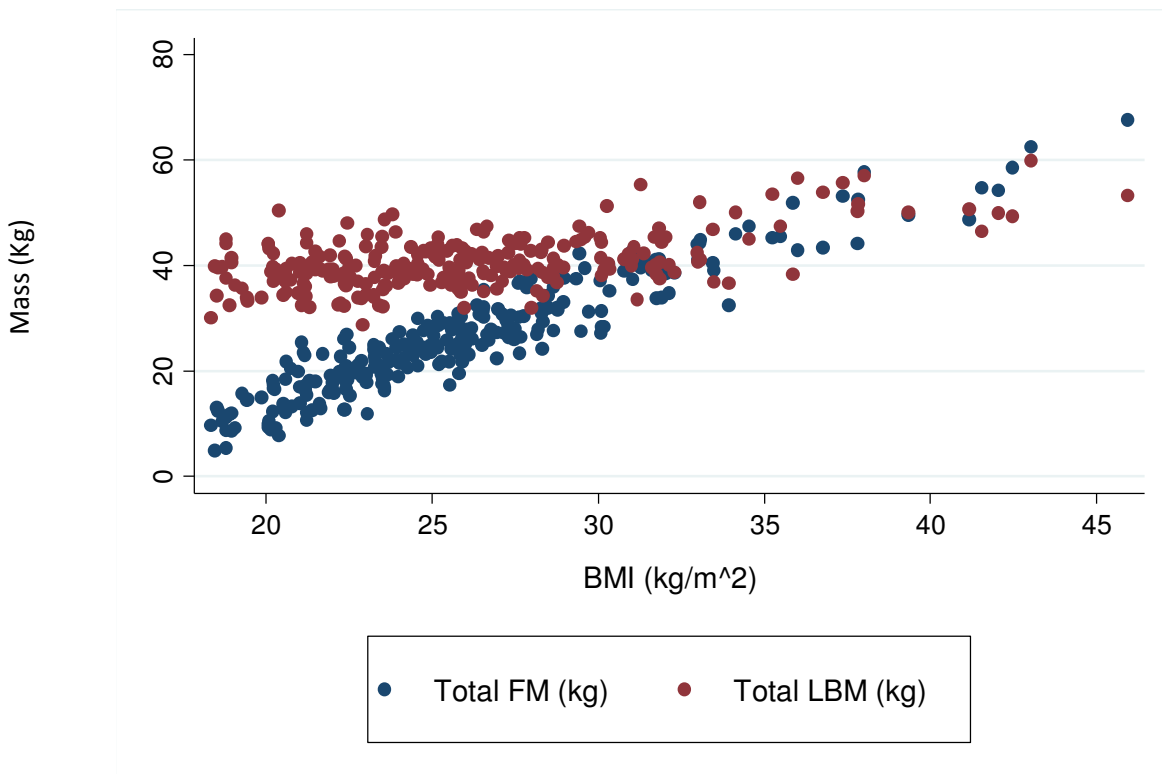


Figure 12 exhibits the changes in total FM and LBM along with BMI. As observed, the FM increases linearly with the BMI while the LBM show increase with BMI only after BMI of 30 kg/m². This indicates that LBM increase can be ignored if in the non-obese group.

4.7.3 Objective three

Table 22 Summary of regression analysis for BMI (kg/m²) predicting FM (kg) of different regions in the whole cohort

	Model 1 (Total FM)			Model 2 (Trunk FM)			Model 3 (Abdominal FM)		
	β	β SE	t	β	β SE	t	β	β SE	t
BMI (kg/m ²)	2.05 ***	0.045	44.87	1.242 ***	0.028	43.37	0.94 ***	0.021	44.44
Constant	-26.83 ***	1.211	-22.15	-18.46 ***	0.75	-24.35	-13.82 ***	0.560	-24.64
R ²	0.884			0.877			0.882		

β = regression coefficient

β SE= Standard error

T = t-test

Three prediction equations can be produced from Table 22 in order to predict FM in different regions based on BMI.

First equation (Equation 5) to predict total FM:

$$FM_T = (-26.836 + (2.055 * BMI)) \quad \text{Equation 5}$$

Where FM_T is the total fat mass (kg)
 BMI is the body mass index (kg/m²)

Second equation (Equation 6) can be used to predict trunk FM:

$$FM_{Tru} = (-18.469 + (1.242 * BMI)) \quad \text{Equation 6}$$

Where FM_{Tru} is the trunk fat mass (kg)
 BMI is the body mass index (kg/m²)

Third equation (Equation 7) is to predict abdominal FM:

$$FM_{Abd} = (-13.823 + (0.941 * BMI)) \quad \text{Equation 7}$$

Where FM_{Abd} is the abdominal fat mass (kg)
 BMI is the body mass index (kg/m²)

Figure 13 Two way scatter plot shows the linear relationship between total (A), abdominal (B), trunk (C) FM and BMI

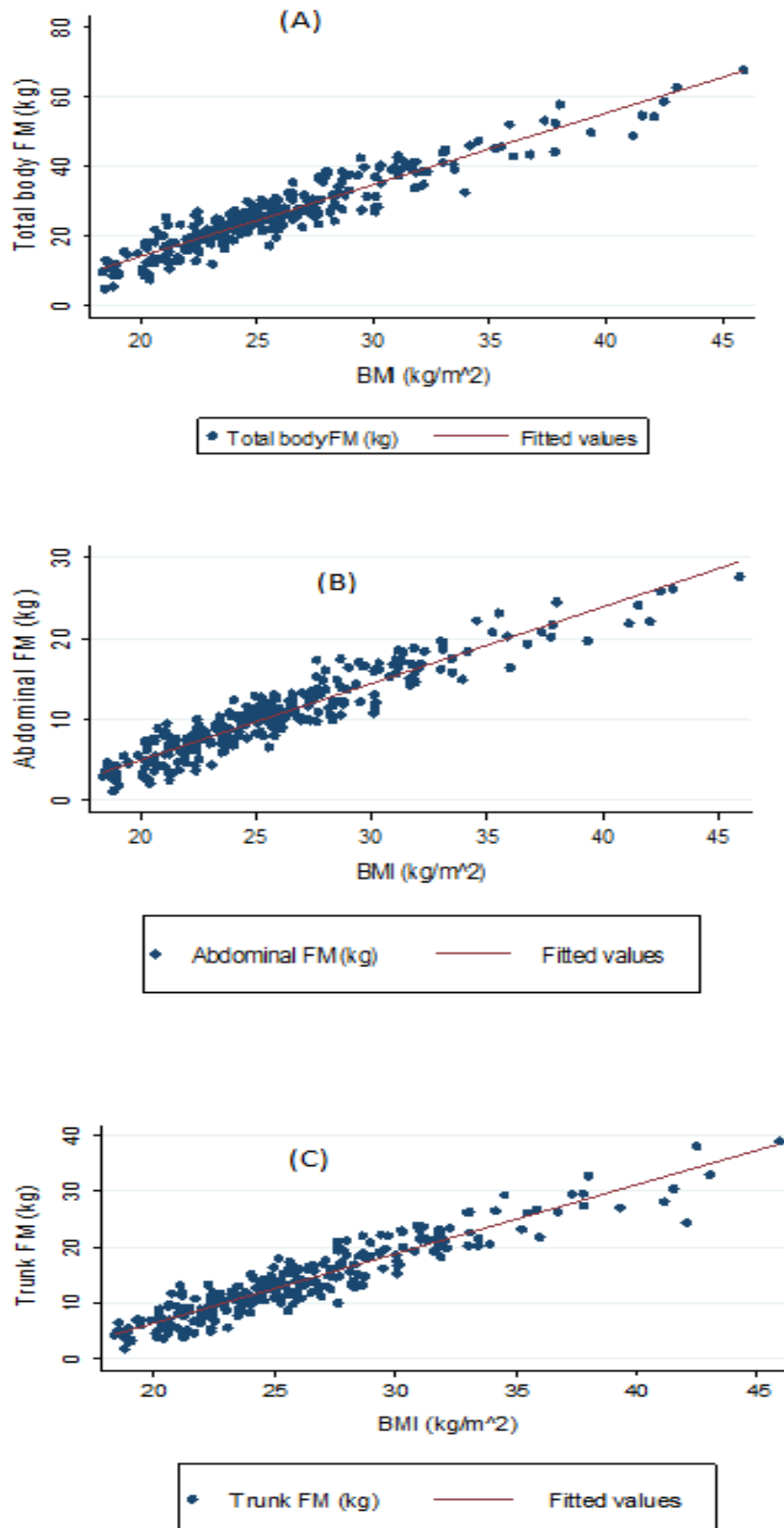


Figure 14 Post estimation test and Sharipo-Wilk to investigate the residual normal distribution

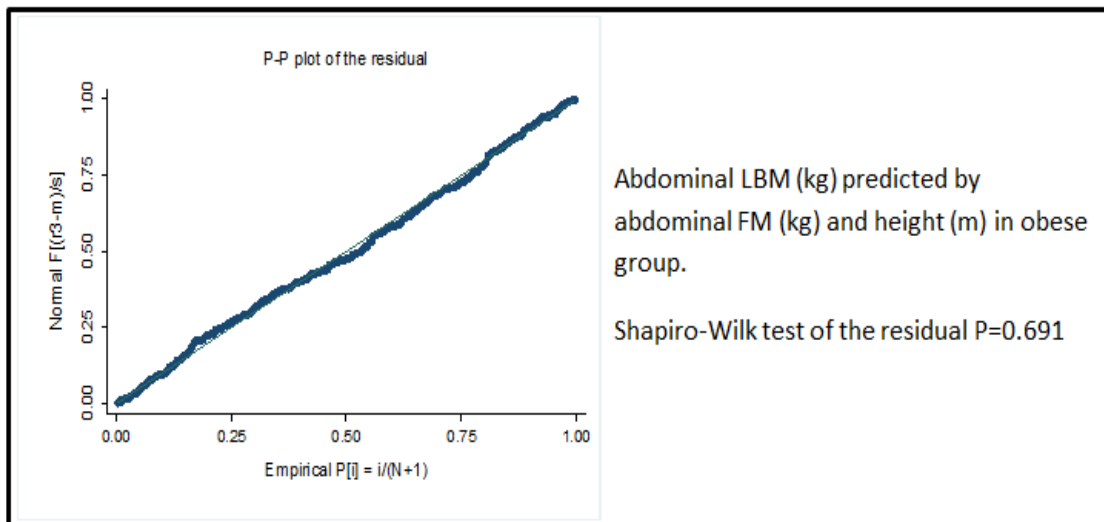
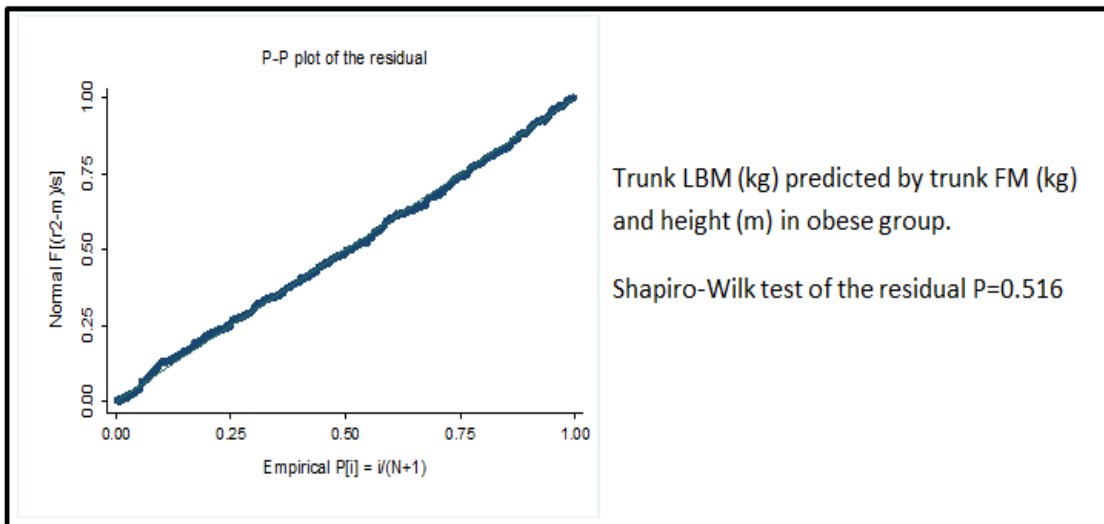
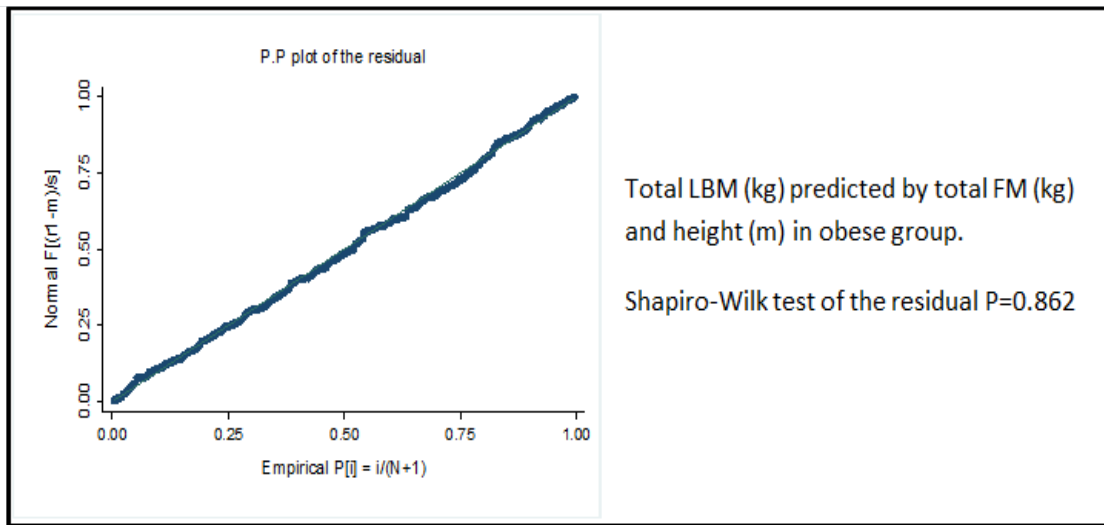


Table 23 Summary of regression analysis for height (m) and total FM (kg)

	Model 1 (whole cohort)			Model 2 (if BMI ≥ 25 kg/m ²)			Model 3 (if BMI ≥ 30 kg/m ²)		
	β	β SE	t	β	β SE	t	β	β SE	t
Total FM (kg)	0.191 ***	0.020	9.45	0.260 ***	0.034	7.50	0.290 ***	0.077	3.77
Height (m)	40.814 ***	3.633	11.23	38.358 ***	4.963	7.70	49.145 ***	9.744	5.04
Constant	-31.88 ***	5.94	-5.37	-29.86 ***	7.89	-3.78	-48.17 **	14.871	-3.24
R ²	0.495			0.558			0.593		

predicting total LBM (kg)

β = regression coefficient

β SE= Standard error

T = t-test

Based on regression models in Table 23, it is clear that total LBM is best predicted when BMI restricted to 30 kg/m² or above. Hence, total LBM can be predicted using the following equation:

$$LBM_T = (-48.176 + (0.290 * FM_T) + (49.145 * H_m)) \quad \text{Equation 8}$$

Where LBM_T is the total lean body mass (kg)

FM_T is the total fat mass (kg)

H_m is the height (m)

Table 24 Regression analysis for height (m) and FM (kg), of different regions, predicting abdominal LBM (kg) in obese group.

	Model 1			Model 2			Model 3		
	β	β SE	t	β	β SE	t	β	β SE	t
Height (m)	12.462 *	4.873	2.56	13.290 **	4.587	2.90	14.298 **	4.626	3.09
Total FM (kg)	0.157 ***	0.038	4.06						
Abdominal FM (kg)				0.378 ***	0.083	4.53			
Trunk FM (kg)							0.259 ***	0.061	4.21
Constant	- 11.305	7.438	- 1.52	- 12.819	7.11	- 1.80	- 13.826	7.22	- 1.91
R ²	0.454			0.485			0.464		

β = regression coefficient

β SE= Standard error

T = t-test

Based on regression result in Table 24, the best regression model to predict abdominal LBM is based on regional FM and height (Model 2). Hence, the following equation can be used to predict abdominal LBM.

$$LBM_{Abd} = (-12.819 + (0.378 * FM_{Abd}) + (13.290 * H_m)) \quad \text{Equation 9}$$

Where LBM_{Abd} is the abdominal lean body mass (kg)

FM_{Abd} is the abdominal fat mass (kg)

H_m is the height (m)

Table 25 Regression analysis for height (m) and FM (kg), of different regions, predicting trunk LBM (kg) in obese group.

	Model 1			Model 2			Model 3		
	β	β SE	t	β	β SE	t	β	β SE	t
Height (m)	16.971 *	6.367	2.67	18.686 **	6.007	3.11	18.525 **	5.557	3.33
Total FM (kg)	0.253 ***	0.050	5.03						
Abdominal FM (kg)				0.592 ***	0.109	5.42			
Trunk FM (kg)							0.471 ***	0.074	6.37
Constant	- 15.848	9.718	- 1.63	- 18.598	9.310	- 2.00	- 18.821 *	8.676	- 2.17
R ²	0.533			0.557			0.613		

β = regression coefficient

β SE= Standard error

T = t-test

As observed in Table 25, trunk LBM is best predicted by trunk FM and height ($r^2=0.61$). The prediction equation that can be used to predict trunk LBM is:

$$LBM_{Tru} = (-18.821 + (0.471 * FM_{Tru}) + (18.525 * H_m))$$

Equation 10

Where LBM_{Tru} is the trunk lean body mass (kg)

FM_{Tru} is the trunk fat mass (kg)

H_m is the height (m)

Figure 15 Two ways scatter plot shows the linear relationship between total (A), abdominal (B), trunk (C) LBM and FM in the same region

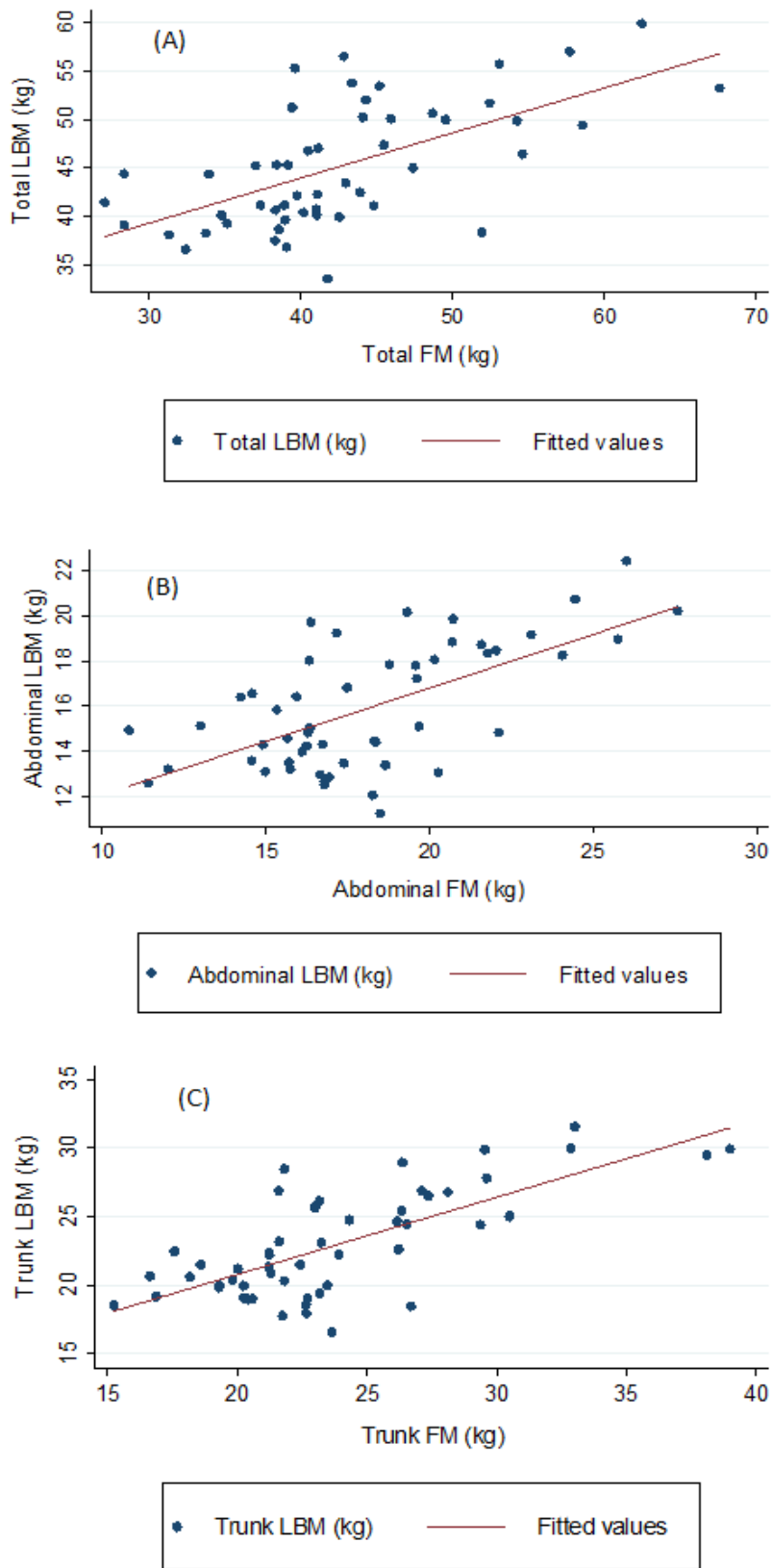


Figure 16 Post estimation test and Shapiro-Wilk to investigate the residual normal distribution

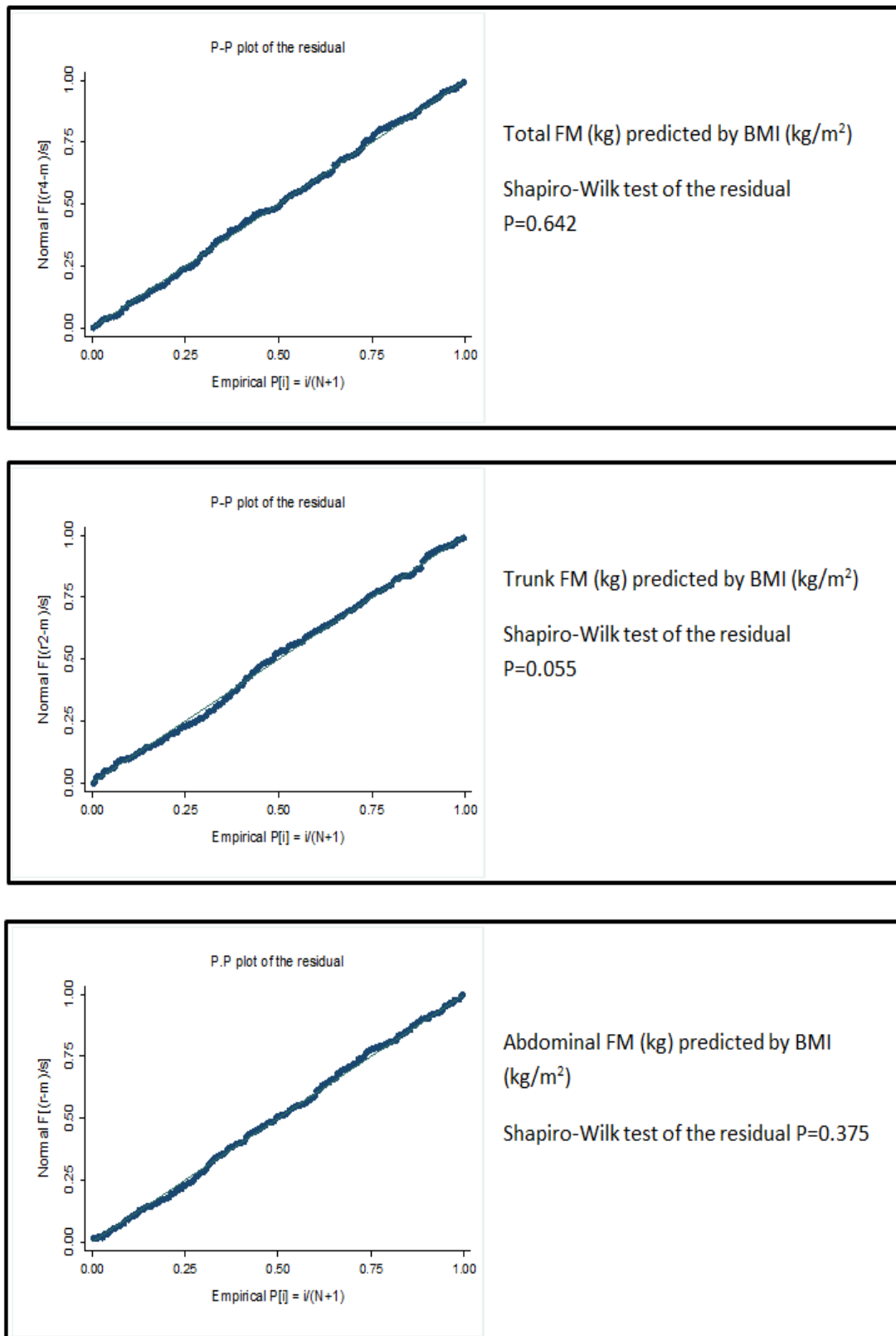
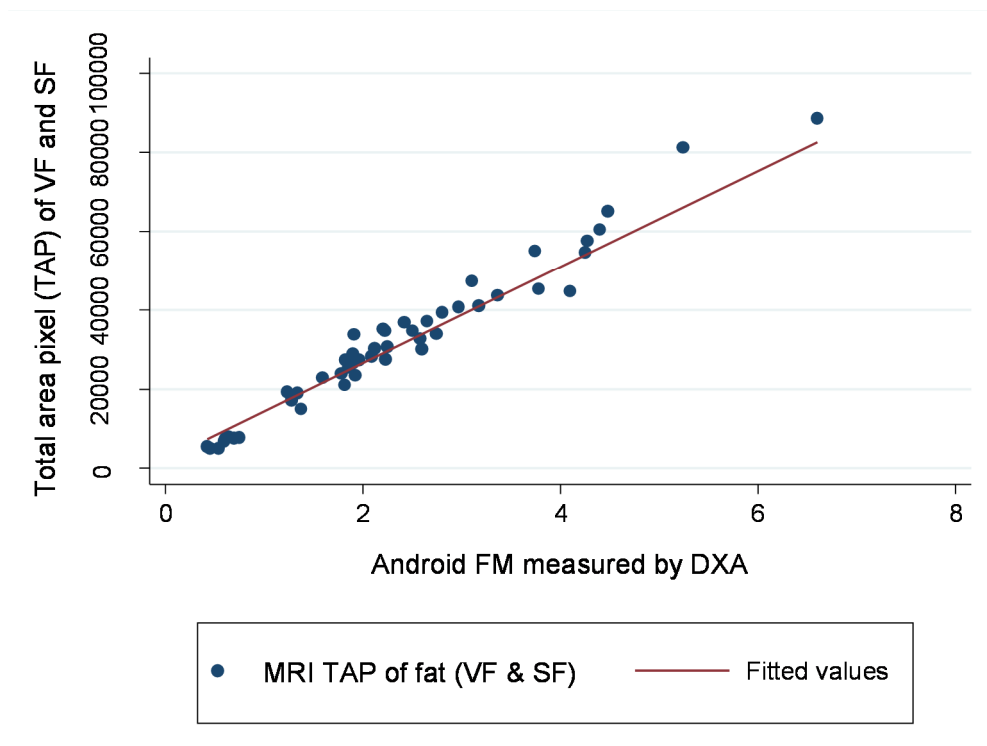


Figure 17 Scatter plot of total pixel area segmented fat in MRI and android FM measured by DXA



Spearman correlation between total pixel area (TPA) of fat segmented using MRI images and the android FM shows a strong spearman correlation, $r^2= 0.88$, $P=0.000$. This is illustrated in Figure 17. This indicates the validity of DXA measured FM compared to the gold standard, MRI.

4.8 Discussion:

The objectives of the current study were to quantify FM and LBM, at the total and regional level, of participants with different BMI based on measurements from DXA scans. It also aimed to investigate the best predictors of FM and LBM across different body parts and produce prediction models that can be used to transform normal weight adult commercially available phantoms into obese phantoms.

These results are in line with those of previous studies, which have reported an increase in total lean mass along with the total fat mass in obese populations using the same cross-sectional approach but a different measurement instrument (Forbes, 1987, Gray and Bauer, 1991, Broyles et al., 2011).

In the current study, the sample size was bigger than that which has been reported in previous studies, 264 compared to 164 and 104, respectively (Forbes, 1987, Gray and Bauer, 1991). It also considered healthy patients only, as certain diseases and endocrine malfunction could alter the fat and /or lean mass (Leenders et al., 2013, Bhasin et al., 1997, Lamberts et al., 1997).

The current study eliminated the number of underweight participants; two only, while in Forbes's study there were twelve with anorexia nervosa, and in Broyles and colleagues study there were a small number of underweight participants, but no exact number revealed (Broyles et al., 2011). The method used in Forbes's study, based on potassium (40K counting), assumes the potassium content of FFM is constant; this might be true for normal weight individuals, but in the obese, the hydration status is different (Das, 2005) and hence the DXA scan is superior to 40K, and less affected by the hydration status (Frisard et al., 2005). In Gray and Bauer's study (1991), two methods of body composition measurement; underwater weighing and body-water determination, were used which give their result great value when the procedure is conducted in optimal conditions. However, despite the high accuracy of the underwater weighing method, it is still conditional on participant performance (Duren et al., 2008). It is specifically challenging with obese children as submerging completely under water is needed,(Duren et al., 2008).In the Gray and Bauer study, the mean BMI in male and female was 31.9 and 34.7 respectively, which indicates they

had obese subjects in their sample but did not explain how they overcame the challenge of submerging in the water tank. In terms of total body water method, it is considered to be of high accuracy when careful attention is paid to patient preparation especially when used in conjunction with other measures (Schoeller and Buchholz, 2005). This jeopardises the accuracy of the Gary and Bauer study since some of their subjects had had a light breakfast prior to the procedure in the late afternoon. Since the Gray and Bauer samples did not include malnourished subjects, they concluded that the link between FM and LBM was linear and they attributed the curvilinear result of Forbes to the inclusion of twelve subjects with anorexia nervosa. Forbes's result was extended to male participants and revised by Broyles and colleagues (Broyles et al., 2011). Despite the large sample, around five thousand, they were restricted in age to between 18-60 years. The main objective of Broyles and colleagues' study was to examine the consistency of Forbes model across different ethnic and gender population. For this reason, the researchers have adjusted the BMI in their sample with BMI ranges in Forbes study. As a result of such adjustment, the slope of the relationship between FM-LBM in both studies did not vary, 9.2 and 10.4.

Despite the fact the ANOVA results seen in Table 19, show significant differences ($p < 0.001$) in age between the first fat percentage groups (fat%,30) and the remaining groups. This could indicate that the increase in LBM is age related but not FM as these two factors affect the LBM proportionally. However, the difference was only between the first fat percentage group and the remaining groups only. While there is no significant difference between the remaining fat percentage groups, the trend of correlations between LBM and FM is positive, this indicates a strong relationship between LBM and FM. Additionally, the correlations between age and LBM across different regions and BMI groups, Table 21, show very low correlations in trunk and abdomen in the overweight BMI group, and mostly no correlation across other subdivision groups. This emphasis on the LBM increase in this cohort is most likely attributed to the FM.

The positive changes in LBM along with FM could be explained by the fact that extra muscle is needed to carry the excess fat mass (Kyle et al., 2001). Also,

the mass of the kidney, pancreas, heart and liver could also contribute to the result (Naeye and Roode, 1970). This is due to the fact that obesity is not just an increase of the number of fat cells but also the size of the fat cell (Spalding et al., 2008). However, the increase in LM is believed to be related mainly to the skeletal muscle (Rice et al., 1999, Janssen and Ross, 1999).

Although the results show a trend for LM to increase with increasing BMI, the relationship based on fat percentage groups was typically greater than the relation based on BMI. This is due to the limitation of BMI in differentiating between FM and LBM. As shown in Figure 11, there are participants placed in the group of normal and overweight groups, while they are obese based on the fat percentage, which is 30% in women. It means, there are participants in high BMI group who have less FM and more LBM, and the opposite is true. In theory, the fat percentage is more accurate in predicting lean mass, but in clinical practice, BMI is the only reasonable measure available to the radiographer when patients present to the medical imaging department for an imaging procedure. It is not possible to scan every patient using a DXA scanner to find out the fat percentage and based on that the lean mass is calculated to determine the right exposure factors on an individual basis. Although other technique can be implemented, such as bioelectrical impedance to calculate the fat percentage in practice this is far beyond the capability and practicability of the medical imaging department.

These results can be taken into account when imaging obese patients as lean and fat tissues attenuate x-ray photons differently. They should also be considered when building a physical or voxel phantom for the purpose of dosimetry or image quality assessment. A number of voxel phantoms, (Cassola et al., 2011, Broggio et al., 2011, Ding et al., 2012), were built to mimic obese patients, but none has considered the increase of lean mass with fat mass. Despite the fact that building a voxel phantom is very complicated, such changes can be adapted when changing phantom size.

4.8.1 Limitations:

The study has several limitations, most noticeably is the single participant gender. This means the relationship between FM and LBM could be different in

males as the fat and lean mass are different to females (Gallagher et al., 2000). Also, since the DXA scans were conducted while the participants were lying down, this means that the models of abdominal fat can be applied to phantoms built for the purpose of dose optimisation in the supine position only. This is due to the dropped fat in the erect position that might alter the amount of fat. It is also limited by the absence of various ethnicity groups, as the dominant ethnicity of participants is Caucasian.

4.9 Conclusion:

The current study demonstrates the body composition changes in obese populations. It shows an agreement with previous studies in demonstrating the increase in FM along with LBM.

The current study concluded that there was an increase in LBM along with FM. The link between the two tissues is higher when accounting for the fat percentage rather than for the BMI. It produces different FM and LBM prediction models that can be used by researcher when modifying normal-weight atom phantoms into obese ones. This can be used in both physical and computational phantoms construction. Models predicting the FM and LBM in abdominal region will be used in the next study in order to build different phantoms with different BMI values for dose optimisation purposes.

The result of this study will help to improve the construction of obese phantoms, both physical and computerised phantoms, by using the different prediction models to build a representative phantom.

5 Chapter 5: Phantom construction

5.1 Introduction:

Based on the conclusion of the previous chapter (Chapter 4), it is clear that the fat is not the only body component that increases along with the BMI, the lean tissue increases as well. Hence, the current chapter will consider construction of obese phantoms that consider body composition changes as described in the previous chapter.

The reader will be introduced to the topic of the phantom, with brief classification and basic principles of different phantom categories. Examples of previous studies that have incorporated obese phantom models will also be discussed.

5.1.1 Overall aim

To construct obese phantoms for dose optimisation purposes

5.1.2 Objectives

- To fabricate and validate fat and lean tissue-equivalent substitutes that can be used to build reusable obese phantoms
- To construct obese phantoms that account for fat and lean changes in order to mimic different body size

5.2 Background to phantoms

This chapter will outline the development of a phantom to mimic obesity using stable and pliable materials which provide an analogue of fat and lean tissue. In the medical dictionary, a phantom can be defined as a model that represents a body or body part for the purpose of simulating the in vivo effects of radiation on tissue (Miller-Keane, 2003b). The ICRU has considered any volume of tissue substitutes as a phantom when used to simulate radiation interactions (White et al., 1989). Phantoms have been used in medical physics since scientists realized the harmful nature of ionising radiation.

The topic of phantoms is very broad and has been the interest of medical physicists, biologists and researchers since the early days of ionising radiation discovery. Hence, covering the full phantom topic is beyond the scope of this

chapter but rather, the reader will be introduced to the topic with some most common examples of types of phantoms and their uses in radiology.

In the next section, types of phantoms used in medical imaging will be discussed briefly with regards to diagnostic radiography and projection radiography in particular.

5.2.1 Types of phantom uses in radiology (Ionising radiation):

Phantoms have been used in radiology for different purposes: radiation dosimetry, image quality and quality assurance (QA) investigations of medical imaging devices. The design, as well as the composition of a phantom, is heavily dependent on the purpose of the phantom. This includes the phantom use for either dosimetry, or image quality assessment and the energy of the radiation that will be used, keV as in diagnostic application or MeV as in therapeutic applications (White et al., 1989). Tissue equivalent substitutes which mimic the radiological and physical properties of human tissue under a certain radiation energy range might not mimic them under higher or lower radiation beam energy. Hence, different phantoms have been developed for the same purpose but for different imaging modalities.

This section will include some examples of each category and will summarise the main principle behind each type and its advantages and limitations. It will focus mainly on phantoms used in diagnostic applications. Due to the large numbers and types of commercially available phantoms that are already used in radiography, only the most commonly used phantoms will be included.

5.2.1.1 Radiation dosimetry phantom:

As named, this category of phantoms is used mainly to measure the dose at certain points of interest. Placing a patient in an ionising radiation main beam for radiation dose measurement is not possible both ethically and morally, while inserting dosimeters inside the patient is even more impracticable, hence, this type of phantom is used. Dosimetry phantoms can be classified into two main types, water and non-water based (Hill et al., 2008). Water based phantoms mainly consist of a tank of water usually 30 x 30 x 30 cm or larger (Podgorsak, 2005). Inside the tank, there is a water subsystem consisting of reservoir, pump

and transfer line. This type of phantom is considered to be the first attempt of dosimetry phantom construction and still used due to its simplicity (Podgorsak, 2005). It also allows an infinite number of dosimetry locations within its confines. They have been used extensively in radiography research (Huda and Gkanatsios, 1998, Baker, 2017, Longo et al., 2018). However, for comparison and research purposes, accurate replication of dose measurements using a water tank is limited due to impracticable reproducibility of dosimeter positioning. Additionally, in order to correctly position the dosimeter, a 3D scanning system is needed which adds more requirement to the water tank phantom system. Along with these required tools, setting up a water phantom is a time consuming and laborious process. Moreover, some TLDs cannot be used in water tanks; a solid dosimeter can be used but has to be waterproofed.

Moreover, the composition of a human body is heterogeneous and not identically represented by a water phantom. Hence, new non-water based generations of dosimeter phantoms have been introduced, in order to fulfil the needs for dose measurements and overcome the limitation of water based phantoms. These types of phantom started with simple materials, such as poly(methyl methacrylate) which is also called PMMA or acrylic (ICRU, 1989, Hill et al., 2008). However, over time, these materials exhibit changes as results of radiation exposure. Additionally, their composition is not identical to water or the desired human tissue properties (Hill et al., 2008). Hence, improved versions of these types of phantoms have been engineered in the form of stacks of plastic that mimic the physical and radiological properties of different tissues. For instance, Virtual Water™, Gammex Solid Water™, CIRS Plastic Water™ and Solid Water® (Schoenfeld et al., 2017, Van Asselen et al., 2017).

5.2.1.2 Quality control phantoms:

These types of phantoms are used primarily for acceptance and quality control (QC) tests. They are made of materials that absorb and scatter radiation in a similar way to human body tissues. Various phantoms have been developed to test different functions (for example, step wedge, line resolution and contrast detailed phantoms). Special requirements need to be met for these types of phantoms. These include the phantom's materials and thickness, which should

mimic human radiation absorption and scattering properties. Phantoms need to be of a practicable size to be used in clinical settings. Examples of these phantoms are REX X-ray Test phantom (PTW, Germany), 07-646 Duke Phantom (Nuclear associates, USA) and CIRS ACR accreditation radiography/fluoroscopy QA phantom.

Despite the use of these types of phantoms mainly for QC purposes, researchers have used them in dose optimisation, utilising their physical metrics to assess image quality (Mackenzie et al., 2016, Andria et al., 2016, Gislason-Lee et al., 2015). However, they are limited to assessing physical measurements such as contrast, signal-to-noise ratio and sharpness, which are at the lowest level of ambition in image quality assessment (Tingberg, 2000).

5.2.1.3 Imaging phantoms:

In this category of phantom, the purpose is more to test the image quality than radiation dose measurement. In the literature, there are numerous types of phantoms that have been used to fulfil this purpose. However, since dose optimisation research usually considers radiation dose and image quality, some dosimetry phantoms have been used for both dosimetry and image quality assessment. These include the RANDO[®] (The Phantom Laboratory, Salem, NY) and ATOM[®] (Computerized Imaging Reference Systems, Norfolk, VA) phantoms. These phantoms are sectioned into 2.5 cm slices and have holes to accommodate TLDs for dosimetry purposes. Despite the fact that these phantoms are not the best for image quality assessment since they are not identical to human tissues, they have been used extensively in previous studies reported in the literature e.g. (Ali et al., 2015, Manninen et al., 2014, Hampel and Pascoal, 2018).

Other phantoms are commercially produced for image quality research purposes and have additional human structures such as kidneys, liver and colon. These include Kyoto N1 Lungman (Kyoto Kagaku, Japan), RS-113T anthropometric pelvis phantom (Radiology Support Devices, Long Beach, CA) as torso only phantoms, and Kyoto PBU-50 (Kyoto Kagaku, Japan) as a full body phantom.

These phantoms have advantages of replicating human body structures and providing more details that can be used to assess the image quality using the European Image Quality (CEC, 1996). However, all physical phantoms that are currently available are demonstrative of average normal weight size patients.

5.2.2 Phantoms used in similar studies:

Due to the high prevalence of obesity and the challenges it poses to the management and assessment of patients in radiological departments, many studies have been conducted in an attempt to optimise the dose and image quality especially in computed tomography. Due to the limited availability of commercial phantoms representing obese patients, different studies used different approaches to achieve the goal of dose optimisation in obese patients. Table 26 outlines ten examples of options and these will be discussed in the next section with regards to their advantages and limitations.

Table 26 List of examples of previous studies and the approaches used to fabricate obese phantoms.

n	Authors name	modality	Aim	Phantom	thickness	
1	(Meinel et al., 2014)	Dual – energy coronary angiography	CT	To assess of tube potential on image quality and radiation dose.	Pseudo-anthropometric thoracic phantom (QRM, Forchheim, Germany) + STER (Unknown source)	QRM thoracic phantom: lateral access: 30 cm Anteroposterior access: 20 cm. Soft-tissue equivalent ring: 5 cm. Maximum QRM + STER thickness: 25 cm
2	(Euler et al., 2015)	Abdominal scan	CT	To assess image quality of obese abdominal CT using integrated circuit (IC) and conventional detectors.	Pseudo-liver phantom (QRM, Moehrendorf, Germany) inserted in a water-filled plastic cylinder	Liver phantom inserted inside the water-filled cylinder: 40 cm.
3	(Morsbach et al., 2014)	Abdominal scan	CT	To assess the effects of IC detector for abdominal CT on image quality.	Pseudo-anthropometric abdominal phantom (QRM-DEP-002, QRM) + Two STER + one FTER	QRM abdominal phantom : 20 x 30 cm With one STER: 25 x 35 cm With two STER: 30 x 40 cm With two STER and FTER: 50 x 60 cm

4	(Schindera et al., 2014)	Abdominal CT scan	To assess the impact of noise reduction technique on image quality, radiation in abdominal CT for obese patients.	Pseudo-liver phantom (QRM, Moehrendorf, Germany) + two FTER (Unknown source)	Liver phantom: 15 cm. Liver phantom inserted the first FTER: 30 cm Liver phantom inside the two FTER: 40 cm
5	(Al-Murshedi et al., 2019)	Projection radiography	To assess the effects of obesity on image quality, radiation dose and acquisition parameters in chest radiograph	Lungman adult chest phantom (Kyoto Kagaku, Japan) + two soft tissue equivalent plate	Lungman AP acces: Unknown Soft tissue plates: 6 cm
6	(Pina et al., 2009)	Projection radiography	To assess image quality	Acrylic plates	Based on examined part. For pelvis: 20 cm max thickness of acrylic represent 30 cm patient thickness

7	(Zheng et al., 2017)	Projection radiography and CT scan	To assess the obesity effects on the exponent of the power law relating dose to x-ray tube potential	Two Standard PMMA CT dose phantom	Head phantom: 16 cm (representing small size) Body phantom: 32 cm (representing large size patient)
8	(Alzyoud et al., 2018)	Projection radiography	To assess the impact of body thickness on image quality, effective dose and to identify the optimum exposure parameters	RS-113T anthropometric pelvis phantom (Radiology Support Devices, CA) + commercial lard	Maximum thickness of lard used: 16 cm RS-113T thickness: unknown
9	(Ching et al., 2015a)	Projection radiography	To compare the accuracy of four systems to predict the required mAs for pelvic radiography	Kyoto abdomen-pelvis anthropometric phantom (Kyoto Kagaku Co. Ltd; Kyoto, Japan) + pork belly	Kyoto phantom: 18 cm Kyoto phantom + pork belly: 21.5 cm

10	(Wang et al., 2013)	Abdominal scan	CT	To assess the radiation dose in obese and non-obese adult	ATOM phantom 701-D (CIRS, USA) + Two FTER	ATOM phantom: unknown FTER: 4 cm each
----	---------------------	----------------	----	-----------------------------------------------------------	-------------------------------------------	------------------------------------------

STER: Soft tissue equivalent ring
FTER: fat tissue equivalent ring

From Table 26, it can be seen that different studies have used different materials and designs to tackle the issue of dose optimisation and image quality in this group of patients. Studies number; 1, 3, 5 and 10 have used normal weight anthropometric phantoms, but with the similar idea of adding fat or soft tissue rings to extend the thickness of the anthropometric phantoms to represent obese patients. These FTER and LTER used in these studies are verified to have similar pixel density, Hounsfield Unit (HU), of fat and lean and they are commercially available. In study number 10, the FTER used had 22 cm width each, this width will limit the use of these materials to small body parts examinations such as extremities but not in large area procedures such as abdomen, lumbar spine and pelvis. If these rings were to be used in the abdominal area, the two FTER would have to be wrapped around the phantom next to each other to extend the normal weight phantom by 8 cm. Hence, fat and soft-tissue rings are good options if available. However, due to the cost of these materials, it was not possible to use them in the current project.

In studies number 2, 4, 6 and 7, much cheaper materials have been used to represent obese patients; PMMA. Despite the cost effectiveness of these materials, their representation of human tissue is limited. Additionally, their use in dosimetry research in low energy procedures, <120 keV, is questionable (Jones et al., 2003). In study number 7, the researcher used readily available and inexpensive cylinders of Perspex with holes in five different regions for dosimetry purposes. Two cylinders were used to represent small (26 cm diameter) and large (32 cm diameter) patients. However, the diameter of these cylinders might be representative to an obese patient's abdomen anteroposterior diameter but it is much smaller than the collimation size used in abdomen radiography. This will reduce the scattered radiation, which is the main source of noise when imaging obese patients, and subsequently will impact on the applicability of the result on clinical practice.

In the studies 8 and 9, animal-based materials have been used to extend average size anthropometric phantoms into obese models. In both studies, the animal-based fat substitutes were added on top of the anthropometric phantom to conduct image quality assessment. Due to the bony structure embedded into

the anthropometric phantom, this will make assessing the image quality subjectively possible. However, fat positioning, i.e anteriorly or posteriorly, will have an impact on image quality as well as the absorbed dose. This is based on the results of Yanch and colleagues' study based on Monte Carlo simulation where fat layers were added to a stylized phantom to assess the effects of fat thickness and orientation on image quality and dose (Yanch et al., 2009). They found that fat orientation impacts heavily on organ dose as well as image quality. Hence, the results of studies 8 and 9 might not be representative of the scenario in clinical practice as the fat was added only to the anterior aspect of the phantom. Additionally, the LBM was not taken into account in these two studies which has been proved to increase along with the FM.

In order to simulate obese patients with different thickness, a large amount of animal fat is needed, this subsequently means a cold-storage facility is needed as well in order to store and reuse the animal fat. This will be impracticable especially if lard or pork belly tissues were used to wrap around the anthropometric phantom, as large amounts would be needed.

5.2.3 Phantom requirements

Based on the literature described above, the phantom intended to be used had to fulfil the following requirements:

- 1- The phantom must have similar absorption and scattering properties to human tissue in diagnostic x-ray range, between 60 and 140 KeV.
- 2- The phantom must facilitate visual image quality assessment, which means the phantom has to be heterogeneous and have bony structures.
- 3- The materials used should be easy and inexpensive to fabricate.
- 4- The fabrication and construction of the tissue equivalent substitutes must be manageable based on the lab facility that is available to the researcher.
- 5- Both fat and lean tissue should be fabricated using the same materials in order to reduce the cost and time.
- 6- The final product should be reusable and easy to store.

With these criteria in consideration, different materials used in the literature were studied in order to select the best option that would fulfil the requirements of this project. Urethane based materials have been used in the literature and they were deemed to be a good option for different reasons (Winslow et al., 2009). Firstly, urethane based materials are fairly cheap and accessible and doesn't need highly equipped lab in order to fabricate them. Additionally, they are more stable and do not degrade over time and loss their radiological properties (Winslow et al., 2009). Moreover, they last for long time which will facilitate more dose optimisation research with regards to obese patients.

5.3 Methods and materials:

Despite the fact that the materials used in this study have already been described in the literature (Winslow et al., 2009), due to the variation in physical and radiological properties between different studies (Kasraie et al., 2018, Nute, 2015), the validation stage was deemed to be essential to ensure the reproducibility of the materials. Additionally, different technical challenges reported in other studies which might impact on the appropriateness of the materials for this project including insufficient dissolving of the additives to the main component resulting in producing a layer of additives at the bottom of the produced slabs (Hall, 2011). Hence, this study was conducted in two phases:

- Tissue equivalent substitutes trial fabrication and validation
- Final phantom construction

Phase one will be described first followed by its validation results. Following that, the final phantom construction will be described and its result will be presented.

5.3.1 Tissue equivalent substitutes trial fabrication:

5.3.1.1 Lean-tissue equivalent substitutes (LTES):

A urethane-based compound was used as the base in the fabrication of the LTES. The material is called PMC 121/30 Dry, and it was sourced from Smooth-On Company in the USA (Smooth-On, Inc.). This material when cured produces a flexible urethane rubber. It is a liquid based material and consists of two-parts; part (A) the hardener, and part (B) the rubber. Smooth-On provides different quantities of this material; 0.9 kg, 7.26 kg, 36.29 kg and 399.17 kg of each part for a set. Since the aim of this stage was to fabricate a trial sample of LTES for validation purposes only, the trial package, containing 0.91 kg of each part A and B, was ordered. This is due to the fact that these materials have a short shelf life and when opened must be used as soon as possible; otherwise, their chemical features will degrade. The package was stored as advised by the provider in a dry and a well ventilated area, with a temperature between 18 and 23 C°. The density of PMC 121/30 is about 1.01 g/cm³. This figure of density is less than the density of human muscle, which is 1.04-1.05 g/cm³ (ICRU, 1989,

Berger, 2005). For this reason, the density had to be increased to match the muscle density value. Calcium carbonate (CaCO_3) was used as an additive and in 2.8 % of the PMC materials weight. The reason for adding this type of material specifically is due its high density value (2.71 g/cm^3). CaCO_3 was sourced from Fisher Scientific UK LTD, and it came with 98% purity in a powder format.

5.3.1.2 Fat Tissue Equivalent Substitute (FTES):

The PMC 121/30 Dry was also used in the fabrication of the FTES. However, as its density is higher than fat density, which is $0.92\text{-}0.95 \text{ g/cm}^3$ (ICRU, 1989, Berger, 2005), a phenolic microsphere, in a form of powder, was used (2% by the weight of the PMC 121/30 Dry) as an additive due to its light density which ranges between 0.20 and 0.80 g/cm^3 . Two kilograms of this material was sourced from Azelis (www.azelis.com). As this material is highly sensitive to humidity and moisture, they were kept sealed, unless used, and placed in a very well ventilated area.

5.3.2 Trial sample moulds:

In order to fabricate a trial sample of LTES and FTES, and for its purpose, the moulds had to have special features to enhance the shape and size of the final products as well as simplify and save time and cost of the process. The first feature is to have a regular shape, i.e square or rectangle. The reason behind this is to simplify the density measurement of the final product using the standard equation of density = mass / volume rather than the sophisticated Archimedes' principle. The reason attributed to this is the lack of required facilities to calculate the density using the Archimede's method. Additionally, immersing the FTES sample in the water was challenging as reported by Winslow and colleagues due to the small density of FTES compared to water (Winslow et al., 2009). Additionally, the mould has to be made of glass, metal or hard plastic in order to reduce the cost by not using a sealing and release agent, especially in this stage. Finally, the moulds had to be of translucent materials in order to visualise the mixture when poured into the mould and identify the level of the mix inside the moulds to ensure the height of the final product is of the same to reduce the volume measurement errors.

Based on these features, and after a search for the type of moulds with the lowest cost possible, a makeup organizer that has six small rectangular drawers and made of Perspex was deemed to be the best choice. Each drawer had a dimension of 9.5 cm (width) x 12.4 cm (length) x 2 cm (depth). The product was sourced from eBay at a cost of £13.

5.3.3 Health and safety and pre fabrication process:

Due to the hazardous nature of PMC 121/30 dry materials, containing diisononyl-phthalate (5-15 % per weight) and toluene diisocyanate (<1 % per weight) in part (A) and diethyl-toluene diamine (1-5 % per weight) and phenyl-mercuric neodecanoate (0.2-0.25 % per weight) in part (B), precautionary measures had to be in place prior to the experiment commencing in order to comply with the health and safety regulation of the university. Firstly, the researcher attended a course on how to handle hazardous materials run by the university. Following that, a full laboratory induction was attended by the researcher in order to be familiar with the laboratory's facilities and health and safety regulations. Based on the success of these two steps, multiple meetings were set with the lab manager, health and safety officer who was one of the supervision team and the lab technicians to discuss the next process of filling the Control Of Substances Hazardous to Health (COSHH) forms for the experiments.

The Material Safety Data Sheet (MSDS) for all materials were read carefully and based on that and the preliminary protocol for the experiments, the COSHH forms were prepared and handed over to the lab manager for final approval. Once final approval was granted, the researcher started preparing for the fabrication.

As the final products needed in this stage were for validation purposes, the first COSHH form was prepared only for the trial experiments using very low amounts of the materials, Appendix 6.

5.3.4 Mixing process:

Due to the limited space inside the fume hood, where the fabrication process was taking place in compliance with the COSHH requirements, all materials

were kept ready in a bench next to the fume hood for easy access. To save money, a 500 ml cuisine measuring mug was sourced from local superstore, and used as a mixing pot. A stainless steel spatula was used for stirring the mix. In order to keep control of the process and to eliminate errors and contaminations, FTES and LTES were fabricated separately. Inside the fume hood, the bench scale, with maximum capacity of 6 kg and 0.2 g precision (WZ-10000-56 Cole-Parmer Symmetry, Cole-Parmer Scientific Experts, UK), spatula, the measuring mug and the mould were kept ready and wiped with clean dry tissue to eliminate humidity.

The first material fabricated was the FTES. In order to save the PMC materials in case the experiments needed to be repeated, 100 g of part (A) and 100 g of part (B) of the PMC 121/30 were used. The first step was to weigh the needed amount of the phenolic microspheres (4 g), which represent 2% of the 200 g of the PMC 121/30. A lab glass beaker was used to pour the needed phenolic microspheres inside. The beaker was then placed in the fume hood and covered with a paper. The reasons for weighing and covering the phenolic microspheres before the PMC 121/30, are to eliminate the contamination of the PMC, and also to avoid the phenolic microspheres from being airborne inside the fume hood as they have a very light weight. Part (B) had to be shaken and opened and the required quantity (100 g) was poured into the mixing mug. The mixing mug was then placed aside inside the fume hood in preparation for mixing, the phenolic microspheres were added and mixed with part (B) by hand for two minutes, using a wooden stirring stick sourced from the same supplier. The scale was then reset to zero with the mixing mug on top, and part (A) was then added to the mix. Since the hardener, part (A), is heavy in weight, it would sink in the mix when poured, which would have eliminated the researcher's control of this material if over-poured, hence, a 50cc syringe was used to add the required amount of part (A) to the mix. The mix was then stirred again by hand for another two minutes and then poured into the mould.

It was hard to pour all the mix into the mould due to its high viscosity; this was taken into account when preparing the LTES.

The preparation of the LTES was similar to that of the FTES apart from:

- The amount of PMC 121/30 used increased from 100 g of each part, A and B, to 130 g. this is to compensate the residual of the mix stuck to the mixing mug.
- The additive used in preparation of the LTES is the Calcium Carbonate (CaCO_3) with 2.8% of the PMC total amount, 7.2 g in this trial.

Both fabricated materials were left to dry in the fume hood for 16 hours. Both materials were peeled out of the moulds easily and did not need a release agent.

5.3.5 Validation process:

In order to compare the radiological interaction properties of the fabricated materials and the human tissues, the density, attenuation coefficient and Hounsfield unit (HU) were investigated for the FTES and LTES and compared to lard and Perspex. The reason for choosing lard and Perspex is their wide use in the literature to represent fat and lean tissues (Mooney and Thomas, 1998, Dance, 1990, Midgley et al., 2017, Alsleem and Davidson, 2015, Ikejimba et al., 2017, Cherif et al., 2018, Kiarashi et al., 2015).

5.3.5.1 Density:

The physical density of the FTES and LTES slabs was calculated using Equation 11

$$\rho = \frac{m}{v} \quad \text{Equation 11}$$

Where ρ is the physical density

m is the sample mass in g

v is the sample volume in cm^3

To measure the mass, the bench scale (WZ-10000-56 Cole-Parmer Symmetry, Cole-Parmer Scientific Experts, UK) was used to measure the mass of each samples. The mass of each slab was measured three times and the average mass calculated. The volume of the each slab was determined by measuring the dimensions of the slab using a Vernier calliper with accuracy of ± 0.02 mm

(#5416C- Forge Steel, China). The thickness of each slab was measured three times while changing the measuring site and the average thickness was considered in the volume calculation.

5.3.5.2 Attenuation coefficient:

In order to compare the radiological properties of the FTES and LTES with lard and Perspex, which had already been used extensively in the literature to mimic human fat and lean, a Black Piranha dosimeter (RTI Group, Sweden) was used with Siemens Multix Fusion Max x-ray generator (Siemens Healthcare, Germany) to measure the x-ray attenuation through each sample. The Piranha dosimeter was placed on the x-ray table while the FTES and LTES slab was placed on top of it. The distance between the source of the beam and the detector inside the Piranha dosimeter was set to 100 cm

The same was repeated for a Perspex slab with similar thickness to the LTES. For the FTES, lard was sourced from a local shop and sliced to match the thickness of the FTES slab. Each slab was exposed to multiple exposures with kVp ranged between 40 kVp and 120 kVp with 10 kVp intervals with fixed mAs, 5. Each exposure was repeated three times and the average exposure readings were used. To maintain constant tube outputs, there was a time gap of two minutes between each exposure. The beam was collimated to the size of the detector inside the Piranha dosimeter.

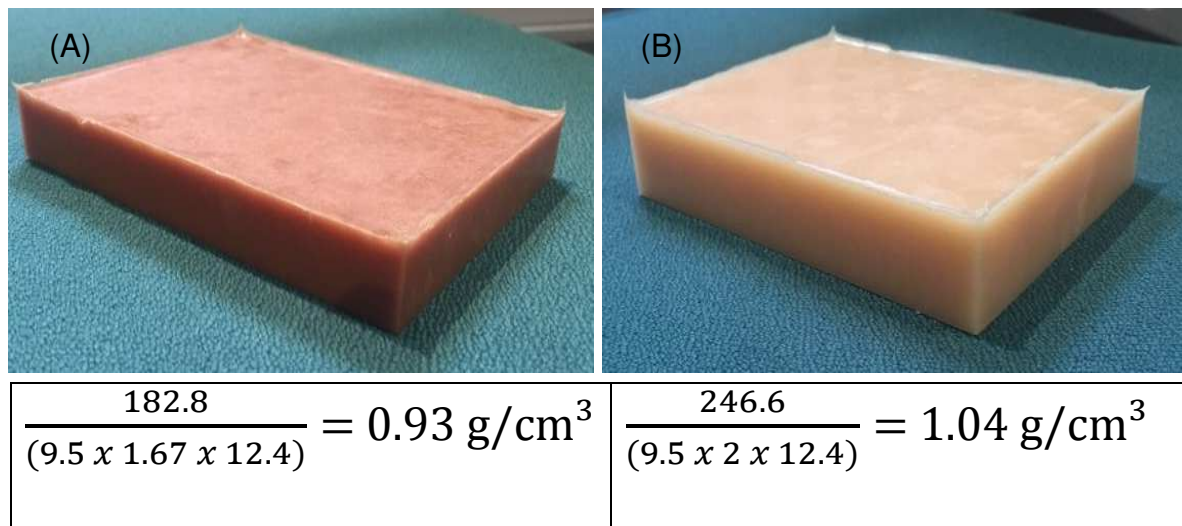
In order to test the consistency of radiological properties across each slab of FTES and LTES compared to the bench mark materials, Perspex and lard, the HU was tested using a CT scan (SOMATOM definition Edge- Siemens, Germany) with 4 kVp level; 80, 100, 120 and 140.

5.4 Validation results:

In this section, the result of the first trial FTES and LTES sample, which was built for validation purposes, will be presented.

5.4.1 Physical density:

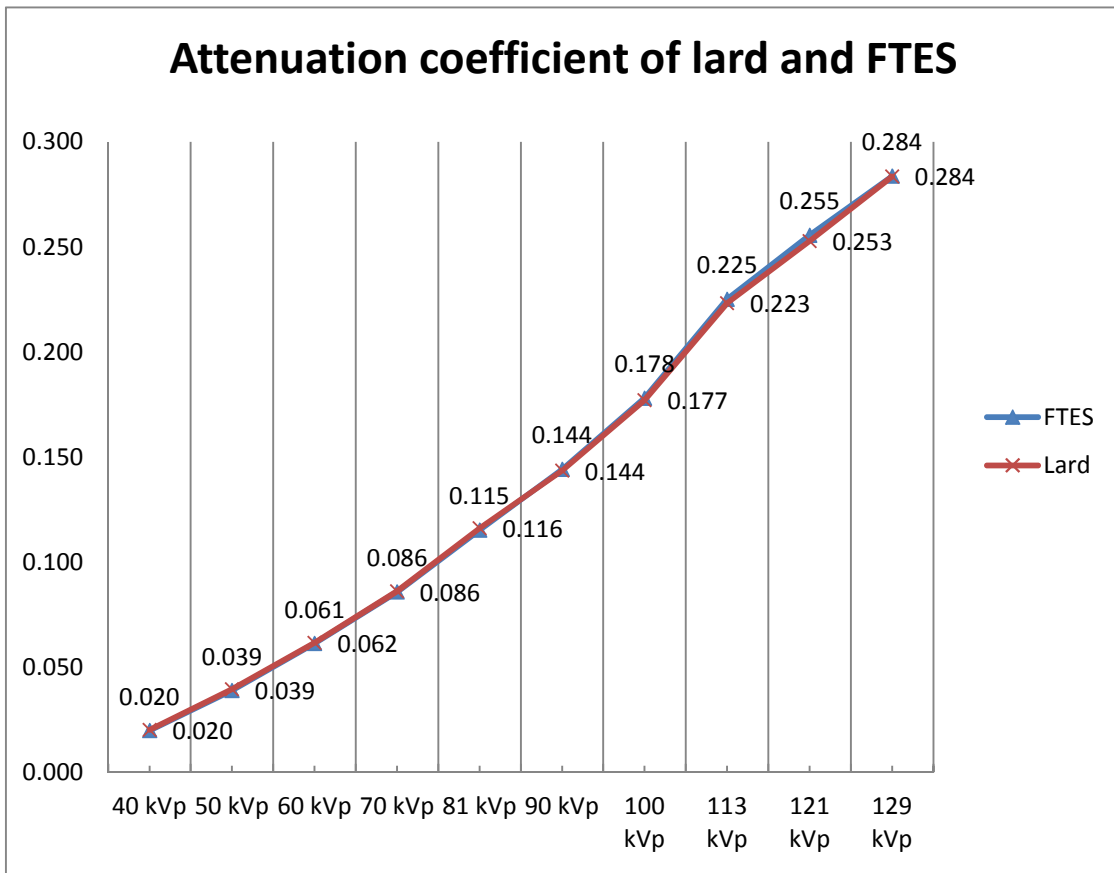
Figure 18 FTES (A) and LTES (B) trial sample and the physical density of each sample



As illustrated in Figure 18, the final product of FTES (A) and LTES (B) are fully cured and in a regular shapes that facilitate the physical density measurements. The thickness of LTES (B) is larger than the FTES (A) thickness due to the amount difference in the PMC 121/30 materials used in fabricating both samples as discussed in (5.3.4). As seen, the additives have dissolved efficiently through both samples as there is no sign of additives collection in either of the two products.

5.4.2 Attenuation coefficient:

Figure 19 FTES attenuation compared to lard (mGy)



As demonstrated in Figure 19, the attenuation coefficient of FTES is identical to lard, the bench mark material. As expected, the attenuation increased with the tube potential.

Figure 20 LTES attenuation compared to Perspex (mGy)

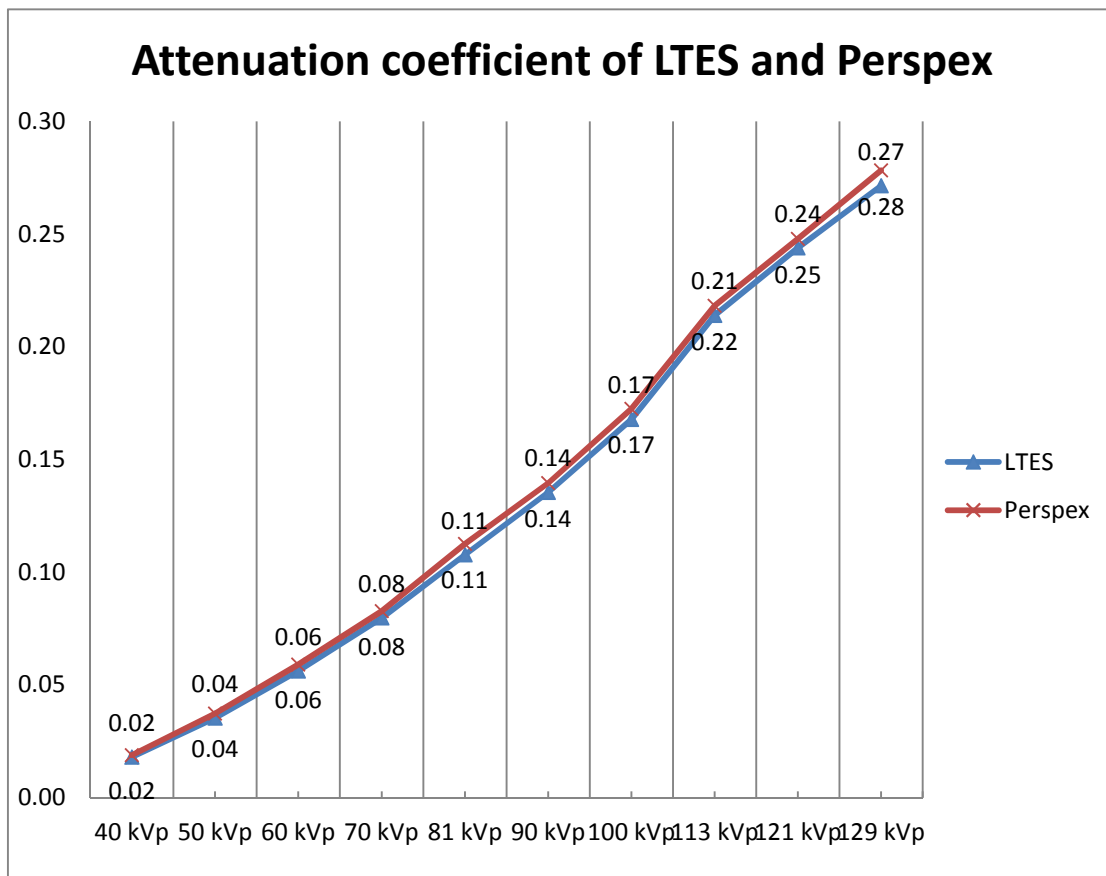


Figure 20 demonstrates the attenuation coefficient of the fabricated LTES compared to Perspex across different kVp levels. Both materials have a similar attenuation coefficient trend with slight difference increases along with the kVp.

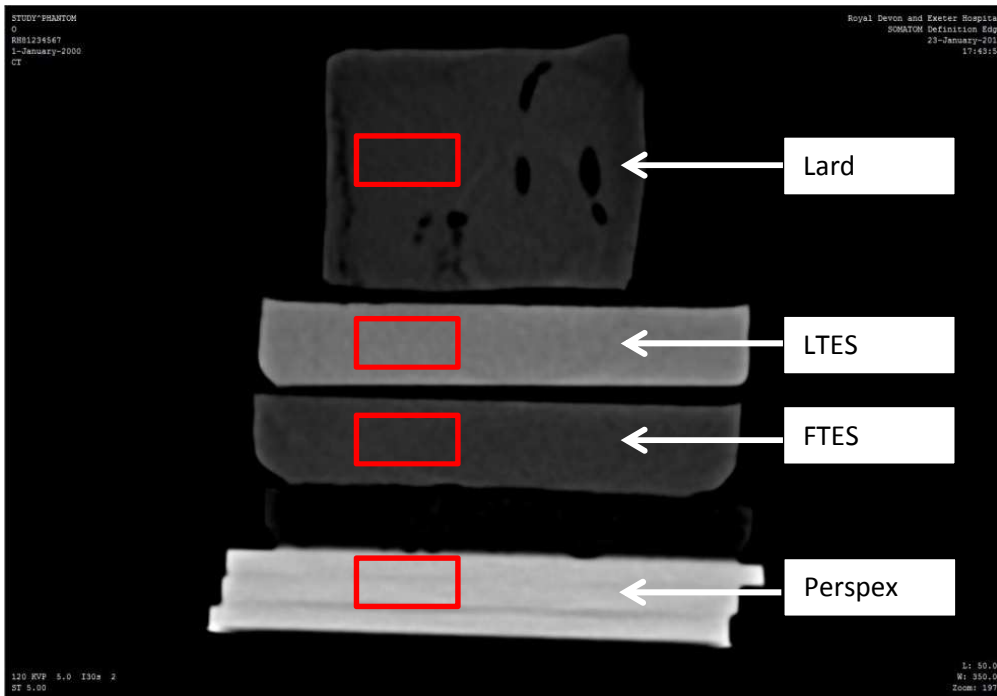
Table 27 Comparison of attenuation coefficient (mGy) difference percentage for LTES compared to Perspex, and FTES compared to lard across various kVp levels.

kVp	LTES	Perspex	%	FTES	Lard	%
40	0.018	0.019	-4.50	0.020	0.020	-1.13
50	0.035	0.037	-5.46	0.039	0.039	-1.33
60	0.056	0.059	-5.18	0.061	0.062	-0.66
70	0.080	0.083	-3.75	0.086	0.086	-0.26
81	0.108	0.113	-4.51	0.115	0.116	-0.81
90	0.136	0.140	-2.95	0.144	0.144	0.43
100	0.168	0.172	-2.80	0.178	0.177	0.56
113	0.214	0.218	-2.02	0.225	0.223	0.81
121	0.244	0.248	-1.68	0.255	0.253	1.07
129	0.271	0.278	-2.50	0.284	0.284	0.04

The fabricated FTES material demonstrated identical attenuation coefficient compared to lard across different kVp levels as shown in table 27. Similarly, the LTES attenuated x-ray identical to Perspex.

5.4.3 Hounsfield Unit (HU):

Figure 21 CT scan image for lard, LTES, FTES and Perspex



The fabricated FTES and LTES as well as the lard and Perspex were CT scanned. In Figure 21 the texture of each material can be seen clearly. The HU for each material was averaged across a 2 cm² area and the HU value for each material is presented in Table 28. All scans were conducted with the room temperature between 20°C and 23°C. The room has air conditioning to maintain room at a constant temperature. Despite the fact that the materials were not tested in different room temperature, which means their HU might change accordingly, the room temperature used during the scan is similar to room temperature used in clinical practice that is recommended by most x-ray vendor to save the system life.

Table 28 Hounsfield Unit (HU) results for fabricated and bench marking materials

	FTES	Lard	LTES	Perspex
80 kVp	-69.7 ± 4.49	-78.0 ± 6.16	34.3 ± 3.86	112 ± 8.0
100 kVp	-67.3 ± 2.86	-80.0 ± 4.02	31.3 ± 4.11	126 ± 2.1
120 kVp	-62.7 ± 1.69	-74.3 ± 2.05	29.7 ± 2.05	127.6 ± 3.0
140 kVp	-67.3 ± 4.49	-68.6 ± 4.78	24.7 ± 2.05	131.6 ± 2.4

The HU of FTES and lard are of similar values. However, the LTES's HU is different compared to the Perspex. The Perspex HU is above +100, which is in line with what has been reported in the literature (Reeves et al., 2012). The LTES is more of muscle representative rather than average soft tissue equivalent substitute.

5.5 Final phantom construction:

FTES and LTES fabricated using PMC 121/30 dry showed a promising agreement in radiological properties compared to the human fat and lean tissues as in the results section. Therefore, these materials were deemed to be suitable for the construction of FTES and LTES layers in order to modify a commercially available phantom already used in dose optimisation in obese phantoms.

5.5.1.1 Calculation stage:

As the aim of this project is to extend a commercially available phantom into a representative obese phantom, the KYOTO PBU-50 was used. The KYOTO PBU-50 phantom (KYOTO KAGAKU.co., LTD) is a full body anthropometric phantom with a synthetic skeleton, lung, liver, mediastinum and kidneys all embedded in the phantom original soft tissue substitute. This phantom has already been used in the literature in dose optimisation studies (Kim et al., 2013, Harbron, 2011, Morishima et al., 2016). The KYOTO phantom has a weight of 50 kg, and a height of 1.65 m. By calculating the BMI for the KYOTO phantom using the formula: $BMI = (\text{weight} / \text{height}^2)$, it has a BMI of 18.3 kg/m². The area of interest is the abdominal region, from the xiphoidal process to the pubic symphysis.

FM and LBM in the abdominal region were predicted using the equations developed by the researcher in Chapter (4), Equation 7 for abdominal FM and Equation 9 for the LBM.

As the DXA study showed no significant increase in LBM along with FM in a BMI group less than 30 kg/m², the LBM was kept the same for BMIs ≤ 30 kg/m².

In order to transform the KYOTO phantom into an obese model, layers of FTES and LTES needed to be wrapped around the abdominal region of the KYOTO phantom as the region of interest in this project. The visceral fat was thought to be far more difficult to fabricate as the phantom comes in a bulk with no possibility of insertion of any other materials as other phantom facilitates, LUNGMAN chest phantom for instance (Szczepura and Manning, 2016).

5.5.1.2 Mould design and laser cutting:

As the abdominal area of the KYOTO phantom has a surface to mimic that of human, moulds needed to be designed using a material that is easy and flexible to fabricate in order to mimic the phantom surface. The mould design needed to fit perfectly on top of the phantom in order to minimise the air gap between the phantom and the constructed FTES and LTES layers. Additionally, the shape of the final transformed phantom must have a shape similar to the abdominal area in the supine position.

To fulfil these two requirements, the material of the moulds had to be flexible in shaping, easy to craft, and strong enough to accommodate the mixed materials when poured in. A few options were available including; Perspex, wood and polystyrene. The Perspex was excluded for it is high cost, where 60 x 40 x 10 cm sheet of Perspex would cost roughly £26. Taking into account that the amount of sheets needed is large, the Perspex was considered a very expensive choice. Also, cutting the Perspex is laborious, would take longer in the laser cutting machine and cost more. Moreover, demoulding the urethane materials from the Perspex would need laser cutting again and the moulds will not be reusable. Despite that, the Perspex wouldn't need a sealing or release agent when pouring the urethane mix, however, it was deemed not to be the best choice that would suit the available technical and financial resources. The same applied to the wood. While a sheet of wood of the required size would cost around £5, the crafting of the wood is much more difficult than Perspex, as most laser cutting companies in the area don't have the facilities to cut wood, which produces more smoke under a laser beam and may damage the laser machine, therefore, a special laser cutting tool is needed. Both Perspex and wood are heavy and if 47 sheets were piled and filled with about 30 to 38 kg of FTES and LTES this may make it impossible to manage and will violate the manual handling health and safety rules. For these reasons, these two materials were excluded. The polystyrene was considered to be a good choice for its low cost, £1 a sheet, light weight and low laser cutting cost. However, different types of polystyrene are available online with different densities. To test the suitability of these materials when laser cut, 10 sheets were ordered from eBay seller (LONGVALLEY PACKAGING LTD). As the seller provides

different grades of polystyrene with density ranged between 10 to 30 g/ltr³, the sheets selected had an ultra-high density, 30 g/ltr³. This option had the highest density offered by the supplier and according to the laser cutting company operator, the higher the density the better at remaining still under the laser beam. Multiple square shapes were cut from two of the polystyrene sheets in order to test the durability of this material to a laser beam and how that might affect the cut accuracy. It showed good accuracy and did not melt at the edge; this indicated the suitability of ultra-high density polystyrene for this project.

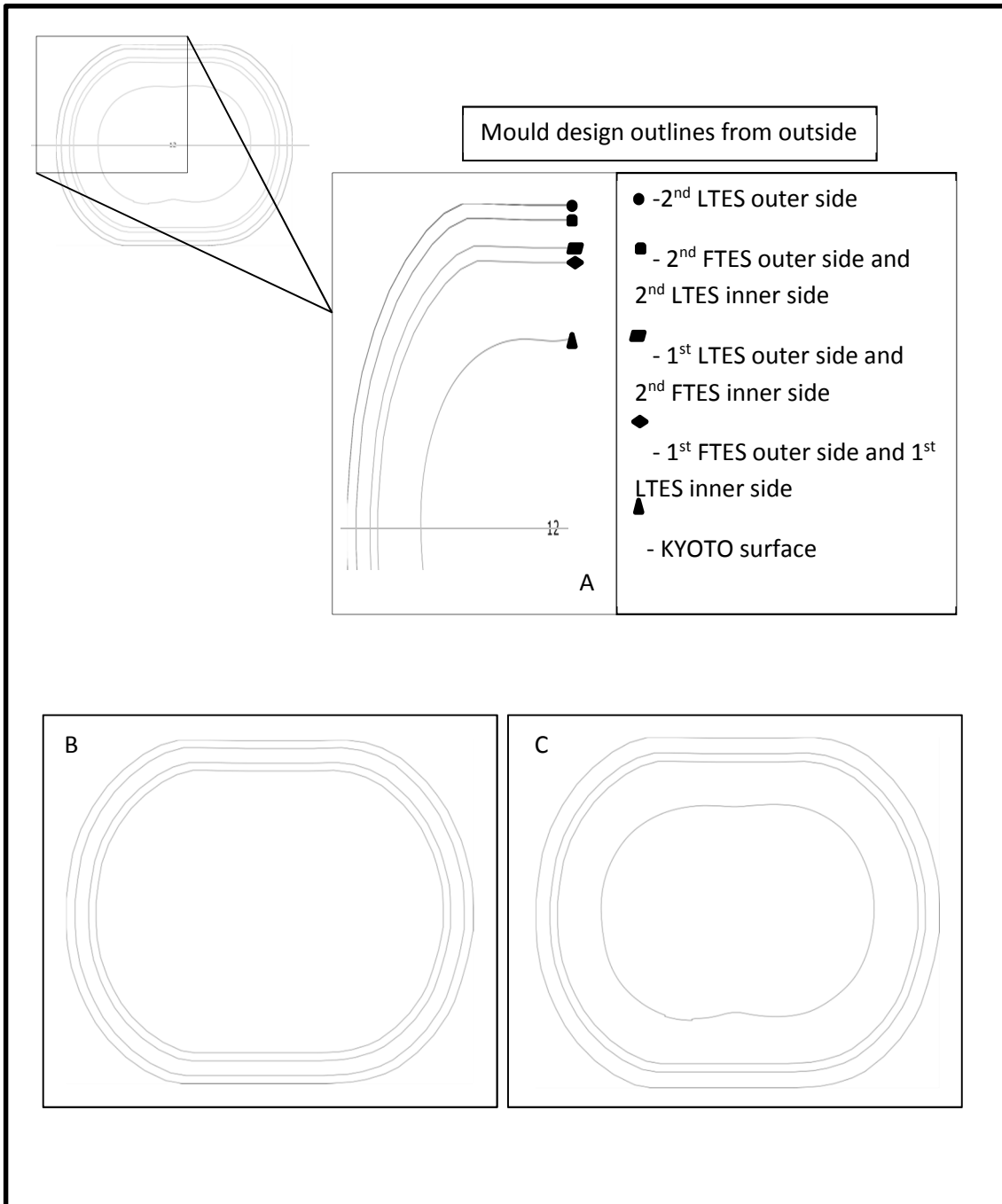
Once a decision was made regarding which materials to use to design the moulds, the second step was to design them. The KYOTO phantom, torso section, was CT scanned (64 Slices – GE VCT Scanner, GE Healthcare, USA) in order to have a 3D shape of the phantom. Images were then transferred into OsiriX Lite software (OsiriX Lite, osirix viewer) in order to reconstruct them into 10 mm thickness with interest in the region between the pubic symphysis and 2 cm above the xiphoidal process. Using 10mm slice thickness was chosen carefully for various reasons. First, to avoid losing some details of the phantom surface shape which would create the possibility of having some air gap between the fabricated FTES and the phantom. Secondly, as the polystyrene sheet will have the same thickness as the image, 10mm, this will eliminate the risk of the polystyrene melting when laser cut as the thicker the polystyrene the more time would be needed for the laser beam to cut the sheet.

In preparation for laser cutting, the outlines of the phantom had to be drawn slice by slice based on the CT images along with the extra layers of FTES and LTES that were intended to be added. In order to achieve that, Computer Aided Design (CAD) software (Inkscape 0.92, www.inkscape.org) was used. All CT images were imported into the CAD software in the correct order. Images were numbered and organised in five rows, each row contained 10 images, apart from the last row which contained seven images. A bitmap was auto-drawn around each image, as the interest here was to outline the shape of the KYOTO phantom in each slice. Once all images were transferred into a bitmap, a line was drawn in the middle of each row and the bitmaps in each row were centred to that line. The reason behind this is to ensure the bitmaps are divided into two equal half that will form the final moulds. The oval shape of the abdomen was

then bitmapped using a CT image of similar phantom reported by Martin and colleagues (Beeres M, 2015). Figure 22 illustrates the designs of the mould of FTES and LTES, while the dimension of each mould is illustrated in Figure 23.

The two sets of polystyrene sheets were then laser cut separately. Each set contained 47 sheets, numbered using holes cut in the left hand side corner in order to avoid confusion when stacked to form the final mould.

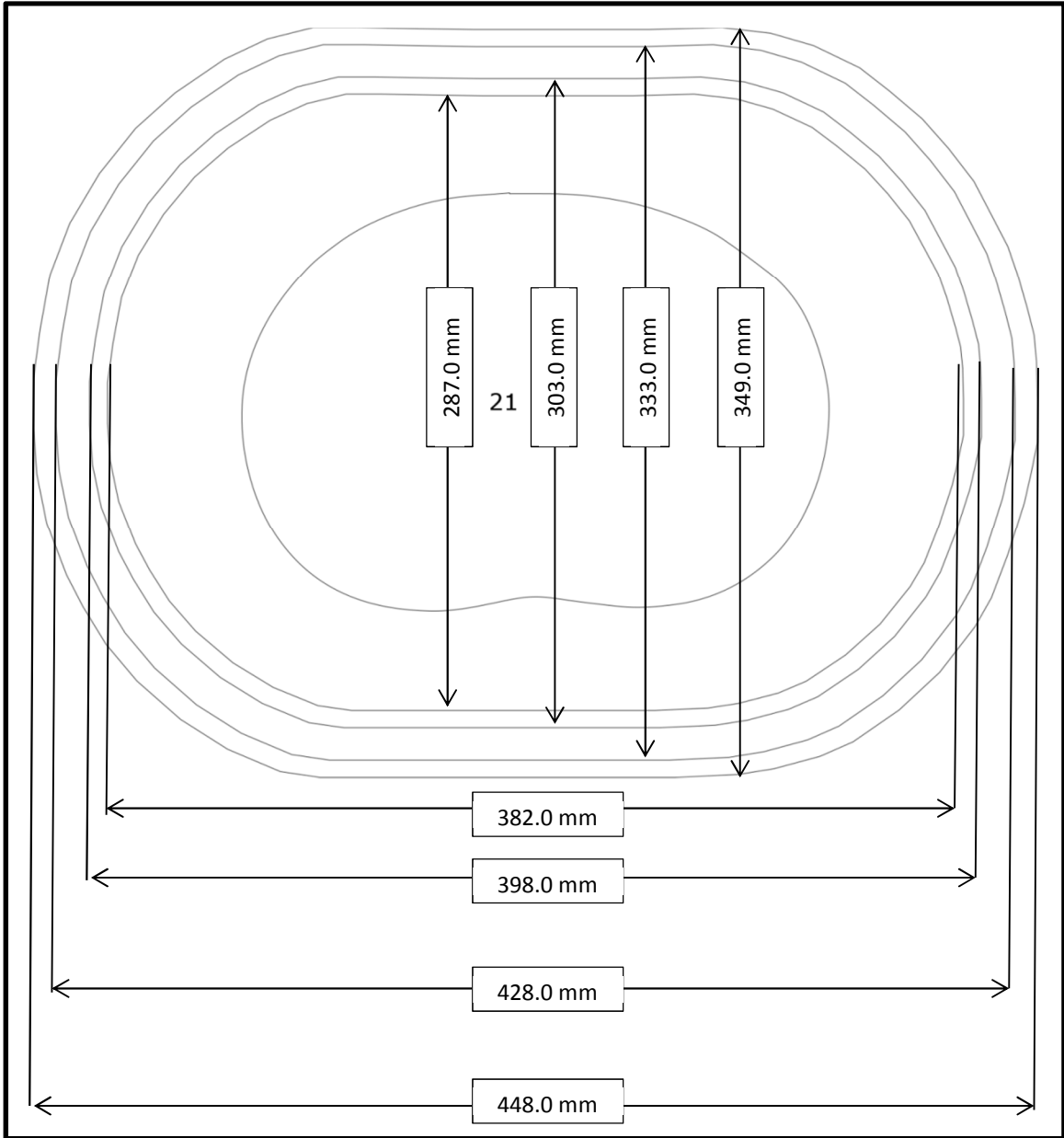
Figure 22 Mould's design cross cut (A) for LTES (B) and FTES (C) prior to laser cutting



A: a cross section for the final design of one slice before imported to the laser cutting machine

B: LTES mould design

Figure 23 Diameters of FTES and LTES final layers



5.5.1.3 Mould assembly and sealing:

For the FTES polystyrene set, packaging tape was used to seal the moulds. This was tested in the lab with a small amount of urethane mix, and it proved to be a good sealer and did not require a release agent to demould the materials after they had cured. As the space inside the two FTES moulds is very small, Figure 24, and it was very hard to insert the tape in and out when the 47 sheets were piled on top of each other. Hence, a set of 10 sheets were aligned together and sealed together at a time. After the 47 sheets were sealed in 10 sheets bulk, they were glued together using Poly(vinyl acetate) (PVA) with two uncut polystyrene sheet at the bottom to form the mould's base.

Figure 24 FTES sealed mould

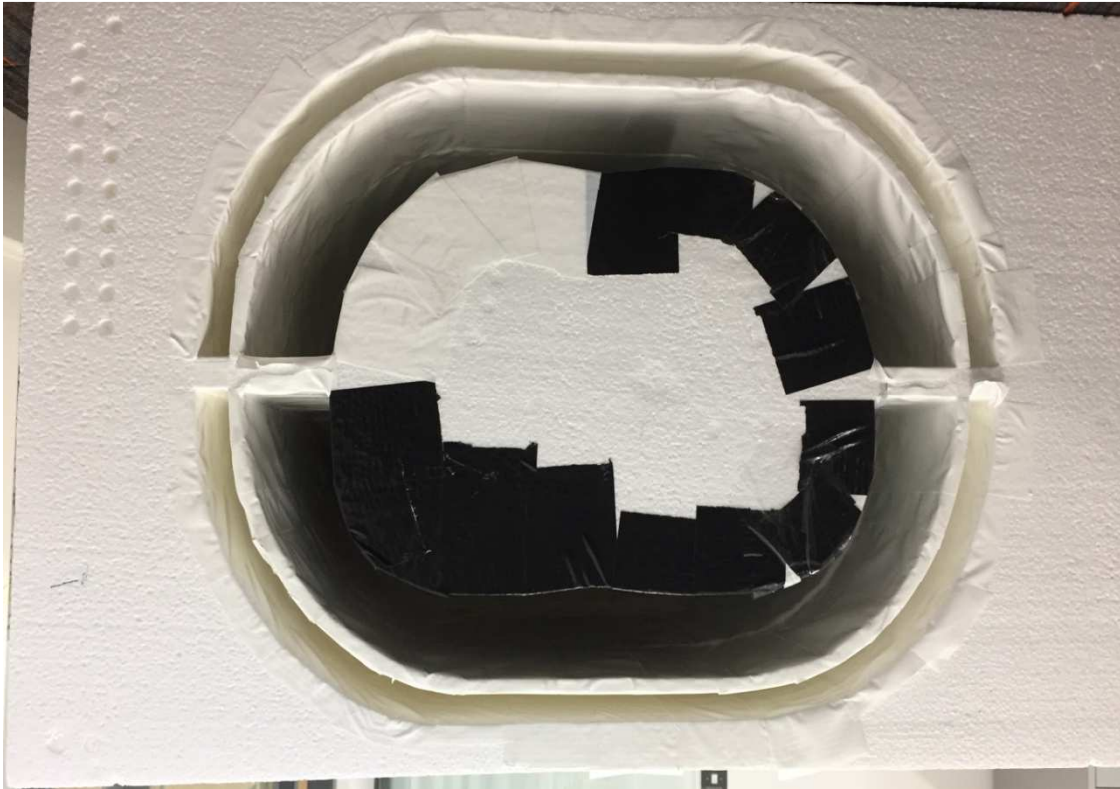


Figure 24 illustrates the FTES final mould after sealing with the packaging tape. As seen on the upper left hand side corner, laser cut holes have been used in order to number the polystyrene sheets in sequence to avoid confusion when combining all sheets together.

In the second set of polystyrene, which has LTES moulds, it was not possible to seal the moulds using the packaging tape as the moulds' spaces are very narrow and any attempt will impose a risk of breaking the separator between the two moulds, Figure 24. Hence, each sheet had to be sealed individually with PVA. In order to ensure a good seal, a second coat of PVA was applied once the first coat had dried. As the polystyrene is not a good absorber of liquid, especially the sheet used in this project as it has high density, this led to extended waiting time for the PVA to fully dry. After the PVA dried, the sheets were stacked on top of each other and glued using a PVA adhesive. The lower sheet was glued to double sheets of polystyrene that were not laser cut, this is to form the base of the moulds.

Figure 25 LTES sealed moulds

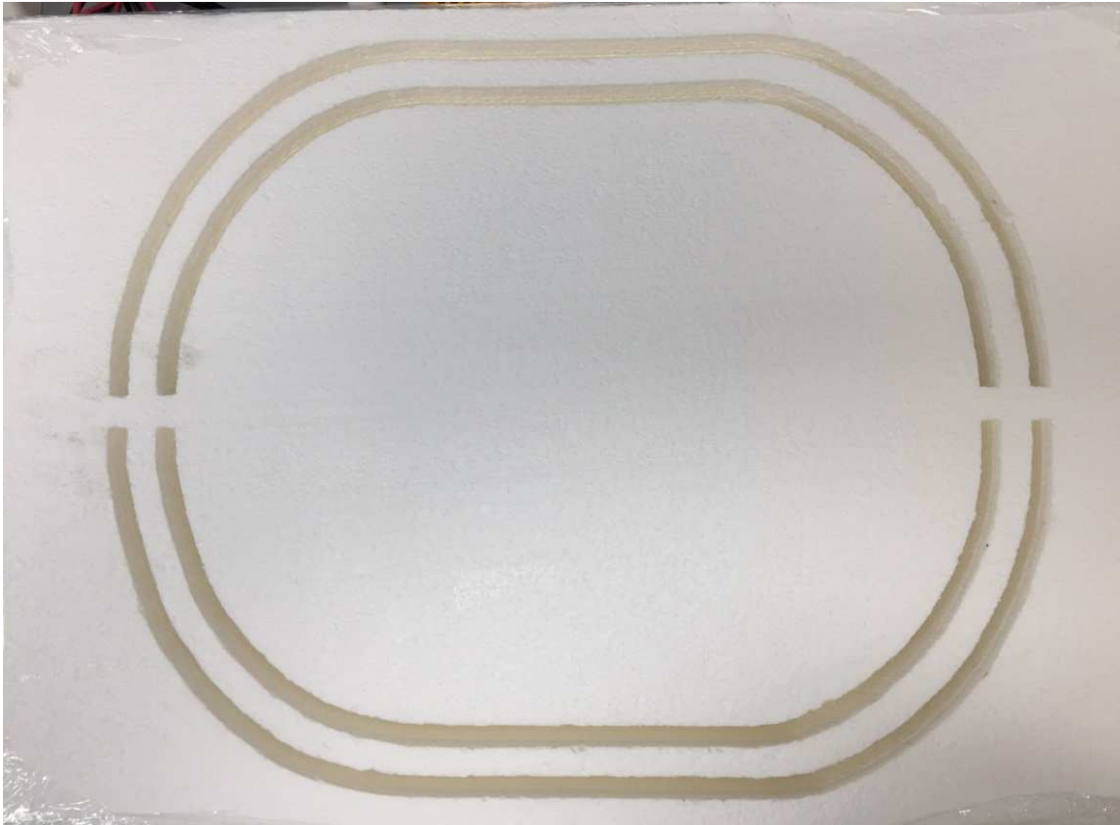


Figure 25 illustrates the LTES moulds after being sealed using PVA and prepared ready for pouring the composite inside. As can be seen, the cavity of the moulds is very narrow causing a difficulty to be sealed using a packaging tape.

5.5.1.4 Mixing stage:

5.5.1.4.1 FTES:

As the two sets of polystyrene sheets were prepared for the mix to be poured in, and with the amounts of materials required pre-calculated, the mixing stage was then conducted. The mixing process followed the same steps described earlier but in a large scale (5.3.4).

The FTES was first fabricated, using 1.5 kg of each part of PMC 121/30 Dry, in addition to the required amount of phenolic microspheres (60 g), the materials were mixed by hand, using a wooden stick sourced from the same supplier of the urethane materials, for about five to eight minutes and poured into one mould. The plan was to conduct all mixing in one day for the FTES moulds and the LTES in another day. After the second round of FTES mix was poured into the moulds, the mould started leaking from one side. Hence, the priority was to control the leak and avoid the mix escaping into the fume hood sink. As the mix set hard when cured, if it passes through the drain pipes it will block the drain in a matter of hours. Eventually, the leak was controlled and the mixing process suspended to the second day in order to allow the materials already in the mould to cure and eventually block the leak.

However, the next day the composite inside the mould had only cured partially. As a result, it was not possible to continue using the materials until investigating the reasons behind the unexpected uncured composite.

A contact was made with the company that produces the urethane materials, Smooth-on, to investigate the reasons behind uncured mix. The reply came back with suggestions that either the materials had passed their expiry date; had a manufacturing fault, or the mixture was under-mixed. In order to test the PMC materials and to ensure they were neither expired nor had a manufacturing fault, a small trial was conducted with no additives. The trial was conducted by adding part (B) and part (A) one to one by weight, mixed manually with a wooden stick for three minutes, poured into Perspex mould and left to cure for 16 hours. The result proved that the PMC materials have no issue and the fault could be due to under-mixing technique.

5.5.1.4.2 LTES:

This was taken into account when mixing the LTES materials. As discussed earlier, the LTES materials were prepared but with an extended time of mixing and poured into the mould. The composite was left to dry over night and on the second day the composite was fully dry. Demoulding the LTES proved to be hard and laborious. Once the LTES was demoulded, the final product was full of air bubbles. This could be due to the fact that the LTES mould height, (47 sheets totalling 47cm), when poured into the moulds created more air bubbles. Additionally, the final product lacked the desired smoothness. It also proved to be a very flexible product. This feature was not clear in the LTES trial sample, which could be attributed to its small size. Therefore, the LTES's mould, which was curved to fit the shape of the phantom in order to avoid density changes when bent around the phantom, could be built using non-curved moulds. For these reasons, the LTES fabrication was repeated with more improvements in mould design.

5.5.1.5 Improved mould design:

The FTES mould was repeated as cleaning the first one proved to be impossible. The new mould has one cavity to cast the first FTES layer. The reason is that it is the only layer that will have irregular surface orientation to fit the KYOTO phantom, Figure 26. In this stage, 47 polystyrene sheets with ultra-high density were sourced from the same supplier and the laser cutting was repeated. As the height of the mould is 49 cm, (i.e. 47 moulding sheets and two base sheets) it presented a challenge at the first round to deal with inside the fume hood. Also, to avoid the air bubbles that had been noticed in the LTES, the new mould was divided into three sections. The first section consisted of the two base sheets and another 16 crafted sheets, the second section consisted of 16 while the third section 15 crafted sheets.

The new mould sealing process was a little different to that used in the first mould. The inner side of the cavity was sealed with packaging tape but the outer side was sealed with A1 sheet of acetate plastic, with 400 micron weight, sourced from a crafting shop (www.veseygallery.co.uk), which was cut to size and glued onto the mould using PVA. The use of acetate plastic sheet to seal

the outer side of the mould attributed to its flexibility to bend around the mould and the less possibility of being separated from the mould with time as noticed in the first mould using packaging tape. The sealing was conducted separately for each section of the three sections.

The first round of the LTES showed that the materials, when cured, are flexible and bending them will not affect their density when wrapped around the KYOTO phantom. Moreover, the remaining FTES and the LTES layers will need to fit on top of the first FTES layer which has a smooth and regular outer surface, hence, the use of laser-cut polystyrene sheets will not improve the quality of the final product, in fact it will make it difficult to deal with when sealing and demoulding as experienced in the first round, see section (5.5.1.3). For these reasons, plates of Perspex were cut in three different lengths to accommodate the increase in the circumference when wrapped around the KYOTO phantoms. The size of the plates is:

- First LTES plate (1) : 56 (cm) x 47 (cm) x 5 (cm)
- First FTES plate (2) : 60.7 (cm) x 47 (cm) x 5 (cm)
- Second LTES plate (3) : 64.5 (cm) x 47 (cm) x 5 (cm)

At a total cost of £75, these three plates were much cheaper than laser cutting of polystyrene. As an advantage of the Perspex, these plates did not require sealing or release agent and were ready to use after constructed.

5.5.1.5.1 Mixing and final construction stage using new and improved

FTES and LTES mould designs:

The mixing time for additives with part (B) was extended to 8 minutes, while the time for mixing part (B) with the additives and part (A) was extended to 17 minutes. There are two reason for choosing these arbitrary time values, the first is the pot life of the material, which is 30 minutes, this means once the mixing process started, the mixture had to be poured into the mould within 30 minutes. This gave the researcher a known time for good mixing compared to the first trial sample. Part (B) is less viscous compared to part (A), hence, 8 minutes was deemed to be sufficient to mix the additives with part (B) thoroughly. Extra time, 17 minutes, for the second part of mixing is due to the high viscosity of part (A) and thus more mixing is needed. All mixing process was conducted

inside plastic mixing containers, which have been sourced from Smooth-On Ltd, with a capacity of 4800 ml each. Wooden sticks were also sourced from the same company for mixing purposes.

Washing the container after the mixing process in order to reuse it was far harder than anticipated; therefore, each mixing process was conducted using a new container and mixing stick to achieve the desired results.

The FTES first layers were fabricated in multiple mixing sets, while the second FTES layers were fabricated in two mixing sets. The quantity of the materials used for each layer is shown in Table 29. The LTES layers were also fabricated in multiple mixing sets, Table 29. In order to ensure equal distribution of the LTES composites across the Perspex plate, a level scale (Stanley Black and Decker, USA) was used to level the Perspex plate inside the fume hood. Final FTES and LTES moulds are illustrated in Figure 26.

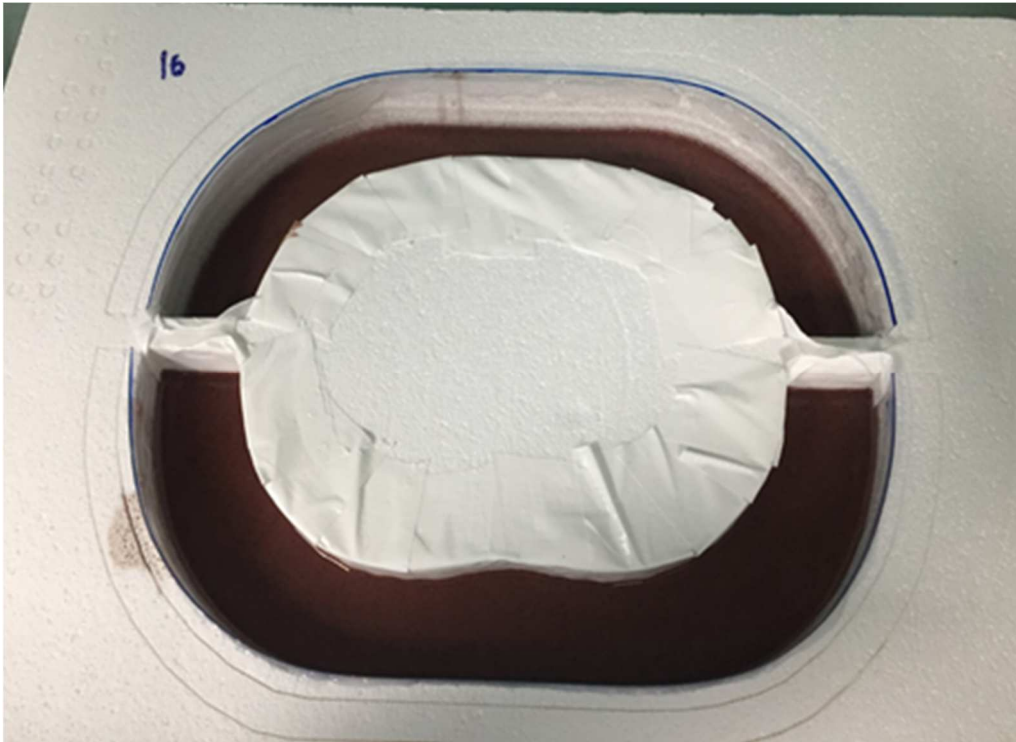
Table 29 Final mixing quantity for each mould

Mould number	Part (A)	Part (B)	Additives	Mixing set	total
1st FTES layer (2)	1545 g	1545 g	61.8 g (Phen. Micr.)	6	18600 g
1st LTES layers (2)	950 g	950 g	53.2 g (CaCo ₃)	2	3800 g
2nd FTES layers	1875 g	1875 g	75 g (Phe. Mic.)	2	7530 g
2nd LTES layers	975 g	975 g	54.6 g (CaCo ₃)	2	3900 g

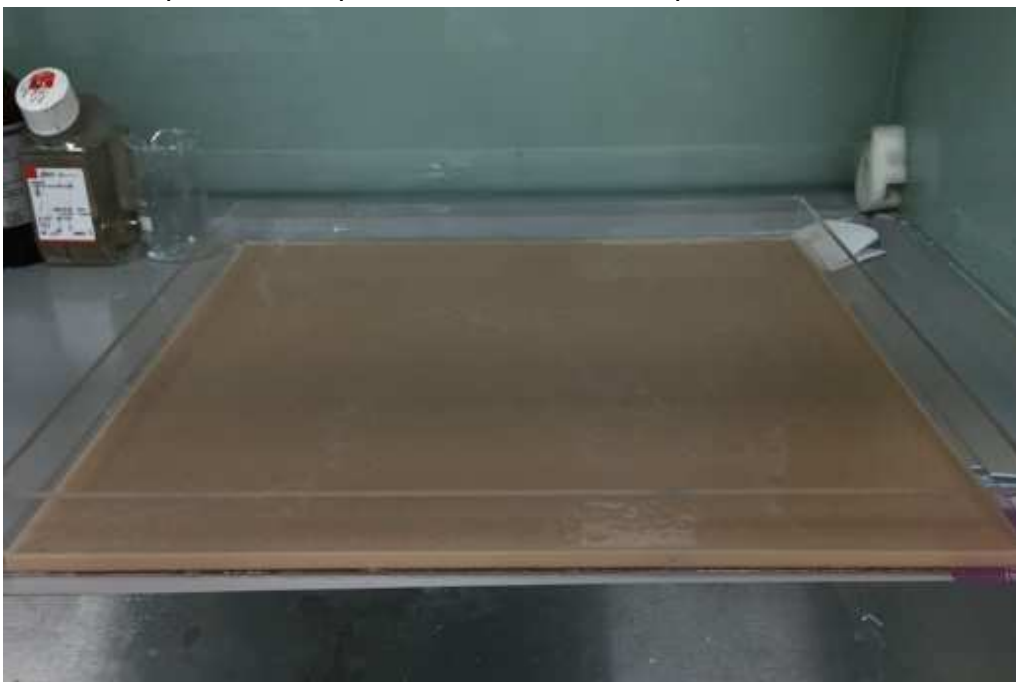
Table 29 listed the amount of each material that have been used in order to construct the final phantoms layers. The first FTES layers were the largest with a total FTES of 18.6 kg.

Figure 26 Improved FTES (A), and LTES (B) moulds with fabricated materials

A: First section of the FTES improved mould with the composite inside



B: LTES improved Perspex mould with the composite inside



5.5.1.6 Validation:

The use of the PMC 121/30 Dry with the calcium carbonate for LTES fabrication, and with phenolic microspheres for FTES fabrication has shown a good agreement with the lean and fat tissue densities, Hounsfield Unit and linear attenuation coefficient as stated in section (5.4). However, the final layers of FTES and LTES were constructed in a large scale and some layers were produced in more than two mixing sets. Hence, it was thought that a CT scan was needed again for the final FTES and LTES layers to investigate the consistency across different sections of these layers. A CT scan (SOMATOM definition Edge- Siemens, Germany) was used to scan all FTES and LTES layers wrapped around the KYOTO phantom using 4 levels of kVp; 80, 100, 120 and 140 kVp, Figure 27. The HU for the FTES was taken from nine different regions, especially the two large FTES slabs, which were constructed in more than three mixing sets. For the LTES, as every layer was constructed in one go, three HU readings from different regions deemed sufficient.

Figure 27 CT scan of all FTES and LTES layers wrapped around the KYOTO phantom



A sagittal CT view shows the LTES and FTES wrapped around the KYOTO phantom demonstrating the minimal air gap between the KYOTO phantom and the fabricated LTES and FTES layers, demonstrated in figure 27.

5.5.2 Validation result of the final FTES and LTES:

Figure 28 FTES final layers HU

Layer number	70 kVp		80 kVp		100 kVp		120 kVp	
	mean	SD	mean	SD	mean	SD	mean	SD
FTES 1 (anterior)	-103.5	11	-77.1	2.8	-81.4	1.2	-85	4.2
FTES 1 (posterior)	-88.6	3.9	-71.6	4.5	-67.7	3.4	-65.8	1.2
FTES 2 (anterior)	-73.6	1.8	-80.5	4.8	-87.5	1.5	-86.6	3.0
FTES 2 (posterior)	-71.7	12.1	-74	4.7	-73.8	3.1	-69.3	2.3

As seen in figure 28, all FTES layers exhibited similar HU across all kVp levels.

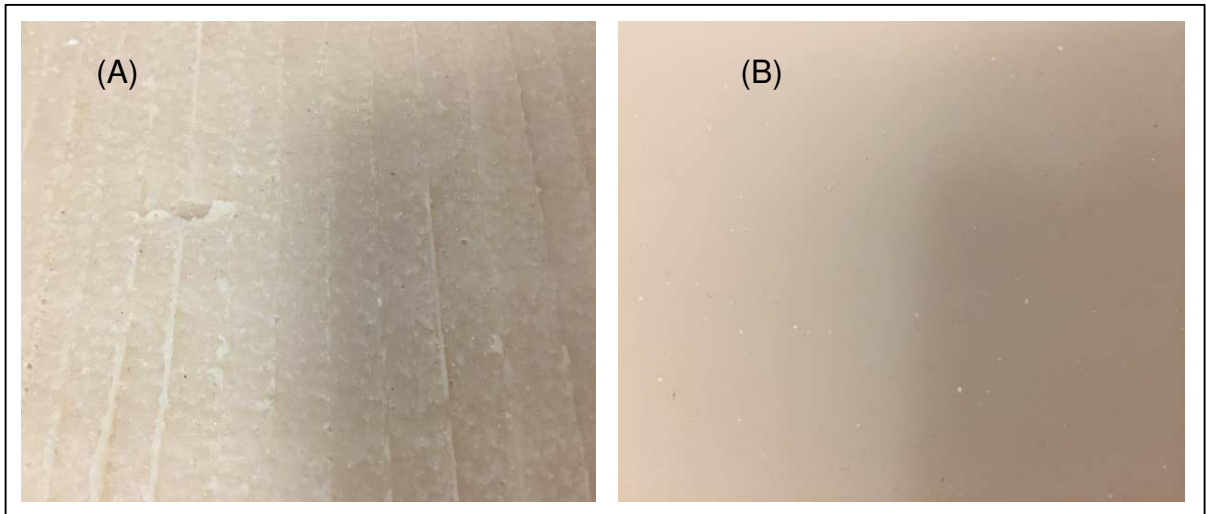
This indicates consistency during the mixing stage.

Figure 29 LTES final layers HU

Layer number	70 kVp		80 kVp		100 kVp		120 kVp	
	Mean	SD	Mean	SD	Mean	SD	Mean	SD
LTES 1 (anterior)	17.6	9.2	24.7	5.1	26	3.5	22.3	5.4
LTES 1 (posterior)	29.3	4.3	19.8	6.2	20.5	6.7	28.3	6.6
LTES 2 (anterior)	25.7	7.9	23.9	5.7	22.5	5.1	21.4	3.2
LTES 2 (posterior)	31.8	4.1	26.6	7.4	27.3	4.6	24.9	5.8

All LTES demonstrated HU values within the HU values of muscle, 10 – 40 HU. This provides assurance that the radiation attenuation across all layers is similar.

Figure 30 First (A) and second (B) LTES showing the improvement in the final product



Improved LTES technique has impacted positively in the final product. As illustrated in Figure 30, the first constructed LTES (A) has a rough surface and air bubbles, which in turn might impact on the x-ray attenuation. In (B), the final improved LTES layer is very smooth and no visible air bubbles produced.

5.6 Discussion:

This chapter describes the first study of extending a normal-weight commercial phantom to obese models using urethane based materials, which were prepared, fabricated and validated in-house.

The FTES and LTES trial samples have shown identical physical densities, Figure 18, to human fat and muscle densities in accordance with ICRU (ICRU, 1989). The density of the FTES reported in this study is 0.93 g/cm^3 while the human fat, adipose tissue, in the ICRU report is 0.916 g/cm^3 . However, variation in fat density is already reported in the literature concerning tissue equivalent substitutes, ranging from 0.91 to 0.95 g/cm^3 , (Watanabe and Constantinou, 2006, Hermann et al., 1986, Homolka et al., 2002, Sanada et al., 1999).

The FTES density reported in the current study, 0.93 g/cm^3 , is different to FTES density (0.88 g/cm^3) produced by Fisher and Hintenlang using similar materials, i.e. PMC 121/30 dry and phenolic microspheres (Fisher and Hintenlang, 2014). This could be attributed to the wide variation of phenolic microspheres densities, $0.20 - 0.80 \text{ g/cm}^3$. Resourcing the phenolic microspheres from a different supplier might be the reason behind such difference. For logistical reasons, it was not possible to source the phenolic microspheres from the same supplier. Additionally, since the fabrication of the FTES is dependent on different factors such as; weighing precision, length of mixing, storage of the materials and the quantity mixed, therefore, the variation in these factors between the current study and Fisher and Hintenlang could explain the difference in FTES density between the two studies.

Likewise, various LTES used in the literature, with regard to muscle tissue, with density variation ranging between 0.840 to 1.4 g/cm^3 (Zoetelief et al., 2001, Yohannes et al., 2012). However, the LTES density reported in this study has an identical muscle density value to the ICRU recommended value, 1.04 g/cm^3 (ICRU, 1989).

As shown in Figure 19, the attenuation coefficient of FTES across different kVp are within the 5% recommended by the ICRU compared with the bench marking material, lard (ICRU, 1989). With regard to the LTES attenuation coefficient

compared to the Perspex, the difference is slightly above the recommended 5%. This could be attributed to the difference in densities between Perspex and LTES, 1.17 and 1.04 g/cm³, which will impact on the linear attenuation coefficient for photoelectric absorption (Graham et al., 2012). Additionally, such differences have been demonstrated by Ali and colleagues between Perspex and muscle linear attenuation coefficient (Ali et al., 2018). However, such small difference is not an issue in case of substitutes used for less sensitive procedures such as radiography compared to mammography (ICRU, 1989).

In terms of HU for FTES, the trial sample demonstrated HU values similar to the bench marking material, lard, as shown in Table 28 . These values are within the range reported in the literature for both subcutaneous and visceral fat (Sato et al., 2018, Lee et al., 2017, Nguyen et al., 2018). However, in terms of LTES, the HU values are different compared to the Perspex (~35 and ~120 HU). This could be attributed to the difference in densities of both materials as discussed earlier. However, both values are in line with what have already been reported in the literature (Amini et al., 2018, Yohannes et al., 2012, White, 1978, Vanderstraeten et al., 2007). Perspex has been used extensively as a soft-tissue equivalent substitute, however, Sandborg and colleagues conducted a study to test the difference between soft tissue and various soft-tissue equivalent substitutes, one of which is Perspex, in terms of equivalent thickness (Sandborg et al., 1993). They concluded that the Perspex showed relatively the great spread in the equivalent thickness. They attributed this to the high density of Perspex (1.17 g/cm³) compared to soft-tissue density (1.00 g/cm³).

Fabrication and construction of the final products of FTES and LTES proved to be more difficult than anticipated. First, the PMC 121/31 Dry materials are supplied solely by Smooth-on Ltd. in the USA. This makes sourcing the materials challenging and needed to be planned in advance to avoid any delay in the experimental timeline. This is more important in a large scale experiment, where availability of spare materials is crucial in the event of problems at any stage. Additionally, these materials have a very short shelf life; which means once opened they should be used soon afterwards. Furthermore, the pot life is also short; hence, before pouring the materials into the mixing pot, all preparation should be accomplished so the mixing can be completed within 30

minutes. This is due to the high viscosity of the composite (1800 CPS, per technical spec) with viscosity increases by the minute (Kasraie et al., 2018). As a result of high viscosity, the composite should be poured into the mould slowly to avoid trapping air bubbles as well as to enhance the homogeneity of the mix.

Due to the hazardous nature of PMC 121/30 dry materials, containing disononyl-phthalate (5-15 % per weight) and toluene diisocyanate (<1 % per weight) in part (A) and diethyl-toluene diamine (1-5 % per weight) and phenyl-mercuric neodecanoate (0.2-0.25 % per weight) in part (B), extra precaution measure had to be in place prior to experiment commencing. These measures include Polyvinyl Chloride (PVC) gloves, good ventilation during the experiment as well as conducting the experiment inside a fume hood in accordance with the university health and safety regulations. Therefore, in-house construction of FTES and LTES using similar materials might be limited to the availability of scientific lab and required facilities.

Another challenge that needs to be taken into account is the mould material and preparation. Polystyrene is the best option in terms of sourcing and laser cutting cost-effectiveness. However, it proved to be challenging when it comes to sealing. In this work, packaging tape was used to insulate the moulds inner-rough surface. Packaging tap tape and polystyrene are not the best combination. Different types of tape were used to achieve good adhesion to the polystyrene; however, the packaging tape was the best option. The laborious process of sealing needs to be factored in to the process and despite packaging tape being the best option, the composite must be poured into the mould as soon as possible after sealing to avoid problems associated with degradation of the tape.

Despite the achieved work presented in this chapter, there is still room for improvement. 3D printing could be used to fabricate the cast of the mould based on the required size using thin Perspex that can be cut easily afterward. This method has been employed in the literature (Ursani et al., 2018).

5.7 Conclusion:

Based on the results from the FTES and LTES trial sample density, attenuation coefficient and HU, the use of PMC 121/30 Dry along with the additives proved to be a good option for fabricating tissue-equivalent substitutes in house with low cost. Calcium carbonate is produced in different purity form, and this should be taken into account when sourcing these materials. The phenolic microspheres are very sensitive to humidity and should be stored in a very well ventilated area and kept sealed when not in use. Due to the hazardous substances contained in the PMC 121/30 dry, health and safety precautions should be in place before conducting the experiments especially fume hood and PVC gloves.

With regard to the conduct of the experiment, attention should be paid to the technical details as this will impact heavily on the physical and radiological properties as well as crudeness of the final product. This includes; good and short shelf storage, precise calculation and weighing of each material, sufficient manual mixing and controllable technique of dispensing the hardener, part (A), into the mix. Sealing the mould is essential unless a metal, glass or Perspex mould is used.

As the fabrication of the LTES and FTES using urethane based materials (PMC 121/30 Dry) is highly dependent on the experimenter, a sample of each substance should be fabricated and tested in a small scale before conducting the experiment in a large scale to avoid repetition of the experiment and doubling the cost.

The protocol used in this study can be replicated to extend any normal weight phantom, such as ATOM and RANDO phantoms, into obese representative phantoms and conduct dosimetry as well as image quality research.

6 Chapter 6: Dose optimisation study

6.1 Introduction:

The first study in this thesis demonstrated high doses (DAP) delivered to patients with obesity especially in lumbar spine and abdominal radiographs. Dose variation was also demonstrated where DAP had moderate to poor correlation with BMI. This indicates that radiographers face difficulties when selecting the exposure factors based on the patients size and emphasizes the need for more dose optimisation in this group of patients specifically. Based on the results from the first study, the second study was conducted in an attempt to quantify body composition in the abdominal region in order to underpin the construction of representative obese phantoms. The third study was conducted to reflect the body composition changes reported in the second study. The current study aimed to conduct dose optimisation experiments to explore the main exposure factors that improve image quality in lumbar spine radiographs using the obese phantoms developed by the researcher.

6.1.1 Overall aim

To conduct dose optimisation experiments in order to improve image quality in patients with obesity

6.1.2 Objectives

14. To investigate the impact of different exposure factors on radiation dose and image quality on the most challenging body part, identified earlier
15. To explore the change in exposure factors effects as the phantom size increases
16. To produce a preliminary guiding model to predict best exposure factors in case of lumbar spine radiography based on patient's size

6.2 Rationale for dose optimisation of Lumbar spine:

The first chapter of this thesis showed a significant radiation dose delivered to patients with obesity in abdominal and lumbar spine radiographs. Such results indicate a clear need for dose optimisation work, especially in these two regions. Choosing lumbar spine radiography instead of abdomen radiography is attributed to different reasons, which will be discussed in the following paragraphs.

In terms of frequency, lumbar spine radiography comprises 2.53 % of 231 types of investigations conducted in two regions in the UK; the West Midlands and the South West, but this is assumed to apply to the rest NHS trusts in the UK (Hart et al., 2010). Such a percentage suggests that lumbar spine radiography is considered to be the second most conducted projection radiography procedure in the UK (Hart et al., 2010, Chaparian et al., 2014).

In terms of radiation dose and radiobiology, Mettler and colleagues conducted a review study in an attempt to report effective dose for various radiological investigations (Mettler Jr et al., 2008). The lumbar spine radiographs effective dose was the highest compared to all projection and dental procedures with average value of 1.5 mSv with a 0.5 mSv difference to the second highest procedure effective dose, the thoracic spine radiographs. In the UK, lumbar spine radiography contributed to the highest effective dose (0.6 mSv) compared to all projection radiography procedures (Hart et al., 2010). The presence of the most radiosensitive organs, with a tissue weighting factor of 0.12, located in the main beam such as colon, stomach and lumbar spine bone marrow (Caracappa et al., 2009), explained the high effective dose of lumbar spine radiography. In a study conducted by Chaparian and colleagues in an attempt to reduce the absorbed dose to various organs in abdominal, lumbar spine and pelvis radiograph using various projections (Chaparian et al., 2014), as shown on Table 30, the absorbed doses during lumbar spine procedures are at the upper border compared to abdominal and pelvis radiograph.

Table 30 Lumbar spine (AP & LAT) absorbed dose adopted and recalculated from Chaparian et al., 2014

Examination		RBM	Breasts (female)	colon	lungs	Ovaries (female)	Prostate (male)	stomach
Abdomen (AP)		0.170	0.019	1.013	0.042	0.732	0.980	1.439
Lumbar spine	AP	0.117	0.014	0.902	0.035	0.613	1.045	1.196
	LAT	0.566	0.032	0.924	0.272	0.735	0.287	0.758
Pelvis (AP)		0.107	0.002	0.698	0.001	0.622	1.129	0.032

RBM= Red Bone Marrow.

Few studies of dose optimisation in obese populations have been reported in the literature. However, none of these studies have considered lumbar spine but rather focused on pelvis and chest radiography. Hence, this study was focussed mainly on lumbar spine radiography.

6.2.1 Operational radiographic acquisition factors:

In projection radiography generally, and in digital radiography specifically, number of interlinked image acquisition factors affect both image quality and radiation dose. These acquisition parameters are; tube potential (kVp), tube current (mA) and mAs, anode angle, focal spot size, filtration, collimation, FID, anti-scatter grid, object to image distance (OID) and AEC. In the next section, the effects of these parameters on image quality and radiation dose will be discussed and examples of previous studies will be given to appreciate the usefulness of each factor.

6.2.1.1 Tube potential (kVp):

This referred to the selected kVp which controls the peak potential difference across the cathode and anode. The greater the difference of peak potential inside the x-ray tube, the greater the attraction of the electron beam towards the anode. Additionally, this beam energy is dependent on the kinetic energy of the electrons as they strike the anode. Therefore, if the kVp is increased, the kinetic energy of the electron beam will increase. While the mean photon energy is

around 30-50 % of the photon maximum energy, this can be increased by increasing the maximum energy of the photon, kVp (Graham et al., 2012). The tube potential (kVp) mainly defines the x-ray power of penetration through the body part which in turns affects the image quality, contrast, and radiation dose (Fauber, 2016).

As kVp is one of the main exposure parameters that affect both image quality and radiation dose, different studies have incorporated this parameter in similar dose optimisation research. A systematic review was conducted by Seeram and colleagues in an attempt to explore the most conducted theme of dose optimisation studies in digital radiography, computed radiography specifically (Seeram et al., 2013). Their conclusion demonstrated that kVp was the favoured parameter to alter in dose optimisation studies. Conflicting results of whether low or high kVp is better in optimising image quality have been concluded by Seeram and colleagues. Geijer and colleagues investigated the optimal exposure setting on lumbar spine radiographs using CDRAD contrast-detail phantom and the resulted exposure techniques were implemented to visual grading analysis of an Alderson phantom (Geijer et al., 2009). They found that a lower tube potential of 60 kVp produced better image quality with no increase in effective dose compared to the default setting of 70 kVp. They also found that 66 kVp, which is still lower than the default 70 kVp, gives the lowest dose without image quality deterioration. Similarly, Alzyoud and colleagues found similar results with low kVp being the favourable parameter in producing the best image quality in pelvis radiography even with large thickness (Alzyoud et al., 2018). Similar studies investigated the impact of kVp on chest (PA) image quality and radiation dose using both CR and DDR system (Compagnone et al., 2013, Tingberg and Sjöström, 2005). Their findings supported the theory of using low kVp to enhance the image quality while reducing the radiation dose.

Other studies have found that a high kVp is better in producing diagnostic image quality with low dose (Brindhaban et al., 2005). They investigated three tube potentials using two different CR systems. Their results demonstrated radiation dose reductions of 25 % and 50%, can be achieved with no statistically significant decrease in visual image quality when increasing kVp. Likewise, Moey and colleagues found similar results; i.e. high kVp being a

better choice in terms of abdomen and lumbosacral (AP) radiographs (Moey and Shazli, 2018). However, they measured the ESD which will be reduced when higher kVp is used.

Based on the discussion above, it is clear that kVp is playing a major role in radiographic optimisation. With the kVp being affected by different factors such as the body part thickness, tube current and types of detectors, and affecting radiation dose and image quality on different levels, based on the value used to measure dose and image quality, it is of importance to investigate its impact in the context of this project.

6.2.1.2 Tube current and tube current-exposure time (mA & mAs)

Tube current describes the quantity of x-ray beam (mA), and mAs the number of photons in the x-ray beam per unit of time (Bushberg and Boone, 2011). Doubling the mA doubles the number of photons in the beam and the beam intensity will increase. This will have a direct impact on patient dose in a linear model. It can be measured in seconds or milliseconds but abbreviated with letter “s” in both cases. Since mA controls the number of photons more than the penetration power, it determines the x-ray quantity travelling through the patient and hitting the detector impacting on both patient’s dose and the image signal to noise ratio (Carver and Carver, 2012, Carroll, 2007).

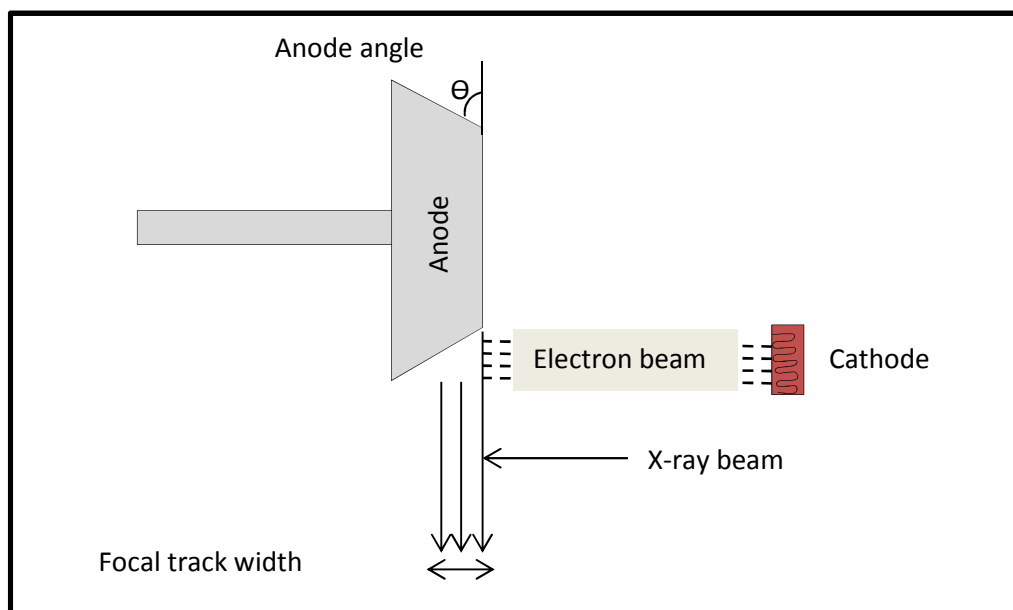
As mAs consists of two factors, rate of the flow of charge and the exposure time, to achieve optimum image quality, there should be an adjustment between these two factors. A high mA with short exposure time is preferred in order to avoid motion artefact and image blur. However, a very short exposure time in a procedure where high tube current is needed for perhaps a thicker body part, may reduce the life expectancy of the tube as a result of the high temperatures generated in a very short time (Bushberg and Boone, 2011, Carlton and Adler, 2012).

6.2.1.3 Angle of anode target:

Inside the x-ray tube, the electron beam is directed from the cathode towards a focal spot on the anode as illustrated in Figure 31. As the electrons strike the tungsten anode, Bremsstrahlung and characteristic emissions occur based on

the electron energies (Poludniowski et al., 2009). Based on the anode angle, the projected focal spot size is determined. The relationship between the anode angle on the one hand, and the focal track width and tube loading on the other, is an inverse one. Therefore, if the anode angle is small, then the focal track will increase as well as the tube load (Bushberg and Boone, 2011, Dowsett et al., 2006). However, the anode angle, ranged between 7° and 20° with 12° to 15° most common, is pre-set by the manufacturer, based on the modality applications, and unchangeable (Bushberg and Boone, 2011). Figure 31 illustrates this.

Figure 31 Anode angle



6.2.1.4 Focal spot size:

This represents the anode area where electron bombardment happens. It is often defined and described as the “line focus principle” (Ball et al., 1997). This principle defines the relationship between the actual focal spot and the effective focal spot (Dendy and Heaton, 2011). The former relates to the actual line in the anode bombarded with electrons, being determined by the filament size of the cathode, while the latter refers to the estimated focal spot as determined by the angle of the anode (Fauber, 2016).

Two sizes of focal spot are usually available fine and broad, with fine typically between 0.5 and 0.6 mm, and broad between 1 and 1.2 mm. The focal spot size can be altered through altering the size of the active filament in the cathode that produces the electron beam (Fauber, 2016). The focal spot size will impact on the geometric unsharpness of the image in proportional relationship (Dendy and Heaton, 2011).

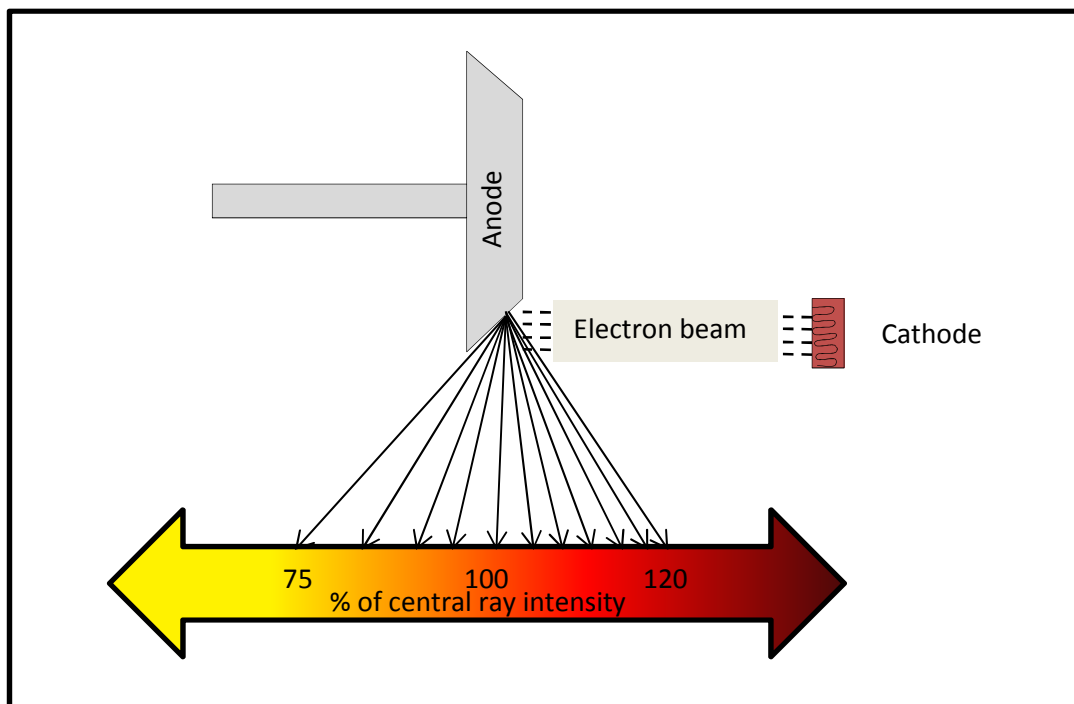
Several studies have considered focal spot size and its effect on image quality in different procedures (Al Qaroot et al., 2014, Kei et al., 2014, Gorham and Brennan, 2010). All studies concluded that there were no significant differences

between large and small focal spot size on image quality even in extremities procedures, where it is common practice to select a small focal spot in order to improve the visualisation of bony trabecular patterns by reducing geometric unsharpness.

6.2.1.5 Anode heel effect:

This phenomenon is related to the reduction in intensity of the x-ray beam at the anode. It is caused by the attenuation of the beam travelling through the anode itself due to the anode angle (Carlton and Adler, 2012). The beam intensity difference between the cathode and anode is around 45 % as shown in Figure 32.

Figure 32 X-ray beam intensity difference between the cathode and anode



However, this effect has less impact when a long focal to image distance (FID) is practiced. Additionally, It can be used to optimise image quality by placing the thicker portion of the examined part on the cathode side as the beam intensity is higher (Graham et al., 2012).

In the literature with regards to the lumbar spine radiography, some studies have tested the best use of anode heel effect and its impact on reducing radiation dose while maintaining the image quality. Fung and Gilboy have investigated the impact of anode heel effect on lumbar spine radiographs in an attempt to find the best orientation (Fung and Gilboy, 2000). Using a Rando phantom with TLDs inserted inside the most sensitive organs; ovaries, breast, testes, thyroid and eyes, they found that the head of a female patient can be placed towards the cathode end of the tube in order to make use of the anode heel effect. This is due to the significant reduction in radiation dose to ovaries, 2259 μGy with head towards the cathode compared to 2644 μGy when placed towards the anode. For male patients, the benefits are less as the dose received by testes is very small, 30 μGy . Similar results have been reported by Ben-Shlomo and colleagues using PCXMC (Ben-Shlomo et al., 2017). Other studies have tested the anode heel effect in pelvis and thoracic spine procedures. Mraity and colleagues investigated the anode heel effect in pelvis radiography and found a significant dose reduction when the patient's head was placed towards the cathode in males, while negligible benefits were found in females (Mraity et al., 2017). In thoracic spine radiography, findings suggested that where the head is positioned towards the anode, radiation dose is reduced by 98% compared to head towards cathode (Ben-Shlomo et al., 2013).

6.2.1.6 Tube filtration:

After electron beam bombardment on the anode, x-rays are produced and projected outside the x-ray tube. The x-ray beam energy is heterogeneous ranging from 10.2 KeV to the maximum tube potential selected prior to the exposure (Fauber, 2016). The x-ray beam travels through a variety of essential parts on its way through the tube. These include the window of the x-ray tube, housing oil, field light mirror, the collimator assembly and any other essential enclosure for the tube (Bushberg and Boone, 2011). As a result, the x-ray beam is attenuated especially those x-rays in the spectrum below 15 KeV (Bushberg and Boone, 2011). This filtration is known as the inherent filtration and usually ranges between 0.5 and 1.0 mm of aluminium equivalent (Carroll, 2007). Whilst this type of filtration cannot be controlled it is essential that it is factored in to any exposure and dose calculations.

Other parts of the beam with low levels of energy need to be stopped before reaching the examined part as they will end up being absorbed by the tissues and contribute to the patient dose significantly whilst making no useful contribution to the image (Fauber, 2016). To achieve this, sheets of metal, usually made from Aluminium or Copper, are added intentionally into the beam to absorb low energy x-rays. This is known as added filtration.

Another type of filtration, called compensating filtration, is used on occasions where the beam intensity needs to be altered in order to produce a consistent exposure to the detector (Bushberg and Boone, 2011). An example of this type of filtration is trough filtration which is used in chest radiography (Bushberg and Boone, 2011). It has low thickness in the middle of the field to compensate for the high attenuation by the sternum.

Different studies have incorporated these parameters in dose optimisation studies. For example, Ekpo and colleagues studied the impact of additional Copper filtration (Cu) on chest (PA) image quality using a digital radiography system (Ekpo et al., 2014). They concluded that effective dose was reduced by 36.6% when using 0.3 mm Cu with no deterioration in SNR. Higher Cu filtration of 0.5 mm shows greater dose reduction (39.7%) but SNR decreased as well. Other studies demonstrated similar results emphasising the importance of filtration in dose optimisation (Brosi et al., 2011, Mraity et al., 2018).

6.2.1.7 Collimation:

Collimation is the process of restricting and confining the x-ray beam to a given area (Miller-Keane, 2003a). Collimation is an integral tool that can be used by the radiographer to eliminate unnecessary radiation and reduce scattered radiation. With regard to this, applying the correct collimation is crucial in digital radiography as image receptors are very sensitive to low radiation energy (Herrmann et al., 2012). In the case of patients with obesity, collimation is even more essential as the scattered radiation is thickness dependent. Proper collimation will reduce image quality deterioration resulting from scattered radiation, and reduce the patient dose by avoiding irradiated tissues.

In digital radiography systems, electron masking software is used in image cropping but collimation is not. The idea of electronic masking is to recognise

the borders of the exposed area of the image detector as the unexposed area outside the collimation usually has a bright appearance, hence, the software reduces eye strain through cropping of the image (Herrmann et al., 2012). However, the electronic masking does not replace the function of collimation, as the literature reported misuses of it leading to unjustified and significant radiation dose to patients (Karami and Zabihzadeh, 2017, Tsalafoutas, 2018). Therefore, manual collimation when applied prior to the radiographic procedure remains a more effective means of radiation dose reduction. Fauber and his colleagues conducted research to investigate the impact of limiting the field size during lumbar spine imaging (Fauber and Dempsey, 2013). They decreased the field size from 35 x 43 cm to 20 x 43 cm while increasing the mAs to maintain exposure to the detector. They found a statistically significant reduction in radiation dose, (>60%), especially in organs further away from the lumbar spine.

6.2.1.8 Source to image distance (SID)

This refers to the distance between the x-ray source and the receptor. Based on the inverse square law; where the intensity of the x-ray beam decreases as the square of the SID increases, hence, the patient radiation dose will decrease, although the inverse square law assumes a point source for the x-radiation. However, as the SID increases, the radiation field divergence increases and the intensity of the x-rays reaching the detector decreases which will impact negatively on image sharpness (Graham et al., 2012, Fauber, 2016, Lanca and Silva, 2012).

Different studies have investigated the impact of SID increase on image quality as well as radiation dose in different procedures (Brennan and Nash, 1998, Heath et al., 2011, Grondin et al., 2004, Joyce et al., 2013, Karami et al., 2017). All studies have demonstrated dose reduction while maintaining the image quality.

6.2.1.9 Anteroposterior and posteroanterior projection:

Based on the text books most commonly utilised by radiographers (Bontrager and Lampignano, 2013, Davey and England, 2015), together with accepted practice in radiology departments, the most favoured and commonly undertaken

view for imaging the lumbar spine is the anteroposterior (AP) view on the grounds that magnification unsharpness is minimised and therefore image quality optimised. However, new literature has emerged suggesting that a PA projection might reduce absorbed and effective doses of lumbar spine radiographs. The idea behind this new approach is that PA is favourable over AP in procedures where radiosensitive organs lie close to the anterior surface (Martin, 2007a). This eventually will reduce the absorbed dose as more x-rays will be attenuated on their way towards the detector and the sensitive organs away located away from the radiation entrance side.

Davey and England studied this phenomena and its impact on effective dose and image quality in lumbar spine radiography (Davey and England, 2015). They found a 20% reduction in effective dose with minor but not significant reduction in image quality compared with the AP projection. Similar results were found in abdomen radiography where a PA projection, taken with the patient prone, reduces the entrance surface dose in different BMI groups (Ismail et al., 2017).

6.2.2 Object-to-image distance (OID)

This technique, also called the “Air gap technique”, is another form of scattered radiation reduction which in this case improves image quality. The principle of OID is based on creating a distance between the exit side of the examined body part and the image receptor in order to reduce of the amount of scattered radiation hitting the detector with consequent degradation of image quality as image contrast increases as the scattered noise is decreased (Bushberg and Boone, 2011). In lateral cervical spine imaging, the airgap is unavoidable due to the position of the shoulder which prevents close positioning of the image receptor to the cervical spine, consequently the SID must be increased in order to reduce magnification unsharpness. However, in other procedures this technique is not applied but some studies have shown its role in optimising image quality. One study conducted by Lanhede and co-authors measured the effect of air gap in chest and lumbar spine radiographs (Lanhede et al., 2002). They compared two scatter radiation reduction techniques, anti-scatter grid and air gap technique, and measured the image quality visually and radiation dose

using ESD. They found that air gap resulted in lower ESD dose but no statistically significant difference between the two techniques in image quality. Similar results have been demonstrated in lumbar spine and pelvis radiography (Chan and Fung, 2015a, Chan and Fung, 2015b). However, the design of x-ray systems used in clinical practice nowadays do not facilitate alteration of OID, although this could be implemented in erect positioning where the patient may be able to stand away from the Bucky to increase the OID.

6.2.2.1 Anti scatter grid:

As the name suggests, the main task of an anti-scatter grid is to eliminate the scattered radiation exiting the examined body part towards the detector. It comes in the form of a flat device comprised of precisely engineered lead strips with a specific thickness and height that are separated by radiolucent interspace materials (Seibert, 2008). Different grid types are characterised by their specification. The alignment of the lead strips can be either parallel or focused (i.e. angled), and the grid can be either stationary or moving (Zarnoch and Guida, 1996). Stationary grids can be placed between the examined body part and the detector. In the case of the moving grid, the grid is placed in a mechanically moving device, called a Bucky, which moves during the exposure to blur the shadows of the grid stripes to avoid grid artefact (Cowen et al., 2008).

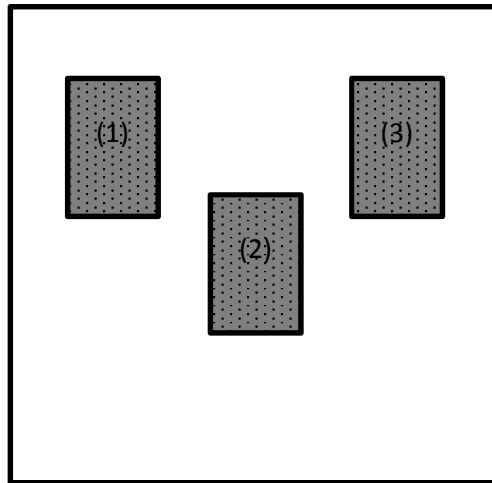
As the scattered radiation passes through the grid, it will be absorbed by the lead strips. This will improve the image quality by reducing the noise in the image. Due to the high sensitivity of CR and DR systems to low energy scattered x-ray photons, using an appropriate anti-scatter grid in these systems is essential (Cowen et al., 2008). However, a higher acquisition dose is required (by a factor of 2 or 3) compared to similar images acquired without an anti-scatter grid (Uffmann and Schaefer-Prokop, 2009). This is attributed to the fact that anti-scatter grids permit transmission of the primary beam but some of this beam is absorbed along with the scattered radiation (Cowen et al., 2008, Holmes et al., 2013, Rana et al., 2016).

6.2.2.2 Automatic exposure control (AEC)

AEC uses ionisation chambers incorporated into the image receptor. Their main task is to automatically terminate the exposure when sufficient signals have reached the detector (Doyle, 2009). This allows the imaging system to control exposure time and produces images with consistent quality for different patient thickness, different body parts and with different tube potential using exposures near the optimum (Herrmann et al., 2012).

In modern x-ray units, three ionisation chambers are usually utilised in the cassette tray between the examined body part and detector panel (Roberts et al., 2006). Figure 33 illustrates the orientation of AEC ionisation chambers typically used in digital radiography. Based on the procedure, the radiographer can choose the appropriate chamber/s in order to ensure a coverage of the anatomy of interest (Manning-Stanley et al., 2012, Geijer and Persliden, 2005).

Figure 33 Automatic Exposure Control (AEC) ionisation chambers orientation in digital radiography detector



Different ionisation chambers are illustrated in Figure 33 where the radiographer can choose the most suitable chamber/s based on the conducted procedure and the region of interest.

Two conditions should be met by the AEC in order to work properly; calibration and positioning (Williams et al., 2007). Inaccurate positioning of the selected ionisation chamber will lead to over or under exposure radiograph as this depends on the density of the area over the selected chambers. Different studies have investigated the importance of the correct combination and positioning of AEC chambers and their role in dose reduction (Moore et al., 2016, Manning-Stanley et al., 2012, Hawking and Elmore, 2009). In lumbar spine radiography, the middle AEC ionisation chamber is usually selected (Hawking and Elmore, 2009).

However, other studies have investigated the impact of manual and AEC mode on image quality and radiation dose. For instance, Reis and colleagues compared the manual and AEC mode effects on image quality and effective dose in chest radiography (Reis et al., 2014). Using an anthropometric phantom with and without inserted lesions, the image quality was assessed visually while the effective dose was calculated using PCXMC. They found that selecting manual mode achieved a lower effective dose in general, but accurate selection of AEC chambers scored the lowest effective dose suggesting that the AEC would be beneficial only if selected and positioned accurately based on the examined body part.

6.2.3 Image quality assessment:

Having discussed the factors that impact on image quality and radiation dose, it is essential to discuss the methods of assessing the image quality. In this section, principles of different image quality assessment tools will be discussed, including each tool's strengths and limitations as well as justifying the use of specific tools used in this study.

According to the ICRU,

“image quality in medicine must be judged in terms of the extent to which a class of images allow real observers, such as radiologists, to correctly determine each patient's state of health or disease” (ICRU, 1995, p. 23).

The medical image transfers to the radiologists or reporting radiographers in two consecutive steps; data acquisition and image formation, and image processing and display. The first step is dependent heavily on the physical and technical features of the imaging system as well as the skill of the radiographer operating it. The second step relies on the observer and his ability to detect abnormalities and interpret the anatomical structures in the produced image (Månsson, 2000). The image quality should be appraised at each step. For assessment of the imaging system physical parameters can be used. In terms of the displayed image, observer performance assessment can be used based on whether the image is phantom or patient based.

In the next subsections, both physical and observer assessments will be discussed with more details in the tools used in this study and the justification behind their application.

6.2.3.1 Physical assessment (objective):

This is defined as the measurements that describe the physical characteristics as well as the overall performance of the imaging system (Alsleem and Davidson, 2012). There are various measurements that fulfil this purpose such as Signal to Noise Ratio (SNR), Contrast to Noise Ratio (CNR), Detective Quantum Efficiency (DQE) and Modulation Transfer Function (MTF). All of these measurements are essential in testing instrumentation performance, however, they do not relate to all components of the imaging chain (Båth, 2010, Sund et al., 2004). Additionally, a review conducted by Tapiovaara, in an attempt to study the link between physical and observer assessment, concluded that physical measurement cannot replace the observer opinion on suitability of clinical image (Tapiovaara, 2008). The result of the review along with the statement quoted earlier from the ICRU emphasised the non-effectiveness of physical measures in judging the image quality.

However, SNR and CNR have been used extensively in similar types of studies for the purpose of identifying a reference image that can be used as a comparator in visual assessment. Additionally, they usually correlated with the visual assessment in order to support the result of such subjective assessment.

6.2.3.1.1 SNR

This physical measurement is a generic term; it measures the ratio of signal, which reflects true anatomy, to the noise. SNR is considered as one of the simplest measures used to define an object visibility in the image (Lanca and Silva, 2012). According to Arnold and Scheibe, SNR can be calculated as the mean signal of the foreground divided by the signal standard deviation of the background, $SNR = S_1/\sigma$, where S_1 is the foreground mean signal values, and σ is the standard deviation of signal value in the background (Arnold and Scheibe, 1984). The use of SNR in digital radiography is widely practiced since the main determinant of image quality is the level of noise (Launders et al., 2001, Doyle et al., 2005, Ekpo et al., 2014, Tugwell et al., 2014).

However, SNR has always been a controversial measure. For instance, the size of the object under investigation is not taken into account when measuring the SNR, hence, this usually results in low correlations with visual assessment (Alsleem and Davidson, 2012). Additionally, in clinical practice, a radiologist is familiar with the texture of the background of a radiographic image which might be influenced by anatomical, detector or system noise (Báth, 2010, Seeram et al., 2014). However, the SNR is based on quantum noise, which is a representative of photon density at the detector (Báth, 2010). Therefore, employing the simple description of noise used in SNR, i.e standard deviation of signal values, is far too basic for an observer who is more sensitive to the noise texture (Mraity et al., 2016). Additionally, high SNR does not always mean a good image quality as an overexposed radiograph will contain high SNR but offer no diagnostic information since noise degrades the image (Vladimirov, 2010, Lyra et al., 2010).

Based on the above discussion, SNR is a valuable physical measure to appraise the performance of an imaging system, however, it should be treated with caution when used in relation to visual assessment (Báth, 2010).

6.2.3.1.2 CNR

Another form of physical assessment of image quality is the CNR. Unlike the SNR, CNR reflects the difference of signal intensity between the foreground and

surrounding background, $CNR = S_1 - S_2 / \sigma$, where S_1 is the mean signal intensity value in the foreground, S_2 is the mean signal intensity value in the background, and σ is the standard deviation of the signal values in the background (Dendy and Heaton, 2011). For this reason, CNR provides superior information on object visibility and differentiation between structures to SNR as it considers both noise and contrast.

However, both SNR and CNR can be used to support the visual assessment but not to replace it as in clinical practice the final decision will be based on the observer, the reporting radiologist/radiographer's, assessment (Båth, 2010).

6.2.4 Visual measurement:

This approach is observer based and can be divided into two categories based on the assessed features and whether the purpose is lesion detection or normal anatomical visualisation. In this thesis, all images are phantom based and the visualisation of normal anatomical structures is the main task. Therefore, types of visual grading that concern normal anatomy structure assessment will be discussed.

6.2.4.1 Fulfilment of image criteria (IC)

The European Commission image quality criteria, can be used to conduct IC assessment. In this task, the observer is presented with the image along with the relevant CEC image quality criteria. The duty of the observer is to state whether the criteria are fulfilled or not (Tingberg, 2000).

The IC score (ICS) is then calculated as the ratio of fulfilled criteria to the sum of criteria assessed (Lanhede et al., 2002). This approach has the advantage of using parametric statistics as the ICS, which is a proportion of the fulfilled criteria, is the average of the variable that can take the value of one or zero (Bath and Mansson, 2007). For this reason, the mean is normally distributed for a large sample based on the central limit theorem (Altman, 1991).

Due to the absence of soft transition from not fulfilled to fulfilled, this may cause some dilemma for the observer regarding the fulfilment of criteria when the reproduction of the criteria is close to the threshold of the observer (Bath and

Mansson, 2007). Additionally, how far the decision threshold from the reproduction is not considered in this approach, this will cause difficulties in interpreting the ICS results (Bath and Mansson, 2007).

6.2.4.2 Visual Grading Analysis (VGA):

In this approach, the observer is presented with the image along with the image quality criteria, CEC for instance, in order to let the observer grade the visibility of each structure stated in the image quality criteria (Bath and Mansson, 2007). This approach is common in studies where the main task is to assess the visibility of normal structures and can be used in studies where the main task is pathology detection, as there is a strong correlation between normal structure visibility and pathology detection (Sund et al., 2004, Herrmann et al., 2000). The VGA can be conducted in one of two ways; either absolute or relative VGA. The absolute scale uses terms like “not visible”, “poorly visible”, “adequately reproduced” and “very well reproduced” when assessing each criterion of image quality (Seeram et al., 2014). The case is different in the relative VGA, where the observer is asked to grade the visibility of anatomical structures against a reference image using a Likert scale of 5 or 3 points (Sund et al., 2004). This can be achieved using 2 alternative forced choice (2AFC). 2AFC is a psychological method used to demonstrate how efficient an observer is in identifying small differences between multiple visual or physical stimuli such as a lesion or different level of noise (Wallraven and Cunningham, 2011). This approach is considered to be less biased and very sensitive to subtle noise differences between two images.

6.3 Methods and materials:

In this section, detailed description and justification of methods employed to accomplish the research's aims and objectives will be presented. A brief overview of the chapter will provide the reader with an outline of the research method used and the justification for method selection. The main method and utilised tools will then be discussed more in depth along with the employed imaging technique. The study design and its framework will be presented with justification of each dependant and independent variables that has been encountered in this study. Finally, the statistical analysis of the data will be defined and the utilised analysis software will be discussed.

6.3.1 Overview:

The study aimed to investigate the impact of multiple independent variables on different dependant variables in order to optimise the image quality and minimise the radiation dose. An experimental approach was deemed to be the most beneficial and applicable. This is attributed to the fact that experimental approach provides the researcher with more space to isolate and control every relevant independent variable that determines the investigated dependant variable (Walliman, 2017). Implementing an experimental approach also increases the validity and reliability of the study by facilitating more control over all variables and reduces the subjectivity bias.

The main aim of the study is to investigate how image quality can be improved in obese populations. The secondary objectives are to investigate the relationship between image quality, radiation dose and phantom size. Finally, to produce prediction models that can be used in clinical practice to aid the radiographer to select the exposure factors based on patient size.

In order to accomplish these objectives, the implemented method utilised imaging a KYOTO anthropometric phantom and a series of phantoms representing different BMI groups that have been extended from the KYOTO normal weight phantom. This permitted multiple exposures to be conducted which would have been ethically, legally and morally unachievable on humans. Lumbar spine (AP) was the procedure investigated. All exposures were

conducted using a ceiling suspended x-ray system in a medical imaging lab at the University.

Tube potential, SID and filtration were used as independent variables to evaluate their individual and combined effects across different levels on radiation dose (DAP) and image quality (VGAS). Based on the numbers of independent variables (factors) and the levels across each factor, and in order to treat these factors separately and combined to fully understand their impact of the dependant variables (outcomes) i.e DAP and VGAS, the factorial design was deemed to be the most suitable design. Hence, this design was implemented across all phantoms with different size.

In order to conduct the VGAS, a reference image had to be chosen prior to the visual assessment. The reference image was selected based on the average SNR. For each phantom, a reference image was selected and the remaining images were scored by two experienced reporting radiographers using Relative Visual Grading Analysis (RVGA) method with five point Likert scale and the CEC image quality criteria. The SNR and CNR were calculated using ImageJ software. The radiation dose utilised in this thesis was the DAP reported directly by the integrated DAP reader in the x-ray unit. All generated data were primarily quantitative enabling meaningful data analysis.

The data were analysed descriptively to illustrate the spectrum of DAP, VGAS and CNR across all phantoms. Main and interaction effects were also used to investigate the impact of factors on the outcomes individually and in combination. Using FOM_{VGAS} , a prediction model for the mAs based on the phantom's thickness was generated.

6.3.2 Imaging equipment:

All equipments that were used in this study have had the usual quality control check prior to the experiments. The check usually carried out by Siemens engineer and in accordance with the manufacturer specification and the IPEM recommendations.

6.3.2.1 X-ray unit:

The dose optimisation experiments were conducted in the medical imaging laboratory at Exeter University. The x-ray equipment used was a ceiling suspended Multi Fusion Max Siemens unit (Siemens Healthcare, Germany) used mainly for teaching and research. The unit has a high-frequency generator, 80 kW, with total filtration of ~2.5 mm Al equivalent and 1 mm broad focal spot. The anode angle in this unit is 12°.

The reciprocating anti-scatter grid used has 10:1 ratio, 50 lines/cm frequency with focussed lead strips (JPI Healthcare Co.,Ltd, Korea). This grid was the only one used in this study, and it has a focal distance of 115 cm.

The tube is equipped with a CAREMAX DAP reader measuring the dose area product (DAP) with up to two digits after the decimal.

The x-ray unit had all quality control (QC) assessments conducted periodically by a Siemens engineer. The system was commissioned in June 2015, and used only for teaching and undergraduate projects.

6.3.2.2 Image receptor:

A wireless flat panel detector made of Amorphous Silicon with TFT/PIN diode technology with a conversion screen Czl, DRZ+ was used (PaxScan4336W, Varian Medical Systems, Salt Lake City, UT, USA). The detector area is 35 x 43 cm² with a pixel matrix of 3072 (v) x 2.476 (h) and pixel pitch of 139 µm. A Lithium-Ion made battery powers the detector with a capacity of 14.8 – 2.1 Ah, 31.1 Wh and runs for up to 3.5 hours (Electrochem Solutions, Inc. USA). A signal of battery life exhibits in the main workstation screens, to maintain good wireless signal output and reduce detector efficiency; the battery was replaced every time the first alert of low battery signal was indicated on the screen. The same image receptor was used throughout the study to maintain consistency in sensitivity and reduce bias.

6.3.2.3 Phantom:

A sectional torso anthropometric phantom (KYOTO PBU-50) was used for image acquisition, which has been used in the literature (Alukic et al., 2018).

The KYOTO phantom is made of urethane-based resin to form soft tissue, kidneys and liver, and epoxy resin based synthetic bone. It comes in a whole body phantom including head, torso and extremities with height of about 1.65 (m) and 50 (kg) weight. The BMI of the phantom is about 18.3 kg/m². Using the FTES and LTES layers developed in the third study, the KYOTO phantom, torso section, was extended to four obese phantoms representative for body composition of 29, 38, 42 and 46 BMI.

In order to extend the KYOTO into obese phantom with BMI of 29 kg/m², a FTES layer weighing 9.3 kg was added to the anterior aspect of the KYOTO phantom. For the 38 BMI phantom, another FTES layer, weighing 9.3 kg, was added posteriorly along with two layers of LTES weighing 3.9 kg in total, added anteriorly and posteriorly. For the 42 BMI phantom, an FTES layer weighing 3.75 kg along with LTES layer weighing 1.9 kg anteriorly. Finally, for the 46 BMI phantom, an FTES layer, 3.75 kg, along with LTES, 1.9 kg, were added posteriorly. Figure 34 shows all phantoms used with their characteristics in Table 31.

Figure 34 phantoms used in dose optimisation study

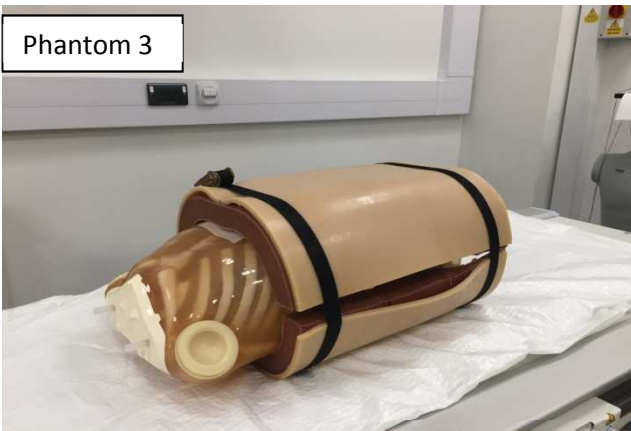
Phantom 1



Phantom 2



Phantom 3



Phantom 4



Phantom 5



Table 31 phantom characteristics

Phantom	BMI (kg/m ²)	AP Thickness (cm)	FTES		LTES		LTES, FTES calculated	
			Added	Total	Added	Total	FTES	LTES
Phantom (1)	18.3	19.6	0	3.40	0	14.19	3.40	14.19
Phantom (2)	29	23.6	9.30	12.70	0	14.19	13.48	14.19
Phantom (3)	38	30	9.30	22.00	3.80	17.99	21.99	17.73
Phantom (4)	42	32.5	3.75	25.75	1.90	19.89	25.72	19.51
Phantom (5)	46	34.7	3.75	29.5	1.90	21.79	29.49	21.29

FTES: fat tissue equivalent substitutes

LTES: lean tissue equivalent substitutes

Calculated: amount calculated based on the prediction models developed in the first study

6.3.2.4 Display monitors and lighting:

Two RadiForce GS320, 21.3 inch, 3MP monochrome liquid crystal (LCD) monitors were used in this study to display the acquired images for both visual and physical images quality assessment purposes. The native resolution of each monitor is 2048 x1536. These monitors are generally used for image interpretation research and have a specifications that meet the requirements for diagnostic display devices as recommended by the Royal College of Radiologists (RCR, 2012). Additionally, all monitors were calibrated for Digital Imaging and Communications in Medicine (DICOM) grayscale standard display function in order to meet the RCR requirements (RCR, 2012).

The lighting intensity was kept at reduced and consistent ambient level through all sessions of visual image quality assessment task for both observers, 60 lux measured using Light Meter App. This is to fulfil the European Guidelines on Quality Criteria for diagnostic radiographic images (Blanc, 1998). The room, where the task was conducted, has no windows, which will alter the lighting condition on different time of the day; hence, the observers were free to do the task at their convenience at any time of the day. No eye test was conducted before the task for any of the observers; however, both observers wear glasses during the task.

6.3.3 Imaging technique:

The KYOTO phantom was extended into four obese phantoms with different BMI and thickness all of which were used in this study. When referring to “phantom” in this section, this applies to each phantom.

The phantom was positioned on the x-ray table-top as for a standard lumbar spine (AP) examination (Bontrager and Lampignano, 2013). The median sagittal plane was parallel to the midline of both table top and the bucky. The vertical central ray was centered at the lower costal margin in the midline at L3 in line with the literature (Davey and England, 2015). The centring point was marked with a blue marker to improve consistency across all phantoms. However, as the FTES and LTES layers were added to the anterior aspect of

the KYOTO, the KYOTO phantom would move and the centring point had to be set at the beginning of every exposure.

For all exposures, the collimation was adjusted to include twelfth thoracic vertebra (T12) superiorly and the sacroiliac joint inferiorly. This was essential in order to control the radiation dose and image quality. The field size impacts on radiation dose and, for the DAP readings to be comparable across the different techniques, the field size had to be fixed. Additionally, this would enable scatter radiation resulting from field size to remain constant (Fauber, 2016).

In order to improve tube output consistency through each set of phantoms, the exposures were conducted for each phantom in one day. Two to three minutes interval between each exposure was kept throughout the study to avoid tube heating.

For each phantom, the images were coded based on excel sheet and phantom number codes. The code of each image was placed at the top left corner after making sure that it would not obscure any assessed features of the image. For each phantom, the exposures were conducted in batches of SID set.

6.3.3.1 Study design:

As discussed in the literature of this chapter, many factors have an impact on image quality and radiation dose in radiography in general and in lumbar spine radiography specifically. In dose optimisation studies, usually one factor or parameter is varied at a time while other factors are constant as the literature showed (Alzyoud et al., 2018, Davey and England, 2015, Tugwell et al., 2014). However, considering one factor only at a time will restrain the possibility of identifying the effect of the interaction that might be happening between all possible factors (Cochran and Cox, 1950). In order to overcome this limitation of one factor at a time design, one way is to conduct a factorial design experiment (Cochran and Cox, 1950). In this design, two or more factors with multiple levels in each factor, for example; kVp (70, 80, 90,), SID (100, 110, 120) and orientation (PA and AP), are crossed against each other resulting in all factors crossed with each other on all levels (Montgomery, 2017). This results in testing all possible combination of factors across all level. The formula used to

calculate the outputs of a factorial design study is the sum of multiplied n^k , where “n” is the level, and “k” is the factor.

Up until 2000, this approach of study design was not commonly implemented in radiography (Wise et al., 1999, Norrman and Persliden, 2005). However, there is growing popularity for this design in studies concerning dose optimisation, and some recommend this approach in similar research in children especially (Matthews and Brennan, 2009, Al Qaroot et al., 2014, Grondin et al., 2004, Båth et al., 2005).

In this study, this approach was applied using the formula n^k , where n refers to the levels (kVp: 6 levels, SID 3 levels and filtration 4 levels) and k to the factors (kVp, SID and filtration in this study). Implementing the factorial design allows investigating the effects of all factors, individually and combined, on different outcomes including radiation dose (DAP) and image quality (VGAS).

Based on this, the factorial design was considered in this study. Including all of the factors that have been discussed in the literature, and have an impact on radiation dose and image quality, was thought to be impossible. The reason behind this is the large number of images that will be produced. Table 32 illustrates this clearly. Producing 960 images for each phantom, 4800 images for all phantoms, will not be possible based on the resources and the timeline available to the researcher.

If 4800 exposures were conducted, with 2 minutes interval between every two exposure to avoid x-ray tube heat, a total 240 hours would be needed to accomplish the exposures. This is equivalent to eight hours continuous exposure work for a month, including the weekends. The challenge is not just in image acquisition but also in image quality assessment as they will need around 40 days of continuous work for eight hours a day. For these reasons, a decision had to be made of which factors to include.

Table 32 Images of each phantom if all technical factors were considered in the factorial design

Factor (^k)	Level (n)	$\Sigma = n_1^k \times n_2^k \times n_3^k \times n_4^k \times n_5^k \times n_6^k$
kVp	6 (70, 75, 80, 85, 90, 95)	$n_1^k = 6$
SID	5 (100, 110, 120, 130, 140)	$n_2^k = 5$
Filtration	4 (0.0, 0.1, 0.2, 0.3)	$n_3^k = 4$
Orientation	2 (FTA, FTC)	$n_4^k = 2$
Projection	2 (PA, AP)	$n_5^k = 2$
Focal spot size	2 (fine, broad)	$n_6^k = 2$
Total number of images for every phantom		960 images

From the clinical perspectives, some of these factors are hard to implement or not possible in patients with obesity. For example, PA and AP orientation cannot be applied in the case of obese patients as this group of patients tend to have difficulties in positioning (Woods et al., 2016).

6.3.3.2 Radiation dose:

The radiation dose unit used in this study is the DAP. Despite the fact that this is a detector dose not a patient dose, calculation of effective dose was deemed to be more complicated than anticipated in obese patients. Different studies have implemented effective dose as it is a commonly accepted indicator of radiation induced cancer (Walter and Slone Richard, 2010, Jang et al., 2018, Al-Murshedi et al., 2018, Notohamiprodo et al., 2018). One method of calculating effective dose is the use of Monte Carlo simulation such as PCXMC (Ladia et al., 2015, Ben-Shlomo et al., 2016, Sharma et al., 2018). However, this software utilises a stylized phantom representative of normal weight but can be modified to represent different patient's sizes. The use of PCXMC in obesity should be treated with caution especially when the purpose is absorbed dose and effective dose to compare different exposure techniques rather than epidemiological purpose. The reason behind this is the absence of fat tissue in the stylized phantom which will affect the distribution and intensity of scattered radiation.

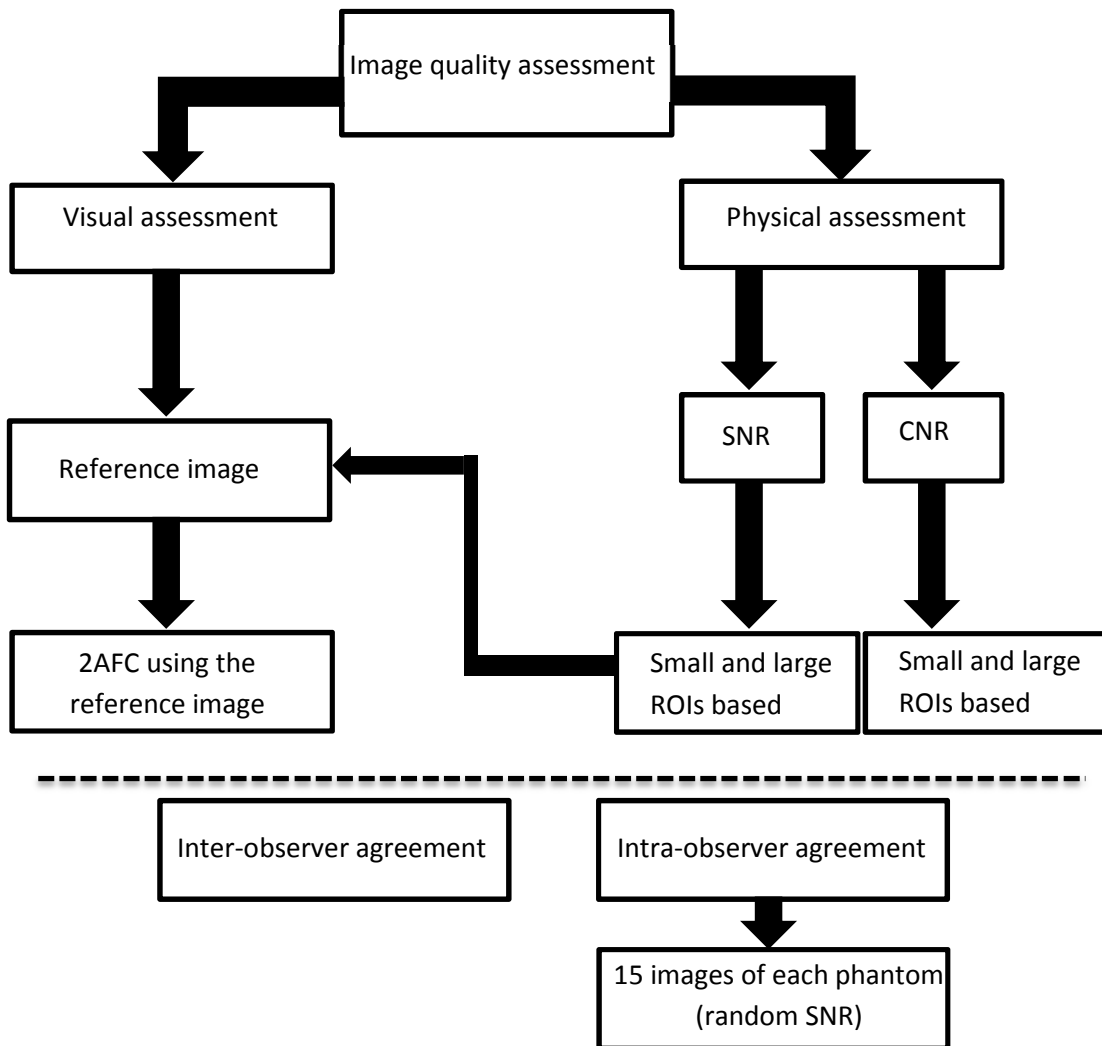
Another method of calculating effective dose is to use commercially available phantoms that facilitate TLD insertion for dosimetry purposes, such as ATOM and RANDO phantoms. This method has been practiced and reported in different research (Davis et al., 2014, Tootell et al., 2014, Ali et al., 2015). However, such method is very laborious and time consuming especially when a factorial design approach is used, as a large number of exposures is conducted. Additionally, these phantoms, ATOM and RANDO, come in standard patient sizes, while the current study deals with obese patients.

Hence, the DAP readings were deemed to be good enough especially since this study is exploratory. Five exposures were conducted across different kVp levels, 70 – 120 kVp with 10 kVp interval, with AEC on for all phantoms in order to calculate the standard error for the DAP reading. The result shows a very negligible standard error (0.003 mGy). Based on this results, one DAP reading for each exposure during the experiments was deemed reliable. This in turn impacted positively on time saving and tube heat avoidance.

6.3.4 Image assessment:

As discussed earlier, visual assessment is the most essential tool in order to investigate image quality. This is attributed to the fact that visual assessment is the only tool used and accepted in clinical practice; hence, it was the main focus in this thesis. However, the physical assessment was also used for two reasons; to determine a reference image to be used in the visual assessment and to verify whether the physical assessment supports the visual results or not. Figure 35 demonstrates the process of image quality assessment approaches that have been employed in this study.

Figure 35 Flowchart of the image quality assessment methods applied in this study.



6.3.4.1 Visual assessment of image quality:

Image quality was visually assessed using paired comparison or what is known as the two alternative forced choice (2AFC) method (Muramatsu, 2018). This approach is advantageous due to its high sensitivity to small differences between two images, the reference and experimental image (Massanes and Brankov, 2016). In this approach, the reference image is presented side by side to the experimental image (appraised image) to facilitate a comparison between the two images based on the provided criteria.

As described in the flowchart earlier, a reference image had to be identified in order to carry out the visual assessment.

6.3.4.1.1 Image quality criteria:

Relative VGA approach using a 2AFC software was used along with the CEC image quality criteria for lumbar spine. The CEC guideline consisting of 7 criteria was used with minor wording amendments as in Table 33.

Due to the variation in the importance of each criteria, weighting factors were applied and the VGAS calculated (Brennan and Madigan, 2000). These weighting factors have been developed by three clinicians who have a minimum experience of five years according to Brennan and Madigan. This method has been employed extensively in the literature (Ismailos et al., 1996, Brindhaban et al., 2005, Davey and England, 2015).

The VGAS was calculated using:

$$VGAS = \sum(WF \times Mean_{score}) \quad \text{Equation 12}$$

Where WF is weighting factor as in Table 33

$Mean_{score}$ is the average image quality scores by the observers

Table 33 Lumbar spine CEC modified image quality criteria

number	Criteria	Weighting factor
1	Visually sharp reproduction of the upper and lower vertebral endplates	2
2	Visually sharp reproduction of the pedicles	2
3	Reproduction of the intervertebral joints	3
4	Reproduction of the spinous and transverse processes	3
5	Visually sharp reproduction of the cortex and trabecular structures	3
6	Reproduction of the adjacent soft tissues, kidneys	1
7	Reproduction of the sacro-iliac joints	2

Despite the fact that CEC image quality criteria have not been validated and might not be suitable for DR, they were the only option available to the researcher based on the literature. The CEC image quality criteria have been amended and used extensively in the literature (Brindhavan et al., 2005, Davey and England, 2015, Alukic et al., 2018, Brennan and Madigan, 2000).

6.3.4.1.2 Observers:

All acquired images for the five sets of phantoms were analysed visually by two experienced radiographers with more than 8 years of reporting experience in clinical practice. It is favourable to have multiple observers assessing the images visually so the inter-observer differences can be assessed (Obuchowski, 2004). Different optimisation studies have used five observers (Allen et al., 2013, Lança et al., 2014, Davey and England, 2015). However, other studies used even larger number of observers with no justification, (Buissink et al., 2016, Mraity et al., 2016, Tugwell et al., 2014). On the other hand, studies have used two or even one observer only (Alzyoud et al., 2018, Mraity et al., 2018). Hence, it is clear that there is no literature indicating the required number of observers. It is more to be pragmatic based on the number of observers available to the researcher during the study.

As this is phase one study, where a new diagnostic test is explored, (Obuchowski, 2004), two observers are needed as the minimum number. As more than 300 images were acquired and considering the amount of time that each image will take the observer to make a decision on 7 criteria for each image, using more than two observers was not practicable. Additionally, the researcher had access to two reporting radiographers, who expressed their interest in assessing the images' quality.

Both observers had a training session prior to commencing the image quality assessment task. Such training is suggested and recommended by Mantiuk and colleagues (Mantiuk et al., 2012). This is to introduce the observers to the task so they can familiarise themselves with the images and criteria and ask any questions on any aspect before conducting the final image assessment task. The session covered two main aspects that are considered most influential on the results. The first is the technical aspect. Both observers were introduced to the software and how to move between criteria and images. The second aspect is image quality related where observers were provided with the definition of all terms used in image quality criteria as shown in Table 34, which is adopted from CEC guideline (CEC, 1996).

Table 34 Definitions of the degree of visibility for anatomical structures in the image

Term	Definition
Visualization	Characteristic features are detectable but details are not fully reproduced; features are just visible.
Reproduction	Details of anatomical structures are visible but not necessarily clearly defined; detail is emerging.
Visually sharp reproduction	Anatomical details are clearly defined; details are clear.

Additionally, the image quality criteria were discussed with the observers and which area to look at when making the final decision. This is justified by the

result from Tingberg and colleagues' study where they found that observers tend to view different parts of the image which resulted in large inter-observer variations. For example, the first criteria in Table 33 indicate visually sharp reproduction of plate surfaces, but there are five lumbar vertebrae. Hence, the observers were provided with a hand-out (Table 35) of anatomical details included in this study adopted from Almén et al. study (Almén et al., 2004).

Table 35 Anatomical details included and the image criteria used in this study

Anatomical structure	Observed area
Plate surfaces	L3
Pedicles	L3
Lateral cortex	
Intervertebral joint	L3 and L5
Spinous and transverse processes	L3 and L5
Adjacent soft tissue	Kidneys

Both observers had the chance to ask any questions as the researcher was available at the beginning of each image quality assessment task.

Each observer conducted the visual assessment task completely blinded to the exposure factors and the phantom thickness. However, it was not possible to mix all images from the five phantoms sets in one set as each phantom has its own reference image from within the set. Hence, each set has 72 images that represent a specific phantom with specific BMI, but this was blinded to the observers. The observers were informed once they started the session that they would not be able to stop and resume later as the software does not provide this feature. However, the researcher offered to split each set of images into two, 36 each, if the observer needed to fit the task with other duties they had in the department. Additionally, this is to eliminate fatigue and reduce the image quality task duration which both have an impact on image perceptual errors (Alers et al., 2011, Pinto and Brunese, 2010).

6.3.4.1.3 Image display:

Each phantom had 72 acquired images that needed to be visually assessed by each assessor using a reference image from within each set. Validated bespoke software was used to accomplish the visual image quality assessment task (Hogg and Blindell, 2012), which has been used in different 2AFC image quality assessment studies (Tugwell et al., 2014, Alzyoud et al., 2018, Davey and England, 2015). The 2AFC software allows the observer to move between the image to be assessed and the quality criteria as many times as needed using a single keyboard key, the space bar. It also presents the images randomly and restricts the manipulation of the window width or zooming. This will subsequently reduce the bias and variability between observers as well as guaranteeing that differences in visual perception are caused by acquisition factors rather than post processing.

The reference image was presented on one monitor while the second monitor was used for the assessed image. In order to mimic the clinical practice setting, the distance between the observer and the monitors was not restricted.

6.3.4.2 Physical assessment of image quality:

The main assessment used in this study was the visual approach. Nevertheless, physical assessments, SNR and CNR, were also conducted for two reasons. The SNR was calculated mainly to determine the reference image in order to conduct the visual assessment. The CNR was derived to support the visual assessment results.

Before describing the physical assessments calculation, it is worth discussing the approach used in drawing the ROIs to calculate SNR and CNR. Despite the fact that physical assessment is objective and based on numbers rather than the observer's preference, as is the case in visual assessment, subjectivity still exists when drawing the ROIs (Sa dos Reis et al., 2017). This includes the size of ROI, the exact location of ROI and the number of ROIs created. The larger the size of the ROI the better as random variation between pixels will be minimised (Sa dos Reis et al., 2017). However, one could argue that a large ROI is not possible in case of small image or small background areas. The

same applies to exact location of the ROI and to the number, as these will depend on the preference of the person carrying out the ROI drawing (Sa dos Reis et al., 2017). Hence, and in order to minimise bias and to ensure that any strong correlation between the physical (CNR) and visual assessment is consistent and not by chance, SNR and CNR ROIs were drawn twice using Image J software (National institute of Health, Bethesda, MD). The software allows the user to specify the measurements needed, mean pixel value and standard deviation in this study. In order to minimise chance of errors, multiple measurement was used for all ROI across all images and the results exported in excel file to conduct the analysis.

In the first round, Figure 36 (A), five smaller ROIs were drawn in homogenous soft tissue areas, along with five similar areas in size in L1, L2, L4 and two other ROIs on the right and left posterior superior iliac spines.

In the second round of drawing the ROIs, four regions were drawn covering most of L1, L2, L3 and L4. Total area of the four regions combined contained 290286 pixels. Two large areas, with total area similar to total area of the first four ROI, 300834 pixels, were drawn covering the adjacent soft tissue, Figure 36 (B). This approach has been implemented by Brindhaban and colleagues (Brindhaban et al., 2005).

SNR and CNR were calculated as using the following formulas which have been used previously in the literature (Marshall, 2009, Moore et al., 2014, Alzyoud et al., 2019, Moore et al., 2016):

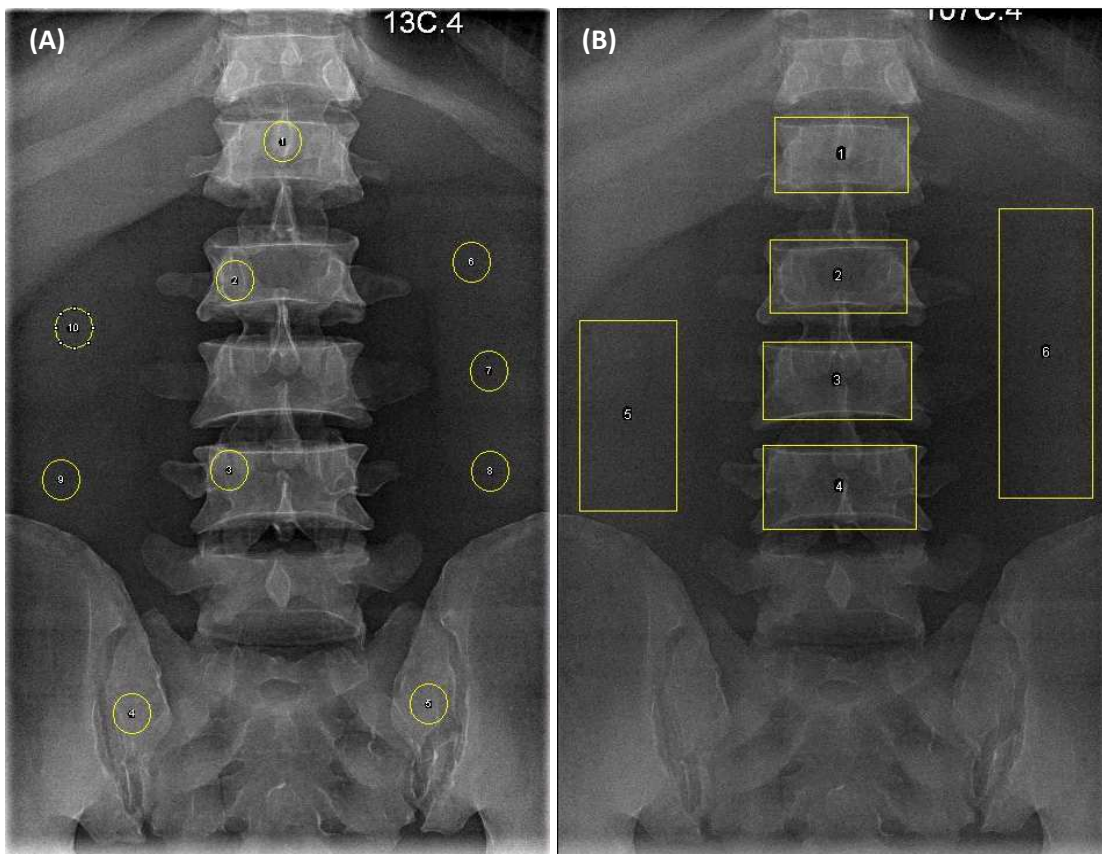
$$SNR = \frac{\text{Mean signal value within the Foreground (Bone ROI)}}{\text{Standard deviation withing the Background (Tissue ROI)}} \quad \text{Equation 13}$$

$$CNR = \frac{\text{Mean signal of Foreground (Bone ROI)} - \text{Mean signal of Background(Tissue ROI)}}{\frac{\sqrt{(\text{Standard deviation of the bone})^2 + (\text{standard deviation of the soft tissue})^2}}{2}} \quad \text{Equation 14}$$

The reference image was subsequently selected based on the average SNR. Out of 72 images in each phantom set, the SNR values were sorted from lowest to highest and the image with an average SNR value was selected. As multiple

images had similar SNR, the reference image was evaluated using the CEC criteria and the image that scored 3 and more of each criteria was selected.

Figure 36 small and large ROIs used to calculate SNR and CNR

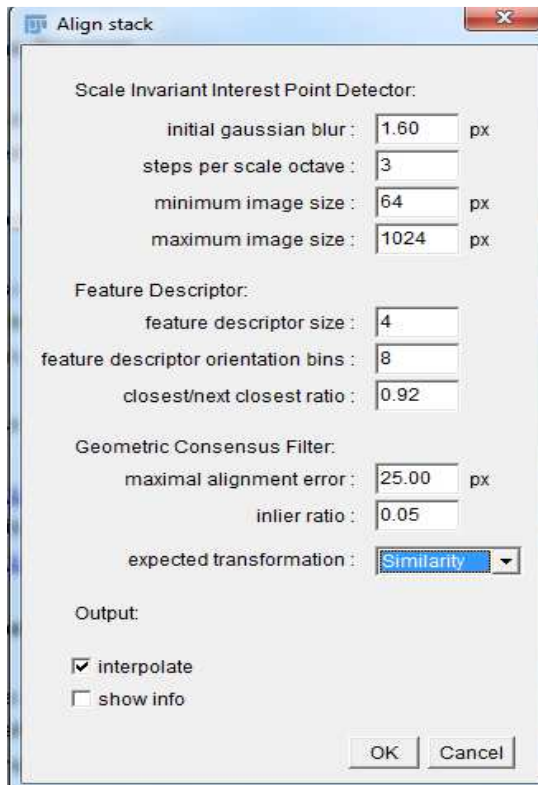


The images were acquired with no changes in collimation, however, cropping some images was inevitable due to the appearance of bright areas outside the exposed area but inside the image. This caused an issue when trying to align all images in order to draw ROIs consistently across each set, Figure 38. One way to overcome this is to repeat the measurement three times and calculate the average. However, this approach is laborious especially with the large amount of images. It also imposes the risk of errors due to the large amount of data that will be produced.

“Linear Stack Alignment with SIFT” was used in order to align the images for the sake of time and errors saving, Figure 39. The plugin identifies invariant features in an image and uses these features in order to enable locating an object in that image (Lowe, 2004). The plugin has been used extensively in the literature, with more than 49 thousand citations, and provides a valuable tool in images alignment.

All scale invariant input point detector, feature descriptor and geometric consensus filter input were kept as default as advised by manual, figure 5 (Saalfeld, 2008). However, the expected transformation was changed to ensure the best image alignment. The best option was the similarity. In this option, the plugin will identify similarity between images and align the image based on the highest value of pixel similarity. Figure 37 illustrates the final plugins settings used in this study.

Figure 37 Feature extraction used in the plugin



In order to ensure that the plugin would not affect the pixel features in the image stack, a pixel profile plot was generated. A line was drawn across the middle of L1 in both the aligned and non-aligned stack. As illustrated in Figure 40, the pixel density across the seventy two images in each stack has a similar trend. The minor difference between the two stacks is attributed to the non-alignment issue rather than to pixel density change due to the application of the plugin. Additionally, drawing an identical line with precise location was not possible, hence, this could also have contributed to the minor difference in the pixel intensity plot profile.

Figure 38 Image with ROIs without alignment

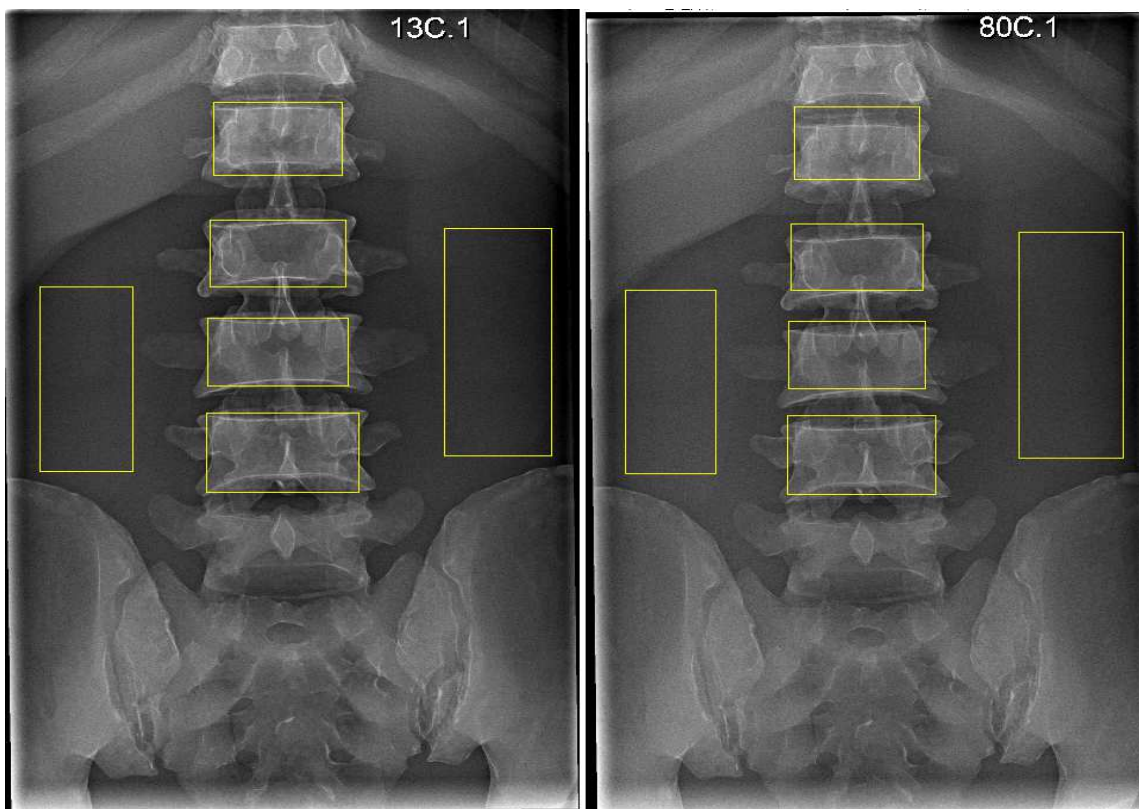


Figure 39 Images with ROIs after alignment

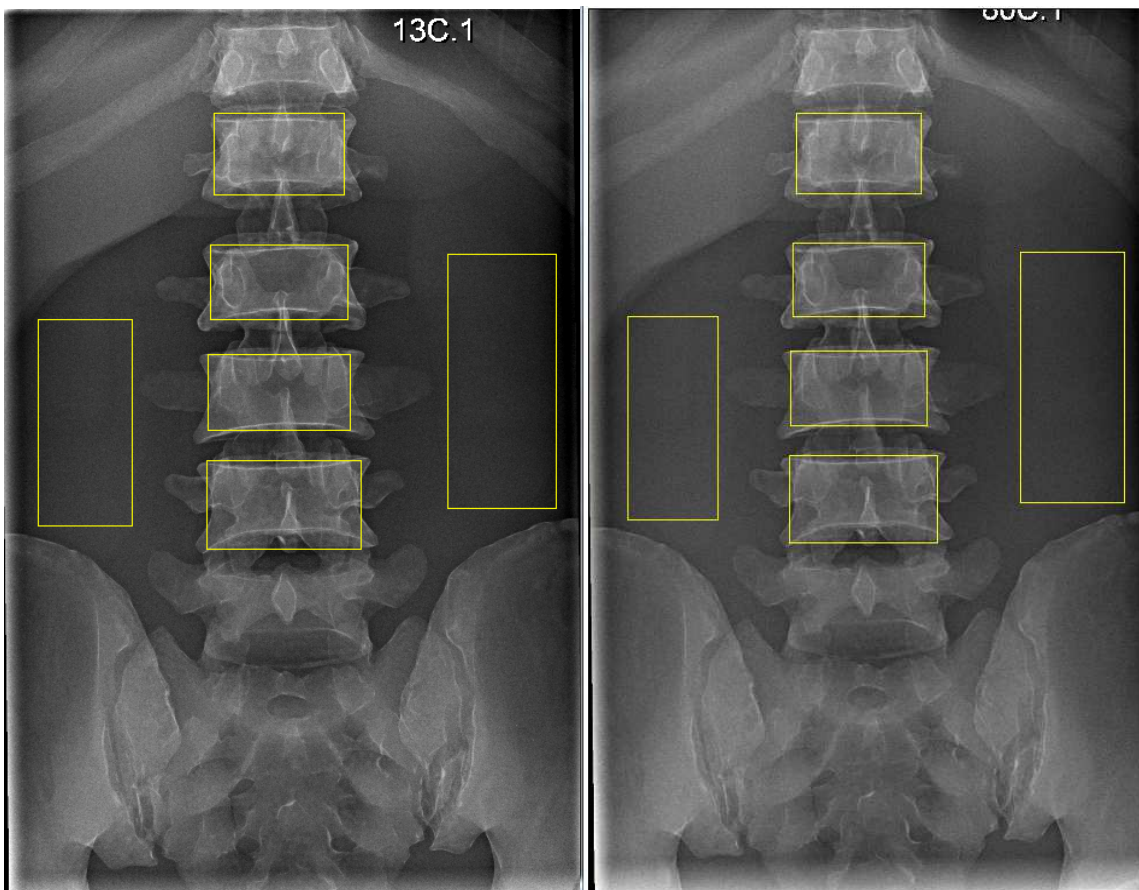
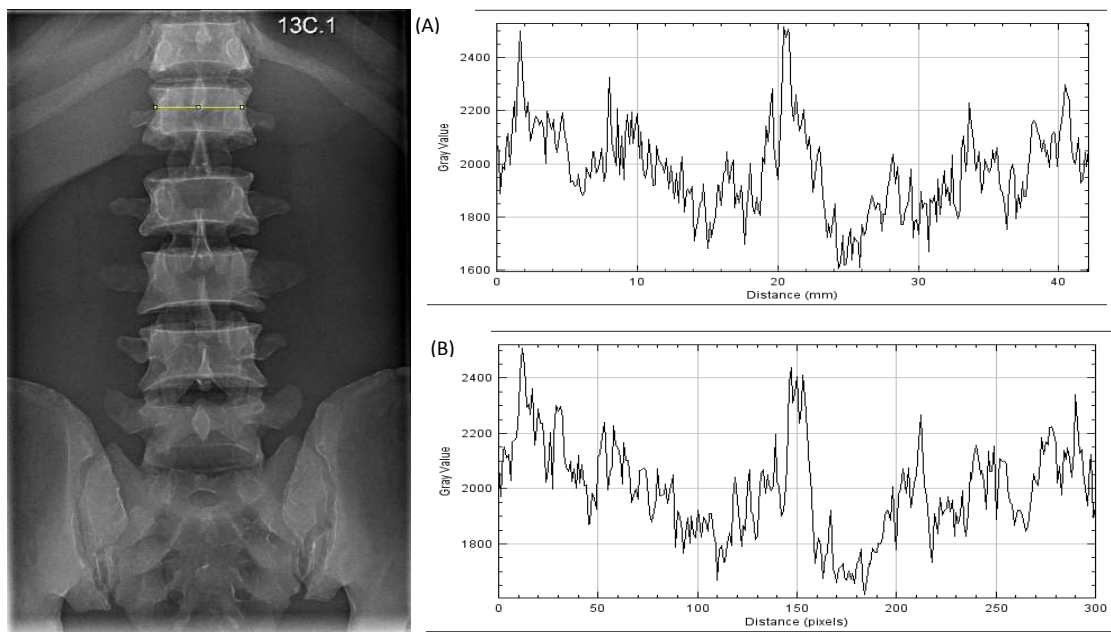


Figure 40 Plot file for image stack before (A) and after alignment (B) plugins



6.3.5 Optimisation score (Figure Of Merit, FOM_{VGAS}):

In accordance with the ALARA principle, the radiation dose to the patient should be kept at the lowest level. However, reducing the radiation dose might compromise the image quality by reducing the x-ray photons that reach the detector and form the image (Amis Jr et al., 2007). ALARA does not certainly mean the lowest radiation dose, nor, when practiced, does it result in the least desired image quality (Seibert, 2004). Different optimisation studies have explored radiation dose and image quality separately (Jang et al., 2018, Alzyoud et al., 2019, Moore et al., 2015, England et al., 2015). However, Doyle and colleagues have proposed and used a method where the image quality and radiation dose are incorporated by dividing the image quality score by the radiation dose to give a figure of merit (FOM), (Doyle et al., 2005, Doyle et al., 2006). According to Samie and colleagues, the FOM is defined as the end point of the optimisation (Samei et al., 2005). By calculating the FOM, one could signify the optimisation score where the highest indicates good image quality at a lower dose and vice versa. In this thesis, the FOM was calculated through dividing the image quality, VGAS, by the radiation dose (DAP).

6.3.6 Statistical analysis:

All data were inputted and saved in an Excel 2010 sheet for each phantom set separately. In terms of visual image quality assessment, the inter- and intra-observer variability was evaluated using the Intra-class Correlation Coefficient (ICC). This statistical test has been used extensively in similar studies (England et al., 2015, Tugwell et al., 2014, Al-Murshedi et al., 2019, Harding et al., 2014). Additionally, the ICC permits investigating the differences in scores for individual sections along with the correlation between the assessors. However, the interpretation of the ICC is a complex issue as various interpretations exist in the literature. In this thesis, the most commonly used and recommended interpretation reported by Fleiss and Rosner was used (Fleiss, 2011, Rosner, 2015). ICC values of less than 0.40 indicates poor reproducibility, ICC values in the region between 0.40 – 0.75 indicate fair to good reproducibility, and an ICC value of greater than 0.75 indicates excellent reproducibility. This was

conducted using SPSS software package (PASW Statistics 25: version 25, SPSS Inc., Chicago, IL).

Descriptive statistics for mAs, DAP, CNR and VGAS for each phantom will be presented to demonstrate the trend of these dependant variables along with the phantom size. Additionally, the scatterplot of the trend between DAP and VGAS, DAP and CNR will be presented.

The main and interaction effects of the acquisition factors (kVp, SID and filtration) on the outcomes (DAP and VGAS) will be investigated using two level factorial design analysis. Despite the fact that the study was conducted in full factorial design, the two level factorial design analysis simplifies the analysis process and provides simple but meaningful results. It allows the ANOVA to be conducted using two levels, the highest and lowest, of a factor and demonstrate the effect and interaction effect based on each factor when changes from low to high. The plot will be generated using Minitab statistical software, version 17 (Minitab Inc., Pine Hall Road, state college, PA).

An mAs prediction model will be produced based on patient's thickness and the optimal acquisition factors.

6.4 Results:

This section presents the results from the optimisation experiments. Results will be presented in three main themes. First, observer agreement along with a descriptive analysis of the DAP, VGAS, and mAs will be presented for all the images in each phantom. This is to show the trend of all the dependant variables based on the phantom size and thickness.

The second theme, is the main effect along with the interaction effects of the primary acquisition factors (kVp, SID and filtration) and the significance of the response variables, mainly VGAS and DAP, will be presented for each phantom. Additionally, Images that have met the reference image VGAS and above will be presented in a bar chart along with the exposure factors used. This includes all images that have similar VGAS to the reference image or above with disregard to the radiation dose. The bar chart will include the DAP, VGAS and FOM_{VGAS} for each satisfactory image sorted by the FOM_{VGAS} . The relationship between CNR, both small and large ROIs, and the VGAS will be presented.

Final theme will include the overlaid contour plot for the best acquisition factors that can be used in each phantom constrained by VGAS (equal or above the reference image) and DAP (first quartile). The mAs prediction model based on the phantom thickness will also be presented.

6.4.1 Inter-observer agreement:

Both observers completed the visual image quality assessments for all images of all five phantoms. As the visual assessment in this thesis was based on assessing normal anatomical structures, each observer set a level of agreement on how clear the anatomical structures in the experimental image compared to the reference image. Unlike the physical measurement, this approach is subjective and vulnerable to inter-and intra-observer variation

Table 36 Intra-Class Correlation (ICC) of observer agreement on visual image quality scores for all phantoms

Phantom set	Absolute agreement	95 % CI	
		lower	upper
Phantom (1)	0.81	0.71	0.87
Phantom (2)	0.90	0.85	0.94
Phantom (3)	0.84	0.75	0.89
Phantom (4)	0.89	0.83	0.93
Phantom (5)	0.69	0.17	0.86

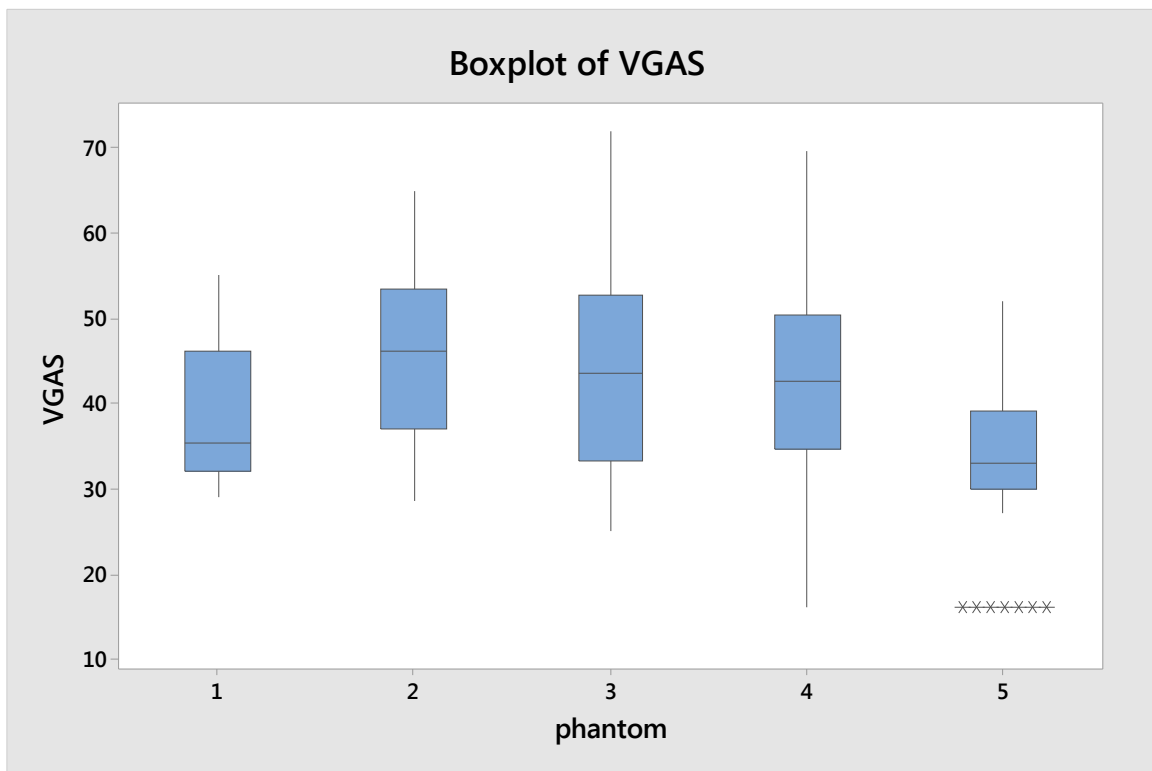
Table 37 Intra-class Correlation Coefficient (ICC) of observer consistency in individual phantom set and for all phantoms

Total/single	Absolute agreement	95 % CI	
		lower	upper
All phantoms	0.89	0.83	0.93
Phantom 1	0.75	0.40	0.91
Phantom 2	0.81	0.53	0.93
Phantom 3	0.88	0.69	0.96
Phantom 4	0.97	0.92	0.99
Phantom 5	0.95	0.88	0.98
 			
All phantoms	0.93	0.90	0.96
Phantom 1	0.90	0.73	0.96
Phantom 2	0.91	0.77	0.97
Phantom 3	0.95	0.87	0.98
Phantom 4	0.93	0.82	0.97
Phantom 5	0.94	0.83	0.98

6.4.2 Descriptive analysis

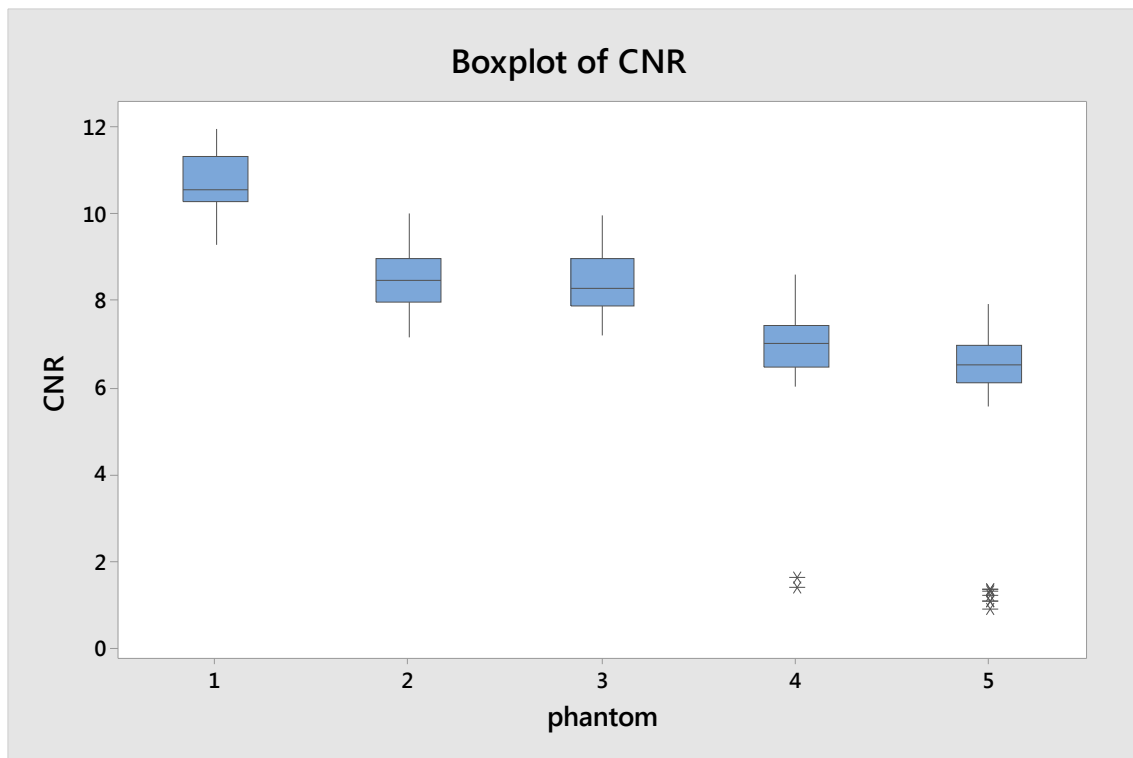
This section illustrates the DAP, VGAS, CNR (large ROIs) and mAs changes across all phantoms in order to demonstrate the trend of these variables' change along with the phantom size.

Figure 41 VGAS values for each phantom



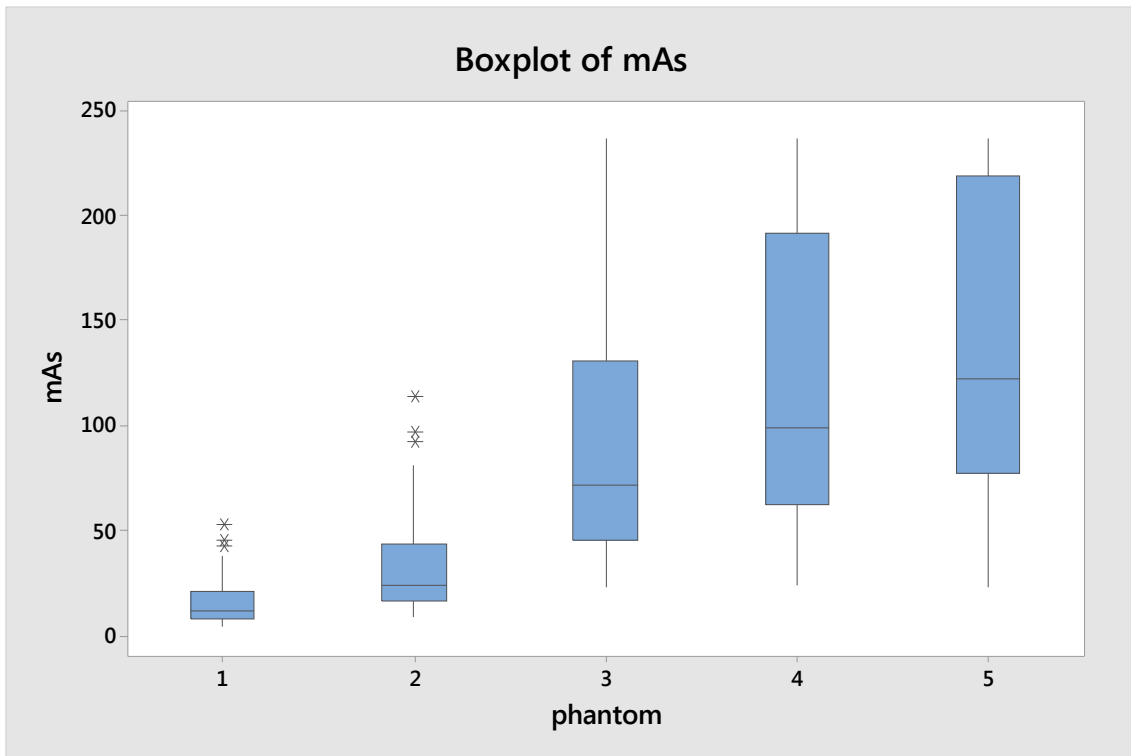
As illustrated in Figure 41, the visual VGAS decreases as the phantom size increase except in the first phantom where the mean VGAS was less than the mean of all phantoms but higher than phantom 5.

Figure 42 CNR values for each phantom



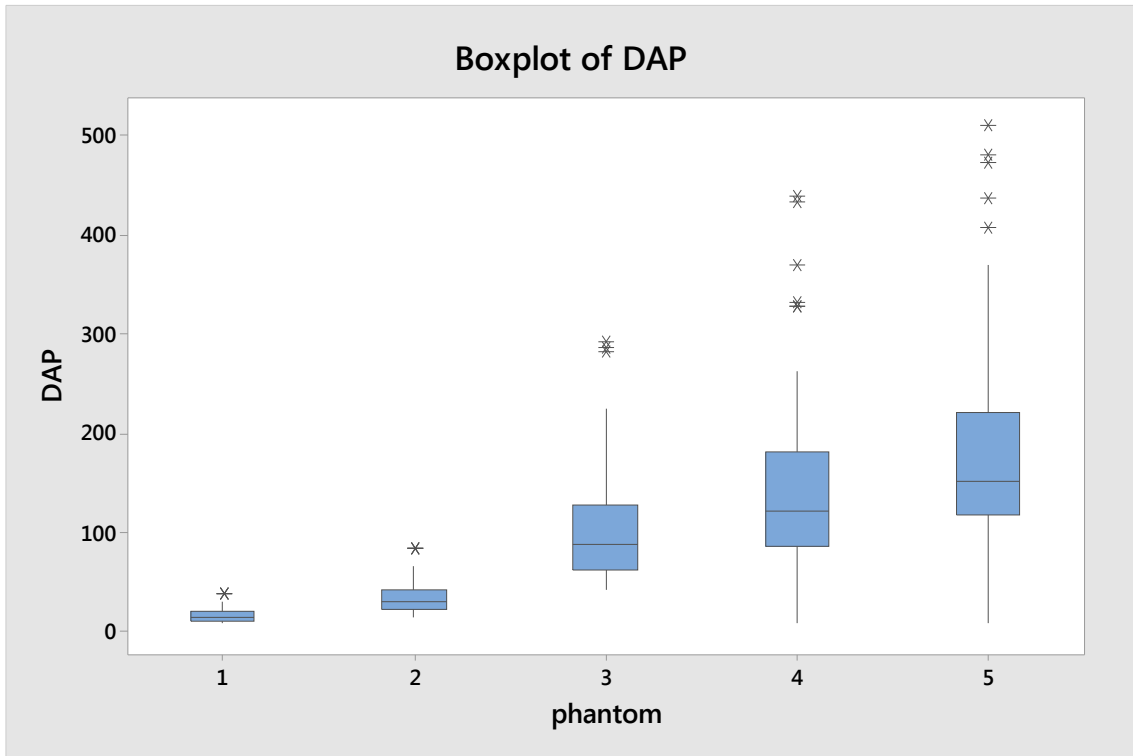
The CNR had an inverse relationship with the phantom size Figure 42.

Figure 43 mAs changes across phantoms



As AEC was used in this experiment, as the phantom's size increases the mAs increases as well in order to allow for more photons to penetrate through the phantom and compensate the scattered photons, figure 43 illustrated.

Figure 44 DAP changes with the phantom size



The DAP readings increases as the phantom thickness increases, figure 44 demonstrates. This is due to the increase in the mAs that has been illustrated in figure 43.

6.4.3 Main and interaction effects of kVp, SID and filtration on DAP and VGAS

In this section, the main effects of all acquisition factors employed in this study (kVp, SID and filtration), along with the interaction effects between them, on DAP and VGAS on phantom basis will be illustrated. The effects will be presented in charts that show the power of the effects of the factors on the outcomes when changed from low to high values. The effect, which is the difference between the highest and the lowest point in the slope, will be presented along with regression coefficient and the significance value. Following each phantom, a bar chart will be presented summarising the combined acquisition factors, in the X axis, that have been used to produce images that match the reference image or above with disregard to the dose.

6.4.3.1 Phantom (1)

Figure 45 Main effect (A) and interaction effect (B) of kVp, SID and filtration on DAP for phantom 1 (BMI: 18.3 kg/m²)

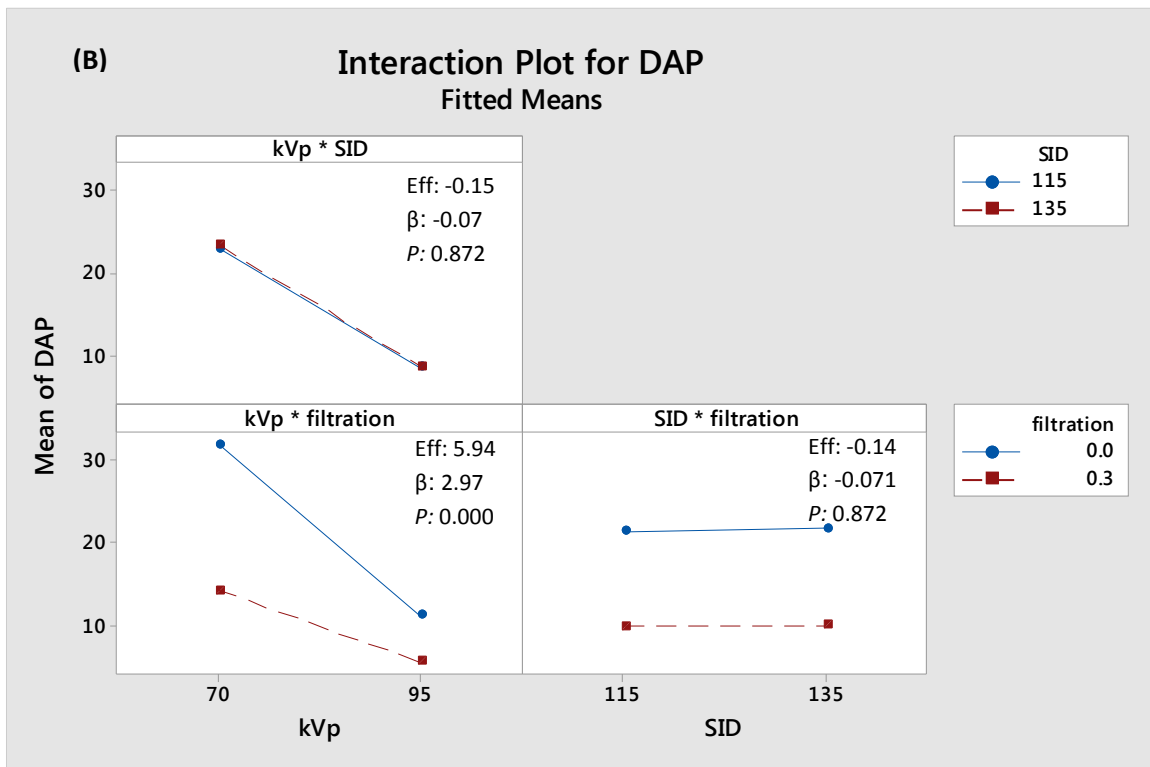
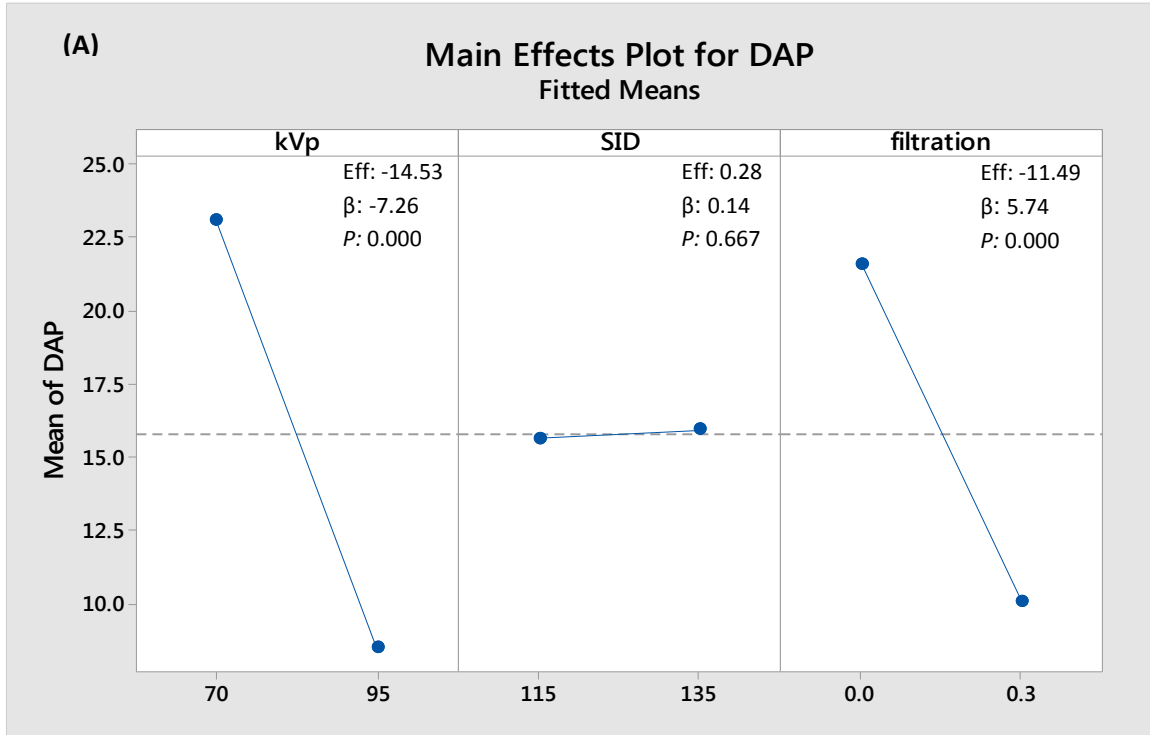
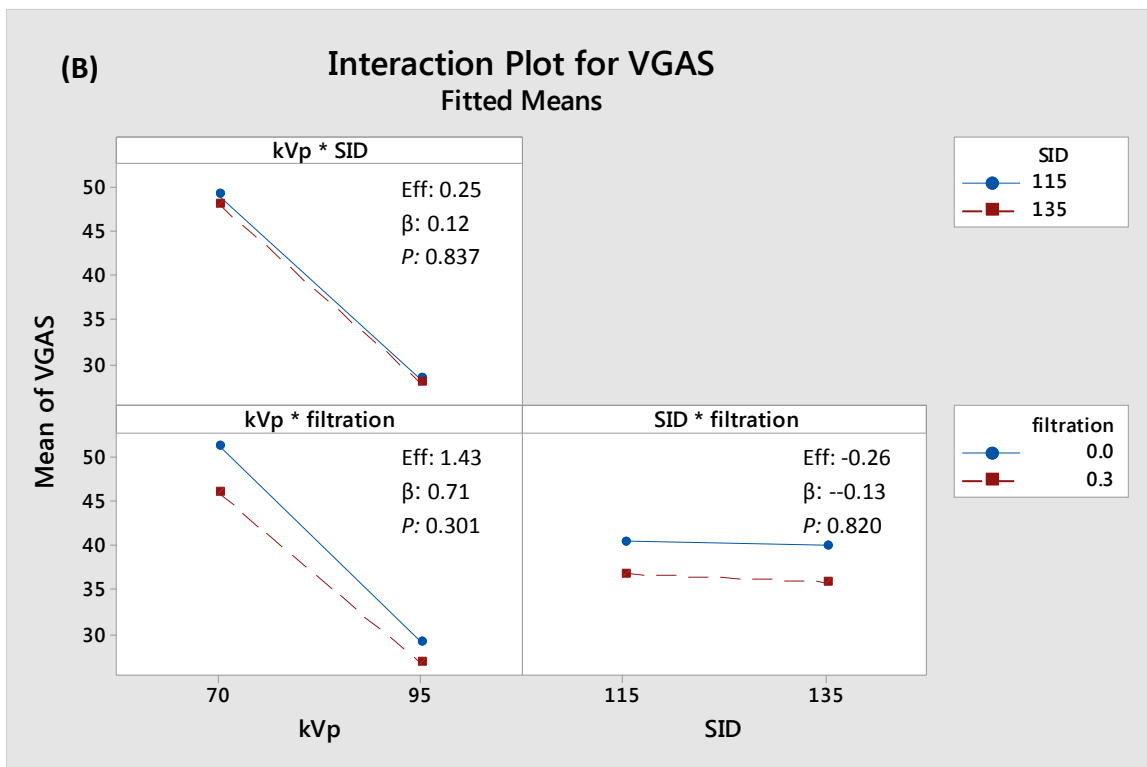
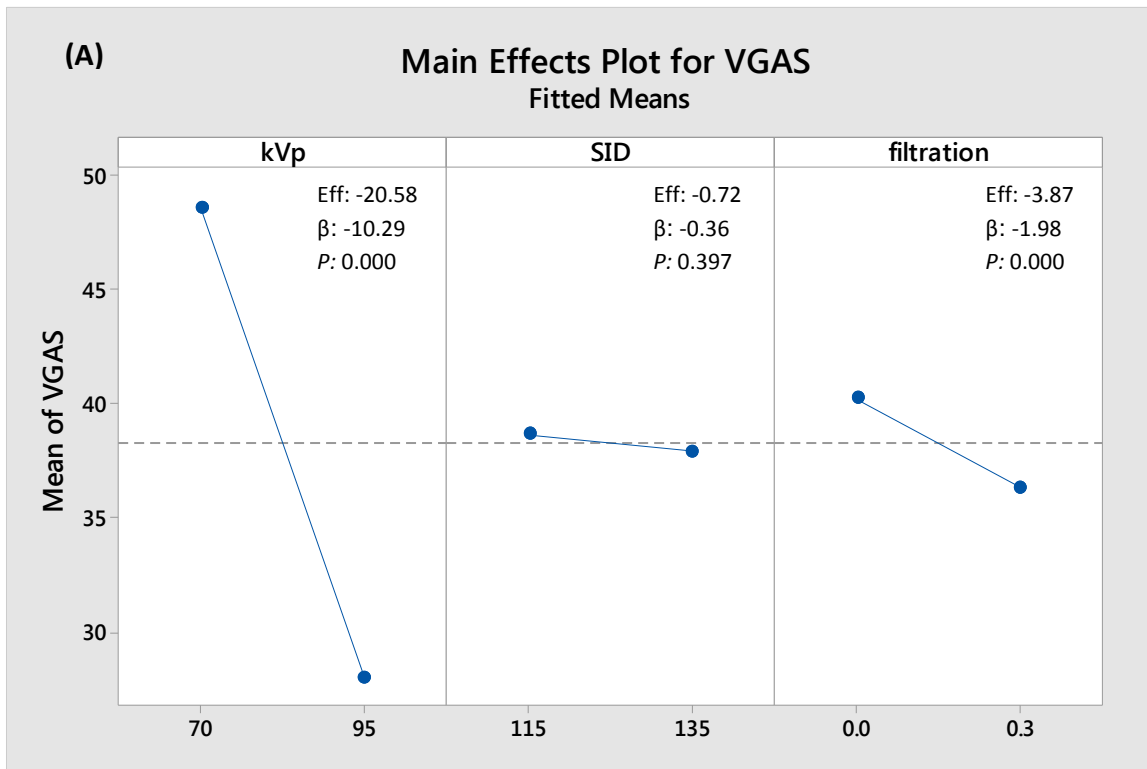


Figure 45 (A) demonstrates that kVp and filtration have the high negative effect on DAP (-14.5 and -11.4 with $P < 0.001$) while the SID has a non-significant positive effect (0.28). In Figure 45 (B) it is clear that when kVp combined with SID, long and short SID performed equally across high and low kVp. However, with kVp and filtration combination, increase in kVp inverse estimated effects across high and low filtration. High filtration (0.3 mm Cu) affects the DAP negatively more than zero filtration but high kVp decreased the effect gap between the types of filtration, zero and 0.3 mm Cu.

Filtration types performed equally across long and short SID with high filtration reducing the DAP more.

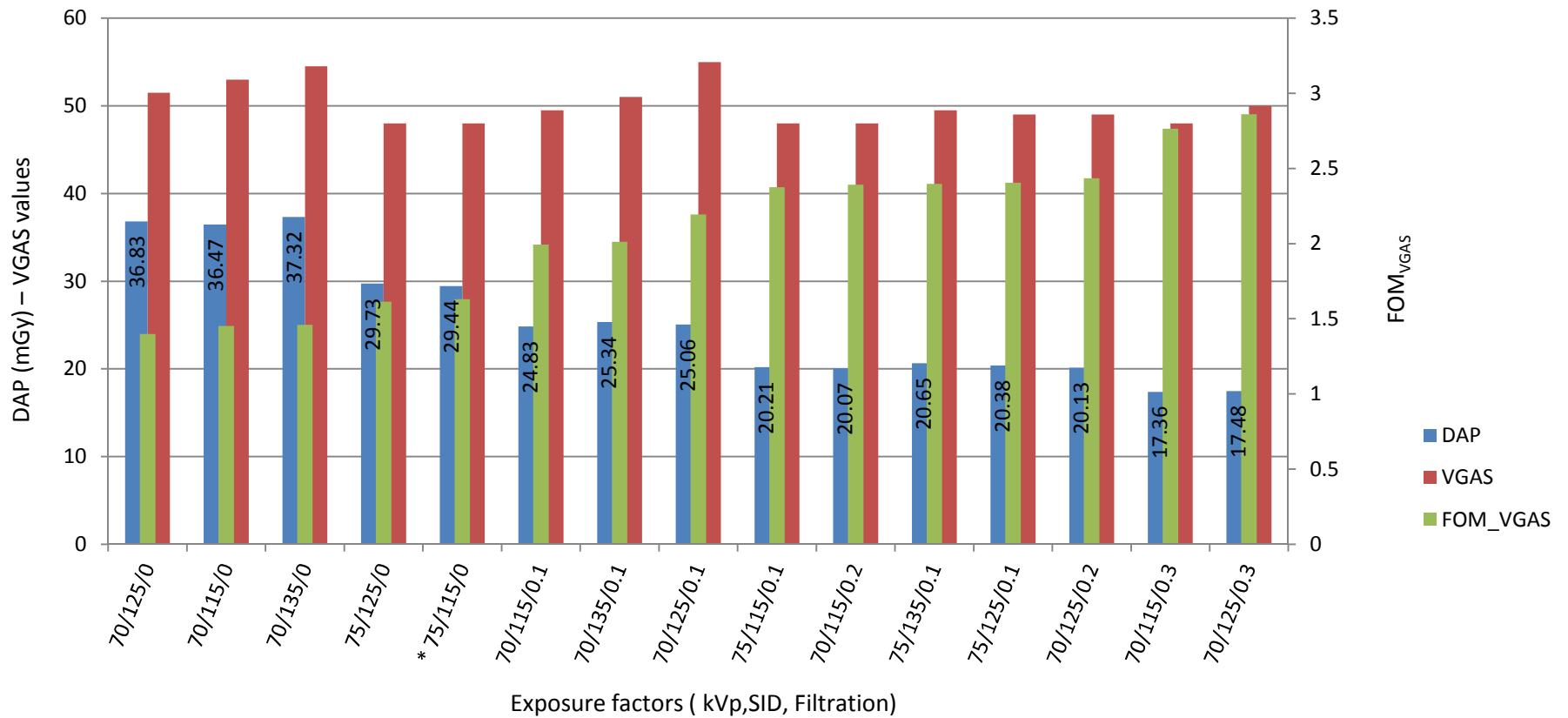
Figure 46 Main effect (A) and interaction effect (B) of kVp, SID and filtration on VGAS for phantom 1 (BMI: 18.3 kg/m²)



As shown in Figure 46(A), kVp has the highest negative impact on image quality when changed from low to high (-20.58, $p=0.000$) followed by filtration (-3.8, $p=0.000$). The SID showed similar but non-significant (-0.72, $p=0.397$) trend of effect on image quality (VGAS) when changed from lower to higher values.

The results of the interaction effect, Figure 46(B), show no significant interaction between the acquisition factors effects on VGAS. However, the VGAS scored higher with low filtration when combined with kVp and SID with equal steady decrease when kVp changed from low to high while remaining equal across short and long SID.

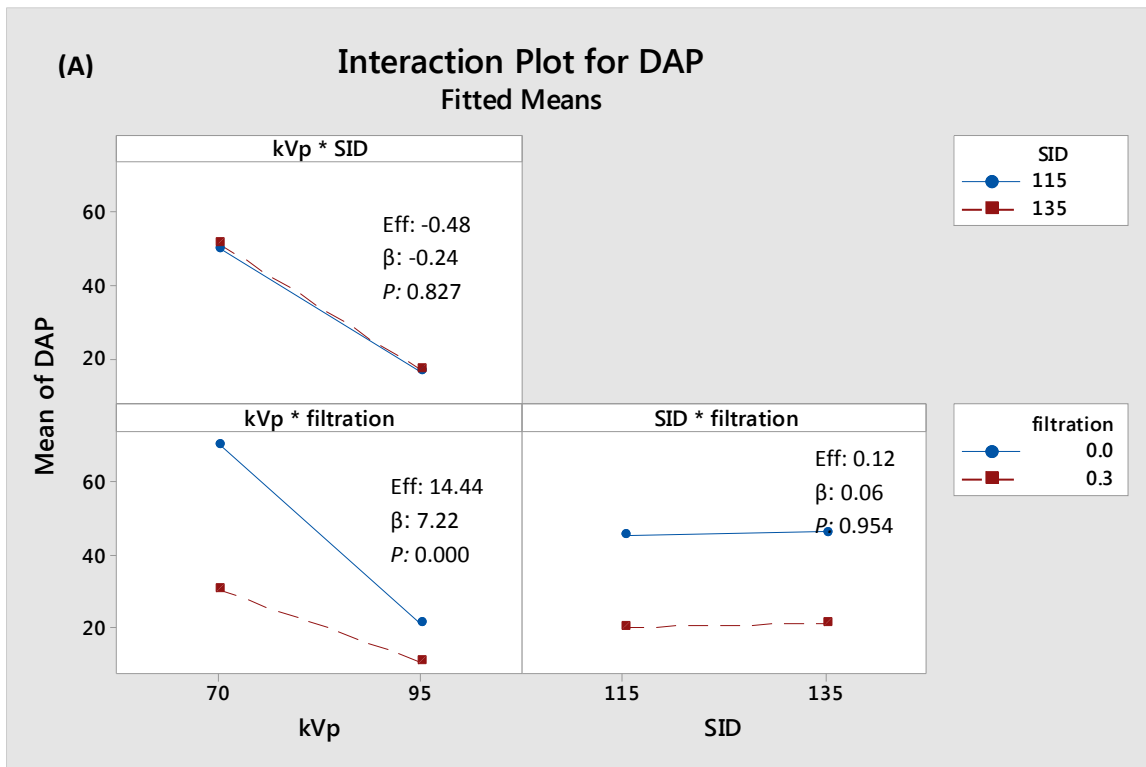
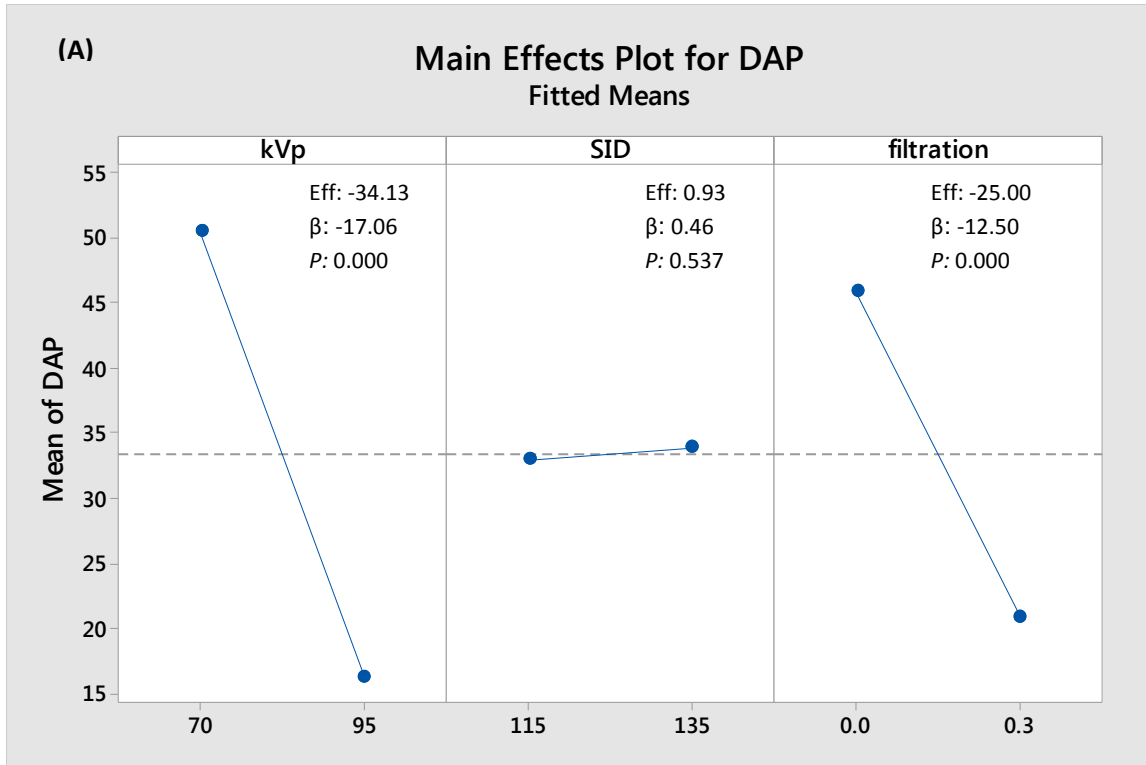
Figure 47 Acquisition factor combination (kVp, SID * filtration) that led to image with similar VGAS to the reference image or above including DAP, VGAS and FOM_{VGAS} for each combination (phantom 1, BMI: 18.3 kg/m²)



* Reference image

6.4.3.2 Phantom (2)

Figure 48 Main effect (A) and interaction effect (B) of kVp, SID and filtration on DAP for phantom 2 (BMI: 29 kg/m²)

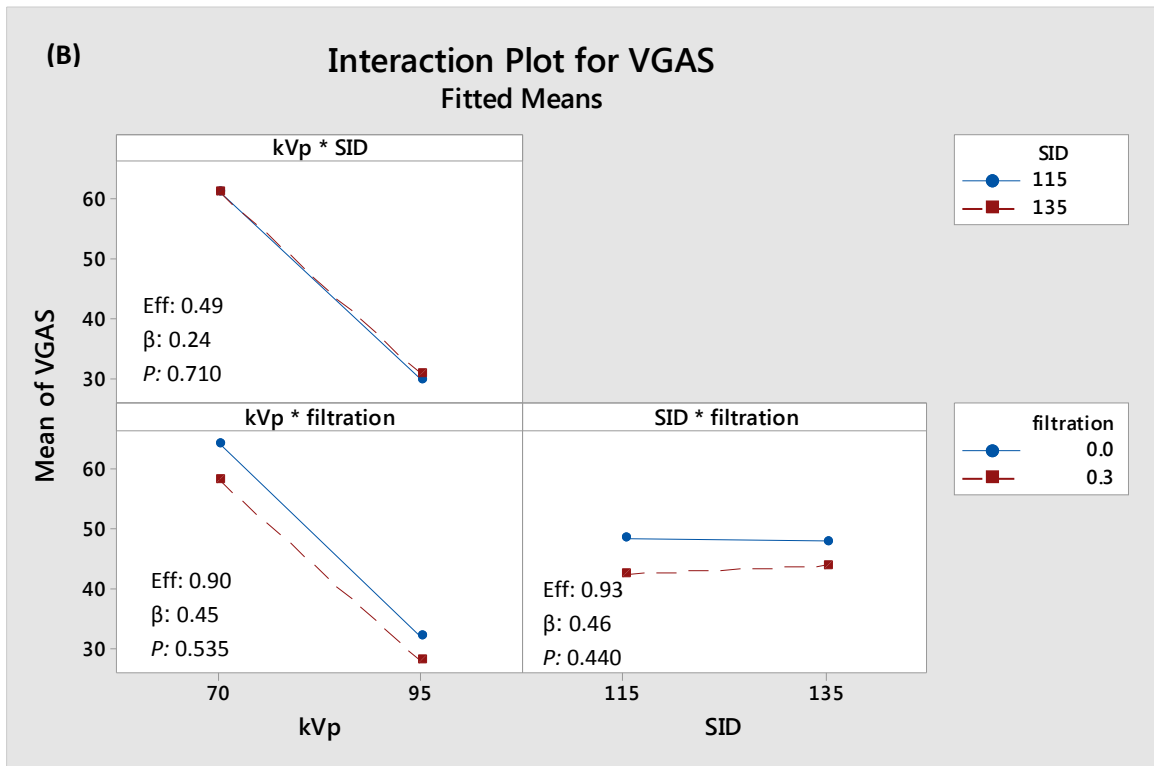
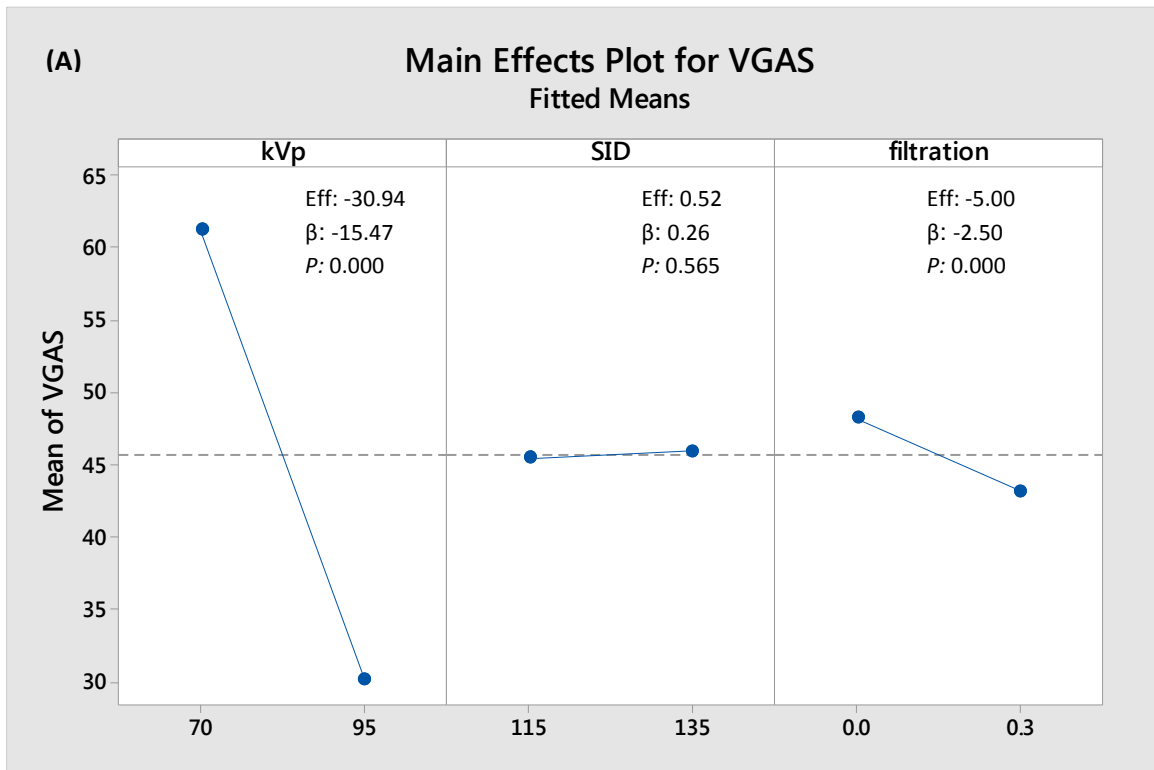


As illustrated in Figure 48(A), the kVp and filtration have the highest negative impact on DAP (-34.13 & -25, $p=0.000$), while the SID has a non-significant positive effect.

In Figure 48(B) it is clear that when kVp combined with SID, long and short SID performed equally across high and low kVp. However, with kVp and filtration combination, increase in kVp inverse estimated effects across high and low filtration. High filtration (0.3 mm Cu) affect the DAP negatively more than zero filtration but high kVp decreased the effect gap between the types of filtration, zero and 0.3 mm Cu.

Filtration types performed equally across long and short SID with high filtration reducing the DAP more.

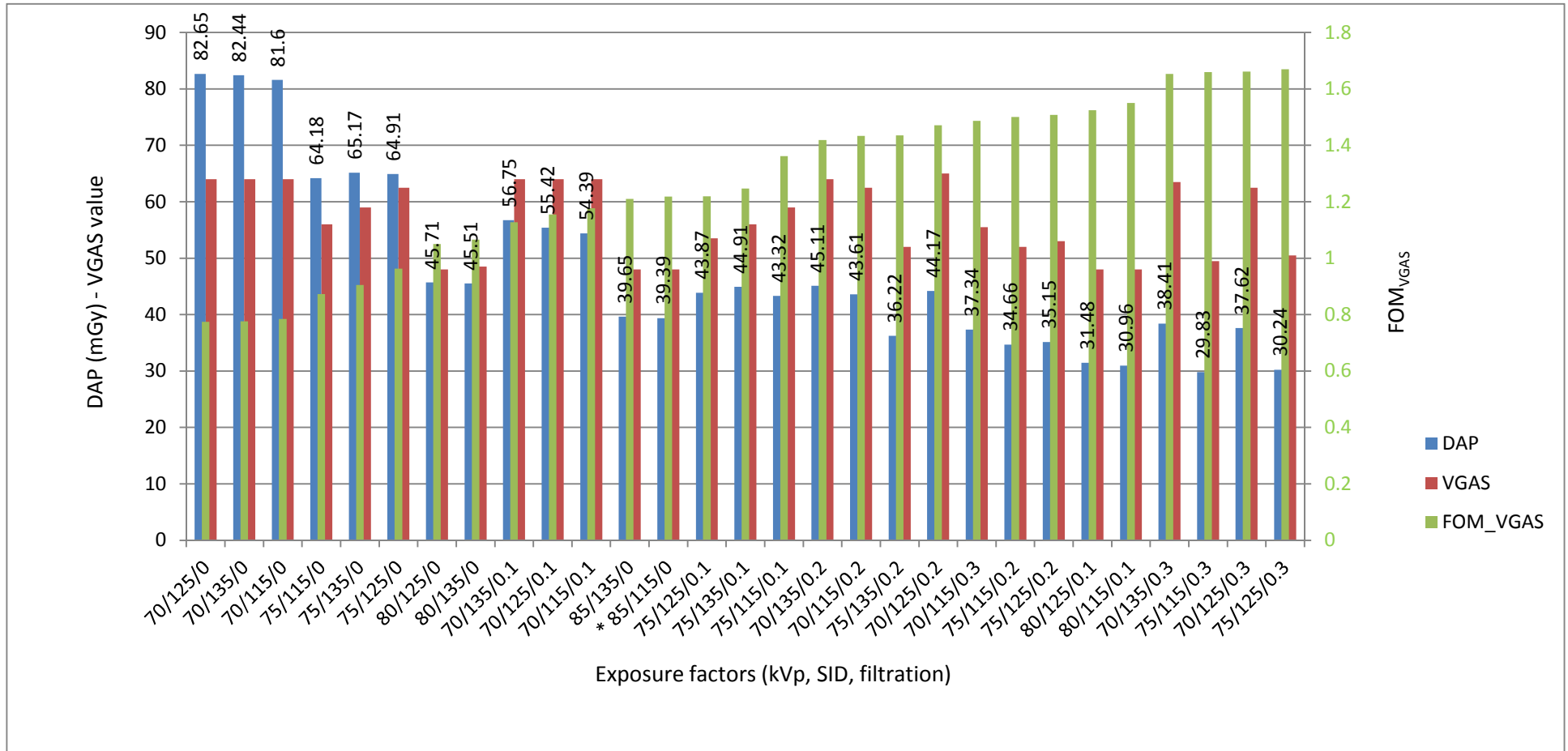
Figure 49 Main effect (A) and interaction effect (B) of kVp, SID and filtration on VGAS for phantom 2 (BMI: 29 kg/m²)



As shown in Figure 49(A), kVp has the highest negative impact on image quality when changed from low to high (-30.94, $p=0.000$) followed by filtration (-5, $p=0.000$). The SID showed positive but non-significant (0.52, $p=0.565$) trend of effect on image quality (VGAS) when changed from lower to higher values.

The results of the interaction effect, Figure 49(B), show no significant interaction between the acquisition factors effects on VGAS. However, the VGAS scored higher with low filtration when combined with kVp and SID with equal steady decrease when kVp changed from low to high while remaining equal across short and long SID.

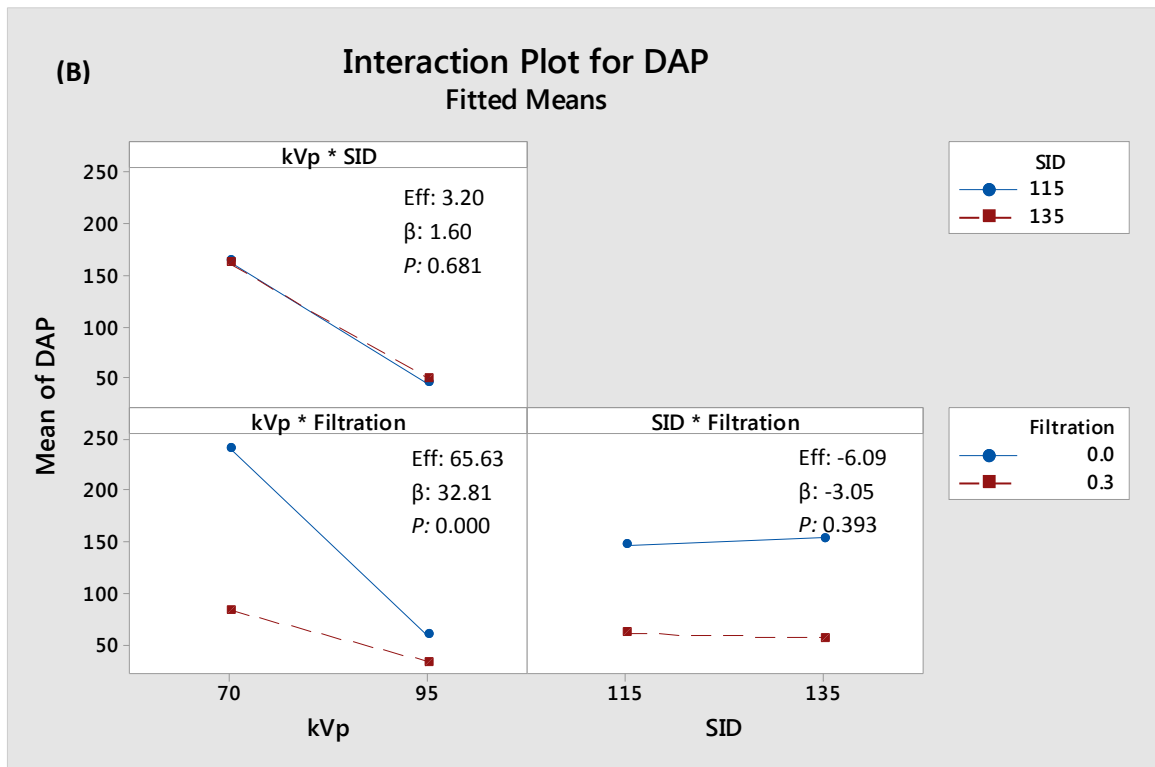
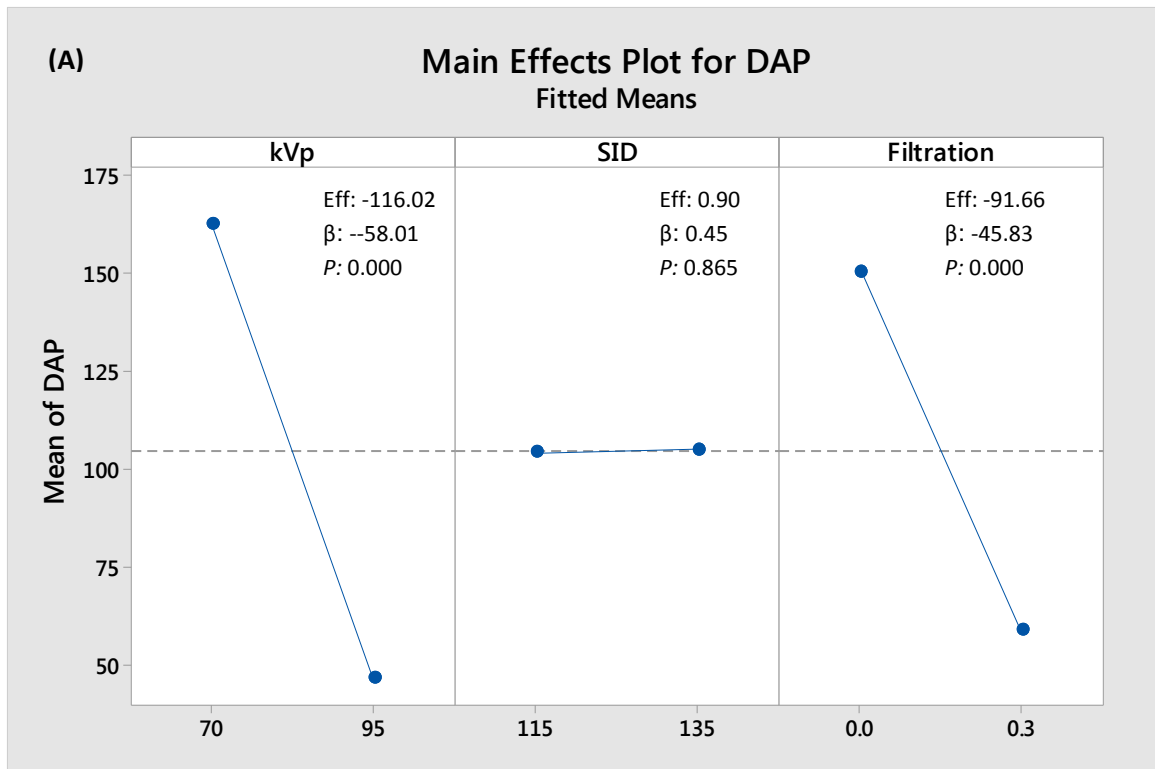
Figure 50 Acquisition factor combination (kVp, SID * filtration) that led to image with similar VGAS to the reference image or above including DAP, VGAS and FOMVGAS for each combination (phantom 2, BMI: 29 kg/m2)



* Reference image

6.4.3.3 Phantom (3)

Figure 51 Main effect (A) and interaction effect (B) of kVp, SID and filtration on DAP for phantom 3 (BMI: 38 kg/m²)

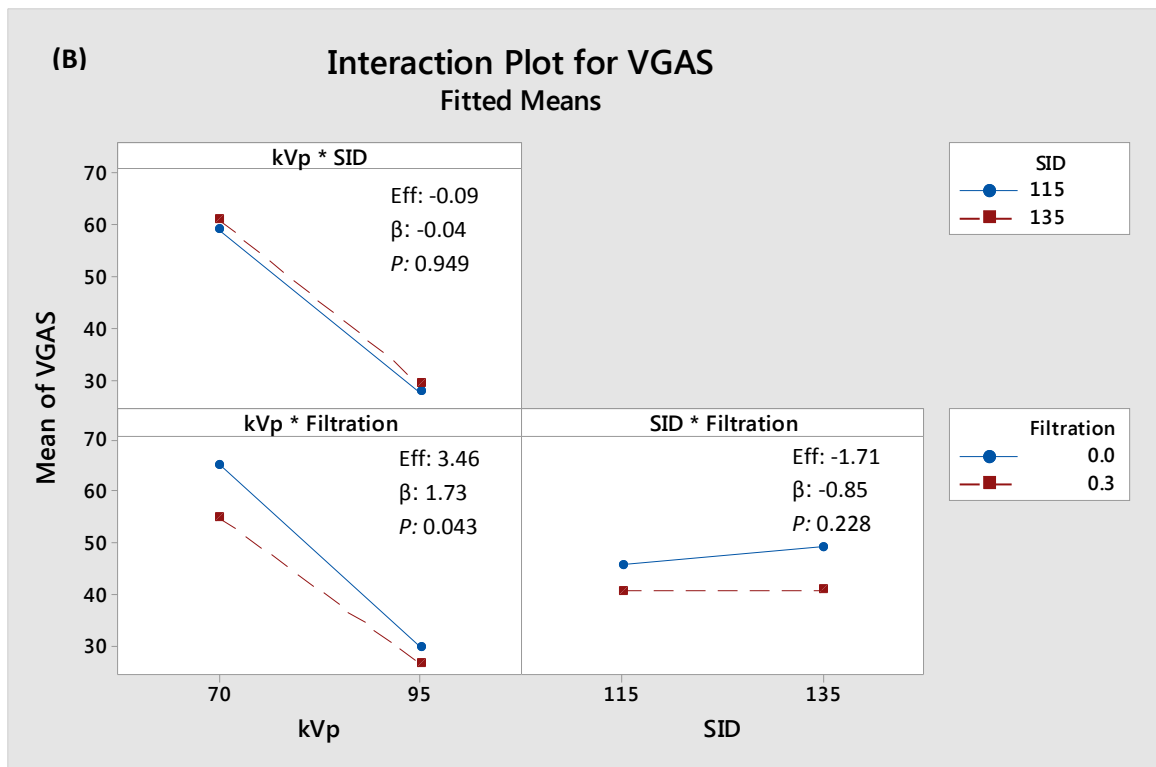
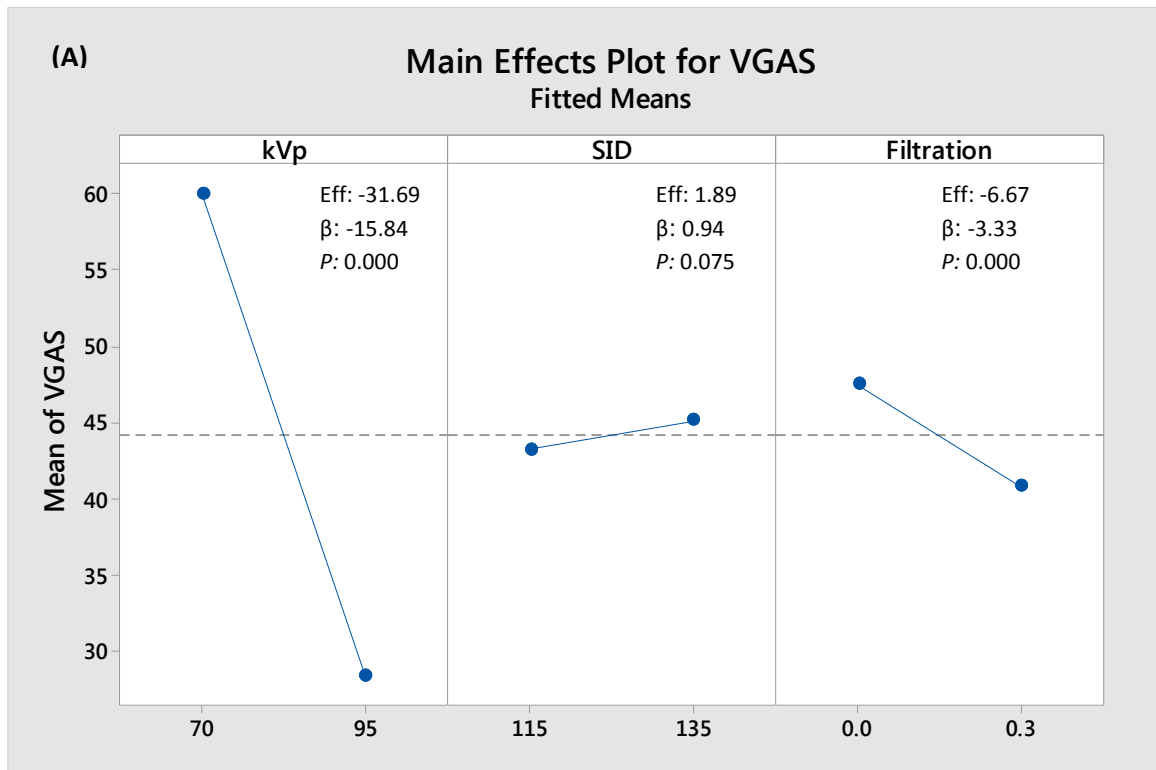


As illustrated in Figure 51(A), the kVp and filtration have the highest negative impact on DAP (-34.13 & -25, $p=0.000$), while the SID has a non-significant positive effect.

In Figure 51(B) it is clear that when kVp combined with SID, long and short SID performed fairly equally across high and low kVp. However, with kVp and filtration combination, increase in kVp inverse estimated effects across high and low filtration. High filtration (0.3 mm Cu) affect the DAP negatively more than zero filtration but high kVp decreased the effect gap between the types of filtration, zero and 0.3 mm Cu.

Filtration types performed equally across long and short SID with high filtration reducing the DAP more.

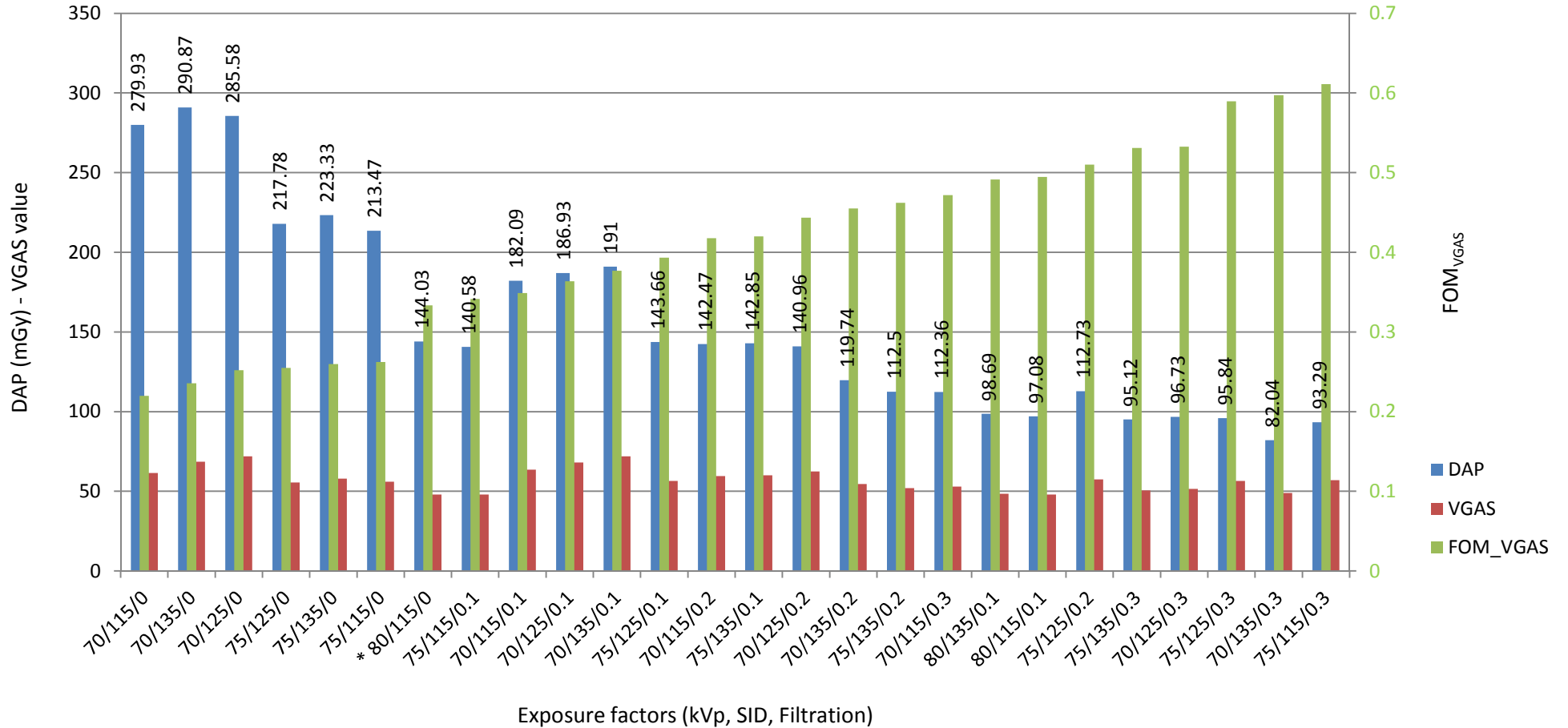
Figure 52 Main effect (A) and interaction effect (B) of kVp, SID and filtration on VGAS for phantom 3 (BMI: 38 kg/m²)



As shown in Figure 52(A), kVp has the highest negative impact on image quality when changed from low to high (-31.96, $p=0.000$) followed by filtration (-6.67, $p=0.000$). The SID showed positive but non-significant (1.89, $p=0.075$) trend of effect on image quality (VGAS) when changed from lower to higher values.

The results of the interaction effect, Figure 52(B), show no significant interaction between the acquisition factors effects on VGAS. However, the VGAS scored higher with low filtration when combined with kVp but the gap between the effects of high and low filtration narrowed in high kVp.

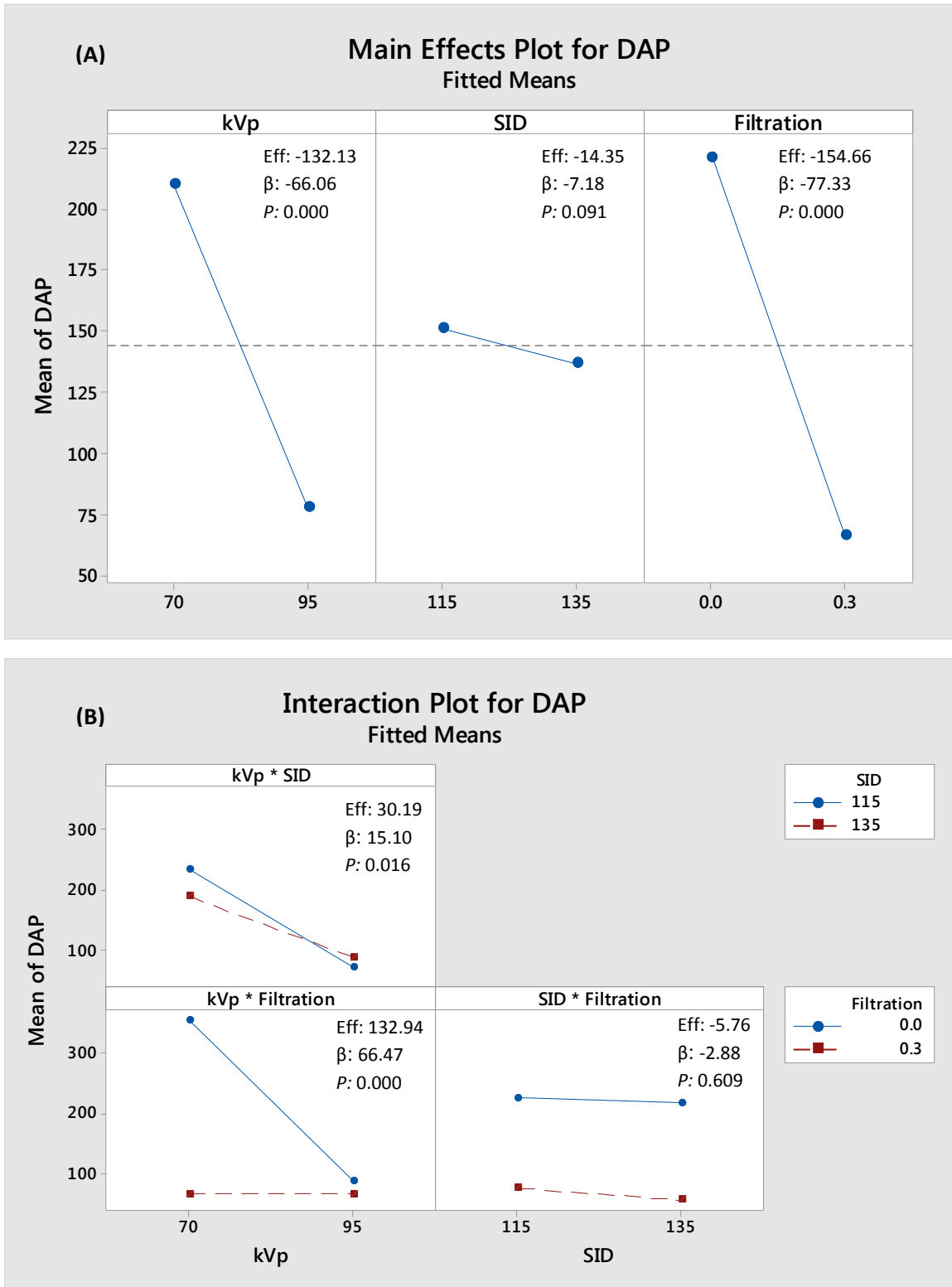
Figure 53 Acquisition factor combination (kVp, SID * filtration) that led to image with similar VGAS to the reference image or above including DAP, VGAS and FOMVGAS for each combination (phantom 3, BMI: 38 kg/m2)



* Reference image

6.4.3.4 Phantom (4)

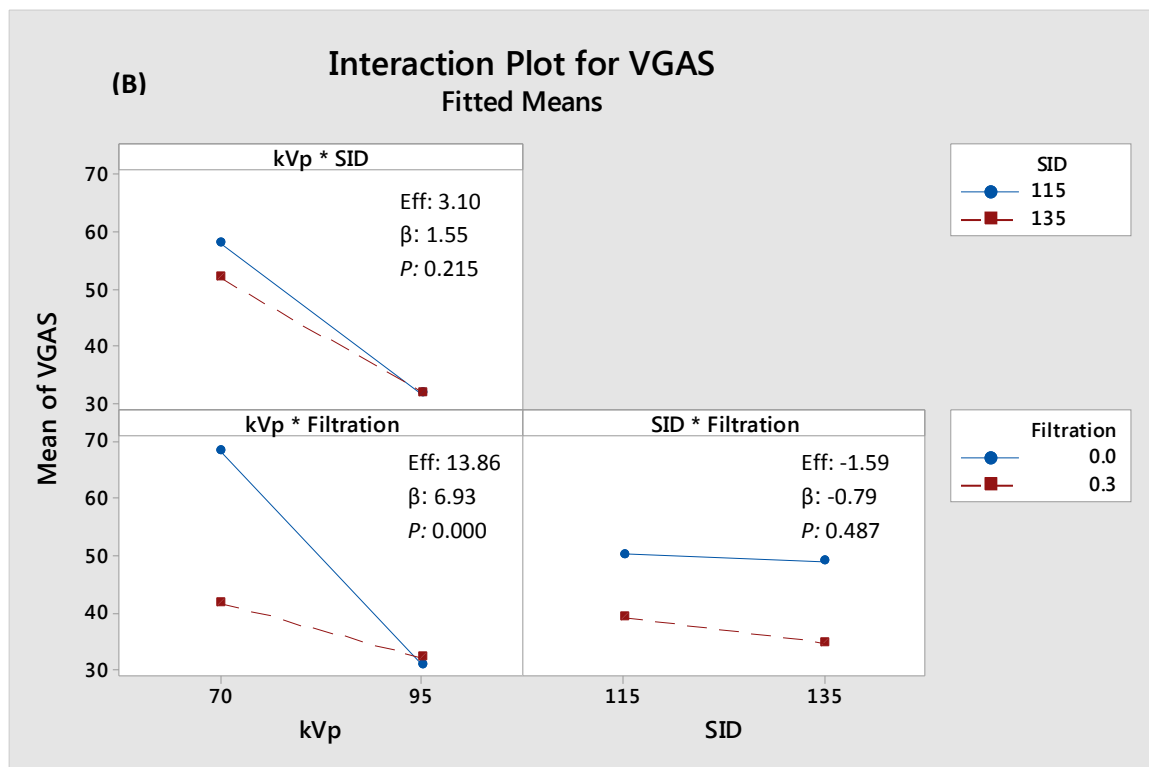
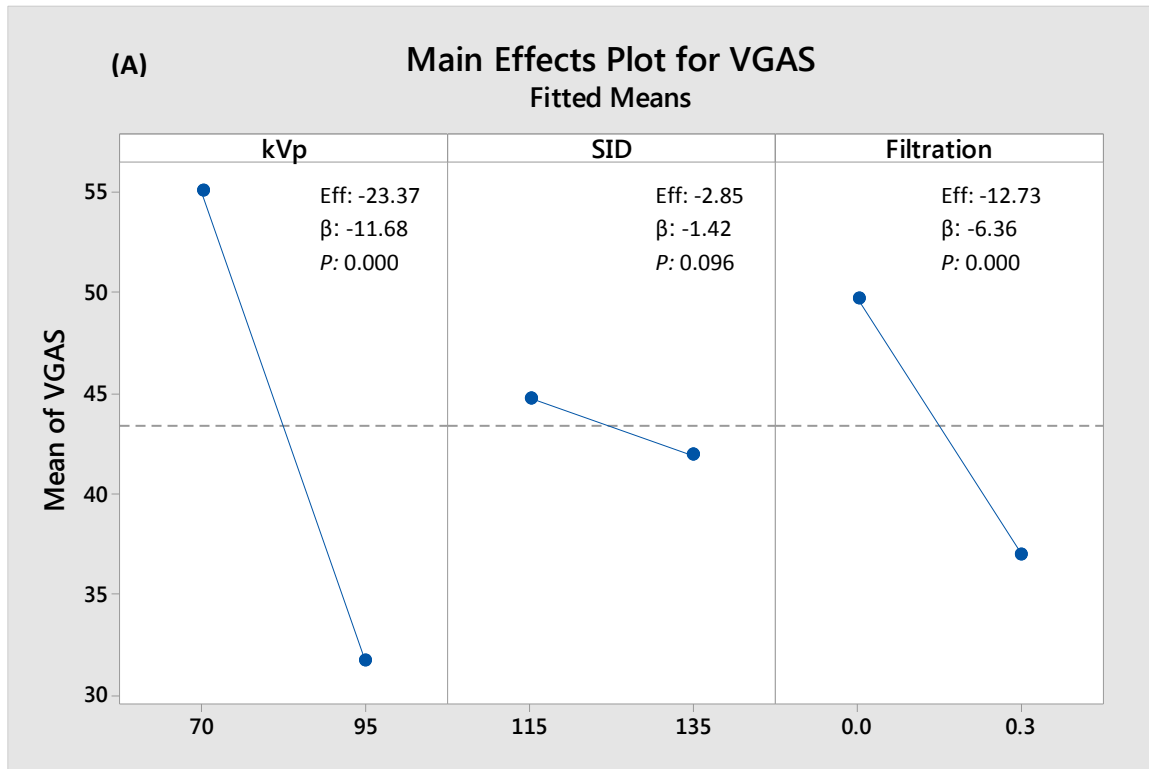
Figure 54 Main effect (A) and interaction effect (B) of kVp, SID and filtration on DAP for phantom 4 (BMI: 42 kg/m²)



As shown in Figure 54(A), all acquisition factors have a significant negative effects of the DAP, with the filtration being the highest (-217.57) when changed from low to high value, followed by kVp and SID (-79.18 and -34.54), respectively.

In Figure 54(B), long SID performed equally across all kVp levels. However, small SID performed better in high kVp. Similar with filtration, high filtration impacted more on the DAP at low kVp but similar to small filtration at higher kVp.

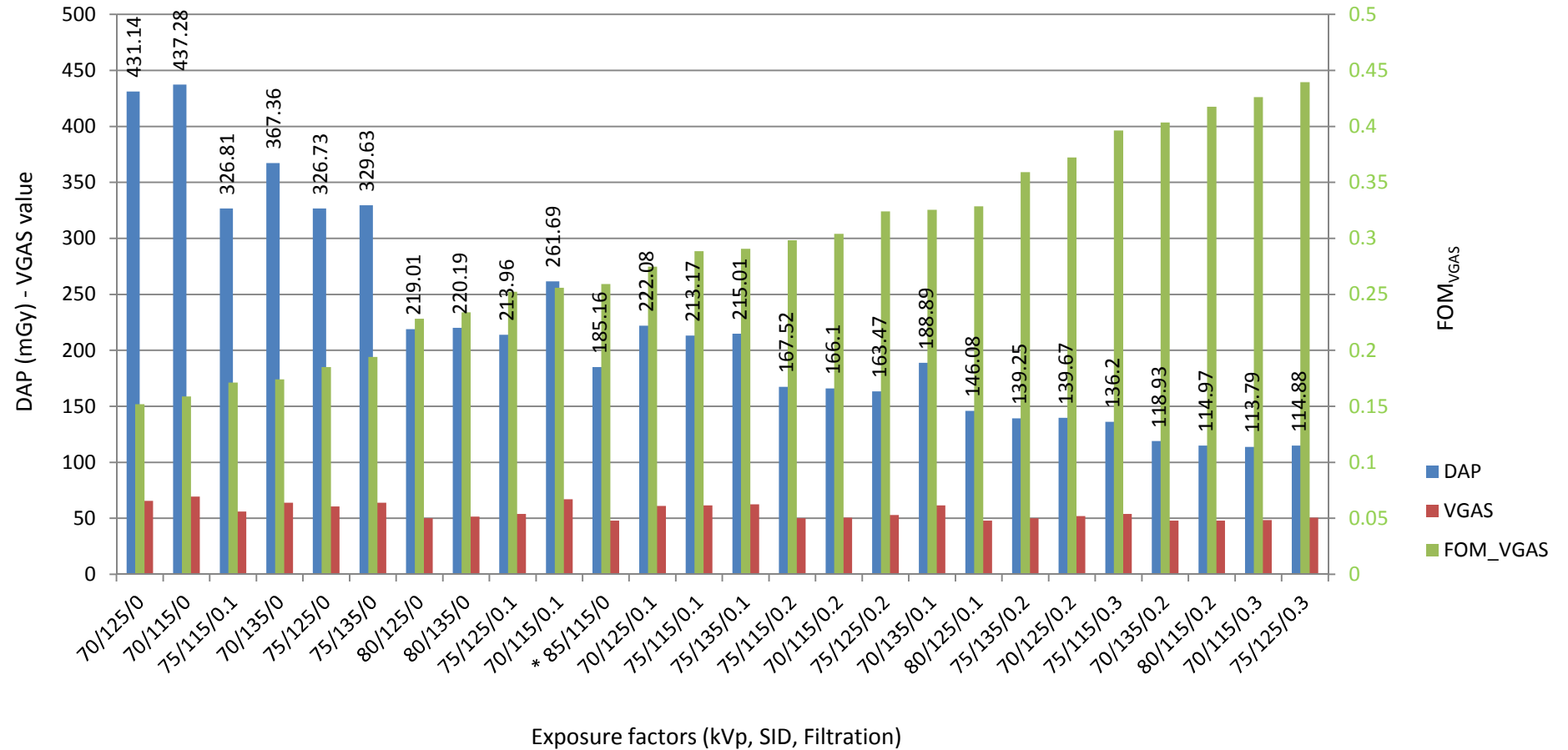
Figure 55 Main effect (A) and interaction effect (B) of kVp, SID and filtration on VGAS for phantom 4 (BMI: 42 kg/m²)



As illustrated in Figure 55(A), all acquisition factors have a significant negative impact on the VGAS, with the filtration being the highest when changed from low to high value, followed by kVp and SID, respectively.

In Figure 55(B), the kVp reverses the estimated effect of SID when changed from low to high, showing that small SID is better with low kVp but in high kVp both filtration performed equally on VGAS.

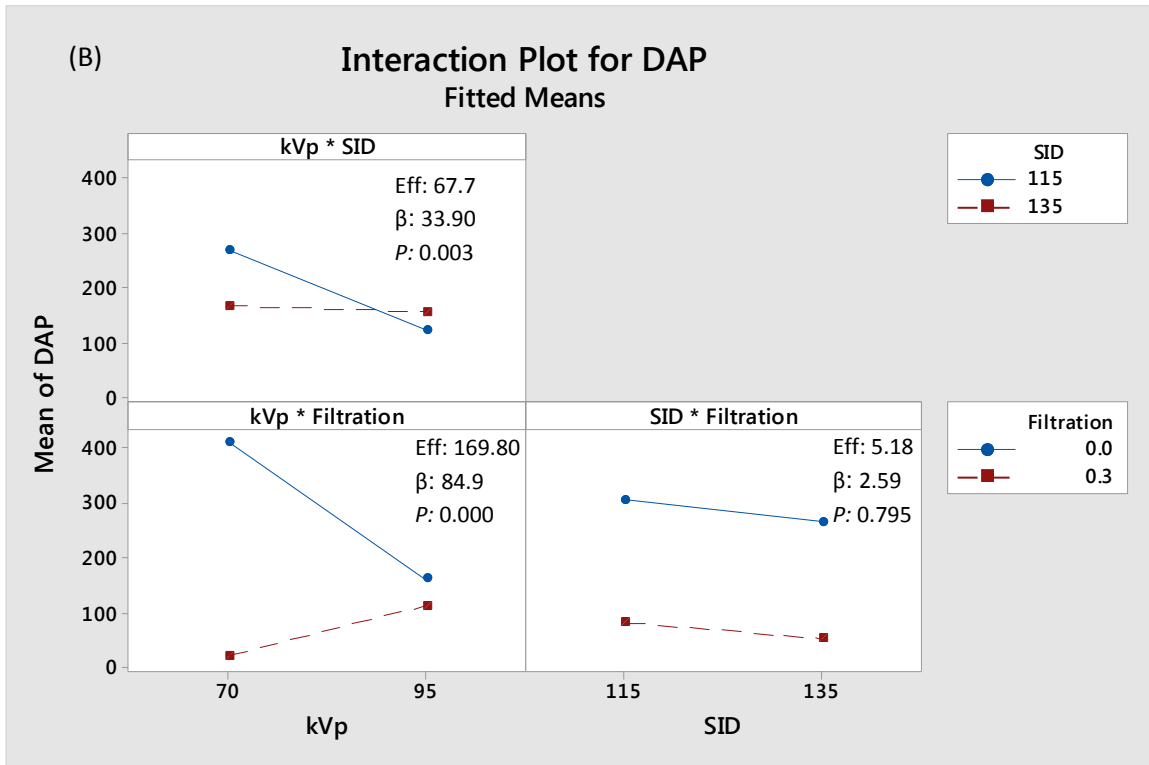
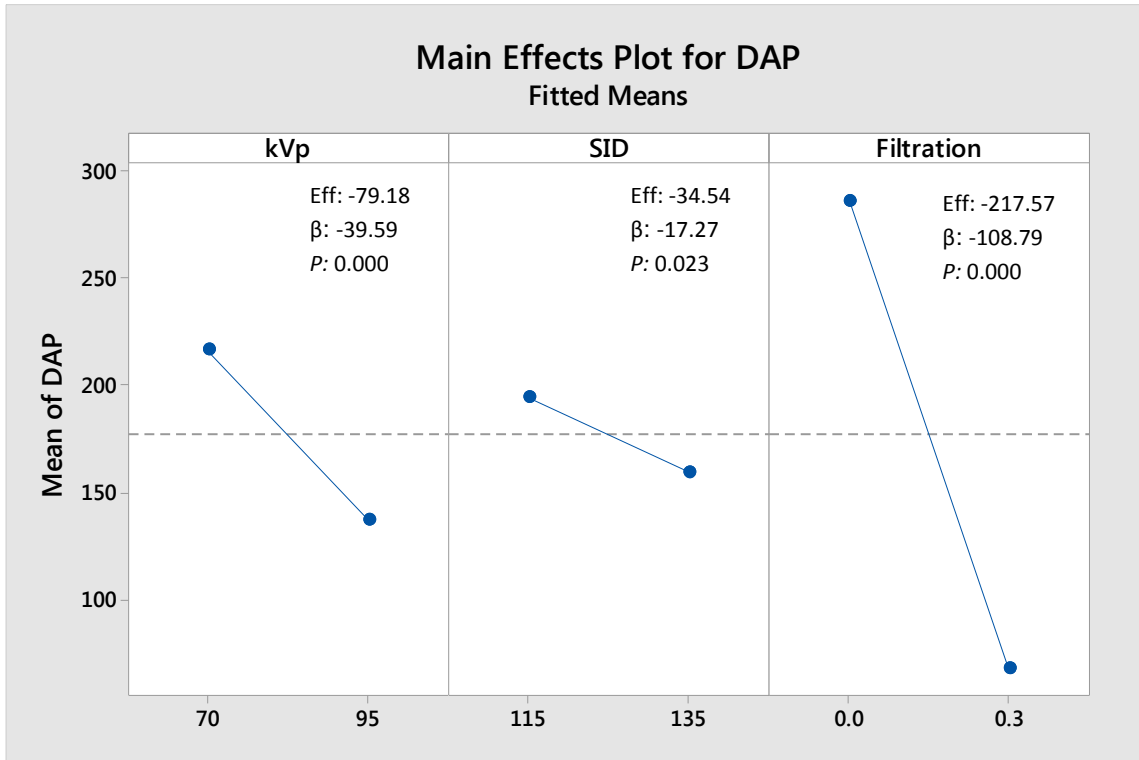
Figure 56 Acquisition factor combination (kVp, SID * filtration) that led to image with similar VGAS to the reference image or above including DAP, VGAS and FOM_{VGAS} for each combination (phantom 4, BMI: 42 kg/m²)



*Reference image

6.4.3.5 Phantom (5)

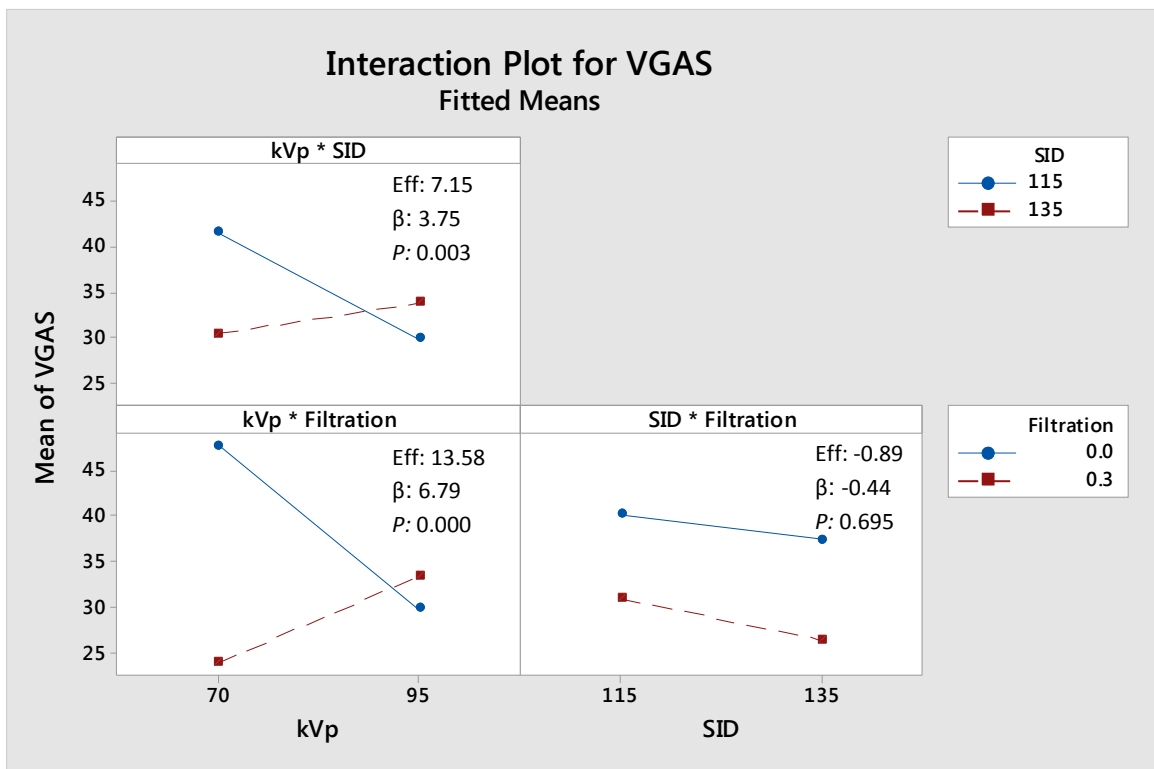
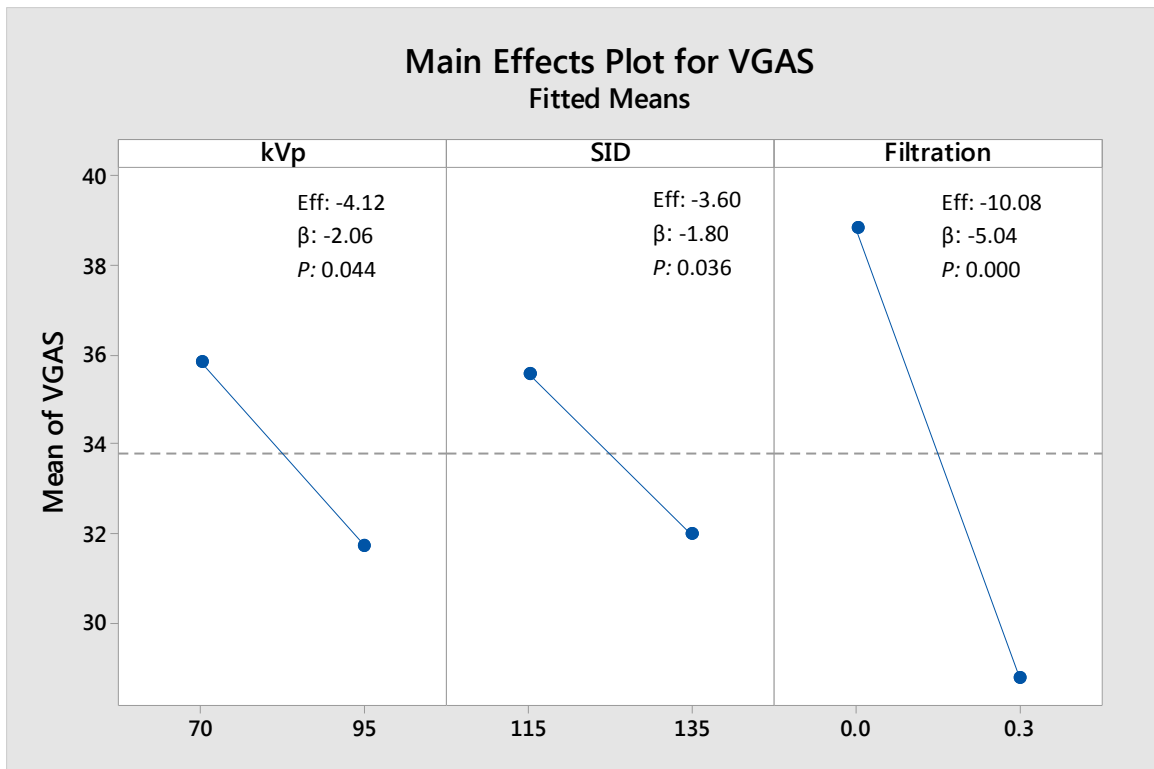
Figure 57 Main effect (A) and interaction effect (B) of kVp, SID and filtration on DAP for phantom 5 (BMI: 46 kg/m²)



As shown in Figure 57(A), all acquisition factors have significant negative effects on the DAP, with the filtration being the highest when changed from low to high value, followed by kVp and SID, respectively.

In Figure 57(B), it is evident that there is interaction between kVp with SID, and kVp with filtration. Large SID performed equally across all kVp levels. However, small SID performed better in high kVp. Similar with filtration, high filtration impacted more on the DAP at low kVp but similar to small filtration at higher kVp.

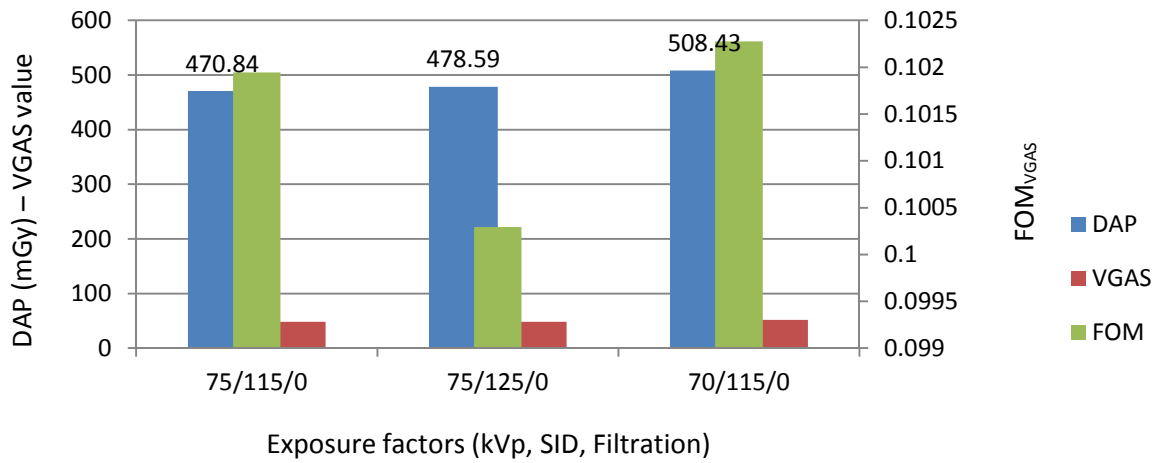
Figure 58 Main effect (A) and interaction effect (B) of kVp, SID and filtration on VGAS for phantom 5 (BMI: 46 kg/m²)



As illustrated in Figure 58(A), all acquisition factors have a significant negative impact on the VGAS, with the filtration being the highest when changed from low to high value, followed by kVp and SID (-10.08, -4.12 and -3.6) respectively.

In Figure 58(B), it is evident that there is interaction between kVp with SID, and kVp with filtration. The kVp reverses the estimated effect of SID when changed from low to high, showing that a small SID is better with low kVp but in high kVp the long SID impacted positively more on the VGAS. Similar with filtration, high filtration impacted more on the DAP at low kVp but similar to small filtration at higher kVp.

Figure 59 Acquisition factor combination (kVp, SID * filtration) that led to image with similar VGAS to the reference image or above including DAP, VGAS and FOM_{VGAS} for each combination (phantom 5, BMI: 46 kg/m²)



6.4.4 Optimal optimisation factors

In this section, the optimal optimisation factors for each phantom will be presented based on the lowest dose and highest images quality score. The VGAS and DAP values for each phantom will be presented. These values represent only images that have similar VGAS to the reference image or above. Based on these values, Contour plots will be presented for each phantom to illustrate the range of optimal exposure factors that produced image quality equal to or above the reference image VGAS with a DAP values that is within the first quartile of DAP values.

Table 38 Descriptive analysis of DAP, VGAS and FOM_{VGAS} for images that match the reference image VGAS score or above for each phantom

Phantom	Variable	mean	SD	median	min	1 st quartile	max	3 rd quartile
1	DAP	25.4	7.0	24.83	17.3	20.1	37.3	29.7
	VGAS	50.1	2.3	49.5	48	48	55	51.5
2	DAP	47.7	15.5	43.87	29.8	36.7	82.6	56.0
	VGAS	56.8	6.5	56	48	50	65	64
3	DAP	155.4	63.2	141.7	82.0	98.3	290.9	196.6
	VGAS	57.2	7.2	56.5	48	51.2	72	61.7
4	DAP	218.4	96.0	201.0	113.8	139.6	437.3	277.9
	VGAS	55.7	6.9	53.5	48	50	69	61.7
5	DAP	486.0	19.8	478.6	470.8	470.8	508.4	508.4
	VGAS	49.3	2.3	48	48	48	52	52

Minimum to 1st quartile DAP values demonstrated in table 38 were used along with the minimum to maximum VGAS value in order to generate the contour plots, in the next page, for each phantom. The minimum VGAS value in table 38 represent the VGAS for the reference image, which means the image that has any VGAS value equal to or above the minimum VGAS value was similar or better than the reference image.

Figure 60 Contour plot of VGAS, DAP of each phantom (1, 2, 3 and 4) constrained by VGAS equal and above reference image and the 1st quartile of DAP

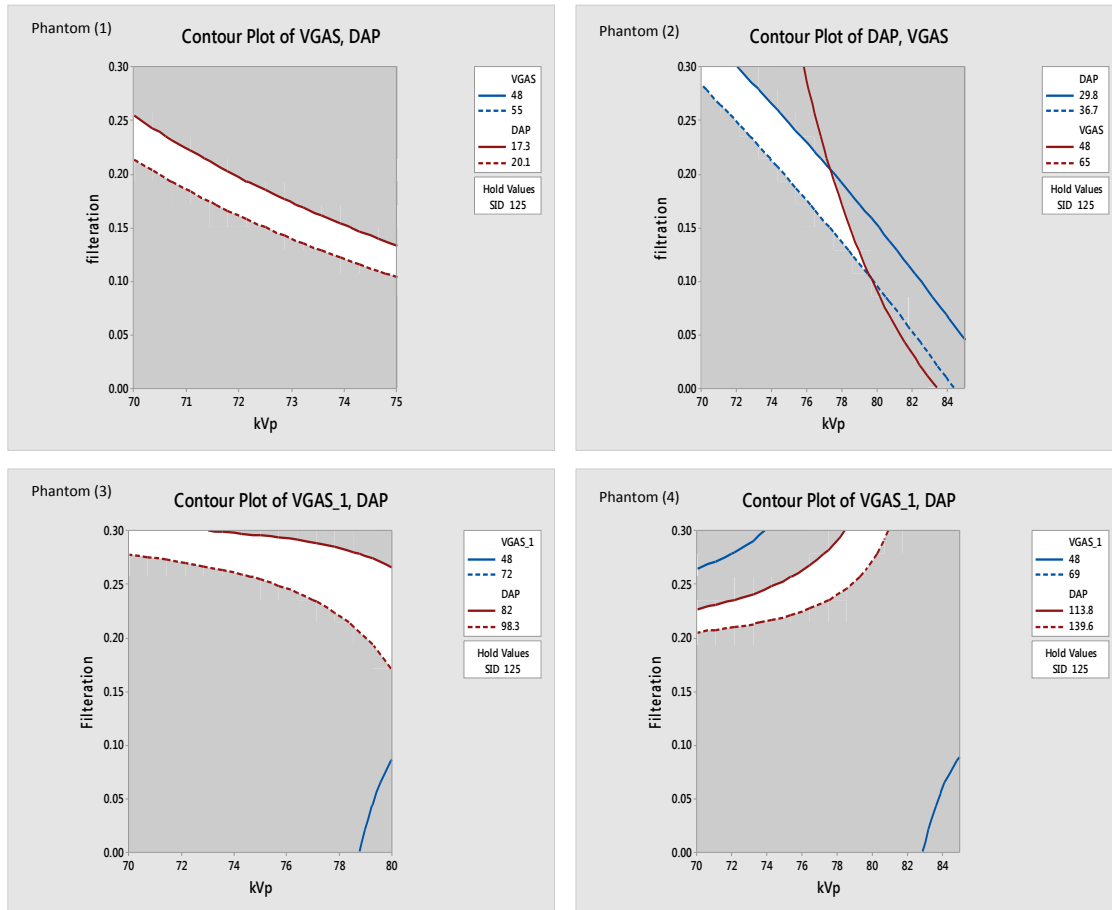
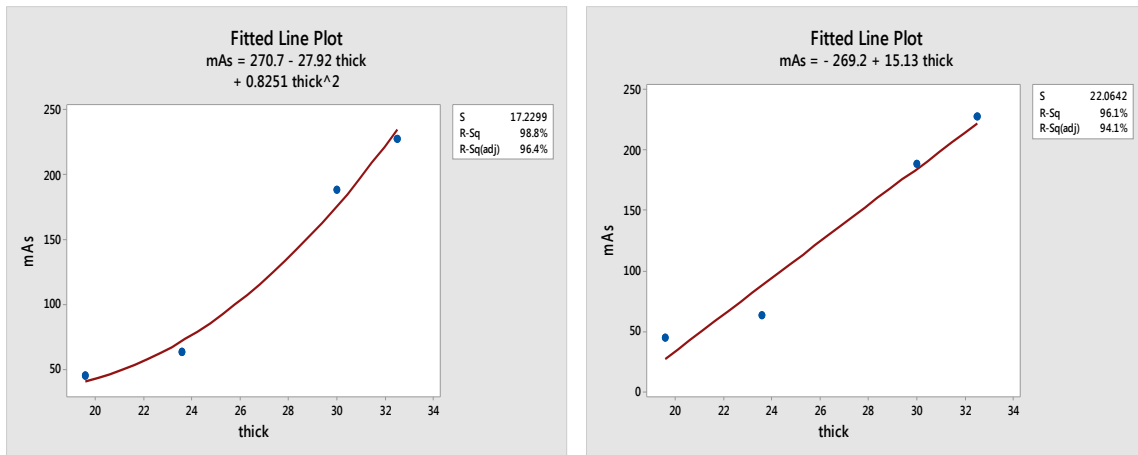


Figure 60 illustrated the range of optimal exposure factors constrained by the 1st quartile values of DAP, and the VGAS equal to or above the reference image. It can be seen that low kVp is favoured across all phantoms with added Cu filtration ranged between 0.2 and 0.3 mm. Phantom 5 was excluded as only three images had VGAS similar to reference image or above acquired with the highest DAP possible, this in turn makes impossible to generate a contour plot.

Figure 61 Quadratic (A), and linear prediction model (B) of mAs with kVp of 75, SID of 125 cm and filtration of 0.3 mm Cu



Two mAs models are produced based on the combined exposure factors that produced 75th percentile of FOM_{VGAS}, shown in Figure 61. The quadratic (A) regression model has the highest r^2 , 0.98 compared to the linear (B), $r^2=0.96$, respectively. Hence, the quadratic seems to be the best model. The kVp is set to 75, except in the first phantom, 70kVp. The remaining acquisition factors, SID and filtration, remain constant across all phantoms; 125 SID and 0.3 mm Cu filtration. mAs can be calculated based on the patients thickness using the following equation:

$$mAs = (270.7 - (27.92 * Thick_{cm}) + (0.8251 * Thick^2)) \quad \text{Equation 15}$$

Where mAs is the tube milliamp second

$Thick_{cm}$ is the patient's thickness in cm

$Thick$ is the patient thickness

6.4.5 Correlation between physical and visual assessment of image quality

In this subsection, the relationship between image quality physical assessment, in the form of CNR, and visual assessment, in form of VGAS, is tested for all produced images in each set of phantom. The spearman's rank correlation coefficient was used as VGAS data are ordinal while CNR data is interval data.

Table 39 Spearman correlation between VGAS and CNR based on two different size ROIs (Significance level: $P < 0.001$)

	CNR (Small ROIs)	CNR (Large ROIs)
Phantom 1	0.78	0.86
Phantom 2	0.88	0.91
Phantom 3	0.91	0.91
Phantom 4	0.98	0.94
Phantom 5	0.88	0.88

Strong correlations between CNR and image quality (VGAS) across all phantoms are illustrated in Table 39. CNR derived from both large and small ROIs are strongly correlated with the VGAS.

6.5 Discussion:

This section will discuss the result of the factorial design dose optimisation experiments. To avoid repetition, the impact of each acquisition factor on outcomes will be discussed individually.

6.5.1 Inter and intra-observer agreement for visual assessment:

The ICC results for the visual assessment demonstrated an excellent inter and intra observer agreement for all phantoms. In terms of inter-observer agreement, a two-way random ICC, an excellent agreement (0.81 – 0.90, 95 % CI 0.71 to 0.94) is achieved indicating an excellent reproducibility (Fleiss, 2011). In the 5th phantom, fair to good agreement is observed (0.69, 95% CI 0.17 to 0.86). This could be attributed to the fact that all images produced for this phantom contain high levels of noise which is reflected in the small number of images that were deemed to be of diagnostic quality, see Figure 59. These agreement figures are consistent with agreement values reported by (Alzyoud et al., 2019, Davey and England, 2015), showing an excellent agreement, and fair to good agreement (Harding et al., 2014).

With regards to observer intra-variability, consistency, the two-way mixed ICC results showed an excellent agreement for both observers across all phantoms, Table 37. The observer did not take any breaks during the assessment of each phantom, which means each set of visual image quality assessment comprised of 72 images, hence, 15 images were extracted from each phantom set including the reference image for the intra-observer agreement. This is to discover if the time spent by the observer during the main task of image assessment had impacted on their grading. However, based on the intra-observer results, no trend of observer consistency is observed across all phantoms.

The viewing conditions utilised during the visual image quality assessment in the current study are similar to what is used in clinical practice, if the RCR recommendations are followed. However, in this study, training was given to each observer regarding the assessment criteria. Additionally, a restriction of image contrast manipulation was implemented. In clinical practice, these restrictions and training are not practiced which indicates that the variation

between observers in clinical environment could be higher than that reported in the current study.

6.5.2 Effects on DAP:

The results demonstrate that both kVp and filtration have a different but significant impact on the DAP across all phantoms. The impact of kVp was higher than filtration in the first three phantoms. In the final two phantoms (BMI: 42 and 46 kg.m²) the filtration was seen to impact more on DAP than kVp (-154.6 and -217.5 for filtration compared to -132.13 and -79.1 for kVp. However, the scenario is different with regard to SID, where a positive but non-significant impact on DAP is visualised across the first three phantoms (BMI: 18.5, 29 and 38 kg.m²) but a negative impact on the obese phantoms (BMI: 42, p=0.09, and 46 kg.m², p=0.02).

The justification of the negative effect of kVp on DAP is the fact that increasing the kVp leads to a reduction on the mAs. As discussed in section (6.2.1.2), the dose is dependent on mAs mainly. Hence, the reduction in mAs means a reduction of the radiation dose. The opposite is also true, with low kVp, the DAPs were high across all phantoms due to the increase in mAs (Carroll, 2007, Fauber, 2016). This result is in line with other studies which show the negative impact of kVp on radiation dose. Brindhaban and colleagues investigated the effect of tube potential on radiation dose and image quality using two computed radiography systems (Brindhaban et al., 2005). They reported a decrease of 25% to 50% when increasing tube voltage from 81 to 104. Similarly, Lanca and colleagues demonstrated similar results with statistically significance difference when kVp was increased from 60 to 120 kVp in pelvis radiography (Lança et al., 2014). Additionally, a study investigating the impact of AEC and manual mode on image quality on chest PA radiographs showed a similar result of radiation dose decrease along with kVp increase (Reis et al., 2014). All the studies discussed earlier conducted the optimisation exposure based on phantoms that are representative of normal weight patient. However, in this study only the first phantom (BMI 18.5 kg/m²) is similar to other phantoms used in the literature in terms of the size. Hence, a different trend of the kVp effect is noticed where the filtration effect is taking over in the two highest BMI phantoms (BMI: 42 and 46

kg/m²). At high kVp, the radiation penetrates the examined body part very easily, and the opposite is true, due to the fact the kVp determines the quality of the beam (Dendy and Heaton, 2011). However, as the radiation passes through the body, its intensity reduces by an amount that is determined by the physical properties of the matter (Dendy and Heaton, 2011). These physical properties include thickness, density and atomic number of the material through which the radiation beam passes. The increase in any of these physical properties causes more attenuation of the beam, hence less signals are recorded in the detector, and subsequently the AEC will provide more time until the required signals are recorded in the ionisation chambers. This will be at the expense of high mAs and radiation dose. The scenario in phantoms 4 and 5 is similar, where the patient thickness is increased causing more attenuation of the beam. However, the AEC terminates the exposure very early to avoid damage to the tube. The justification for this phenomenon is the fact that AEC reached the cut-off point especially at 70 and 75 kVp. As a result, the DAPs in low kVp range for the two largest phantoms are less than the DAPs recorded when using high kVp. The low DAP recorded at low kVp in these two phantoms (4 & 5) compared to the DAPs in higher kVp level caused decreases in the regression slope. This result should be taken with precaution as it might not apply to other x-ray systems where a higher cut off point is possible.

The filtration had similar trends of affecting the DAP negatively across all phantoms. This effect of filtration came in second place after the kVp in the first three phantoms, but the highest in the two large phantoms. This is attributed to the fact that filtration absorbed the low x-ray energy. As discussed in section (6.2.1.1), 30 to 50 % only of the beam will have the maximum photon energy, this indicates that the remaining low energy beam, will exit the tube towards the detectors but will end up absorbed by the tissues of the examined body part. This will result in increase of the patient dose with no contribution to image quality (Fauber, 2016). Applying filtration, like Copper, will absorb these low energy photons before reaching the patient.

These results agreed with many studies that have investigated the impact of added filtration on radiation dose and image quality. For instance, in a study conducted by Ekpo and colleagues testing the impact of added Copper filtration

on image quality and radiation dose (DAP) and effective dose, they found that using 0.3 mm of Cu filtration reduces the DAP by 37% while still producing a diagnostic image (Ekpo et al., 2014). Other studies have demonstrated comparable results in different projection radiography examinations (Brosi et al., 2011, Smans et al., 2010, Vassileva, 2004). Other studies that investigated radiation dose to two different sets of chest phantom size reported similar trends in similar x-ray systems with 0.2 added Cu filtration (Al-Murshedi et al., 2019). This indicates the effectiveness of filtration in reducing the radiation dose.

However, the sharp increase in filtration effects on DAP in the largest two phantoms is not clinically beneficial. The reason attributed to this is the fact that the x-ray tube terminated the exposure very early when high filtration is used. This is because the use of filtration forces increase in the mAs, therefore, increases the x-ray tube heating.

With regards to SID, it has impacted positively but not significantly on DAP except in the largest two phantoms (BMI: 42 and 46 kg/m²) where the SID is inversely related with the DAP. This finding is surprising as it contradicts the inverse square law. However, it could be justified by the fact that increases in SID causes decrease in the beam intensity. With the AEC ON, the mAs will subsequently increase to compensate for dose reduction in the detector. This is supported by the result found by Brennan et al, that reported 60% increase in mAs when AEC was used alongside changing the SID in lumbar spine radiography (Brennan et al., 2004). Likewise, this reflects those of Joyce et al, who also reported mAs increase as a result of SID increase when the AEC is in use (Joyce et al., 2013).

Previous studies have demonstrated results that are in line with the inverse square law. For example, Tugwell and colleagues investigate the effects of SID on radiation dose and image quality in pelvic radiography (Tugwell et al., 2014). Using computed tomography and an anthropometric phantom, the impact of SID when changed from 90 - 140 cm and a constant kVp with manual and AEC mode, was studied. They found that increasing the SID from 110 to 140 cm reduces the ESD by 37 % and effective dose by 3.7 % when using AEC. Higher

reduction in the ESD and effective dose (50 % and 41 %) was reported when mAs was kept constant while increasing the SID. However, they applied this protocol while the kVp was constant. In the current study, the effects of SID on DAP is averaged across different level of kVp and filtration which makes the justification of this unexpected phenomenon difficult to explain. Similarly, other studies have reported higher dose reduction using long SID when mAs is controlled (Grondin et al., 2004, Farrell et al., 2008).

The sharp decrease in DAP is again justified by the fact that the tube terminated the exposure to avoid damage.

This could mean that filtration should be looked at instead of SID as the dose reduction showed by filtration is greater than the effects of SID ((Poletti and McLean, 2005).

However, explaining the main effects in factorial design should not be undertaken without investigating the interaction effects (Montgomery, 2017). The reason is that a significant effect of a factor might be dependent on another factor. For this reason, looking at the interaction effect between kVp and filtration is essential before making the final decision regarding the main effects of individual factors on the outcomes.

Across all phantoms, SID and filtration did not have any interaction, which means they are independent of each other. Filtration, both low and high, performed equally across SID. With regards to SID and kVp, both long and short SID performed equally across the first three phantoms, an interaction is observed in the fourth phantom at high kVp, where short SID performed better than long SID, however, the gap between the effects of SID at high kVp is very small. In the fifth phantom, an interaction is seen at high kVp where short SID impacted more on DAP than long SID. The same trend was observed in the interaction between kVp and filtration; where high filtration appears to impacted more on DAP at a lower kVp range in the largest two phantoms. This can be explained by the fact that in these two large size phantoms (42 and 46 BMI) at lower kVp, the AEC terminated the exposure very quickly to avoid tube heat, when adding more filtration or increasing the SID, the load is even bigger and

thus, in lower kVp with long SID and high filtration, the DAP was very low due to the early termination of the exposure.

As a result, the large effects of high filtration and long SID in phantom 4 and 5 should not be misunderstood. Clinically, it is not beneficial but it could signify the importance of knowing the limit of the x-ray system used and employing exposure factors accordingly.

6.5.3 Effects on VGAS:

In the present study, an improved grade of the image quality (VGAS) is observed across all phantoms at a lower kVp range. This result is in line with many studies that have investigated the effect of tube potential on image quality (Uffmann et al., 2005, Geijer et al., 2009, Shaw et al., 2013, Alzyoud et al., 2019). The reason for this is attributed to the fact that increasing the kVp while using AEC mode will result in mAs decrease which results subsequently in heightening of the noise level (Geijer et al., 2009). Additionally, this is attributed to the reduction of subject contrast as a result of high kVp. The subject contrast can be defined as the ratio of the intensity of transmitted radiation of a body part to the intensity transmitted by the adjacent part with high absorption rate (McEntee et al., 2004). The intensity of the radiation will be reduced as the radiation passes through the examined part depending on the body part density, thickness, atomic number, scattered radiation and tube potential. With the limited control of all factors except the tube potential, the relationship between subject contrast and tube potential is the key to the low subject contrast resulted when using high kVp. with a given body thickness, the relationship between subject contrast and tube potential is an inverse relationship (Bushberg and Boone, 2011, Fauber, 2016). When high kVp applied, the penetration power

Additionally, as the kVp decreases, the scattered beam energy decreases which subsequently reduces the scattered radiation reaching the detector (Dendy and Heaton, 2011). However, the opposite is true, with high kVp the scattered radiation energy increases and can reach the detector easily and impact on the noise level. This is very critical in digital radiography systems as they are more sensitive to low energy scattered radiation.

This result contradicts what is known and practiced clinically (Doherty et al., 2003). However, this is true in the case of analogue x-ray systems which have a limited sensitivity spectrum (Vassileva, 2004). In digital radiography the scenario is different where image post processing offers more options to enhance the image quality independent of the dose. De Vries and colleagues reported contradictory results using a similar detector (de Vries et al., 2015). They utilised a 20cm slab of PMMA along with CDRAD 2.0 contrast phantom sandwiched inside in an attempt to mimic the Alderson anthropometric phantom. Using CDRAD analyser, the image quality was measured. They found that at a lower kVp, the image quality is far less compared to higher kVp. However, the image quality assessment was based on physical measurements which do not reflect visual perception. Additionally, the phantom used in their study is very simple and not representative of heterogeneous human tissues.

In the highest BMI phantom (46 BMI), the effects of kVp are lower, this is due to the termination of the exposure at low kVp to avoid tube damage.

With regards to added Cu filtration, it is observed across all phantoms that increased filtration impacted negatively on VGAS. Compared to the filtration effects on DAP, as discussed earlier, it is apparent that filtration reduction impacted more positively on DAP than on VGAS. This can be seen clearly on Figures 47, 50, 53, 56 and 59 where protocols that use high filtration produced images with high optimisation index score (FOM_{VGAS}). This finding is supported by different studies that have reported similar findings in case of normal weight representative phantom studies. Ekpo and his colleagues investigated the impact of added Copper filtration on radiation dose and image quality at a constant tube potential, 120 kVp (Ekpo et al., 2014). They observed up to 37% patients dose reduction, (effective dose), while the image was considered of a diagnostic quality. This phenomenon has been reported extensively in the literature with the use of DR systems, which support the findings of the current study (Brosi et al., 2011, Smans et al., 2010, Hamer et al., 2005, Lança et al., 2018).

The impact of SID on VGAS fluctuated across phantoms. However, its effect was not significant except in the morbidly obese phantom, (number five). In the

literature, most studies reported no significant reduction in image quality when the SID was increased. For instance, Tugwell and colleagues investigated the effects of SID on image quality with regards to pelvis radiography (Tugwell et al., 2014). Using both visual image quality assessment as well as SNR, no significant image quality score difference was observed between short and long SID (90 – 140 CM). However, a slight decrease in the SNR was reported when SID increased. Similarly, Joyce and his colleagues found similar results when increasing the SID from 100 to 150 cm in cranial radiography with no deterioration in image quality.

Based on the discussion above, it can be seen that both kVp and filtration are the most influential acquisition factors that can be employed in dose optimisation across different thickness. Lower kVp is favourable with no filtration when the image quality is more relevant. However, filtration reduced the radiation dose significantly but with image quality still of a diagnostic range, see Appendix 7-10. The results of this study can be implemented in clinical practice in order to reduce patient dose to patients with obesity and to improve the image quality.

In order to simplify the transference to clinical practice, prediction models (Figure 61) have been produced to aid radiographers selecting exposure factors and reduce the variation in mAs, radiation dose and image quality. As multiple acquisition factors were used across different phantom that varied in size, it was not possible to produce a regression model based on best acquisition factors.

6.5.4 Correlation between VGAS and CNR

A strong positive correlation is observed between VGAS and CNR across all phantoms with regard to the ROI size, Table 39. This indicates that the size of the ROIs did not impact on the relationship between VGAS and CNR. The results from this study strongly agree with many results that have been reported in the literature (Alzyoud et al., 2019, Jones et al., 2015, Moore et al., 2013). This supports the visual assessment of image quality and may permit the use of physical measure to predict the image quality. However, this cannot replace the visual assessment especially in clinical situation (Båth, 2010).

6.6 Conclusion

The current study showed a promising future for image quality improvement in patients with obesity. kVp and filtration had the biggest impact on radiation dose and image quality. As the kVp increases the radiation dose is reduced as well as the image quality. This indicates that low kVp is favourable when the main focus is the image quality.

Similarly, Copper filtration showed a significant negative impact on the radiation dose but positive impact on the image quality due to the improvement in beam quality by filtering the soft component. This proves the efficiency of employing filtration in clinical practice, especially in patients with obesity in order to improve the beam quality and reduce scattered radiation.

The cut-off point of x-ray system should be known to the operator in order to employ the lower kVp and high filtration techniques in case of patients with obesity.

The mAs prediction model reported in this thesis can be used as a preliminary prediction model in clinical practice as there is no guideline in place currently.

7. Chapter 7: Conclusion

7.1. The story of the thesis:

The first study of this thesis was conducted in an attempt to identify the current practice employed in projection radiography with regards to patients with obesity. The first study was conducted in order to identify the most challenging parts when examining obese patients in order to act accordingly and come up with a result that can be implemented to solve a clinical practice issue. This was considered essential since the literature review demonstrated a lack of related studies. Based on the findings of the first study, abdominal and lumbar spine radiographs were proved to be the most challenging parts. However, conducting a dose optimisation study directly was not possible as no obese phantom is commercially available. Therefore, constructing an obese phantom was a primary goal. However, body composition must be accounted for since different tissues attenuate x-ray differently. Hence, the second study was carried out in order to quantify body composition in the most challenging areas in order to underpin the construction of representative obese phantoms. Different prediction models for fat and lean tissues in different body parts were produced to aid the research to construct the different phantoms for different BMI groups. Tissue equivalent substitutes were fabricated and validated in order to be used in the construction of obese phantoms. Fabrications of these tissue equivalent substitutes were successful and the final phantoms were constructed based on the body composition models reported in the second study.

For the purpose of consistency, final fabricated phantoms were validated and upon the satisfactory results they were used in dose optimisation experiments. A factorial design study was conducted using the constructed phantoms in order to investigate the impact of different acquisition factors on radiation dose and image quality across different size phantoms.

Conducting this thesis in this order improved its robustness as every conducted stage was based on evidence from the former stage results.

The next few sections of the conclusion will summarise research achievements, novelty and limitations of all studies briefly. The final conclusion will be drawn to provide a take home message for the reader. As with any research, raised

questions are of the same importance as answered ones, thus, further studies recommended will be listed to direct other researchers for further research that can be conducted to improve and strengthen the evidence in the radiation dose optimisation in this group of patients.

7.2. Research achievement:

- The current practice of imaging patients with obesity has been identified in more than 600 patients who have had projection radiography.
- The most challenging parts of the body, based on the reported radiation dose, have been identified.
- The relationships between patients' sizes and radiation dose in different projection radiography procedures have been identified.
- Radiation related lifetime-cancer risks of patients with obesity have been estimated based on the reported DAPs and compared with normal weight patients using the NDRL radiation dose values.
- Body compositions, FM and LBM, have been quantified in different body parts and different prediction models of FM and LBM have been developed to aid researchers when developing non-standard size phantoms.
- Fat and lean tissue equivalent substitutes have been fabricated and validated in order to construct phantoms representative of obese patients.
- A protocol for extending commercially available normal weight phantoms has been developed.
- The KYOTO phantom has been extended to four phantoms with different BMI.
- Dose optimisation experiments have been conducted using five phantoms of different sizes.
- A factorial study design has been implemented to conduct the experiments using three factors with different levels of each factor.
- Radiation doses in form of DAP have been reported for all produced images.
- Physical (CNR) and visual image quality (VGAS) assessments have been used in order to assess the quality of all produced images.

- Main and interaction effects of all acquisition factors on DAP and VGAS have been investigated in order to fully understand the effects of the acquisition factors when combined.
- The mAs prediction models have been produced in order to guide radiographers selecting the exposure factors based on patient size to yield a diagnostic image with low dose.

7.3. Strengths of this research:

- The first phase of this research was the first study that has reported radiation dose in patients with obesity based on actual clinical practice indicating the challenges of imaging this group of patients.
- It also produced an evidence based overview of the variations in radiation dose received by patients with obesity signifying the negative effects of the absence of any guidelines to aid radiographers selecting the most appropriate exposure factors based on the patient size in order to adhere with the ALARA principle.
- Effective risk and effective dose are also reported giving more insight and guidance to clinicians and radiographers when justifying radiographic exposures in the case of patients with obesity.
- Obese phantoms were built based on the best evidence with regards to the body composition of obese patients.
- The materials used in the phantom construction permit limitless reuse in dose optimisation research which in turn facilitate comparison of results from different dose optimisation protocols
- The protocol developed is valid to extend any commercial normal weight phantoms into obese models
- Factorial design methods have been employed promoting the investigation into the effect of multiple acquisition factors simultaneously rather than only one factor
- Optimisation index was used to identify highest image quality with the lowest dose which provide more understanding of the best exposure factors for both image quality and radiation dose instead of considering these outcomes separately

7.4. Limitations:

- The dose audit study was conducted retrospectively, which in turn imposed a more restricted inclusion and exclusion criteria, and resulted in limiting the numbers of investigations in the final analysis of radiation dose
- The patients size was based on BMI while the thickness of the body part is more relevant when considering radiation dose
- Radiation doses reported were based on radiographer entry and errors may be present resulting from entry mistakes
- Body composition was reported based on female participants, which implies that the result is more relevant to females than males.
- Abdominal FM was calculated in total with no configuration of visceral and subcutaneous FM separately
- Obese phantoms were constructed taking into account the FM and LBM in total but no visceral fat was employed
- The extended phantoms represent obese patients in supine position only which limits their use in erect position due to the fat redistribution
- Dose optimisation experiments were conducted using a single x-ray system which in turns influences the applicability of the results to other x-ray systems.
- Three acquisition factors were employed in the current thesis while other factors can be used to optimise the image quality and reduce the radiation dose.
- The results have not been implemented in clinical practice

7.5. Overall conclusion of the thesis:

A significantly high Radiation dose (DAP) is delivered to patients with obesity in all radiographic procedures reported in this thesis. Body parts with most sensitive organs are receiving the highest dose, abdominal and lumbar spine radiographs. Hence, the radiation-related lifetime cancer risk can reach up to 153% in patients with obesity compared to normal weight patients especially in younger patients. This provides the rationale for radiation dose auditing processes in medical imaging departments in order to identify similar results and act upon them. Additionally, the results provide more evidence based

understanding of the radiation dose issue especially in projection radiography which advocate more dose optimisation research for non-standard size patients.

However, caution should be exercised when an attempt is made to conduct such research. This includes utilisation of phantoms, physical or computational, that encounter fat as well as lean mass increase. The current thesis demonstrated a statistically significant increase of LBM along with FM and height.

In order to standardise the construction of phantoms representing obese patients, taking these two body compartments into account will facilitate reduction of discrepancies in dosimetry that is attributed to phantom construction and size. In this thesis, multiple prediction equations have been developed to help researchers estimating FM and LBM increase across different body parts.

With the high cost of commercially available phantoms, in-house FTES and LTES can be constructed in order to extend normal weight phantoms into obese phantoms. This can be conducted only if the required lab facilities are available. Due to the hazardous nature of these materials, one should ensure health and safety measures are in place before conducting the experiment. Good planning in advance will produce satisfactory results as these materials need special handling, storage and mixing. The materials constructed in this thesis provided an opportunity to conduct dose optimisation experiments in order to optimise radiation dose and image quality in non-standard size of patients.

The factorial design implemented in this thesis provided more insight into the effect of different acquisition factors on both image quality and radiation dose. Based on the results of this thesis, with regards to the main research question, manipulating different acquisition factors produced improvements in image quality and reduction in radiation dose across different size models. It can be concluded that low kVp is favourable (~75 kVp) when the main focus is a radiographic image of a high quality. The radiation dose can be reduced significantly, while the acquired image of a diagnostic quality, by adding up to 0.3 mm of Cu filtration. These two exposure factors when combined proved to produce a radiographic image with high optimisation index.

However, tube load should be considered and the cut-off point of the x-ray system AECs should be investigated in order to adapt the current exposure factor selection to other systems. In this project, phantom thickness above 33 cm proved to be challenging as the x-ray system was working at its limit.

7.6. Research impacts:

The results of this thesis will have a direct impact on imaging obese patients in clinical practice as well as on the quality of patient care. With regards to the impact on patient's care, the mAs prediction model will help in reducing patient's radiation dose and dose variation. It will serve as a reference for the radiographers to choose the best exposure factors based on patient thickness rather than speculating these factors. Additionally, in healthcare centres, where more manufacturer variety of x-ray systems is available, the patient can be directed to the best system based on the cut-off point when similar mAs prediction model is produced for other DR systems.

Clinicians can use the result of this thesis to decide whether projection radiography will improve the patient diagnosis or not based on the estimated lifetime cancer risk for obese patients, which is different when compared to normal-weight patients. This thesis forms the foundation for future work in this area.

7.7. Recommendations for further studies:

- Further radiation dose evaluation studies to be conducted in order to investigate if similar results found and to explore challenges in other procedures that have not been included in this thesis
- Investigating the causes of radiation dose variation to understand the causes and act upon them
- More body composition quantification studies are needed in order to understand body composition changes across males, children and different ethnicity groups in order to standardise phantom construction across different populations
- Obese phantoms with visceral fat is of importance in order to understand the impact of fat redistribution on internal organs' absorbed dose

- More acquisition factors should be explored in order to have a full picture of how the dose and image quality could be optimised in this group of patients
- Similar experiments could be conducted with the use of manual mode, i.e mAs manipulated manually, in order to investigate any further dose reduction opportunities
- Effective dose is advised to be implemented instead of DAP in future similar studies as it is more efficient in dose optimisation studies than DAP.

8. Appendices:

Appendix 1 Invitation letter for engagement in the study



MEDICAL SCHOOL
MEDICAL IMAGING
DEPARTMENT.

South Cloisters 1.44
St Luke's Campus
Heavitree Road
Exeter
UK EX1 2LU

t +44 (0) 1392 724133
e K.M.Knapp@exeter.ac.uk

Dear

We are writing to request your engagement in a study into the impact of obesity on radiographic image quality and radiation dose in this group. We are researchers based in the Medical Imaging Department at the University and this study forms part of a PhD project being undertaken by Saeed Alqahtani. As you are aware of the prevalence of obesity within the UK population is increasing, which in turn has created a new challenge in delivering good quality radiology services in the obese population.

We are looking to collect retrospective data for one thousand patients who meet the inclusion criteria of a BMI >30. We need to collect the heights, weights and hospital numbers for these patients (aged over 18) to understand the range of obese patients presenting within some of the services. These data will be used to underpin the sizes of a range of phantoms, which will be developed to undertake experiments to optimise the exposure factors for common radiographic examinations. The hospital numbers are required so that (with the appropriate R&D / ethics approvals in place) any imaging the patients have had completed can be reviewed to evaluate the current radiation doses they receive along with a measurement of the diagnostic quality of the images achieved. These doses will then be compared to the dose reference levels for the UK. The reports will also be reviewed to explore how many of the images were suboptimal due to patient body habitus.

The research and development department will be contacted to ensure the appropriate approvals are in place for the study to take place.

If you have a database of patient heights and weights, this would be very useful to the research team and we would be interested to discuss this study proposal further with you.

Thanking you in advance for your time.

Yours sincerely,

Karen Knapp PhD

Associate Professor in MSK Imaging
Head of Medical Imaging
University of Exeter Medical School
University of Exeter

Appendix 2 Draft of the study protocol

Title:

Projection radiography doses and image quality in obesity.

Background:

In the last few decades, the prevalence of obesity across the world has nearly been doubled between 1980 and 2008 ⁽¹⁾. Finucane et al. reported that across 199 countries included in their study, 1.46 billion people were overweight and 502 million obese. In the UK, the Office of National Statistics reported nearly more than half of men and women in the UK to be overweight or obese ⁽²⁾. Obesity is one of the causes leading to diseases such as insulin resistance, type 2 diabetes, dyslipidemia, hypertension, heart diseases and non-alcoholic fatty liver disease ^{(3) (4)}. Such a high prevalence of obesity and associated health consequences increases the demand on healthcare services. However, the equipment and current evidence base struggles in some circumstances to accommodate the obese population fully. For example, within medical imaging, higher radiation doses are delivered to obese patients and low image quality or in certain occasion non-diagnostic images ⁽⁵⁾. In terms of radiation dose, the International Commission of Radiation Protection (ICRP) 1996⁽⁶⁾, have introduced the term Diagnostic Reference Level (DRL) as an investigation levels or a quality assurance tool in order to improve the regional, national or local distribution of the radiation dose of general medical imaging procedures and to keep the dose in standard range. In the UK, the DRL was established in 2000 depending on the data of patient dose in 371 hospitals between 1996 and 2000 ⁽⁷⁾. Since the patient's dose is dependent on patient size, the range of patient weights included in the Hart et al. study was 65 to 75 Kg. With the increasing rate of obesity within the population, the DRL measure is becoming less applicable to obese patients since their weight is out of the range weight used in DRL establishments. This has brought a new challenge to health professionals in medical imaging department in order to produce optimal image with the lowest dose and to comply with the ALARA principle while maintaining doses close to the DRL for the investigation. In terms of image quality, in the USA, Uppot and his colleagues have reported an increase in radiological reports citing limitations due to body shape and size⁽⁸⁾. Their study retrospectively evaluated the radiological reports at Massachusetts General Hospital from 1989 to 2003 citing any terms "limited due to body habitus". The results revealed a small but a progressive increase in radiology reports numbers of habitus-limited. Out of 5,253,014 reports, 7778 (15%) were habitus-limited with linear increase of 0.010% per year. This will lead to a negative effect on diagnosis preciseness and delay the treatment process of such patients. Such evidence might exist in the UK, but this has yet to be confirmed through a similar audit of radiology reports.

Appendix 3 Follow up justification of the study protocol

“The quantity of records it is proposed to access (1000). There seems no clear justification for the need for this volume

Since the current study has the objective to estimate the average height, weight, age and waist circumference of obese population at Musgrove Park hospital, therefore, one thousand subjects seems to be statistically good number to have a normal distribution of all requested anthropometric variables. This number has been discussed with the bariatric surgeon at the hospital, who is engaged in this study, and he strongly agreed with this number of subjects in order to achieve good and locally generable result. Additionally, the research team at Exeter University will build up x-ray phantom simulate obese patients, of different BMI groups, to conduct some lab based projection exposures for dose optimisation and image quality enhancement. If average age, weight, height and waist circumference estimated accurately, this will impact on the applicability and usefulness of the lab experimental studies to optimise patient dose. The advice of the bariatric team was taken into account since Taunton is a regional centre and therefore many of the patients will not have undergone imaging at this hospitals and hence dose data will not be available for them. At present we do not know the percentage of these patients who will have undergone imaging and therefore this number of subjects will increase the likelihood of sufficient patients having had a previous history of x-ray imaging. This will strengthen the evidence around the radiation dose received by obese patients at Musgrove Park Hospital.

The intention to pass the data (anonymised according to the description) onto the research team at Exeter University – there is a degree of uncertainty about what happens to the information from that point onwards.

Once the data passed onto the research team at Exeter University, statistical analysis and lab works will be developed based on the provided data. First, the radiation dose will be analysed according to body parts and projections to compare with the national diagnostic reference level (DRL). Secondly, the radiological reports limited by body habitus will be analysed to configure how many diagnoses were limited by patient size and to identify the most common body parts that radiologists find it difficult to achieve a robust diagnosis. This will help the research team to focus on the most common areas that are difficult to image in this population For the basis of future in-vitro studies. Tissue equivalent phantoms will be constructed simulating different BMI groups to conduct further lab based x-ray exposures with exposure factors manipulation to minimise the radiation dose and optimise the image quality for each BMI group. All results will then be shared with the Musgrove Park Hospital and it is hoped the results from this work will impact on improving imaging while reducing patient dose in this population, who are frequently attend hospitals due to their multiple co-morbidities.

The proposed inclusion of the hospital number within the information provided by our clinical team, thus potentially jeopardising true anonymization.

The hospital number will be provided by the collaborator bariatric surgeon to the healthcare team only to be able to access data for the right patient. The ID hospital

number will not be transferred to the research team at Exeter University at any stage of the study, but are required by the healthcare team to link the obese patients to their imaging histories. The data will remain anonymous to the research team.

As an associated issue these is no stated engagement between student and Radiology team. Their critique and approval of this would appear important prior to any data collection.”

Sue Rimes has been engaged with the research team regarding this project and introduced us to the Bariatric team. We have also undertaken some previous student projects with Taunton and some other work with Sue Rimes and have found the engagement and enthusiasm for service evaluation at Musgrove Park to be exceptional in the past. This is why we have requested to work with yourselves, rather than a hospital more local to us.

Appendix 4 Permission to conduct the study

RE: Saeed,

Karen Tanner <Karen.Tanner@tst.nhs.uk>

Fri 27/11/2015 03:33

To: Alqahtani, Saeed Jaber M. <sa512@exeter.ac.uk>;

Dear Saeed,

From the clarifications that you sent, the Clinical Audit Department have said that they are content that your project can go ahead, and be managed as a service evaluation, not audit or research.

I have also been in contact with the Trust service improvement team who are in the early stage of setting up a register of projects being undertaken in the Trust. It may be that they will require some sort of registration from you at a later date but this has not been stipulated as a mandatory requirement at present so as long as the Managers and Clinical Director for contributing departments are happy for the data to be provided, it is fine to commence your project.

All the best.

Kind regards,
Karen

Karen Tanner

Research Manager
Department of Clinical Research
Musgrove Park Hospital
Taunton
TA1 5DA

(01823) 34 2638

CONFIDENTIALITY NOTICE

This message is private and confidential. If you have received this message in error please notify me and remove it from your system.

Please note that the contents of this email may be subject to disclosure under the Freedom of Information Act 2000, subject to specified exemptions.



<https://www.joindementiaresearch.nihr.ac.uk/>

Appendix 5 Radiation related lifetime cancer risk of organs for both groups, normal weight and obese, for all reported procedures

Table 1. Lifetime cancer risk (per 10⁶) as a result of abdominal AP in normal-weight group

organ	Age at exposure (Y)						
	20-29	30-39	40-49	50-59	60-69	70-79	80-89
Males							
Lung	0.5525443	0.5903898	0.605528	0.5752516	0.4617151	0.2876258	0.1135365
Stomach	4.2601572	3.2138028	2.3169276	1.494792	0.8968752	0.4484376	0.1494792
Colon	5.0652672	4.0832256	3.101184	2.2225152	1.29216	0.6202368	0.1550592
RBM	0.8369361	0.8260668	0.8478054	0.7065045	0.5325957	0.3586869	0.1847781
Bladder	5.231408	4.426576	3.7022272	2.816912	1.8511136	0.9657984	0.3219328
Liver	1.7830246	1.3634894	0.9439542	0.6293028	0.3670933	0.1573257	0.0524419
Thyroid	0.0000865	0.0000519	0.0000173	0.0000173	0	0	0
Oesophagus	0.1024243	0.1024243	0.1117356	0.1303582	0.1396695	0.1396695	0.093113
Other	3.9916425 5	2.8060061 5	1.8970182 4	1.1856364	0.6125788 1	0.2371272 8	0.0592818 2
All cancers	21.823490 7	17.412032 7	13.526397 5	9.76129	6.1538012 1	3.2149079 8	1.1296225 2
Females							
Breast	0.4179331	0.2723184	0.1588524	0.0850995	0.0397131	0.0151288	0.0037822
Lung	1.1959178	1.286747	1.3472998	1.3018852	1.0521049	0.6206662	0.2195039
Stomach	6.5770848	5.0075532	3.5875008	2.4664068	1.494792	0.747396	0.2242188
Colon	2.4809472	1.9640832	1.4989056	1.0854144	0.7236096	0.3618048	0.1033728
RBM	0.543465	0.4891185	0.8369361	0.5325957	0.3152097	0.1630395	0.0652158
Bladder	4.1851264	3.621744	3.1388448	2.5754624	1.9315968	1.1267648	0.402416
Liver	0.7866285	0.5768609	0.4195352	0.3146514	0.1573257	0.1048838	0
Thyroid	0.0004498	0.0002249	0.0001038	0.0000346	0.0000173	0	0
Oesophagus	0.093113	0.1117356	0.1396695	0.1955373	0.2607164	0.279339	0.1769147
Ovary	1.17676	0.91104	0.64532	0.41756	0.22776	0.07592	0.03796
Other	3.0482597 6	2.1689540 6	1.4655095	0.9379260 8	0.5275834 2	0.2540216 5	0.0781605 1
All cancers	20.505685 4	16.410379 8	13.238477 5	9.9125733 8	6.7304289 2	3.7489645 5	1.3115447 1

Table 2. Lifetime cancer risk (per 10⁶) as a result of abdominal AP in patients with obesity group

organ	Age at exposure (Y)						
	20-29	30-39	40-49	50-59	60-69	70-79	80-89
Males							
Lung	1.2761568	1.3635648	1.398528	1.3286016	1.0663776	0.6643008	0.262224
Stomach	9.7981119	7.3915581	5.3287977	3.437934	2.0627604	1.0313802	0.3437934
Colon	14.967696 8	12.065796 4	9.163896	6.5674588	3.81829	1.8327792	0.4581948
RBM	1.6600276	1.6384688	1.6815864	1.401322	1.0563812	0.7114404	0.3664996
Bladder	14.399658	12.184326	10.190527 2	7.753662	5.0952636	2.6583984	0.8861328
Liver	3.746681	2.865109	1.983537	1.322358	0.7713755	0.3305895	0.1101965
Thyroid	0.001087	0.0006522	0.0002174	0.0002174	0	0	0
Oesophagus	0.1499773	0.1499773	0.1636116	0.1908802	0.2045145	0.2045145	0.136343
Other	9.1209086 9	6.4117278 9	4.3346892 8	2.7091808	1.3997434 1	0.5418361 6	0.1354590 4
All cancers	55.120305 1	44.071180 5	34.245390 6	24.711614 8	15.474706 2	7.9752391 6	2.6988431 4
Females							
Breast	1.967121	1.281744	0.747684	0.400545	0.186921	0.071208	0.017802
Lung	2.7620928	2.971872	3.1117248	3.0068352	2.4299424	1.4334912	0.5069664
Stomach	15.126909 6	11.517078 9	8.2510416	5.6725911	3.437934	1.718967	0.5156901
Colon	7.3311168	5.8038008	4.4292164	3.2073636	2.1382424	1.0691212	0.3054632
RBM	1.07794	0.970146	1.6600276	1.0563812	0.6252052	0.323382	0.1293528
Bladder	11.519726 4	9.968994	8.6397948	7.0890624	5.3167968	3.1014648	1.107666
Liver	1.6529475	1.2121615	0.881572	0.661179	0.3305895	0.220393	0
Thyroid	0.0056524	0.0028262	0.0013044	0.0004348	0.0002174	0	0
Oesophagus	0.136343	0.1636116	0.2045145	0.2863203	0.3817604	0.409029	0.2590517
Ovary	2.9088292	2.2519968	1.5951644	1.0321652	0.5629992	0.1876664	0.0938332
Other	7.4067510 4	5.2701882 4	3.560938	2.2790003 2	1.2819376 8	0.6172292 5	0.1899166 9
All cancers	51.895429 7	41.41442	33.082982 5	24.691878 1	16.692546	9.1519518 5	3.1257420 9

Table 3. Lifetime cancer risk (per 10⁶) as a result of chest PA in normal-weight group

	20-29	30-39	40-49	50-59	60-69	70-79	80-89
Males							
Lung	0.3601893	0.3848598	0.394728	0.3749916	0.3009801	0.1874958	0.0740115
Stomach	0.0215004	0.0162196	0.0116932	0.007544	0.0045264	0.0022632	0.0007544
Colon	0.0013426	0.0010823	0.000822	0.0005891	0.0003425	0.0001644	0.0000411
RBM	0.1248093	0.1231884	0.1264302	0.1053585	0.0794241	0.0534897	0.0275553
Bladder	0.0000195	0.0000165	0.0000138	0.0000105	0.0000069	0.0000036	0.0000012
Liver	0.0285634	0.0218426	0.0151218	0.0100812	0.0058807	0.0025203	0.0008401
Thyroid	0.0021315	0.0012789	0.0004263	0.0004263	0	0	0
Oesophagus	0.0238216	0.0238216	0.0259872	0.0303184	0.032484	0.032484	0.021656
Other	0.1072000 5	0.0753584 5	0.0509465 6	0.0318416	0.0164514 9	0.0063683 2	0.0015920 8
All cancers	0.6695776 5	0.6476681 5	0.6261690 6	0.5611612	0.4400961 9	0.2847893 2	0.1264516 8
Females							
Breast	0.2454647	0.1599408	0.0932988	0.0499815	0.0233247	0.0088856	0.0022214
Lung	0.7795878	0.838797	0.8782698	0.8486652	0.6858399	0.4045962	0.1430889
Stomach	0.0331936	0.0252724	0.0181056	0.0124476	0.007544	0.003772	0.0011316
Colon	0.0006576	0.0005206	0.0003973	0.0002877	0.0001918	0.0000959	0.0000274
RBM	0.081045	0.0729405	0.1248093	0.0794241	0.0470061	0.0243135	0.0097254
Bladder	0.0000156	0.0000135	0.0000117	0.0000096	0.0000072	0.0000042	0.0000015
Liver	0.0126015	0.0092411	0.0067208	0.0050406	0.0025203	0.0016802	0
Thyroid	0.0110838	0.0055419	0.0025578	0.0008526	0.0004263	0	0
Oesophagus	0.021656	0.0259872	0.032484	0.0454776	0.0606368	0.064968	0.0411464
Ovary	0.0000093	0.0000072	0.0000051	0.0000033	0.0000018	0.0000006	0.0000003
Other	0.0828110 4	0.0589232 4	0.039813	0.0254803 2	0.0143326 8	0.0069009 2	0.0021233 6
All cancers	1.2681259 4	1.1971854 4	1.1964732	1.0676701 2	0.8418315 8	0.5152171 2	0.1994662 6

Table 4. lifetime cancer risk (per 10⁶) as a result of chest PA in patients with obesity group

	20-29	30-39	40-49	50-59	60-69	70-79	80-89
Males							
Lung	0.4119755	0.440193	0.45148	0.428906	0.3442535	0.214453	0.0846525
Stomach	0.0364173	0.0274727	0.0198059	0.012778	0.0076668	0.0038334	0.0012778
Colon	0.005831	0.0047005	0.00357	0.0025585	0.0014875	0.000714	0.0001785
RBM	0.1695155	0.167314	0.171717	0.1430975	0.1078735	0.0726495	0.0374255
Bladder	0.0003705	0.0003135	0.0002622	0.0001995	0.0001311	0.0000684	0.0000228
Liver	0.0490144	0.0374816	0.0259488	0.0172992	0.0100912	0.0043248	0.0014416
Thyroid	0.005162	0.0030972	0.0010324	0.0010324	0	0	0
Oesophagus	0.0288926	0.0288926	0.0315192	0.0367724	0.039399	0.039399	0.026266
Other	0.18791387	0.13209787	0.0893056	0.055816	0.02883827	0.0111632	0.0027908
All cancers	0.89509267	0.84156297	0.7946411	0.6984595	0.53974087	0.3466053	0.1540555
Females							
Breast	0.1967563	0.1282032	0.0747852	0.0400635	0.0186963	0.0071224	0.0017806
Lung	0.891673	0.959395	1.004543	0.970682	0.7844465	0.462767	0.1636615
Stomach	0.0562232	0.0428063	0.0306672	0.0210837	0.012778	0.006389	0.0019167
Colon	0.002856	0.002261	0.0017255	0.0012495	0.000833	0.0004165	0.000119
RBM	0.110075	0.0990675	0.1695155	0.1078735	0.0638435	0.0330225	0.013209
Bladder	0.0002964	0.0002565	0.0002223	0.0001824	0.0001368	0.0000798	0.0000285
Liver	0.021624	0.0158576	0.0115328	0.0086496	0.0043248	0.0028832	0
Thyroid	0.0268424	0.0134212	0.0061944	0.0020648	0.0010324	0	0
Oesophagus	0.026266	0.0315192	0.039399	0.0551586	0.0735448	0.078798	0.0499054
Ovary	0.0007595	0.000588	0.0004165	0.0002695	0.000147	0.000049	0.0000245
Other	0.145314	0.1033965	0.0698625	0.044712	0.0251505	0.0121095	0.003726
All cancers	1.4786858	1.396772	1.4088639	1.2519891	0.9849336	0.6036369	0.2343712

Table 5. Lifetime cancer risk (per 10⁶) as a result of lumbar spine AP in normal-weight group

	20-29	30-39	40-49	50-59	60-69	70-79	80-89
Males							
Lung	0.1171796	0.1252056	0.128416	0.1219952	0.0979172	0.0609976	0.024078
Stomach	4.6248033	3.4888867	2.5152439	1.622738	0.9736428	0.4868214	0.1622738
Colon	5.574191	4.4934805	3.41277	2.4458185	1.4219875	0.682554	0.1706385
RBM	0.5539688	0.5467744	0.5611632	0.467636	0.3525256	0.2374152	0.1223048
Bladder	8.248968	6.979896	5.8377312	4.441752	2.9188656	1.5228864	0.5076288
Liver	0.8414898	0.6434922	0.4454946	0.2969964	0.1732479	0.0742491	0.0247497
Thyroid	0.0000085	0.0000051	0.0000017	0.0000017	0	0	0
Oesophagus	0.0714175	0.0714175	0.07791	0.090895	0.0973875	0.0973875	0.064925
Other	4.7589206	3.3453798	2.2616652	1.4135408	0.7303294	0.2827081	0.0706770
All cancers	24.790947	19.694537	15.240395	10.901373	6.7659035	3.4450193	1.1472756
	2	9	9	6	1	6	4
Females							
Breast	0.1649102	0.1074528	0.0626808	0.033579	0.0156702	0.0059696	0.0014924
Lung	0.2536216	0.272884	0.2857256	0.2760944	0.2231228	0.1316264	0.0465508
Stomach	7.1400472	5.4361723	3.8945712	2.6775177	1.622738	0.811369	0.2434107
Colon	2.730216	2.161421	1.6495055	1.1944695	0.796313	0.3981565	0.113759
RBM	0.35972	0.323748	0.5539688	0.3525256	0.2086376	0.107916	0.0431664
Bladder	6.5991744	5.710824	4.9493808	4.0610304	3.0457728	1.7767008	0.634536
Liver	0.3712455	0.2722467	0.1979976	0.1484982	0.0742491	0.0494994	0
Thyroid	0.0000442	0.0000221	0.0000102	0.0000034	0.0000017	0	0
Oesophagus	0.064925	0.07791	0.0973875	0.1363425	0.18179	0.194775	0.1233575
Ovary	1.6106019	1.2469176	0.8832333	0.5715039	0.3117294	0.1039098	0.0519549
Other	3.7975028	2.7020693	1.8257225	1.1684624	0.6572601	0.3164585	0.0973718
All cancers	23.092008	18.311667	14.400183	10.620027	7.1372847	3.8963810	1.3555995
	8	8	8			7	7

Table 5. Lifetime cancer risk (per 10⁶) as a result of lumbar spine AP in patients with obesity group

	20-29	30-39	40-49	50-59	60-69	70-79	80-89
Males							
Lung	0.2888537	0.3086382	0.316552	0.3007244	0.2413709	0.1503622	0.0593535
Stomach	4.2694197	3.2207903	2.3219651	1.498042	0.8988252	0.4494126	0.1498042
Colon	7.8563856	6.3332088	4.810032	3.4471896	2.00418	0.9620064	0.2405016
RBM	0.6546309	0.6461292	0.6631326	0.5526105	0.4165833	0.2805561	0.1445289
Bladder	18.273567	15.462249	12.9320628	9.839613	6.4660314	3.3735816	1.1245272
Liver	2.1110702	1.6143478	1.1176254	0.7450836	0.4346321	0.1862709	0.0620903
Thyroid	0.000268	0.0001608	0.0000536	0.0000536	0	0	0
Oesophagus	0.1451384	0.1451384	0.1583328	0.1847216	0.197916	0.197916	0.131944
Other	8.29322177	5.82988857	3.94133312	2.46333325	1.27272215	0.49266664	0.12316666
All cancers	41.8925553	33.5605511	26.2610894	19.0313715	11.9322611	6.09277244	2.03591636
Females							
Breast	0.5408312	0.3523968	0.2055648	0.110124	0.0513912	0.0195776	0.0048944
Lung	0.6251902	0.672673	0.7043282	0.6805868	0.5500091	0.3244658	0.1147501
Stomach	6.5913848	5.0184407	3.5953008	2.4717693	1.498042	0.749021	0.2247063
Colon	3.8480256	3.0463536	2.3248488	1.6835112	1.1223408	0.5611704	0.1603344
RBM	0.425085	0.3825765	0.6546309	0.4165833	0.2465493	0.1275255	0.0510102
Bladder	14.6188536	12.650931	10.9641402	8.9962176	6.7471632	3.9358452	1.405659
Liver	0.9313545	0.6829933	0.4967224	0.3725418	0.1862709	0.1241806	0
Thyroid	0.0013936	0.0006968	0.0003216	0.0001072	0.0000536	0	0
Oesophagus	0.131944	0.1583328	0.197916	0.2770824	0.3694432	0.395832	0.2506936
Ovary	2.2334911	1.7291544	1.2248177	0.7925291	0.4322886	0.1440962	0.0720481
Other	6.26643888	4.45881228	3.012711	1.92813504	1.08457596	0.52220324	0.16067792
All cancers	36.2139925	29.1533612	23.3813024	17.7291877	12.2881279	6.90391754	2.44477402

Table 6. Lifetime cancer risk (per 10⁶) as a result of lumbar spine LAT in normal-weight group

	20-29	30-39	40-49	50-59	60-69	70-79	80-89
Males							
Lung	0.1444195 5	0.1543113	0.158268	0.1503546	0.1206793 5	0.0751773	0.0296752 5
Stomach	1.8652737	1.4071363	1.0144471	0.654482	0.3926892	0.1963446	0.0654482
Colon	4.3686293	3.5216501 5	2.674671	1.9168475 5	1.1144462 5	0.5349342	0.1337335 5
RBM	1.6360613 5	1.6148138	1.6573089	1.3810907 5	1.0411299 5	0.7011691 5	0.3612083 5
Bladder	0.548314	0.463958	0.3880376	0.295246	0.1940188	0.1012272	0.0337424
Liver	1.8744999	1.4334411	0.9923823	0.6615882	0.3859264 5	0.1653970 5	0.0551323 5
Thyroid	0.000007	0.0000042	0.0000014	0.0000014	0	0	0
Oesophagus	0.0384213 5	0.0384213 5	0.0419142	0.0488999	0.0523927 5	0.0523927 5	0.0349285
Other	4.1767688 1	2.9361444 1	1.9849990 4	1.2406244	0.6409892 7	0.2481248 8	0.0620312 2
All cancers	14.652395 6	11.569880 6	8.9120295 4	6.3491348	3.9422720 2	2.0747671 3	0.7758998 2
Females							
Breast	0.0951847	0.0620208	0.0361788	0.0193815	0.0090447	0.0034456	0.0008614
Lung	0.3125793	0.3363195	0.3521463	0.3402762	0.2749906 5	0.1622247	0.0573721 5
Stomach	2.8797208	2.1925147	1.5707568	1.0798953	0.654482	0.327241	0.0981723
Colon	2.1397368	1.6939583	1.2927576 5	0.9361348 5	0.6240899	0.3120449 5	0.0891557
RBM	1.0623775	0.9561397 5	1.6360613 5	1.0411299 5	0.6161789 5	0.3187132 5	0.1274853
Bladder	0.4386512	0.379602	0.3289884	0.2699392	0.2024544	0.1180984	0.042178
Liver	0.8269852 5	0.6064558 5	0.4410588	0.3307941	0.1653970 5	0.1102647	0
Thyroid	0.0000364	0.0000182	0.0000084	0.0000028	0.0000014	0	0
Oesophagus	0.0349285	0.0419142	0.0523927 5	0.0733498 5	0.0977998	0.1047855	0.0663641 5
Ovary	1.2958434	1.0032336	0.7106238	0.4598154	0.2508084	0.0836028	0.0418014
Other	3.435315	2.4443587 5	1.6515937 5	1.05702	0.5945737 5	0.2862762 5	0.088085
All cancers	12.521358 9	9.7165356 5	8.0725668	5.6077391 5	3.489821	1.8266971 5	0.6114754

Table 7. Lifetime cancer risk (per 10⁶) as a result of lumbar spine LAT in patients with obesity group

	20-29	30-39	40-49	50-59	60-69	70-79	80-89
Males							
Lung	0.6107727 5	0.6526065	0.66934	0.635873	0.5103717 5	0.3179365	0.1255012 5
Stomach	3.6930898 5	2.7860151 5	2.0085225 5	1.295821	0.7774926	0.3887463	0.1295821
Colon	8.0880968	6.5199964	4.951896	3.5488588	2.06329	0.9903792	0.2475948
RBM	3.0682844 5	3.0284366	3.1081323	2.5901102 5	1.9525446 5	1.3149790 5	0.6774134 5
Bladder	1.0495712 5	0.8880987 5	0.7427735	0.5651537 5	0.3713867 5	0.193767	0.064589
Liver	4.6707279	3.5717331	2.4727383	1.6484922	0.9616204 5	0.4121230 5	0.1373743 5
Thyroid	0.0013172 5	0.0007903 5	0.0002634 5	0.0002634 5	0	0	0
Oesophagus	0.0931249	0.0931249	0.1015908	0.1185226	0.1269885	0.1269885	0.084659
Other	7.8126462 7	5.4920582 7	3.7129408	2.320588	1.1989704 7	0.4641176	0.1160294
All cancers	29.087631 4	23.03286	17.768197 7	12.723683 1	7.9626651 7	4.2090372	1.5827433 5
Females							
Breast	0.3048916	0.1986624	0.1158864	0.062082	0.0289716	0.0110368	0.0027592
Lung	1.3219465	1.4223475	1.4892815	1.439081	1.1629782 5	0.6860735	0.2426357 5
Stomach	5.7016124	4.3410003 5	3.1099704	2.1381046 5	1.295821	0.6479105	0.1943731 5
Colon	3.9615168	3.1362008	2.3934164	1.7331636	1.1554424	0.5777212	0.1650632
RBM	1.9923925	1.7931532 5	3.0682844 5	1.9525446 5	1.1555876 5	0.5977177 5	0.2390871
Bladder	0.839657	0.7266262 5	0.6297427 5	0.516712	0.387534	0.2260615	0.0807362 5
Liver	2.0606152 5	1.5111178 5	1.0989948	0.8242461	0.4121230 5	0.2747487	0
Thyroid	0.0068497	0.0034248 5	0.0015807	0.0005269	0.0002634 5	0	0
Oesophagus	0.084659	0.1015908	0.1269885	0.1777839	0.2370452	0.253977	0.1608521
Ovary	1.9697958	1.5250032	1.0802106	0.6989598	0.3812508	0.1270836	0.0635418
Other	6.2309696 8	4.4335745 8	2.9956585	1.9172214 4	1.0784370 6	0.5192474 7	0.1597684 5
All cancers	24.474906 2	19.192701 8	16.110015	11.460426	7.2954544 6	3.9215780 2	1.308817

Table 8. Lifetime cancer risk (per 10⁶) as a result of cervical spine AP in normal-weight group

	20-29	30-39	40-49	50-59	60-69	70-79	80-89
Males							
Lung	0.0407632	0.0435552	0.044672	0.0424384	0.0340624	0.0212192	0.008376
Stomach	0.0003363	0.0002537	0.0001829	0.000118	0.0000708	0.0000354	0.0000118
Colon	0.0000294	0.0000237	0.000018	0.0000129	0.0000075	0.0000036	0.0000009
RBM	0.0585739	0.0578132	0.0593346	0.0494455	0.0372743	0.0251031	0.0129319
Bladder	0	0	0	0	0	0	0
Liver	0.0005066	0.0003874	0.0002682	0.0001788	0.0001043	0.0000447	0.0000149
Thyroid	0.1409155	0.0845493	0.0281831	0.0281831	0	0	0
Oesophagus	0.0084678	0.0084678	0.0092376	0.0107772	0.011547	0.011547	0.007698
Other	0.4643064	0.3263936	0.2206604	0.1379128	0.0712549	0.0275825	0.0068956
All cancers	0.7138991	0.5214439	0.3625568	0.2690667	0.1543212	0.0855355	0.0359291
	3	3	8	5	6	4	
Females							
Breast	0.025857	0.016848	0.009828	0.005265	0.002457	0.000936	0.000234
Lung	0.0882272	0.094928	0.0993952	0.0960448	0.0776176	0.0457888	0.0161936
Stomach	0.0005192	0.0003953	0.0002832	0.0001947	0.000118	0.000059	0.0000177
Colon	0.0000144	0.0000114	0.0000087	0.0000063	0.0000042	0.0000021	0.0000006
RBM	0.038035	0.0342315	0.0585739	0.0372743	0.0220603	0.0114105	0.0045642
Bladder	0	0	0	0	0	0	0
Liver	0.0002235	0.0001639	0.0001192	0.0000894	0.0000447	0.0000298	0
Thyroid	0.7327606	0.3663803	0.1690986	0.0563662	0.0281831	0	0
Oesophagus	0.007698	0.0092376	0.011547	0.0161658	0.0215544	0.023094	0.0146262
Ovary	0	0	0	0	0	0	0
Other	0.3585732	0.2551386	0.172391	0.1103302	0.0620607	0.0298811	0.0091941
All cancers	1.2519081	0.7773346	0.5212448	0.3217367	0.2141000	0.1112013	0.0448304
	8	8	4	6	1	9	
	8	8	4	6	1	9	

Table 8. Lifetime cancer risk (per 10⁶) as a result of cervical spine AP in patients with obesity group

organ	Age at exposure (Y)						
	20-29	30-39	40-49	50-59	60-69	70-79	80-89
Males							
Lung	0.0351787	0.0375882	0.038552	0.0366244	0.0293959	0.0183122	0.0072285
Stomach	0.0007866	0.0005934	0.0004278	0.000276	0.0001656	0.0000828	0.0000276
Colon	0.0000686	0.0000553	0.000042	0.0000301	0.0000175	0.0000084	0.0000021
RBM	0.0581658	0.0574104	0.0589212	0.049101	0.0370146	0.0249282	0.0128418
Bladder	0	0	0	0	0	0	0
Liver	0.0009384	0.0007176	0.0004968	0.0003312	0.0001932	0.0000828	0.0000276
Thyroid	0.1169285	0.0701571	0.0233857	0.0233857	0	0	0
Oesophagus	0.0053614	0.0053614	0.0058488	0.0068236	0.007311	0.007311	0.004874
Other	0.5281801	0.3712949	0.2510163	0.1568852	0.0810573	0.0313770	0.0078442
	7	7	2		5	4	6
All cancers	0.7456081	0.5431783	0.3786906	0.2734572	0.1551551	0.0821024	0.0328458
	7	7	2		5	4	6
Females							
Breast	0.0417248	0.0271872	0.0158592	0.008496	0.0039648	0.0015104	0.0003776
Lung	0.0761402	0.081923	0.0857782	0.0828868	0.0669841	0.0395158	0.0139751
Stomach	0.0012144	0.0009246	0.0006624	0.0004554	0.000276	0.000138	0.0000414
Colon	0.0000336	0.0000266	0.0000203	0.0000147	0.0000098	0.0000049	0.0000014
RBM	0.03777	0.033993	0.0581658	0.0370146	0.0219066	0.011331	0.0045324
Bladder	0	0	0	0	0	0	0
Liver	0.000414	0.0003036	0.0002208	0.0001656	0.0000828	0.0000552	0
Thyroid	0.6080282	0.3040141	0.1403142	0.0467714	0.0233857	0	0
Oesophagus	0.004874	0.0058488	0.007311	0.0102354	0.0136472	0.014622	0.0092606
Ovary	0	0	0	0	0	0	0
Other	0.4079015	0.2902376	0.1961065	0.1255081	0.0705983	0.0339917	0.0104590
	2	2		6	4	9	1
All cancers	1.1781007	0.7444585	0.5044384	0.3115480	0.2008553	0.1011690	0.0386475
	2	2		6	4	9	1

Table 9. Lifetime cancer risk (per 10⁶) as a result of cervical spine LAT in normal-weight group

	20-29	30-39	40-49	50-59	60-69	70-79	80-89
Males							
Lung	0.0201151 5	0.0214929	0.022044	0.0209418	0.0168085 5	0.0104709	0.0041332 5
Stomach	0.0002451	0.0001849	0.0001333	0.000086	0.0000516	0.0000258	0.0000086
Colon	0.0000098	0.0000079	0.000006	0.0000043	0.0000025	0.0000012	0.0000003
RBM	0.0610109 5	0.0602186	0.0618033	0.0515027 5	0.0388251 5	0.0261475 5	0.0134699 5
Bladder	0	0	0	0	0	0	0
Liver	0.0002737	0.0002093	0.0001449	0.0000966	0.0000563 5	0.0000241 5	0.0000080 5
Thyroid	0.086189	0.0517134	0.0172378	0.0172378	0	0	0
Oesophagus	0.0043241	0.0043241	0.0047172	0.0055034	0.0058965	0.0058965	0.003931
Other	0.4946340 3	0.3477130 3	0.2350736	0.146921	0.0759091 8	0.0293842	0.0073460 5
All cancers	0.6668018 3	0.4858641 3	0.3411601	0.2422936 5	0.1375498 3	0.0719503	0.0288972
Females							
Breast	0.0071935 5	0.0046872	0.0027342	0.0014647 5	0.0006835 5	0.0002604	0.0000651
Lung	0.0435369	0.0468435	0.0490479	0.0473946	0.0383014 5	0.0225951	0.0079909 5
Stomach	0.0003784	0.0002881	0.0002064	0.0001419	0.000086	0.000043	0.0000129
Colon	0.0000048	0.0000038	0.0000029	0.0000021	0.0000014	0.0000007	0.0000002
RBM	0.0396175	0.0356557 5	0.0610109 5	0.0388251 5	0.0229781 5	0.0118852 5	0.0047541
Bladder	0	0	0	0	0	0	0
Liver	0.0001207 5	0.0000885 5	0.0000644	0.0000483	0.0000241 5	0.0000161	0
Thyroid	0.4481828	0.2240914	0.1034268	0.0344756	0.0172378	0	0
Oesophagus	0.003931	0.0047172	0.0058965	0.0082551	0.0110068	0.011793	0.0074689
Ovary	0	0	0	0	0	0	0
Other	0.3819946 5	0.2718038 5	0.1836512 5	0.1175368	0.0661144 5	0.0318328 8	0.0097947 3
All cancers	0.9249603 5	0.5881793 5	0.4060413	0.2481443	0.1564337 5	0.0784264 3	0.0300868 8

Table 10. Lifetime cancer risk (per 10⁶) as a result of cervical spine LAT in patients with obesity group

	20-29	30-39	40-49	50-59	60-69	70-79	80-89
Males							
Lung	0.0292547 5	0.0312585	0.03206	0.030457	0.0244457 5	0.0152285	0.0060112 5
Stomach	0.0006298 5	0.0004751 5	0.0003425 5	0.000221	0.0001326	0.0000663	0.0000221
Colon	0.0000686	0.0000553	0.000042	0.0000301	0.0000175	0.0000084	0.0000021
RBM	0.0596288	0.0588544	0.0604032	0.050336	0.0379456	0.0255552	0.0131648
Bladder	0	0	0	0	0	0	0
Liver	0.0007259	0.0005551	0.0003843	0.0002562	0.0001494 5	0.0000640 5	0.0000213 5
Thyroid	0.0759387 5	0.0455632 5	0.0151877 5	0.0151877 5	0	0	0
Oesophagus	0.004433	0.004433	0.004836	0.005642	0.006045	0.006045	0.00403
Other	0.4578175 1	0.3218321 1	0.2175766 4	0.1359854	0.0702591 2	0.0271970 8	0.0067992 7
All cancers	0.6284971 6	0.4630268 1	0.3308324 4	0.2381154 5	0.1389950 2	0.0741645 3	0.0300508 7
Females							
Breast	0.0103538 5	0.0067464	0.0039354	0.0021082 5	0.0009838 5	0.0003748	0.0000937
Lung	0.0633185	0.0681275	0.0713335	0.068929	0.0557042 5	0.0328615	0.0116217 5
Stomach	0.0009724	0.0007403 5	0.0005304	0.0003646 5	0.000221	0.0001105	0.0000331 5
Colon	0.0000336	0.0000266	0.0000203	0.0000147	0.0000098	0.0000049	0.0000014
RBM	0.03872	0.034848	0.0596288	0.0379456	0.0224576	0.011616	0.0046464
Bladder	0	0	0	0	0	0	0
Liver	0.0003202 5	0.0002348 5	0.0001708	0.0001281	0.0000640 5	0.0000427	0
Thyroid	0.3948815	0.1974407 5	0.0911265	0.0303755	0.0151877 5	0	0
Oesophagus	0.00403	0.004836	0.006045	0.008463	0.011284	0.01209	0.007657
Ovary	0	0	0	0	0	0	0
Other	0.3535625 6	0.2515733 6	0.169982	0.1087884 8	0.0611935 2	0.0294635 5	0.0090657 1
All cancers	0.8661926 6	0.5645738 1	0.4027727	0.2571172 8	0.1671058 2	0.0865639 5	0.0331191 1

Table 11. Lifetime cancer risk (per 10⁶) as a result of pelvis AP in normal-weight group

	20-29	30-39	40-49	50-59	60-69	70-79	80-89
Males							
Lung	0.0033945	0.003627	0.00372	0.003534	0.0028365	0.001767	0.0006975
Stomach	0.1333344	0.1005856	0.072515 2	0.046784	0.0280704	0.0140352	0.0046784
Colon	4.4179772	3.5614306	2.704884	1.9385002	1.127035	0.5409768	0.1352442
RBM	0.6151838	0.6071944	0.623173 2	0.519311	0.3914806	0.2636502	0.1358198
Bladder	6.7376595	5.7010965	4.768189 8	3.6279705	2.3840949	1.2438756	0.4146252
Liver	0.0429964	0.0328796	0.022762 8	0.0151752	0.0088522	0.0037938	0.0012646
Thyroid	0	0	0	0	0	0	0
Oesophagus	0.0013926	0.0013926	0.001519 2	0.0017724	0.001899	0.001899	0.001266
Other	2.2120144 7	1.5549804 7	1.051254 4	0.657034	0.3394675 7	0.1314068	0.0328517
All cancers	14.163952 9	11.563186 8	9.248018 6	6.8100813	4.2837361 7	2.2014044	0.7264474
Females							
Breast	0.0337025	0.02196	0.01281	0.0068625	0.0032025	0.00122	0.000305
Lung	0.007347	0.007905	0.008277	0.007998	0.0064635	0.003813	0.0013485
Stomach	0.2058496	0.1567264	0.112281 6	0.0771936	0.046784	0.023392	0.0070176
Colon	2.1639072	1.7130932	1.307360 6	0.9467094	0.6311396	0.3155698	0.0901628
RBM	0.39947	0.359523	0.615183 8	0.3914806	0.2316926	0.119841	0.0479364
Bladder	5.3901276	4.6645335	4.042595 7	3.3170016	2.4877512	1.4511882	0.5182815
Liver	0.018969	0.0139106	0.010116 8	0.0075876	0.0037938	0.0025292	0
Thyroid	0	0	0	0	0	0	0
Oesophagus	0.001266	0.0015192	0.001899	0.0026586	0.0035448	0.003798	0.0024054
Ovary	1.3250671	1.0258584	0.726649 7	0.4701851	0.2564646	0.0854882	0.0427441
Other	1.5275790 4	1.0869312 4	0.734413	0.4700243 2	0.2643886 8	0.1272982 5	0.0391686 9
All cancers	11.073285	9.0519605 4	7.571587 2	5.6977013 2	3.9352252 8	2.1341376 5	0.7493699 9

Table 12. Lifetime cancer risk (per 10⁶) as a result of pelvis AP in patients with obesity group

	20-29	30-39	40-49	50-59	60-69	70-79	80-89
Males							
Lung	0.0072124	0.0077064	0.007904	0.0075088	0.0060268	0.0037544	0.001482
Stomach	0.1986165	0.1498335	0.1080195	0.06969	0.041814	0.020907	0.006969
Colon	4.343213	3.5011615	2.65911	1.9056955	1.1079625	0.531822	0.1329555
RBM	0.4821663	0.4759044	0.4884282	0.4070235	0.3068331	0.2066427	0.1064523
Bladder	7.97303	6.74641	5.642452	4.29317	2.821226	1.471944	0.490648
Liver	0.0649536	0.0496704	0.0343872	0.0229248	0.0133728	0.0057312	0.0019104
Thyroid	0	0	0	0	0	0	0
Oesophagus	0.0021274	0.0021274	0.0023208	0.0027076	0.002901	0.002901	0.001934
Other	2.3758916	1.6701812	1.1291366	0.7057104	0.3646170	0.1411420	0.0352855
All cancers	15.447210	12.602994	10.071758	7.4144306	4.6647532	2.3848443	0.7776367
	9	9	3		4	8	2
Females							
Breast	0.0846209	0.0551376	0.0321636	0.0172305	0.0080409	0.0030632	0.0007658
Lung	0.0156104	0.016796	0.0175864	0.0169936	0.0137332	0.0081016	0.0028652
Stomach	0.306636	0.2334615	0.167256	0.1149885	0.06969	0.034845	0.0104535
Colon	2.127288	1.684103	1.2852365	0.9306885	0.620459	0.3102295	0.088637
RBM	0.313095	0.2817855	0.4821663	0.3068331	0.1815951	0.0939285	0.0375714
Bladder	6.378424	5.51979	4.783818	3.925184	2.943888	1.717268	0.61331
Liver	0.028656	0.0210144	0.0152832	0.0114624	0.0057312	0.0038208	0
Thyroid	0	0	0	0	0	0	0
Oesophagus	0.001934	0.0023208	0.002901	0.0040614	0.0054152	0.005802	0.0036746
Ovary	1.1574315	0.896076	0.6347205	0.4107015	0.224019	0.074673	0.0373365
Other	1.5828352	1.1262481	0.7609785	0.4870262	0.2739522	0.1319029	0.0405855
All cancers	11.996531	9.8367329	8.18211	6.2251697	4.3465238	2.3836345	0.8351995
	1	8		4	6	4	2

Appendix 6 COSHH form for the fabrication of trial samples

Assessment Reference Number:	Physical Phantom- Saeed Alqahtani Trial			
Date of Assessment :	07/10/16			
Review Date:				
<i>Annually as standard or more frequently if (see examples below):</i>				
<i>Change to process or substance</i>		<i>Changes in personnel (vulnerability)</i>		
<i>Control measures are failing</i>		<i>Following an incident/accident/case of ill health</i>		
<i>Changes in toxicity information/ revised MSDS</i>		<i>Changes in frequency/quantity used</i>		
Building / Laboratory / Work Area:	The Main Laboratory, University of Exeter Medical School St Luke's Campus			
COSHH Assessors Name:	Georgina Hudson			
Identify the persons carrying out the process / using this/these substance(s)	Saeed Alqahtani			
Who is likely to be exposed? (highlight as appropriate)	Staff and/or Student(s)	Visitors	Maintenance	Other Groups <i>Give details</i>
How many people are likely to be exposed? (highlight as appropriate)	0-5	6-9	>10	
Any vulnerable or high risks groups likely to be exposed? (highlight as appropriate)	Young Person (staff or student under 18)	Pregnant Workers (staff or student)	Other Groups <i>Give details</i>	
List relevant MSDS forms	caco3.pdf, MSDSGY 6010.pdf, PhenolicMicroBalloonsMSDS.pdf, PMC-121-SERIES.pdf, Silicone dioxide.pdf COSHH_assessment_Medical imaging Torso build (2.).doc			
Process details:				
NB: If you are working with micro-organism(s) or biological agents please refer to the <u>Microbiology Risk Assessment for information.</u>				

If working with Nano-materials please refer to the Working Safely with Nanomaterials in Research & Development guidance document

For work with chemicals continue completing this form.

The materials noted in this document will be used to produce trial sample of urethane rubber which will eventually be produced in larger quantities (See COSSH_assessment_Medical imaging Torso build.doc). The aim of this trial will be to assess potential health and safety risks of using larger quantities, and to establish an effective method of mixing the materials effectively.

PMC 121/30 dry will be used to mimic soft tissue density. Part A and B of the PMC will be mixed 1:1, then 23% of Calcium Carbonate will be added. A second lot of PMC A & B will be mixed 1:1 and then added to 2% of phenolic micro-spheres to achieve the desired density. The rubber will then be left to set for approximately 16 hours.

What products/substances are being used in the process?

Products / Substance(s) in process	Hazard or Risk phrases defined for this product in the Material Safety Data Sheet	Red, Amber, Green, (R,A,G,)	What form is this hazard?	Quantity Used / Stored?	Length of Time Used? (Duration)	How often is it used? (Frequency)	Is there a <u>Workplace Exposure Limit</u> for this product / substance?
PMC-121 Series (Polyurethane Elastomer)	H302/H312/H332/H315/H319/H335/H351/H360FD/ Harmful if swallowed/if in contact with skin/if inhaled/ causes skin irritation/ causes serious eye irritation/ suspected of causing cancer/ may damage fertility or the unborn child	R	Gas	750g	1hr	<5 times a year	Contains Toluene-2,6-diisocyanate and Toluene-2,4-diisocyanate TWA: 0.005 ppm 0.04 mg/m3
			Liquid				
			Vapour				
			Fume				
			Solid/ Powder/ Dust				

Calcium Carbonate	Not considered hazardous	G	Gas	20g	1hr	<5 times a year	N/A
			Liquid				
			Vapour				
			Fume				
			Solid/ Powder/ Dust				










Phenoseal Microspheres	May cause eye irritation	G	Gas		20g	1hr	<5 times a year	N/A
	This material may contain trace amount (<0.001%) of free formaldehyde, which is listed by IARC, NTP and OSHA as a carcinogen.		Liquid					
			Vapour					
			Fume					
			Solid/ Powder/ Dust					
			Gas					
			Liquid					
			Vapour					
			Fume					
			Solid/ Powder/ Dust					
			Gas					
			Liquid					
			Vapour					
			Fume					
			Solid/ Powder/ Dust					

STOP CHECK AND CONSIDER THE NEXT QUESTION CAREFULLY					
Can product(s) / substance(s) be substituted?		Y/N	Describe the options and the elimination / substitution process		
Can you eliminate any of the substances?		N			
Can you substitute any of the substances with less hazardous products?		N			
Are any of the substances being mixed?					
Number of substances being mixed		Highest risk (RAG) of the substances to be mixed?		OVERALL RISK OF THE SUBSTANCE(S) (without control measures in place)	RED AMBER GREEN
NB: Treat overall assessment as highest risk (RAG)					
Is the process likely to create new hazards or enhance any existing hazards e.g. producing a violent or highly exothermic reaction, toxic fumes, by-products etc.?					Y / N
If Yes, detail any additional control measures that need to be in place					
What are the risks of fire and/or explosion etc.?					
Is there a risk of fire?					Y / N
Is there a risk of explosion?					Y / N
Is there a risk of toxic fumes?					Y / N
Is there any other associated fire related risk with this process?					Y / N
If Yes to any of the above, detail any additional control measures that need to be in place.					
NB: A separate risk assessment may be also required in accordance with the Dangerous Substances and Explosive Atmospheres Regulations (DSEAR).					

What are the health effects?		
Possible route of entry into the body?		Detail the health effects? (refer to the Material Safety Data Sheet) <i>Consider both short-term and long-term health effects where applicable</i>
Ingestion	Y / N	Polyurethane Elastomer may cause cancer. Organ specific damage: Respiratory. Polyurethane Elastomer may also affect fertility or an unborn child.
Inhalation	Y / N	Polyurethane Elastomer may cause asthma, lung edema, wheezing, shortness of breath, breathing difficulties and reduced lung function.
Contact e.g. skin	Y / N	Chemicals may cause irritation, allergic skin reactions, and can causes burns to the skin. Polyurethane Elastomer may also cause eczema
Absorption via skin and/or mucus membrane e.g. eyes, nose, mouth	Y / N	Can cause serious eye irritation and is harmful.
Other e.g. young persons, pregnancy	Y / N	
What are the first aid requirements: (consult the MSDS for details)		
Ingestion	Get medical attention immediately. Wash out mouth with water. Move exposed person to fresh air. Do not induce vomiting unless directed to do so by medical personnel. Chemical burns must be treated promptly by a physician. Never give anything by mouth to an unconscious person.	
Inhalation	Get medical attention immediately. Move exposed person to fresh air. If it is suspected that fumes are still present, the rescuer should wear an appropriate mask or self-contained breathing apparatus. Keep person warm and at rest. If not breathing, if breathing is irregular or if respiratory arrest occurs, provide artificial respiration or oxygen by trained personnel. It may be dangerous to the person providing aid to give mouth-to-mouth resuscitation. If unconscious, place in recovery position and get medical attention immediately. Maintain an open airway. Loosen tight clothing such as a collar, tie, belt or waistband. In case of inhalation of decomposition products in a fire, symptoms may be delayed. The exposed person may need to be kept under medical surveillance for 48 hours.	
Contact e.g. skin	Get medical attention immediately. Flush contaminated skin with plenty of water. Remove contaminated clothing and shoes. Wash contaminated clothing thoroughly with water before removing or wear gloves. Continue to rinse for at least 10 minutes. Chemical burns must be treated promptly by a physician. Wash clothing before reuse. Clean shoes thoroughly before reuse.	
Absorption e.g. eyes, nose, mouth, skin	Get medical attention immediately. Immediately flush eyes with plenty of water, occasionally lifting the upper and lower eyelids. Check for and remove any contact lenses. Continue to rinse for at least 15 minutes. Chemical burns must be treated promptly by a physician.	
What are the required controls measures?		
Describe the arrangements		

Enclosed System e.g. glove box	Y / N	
Fume Cabinet	Y / N	
Extractor / Hood / Local Exhaust Ventilation	Y / N	For this trial we will be using a fume hood situated in the main laboratory.
Ventilation / Air Change <i>(If unknown seek advice from EDS/Campus Services)</i>	Y / N	
Biological Safety Cabinet	Y / N	
Sensors and / or alarms	Y / N	
Personal Protective Equipment <i>(see details below)</i>	Y / N	
Other:	Y / N	Sensible shoes and emergency shower and eye wash stations recommended.

What are the PPE requirements (in addition to the standard issue laboratory coat)

									Other:
Eye Protection	Respiratory Protection	Face protection	Gloves	Hard Hat	Ear Defenders	Safety footwear	Outer layer	Apron	
Y / N	Y / N	Y / N	Y / N	Y / N	Y / N	Y / N	Y / N	Y / N	Y / N

Describe the type / make/ model of PPE to be used – refer to the Material Safety Data Sheet(s) for guidance

		<i>e.g. Non UV resistant / UV resistant</i>	Butyl or PVC			<i>e.g. toe protection / sole protection</i>			
--	--	---------------------------------------------	--------------	--	--	----------------------------------------------	--	--	--

STOP CHECK AND CONSIDER THE USE OF PERSONAL PROTECTIVE EQUIPMENT (PPE) CAREFULLY

Where Respirators (inc. FFP2 or 3 disposable masks) are required - face fit tests can be arranged for staff and students? Consult your Supervisor for advice or contact Safety@exeter.ac.uk to book an appointment.

Are there any Health Surveillance requirements to be considered?

Consult your Supervisor for advice and guidance or contact occupationalhealth@exeter.ac.uk to book an appointment


What actions to be taken in the event of spillage(s) and/or other emergency situations?	
NB: Refer to Material Safety Data Sheet(s) for guidance	
Small Quantity <500ml	PPE should be worn at all times. Absorbent material such as paper towels should be used to clean up the spillage. It should then be placed into an appropriate container (As supplied in the spill kit) and disposed of via an approved clinical waste contractor. The spill area should then be washed in diluted ammonia solution.
Large Quantity >500ml	PPE should be worn at all times. Only attempt to clean if it is safe to do so (i.e. the area is well ventilated and there is low volumes of dust and vapour). Approach released substance from upwind. Contain and collect spillage with non-combustible absorbent material i.e. sand, earth, vermiculite or diatomaceous earth. Place in an appropriate container (as supplied in spill kit) and dispose of via an approved clinical waste contractor. Prevent entry into sewers and water systems. The spill area should then be washed in diluted ammonia solution.
Do you have correct spill kit provisions to deal with spills (should they occur)?	Y / N
Are there any other emergency situations (<i>not referenced above</i>) to be considered?	Y / N
If Yes, detail any additional control measures that need to be in place	
What are the storage requirements for substances used during this process?	
NB: Refer to Material Safety Data Sheet(s) for guidance	
Are there any specific storage requirements for substances? <i>(Is there a maximum recommended volume/quantity to be stored in one place or a specific temperature, type of cabinet, segregation etc.?) Also consider in laboratory and in holding areas for disposal</i>	Y / N
If Yes, detail the storage arrangements that need to be in place Refer to Material Safety Data Sheet(s) for guidance	PMC-121 Series (Polyurethane Elastomer) : Store in a cool, dry well ventilated space. Calcium Carbonate: Keep container tightly sealed, in a cool well ventilated area. Phenaset Microspheres: May undergo spontaneous smouldering if stored in temperatures above 35 degrees. Store in a cool, well ventilated area.

How should the substances used be disposed of?				
<i>(include environmental impacts and by-products in your explanation if appropriate)</i>				
NB: Refer to Material Safety Data Sheet(s) for guidance				
Dispose of as hazardous waste via approved chemical waste contractor. Do not dispose waste into drains or sinks.				
What are the management arrangements i.e. Training, SOP's, Communication etc.?				
How will this risk assessment be communicated?				
<i>(i.e. how will staff/students be informed of this assessment?)</i>				
All individuals exposed will be directed to relevant COSHH forms, SOP's and MSDS available on the shared network (PCMD- UEMS Medical Imaging- UEMS MI Health and Safety). Paper copies available in the lab.				
Are Safe Systems of Work (SSoW) / Standard Operating Procedure (SOP) needed for this product/task/process in addition to this risk assessment?				Y / N
If Yes, detail / append the SSoW and/or the SOP if applicable				
Are training requirements necessary and who will provide this?				Y / N
If Yes, detail any specialist training required to undertake this process and who will provide said training				
Are there any remaining (residual) risks to be operationally managed?				Y / N
If Yes, detail any specific risks to be considered (e.g. pregnancy, vulnerable people, etc.)?				
Actions				
<i>Use the table below to record actions to be taken if additional control measures are needed to meet the requirements of this risk assessment (identified above)</i>				
No.	Action (describe)	By	Target	Date

		Who?	Date	Completed

OVERALL RISK RATING OF THIS PROCESS (with control measures in place)	
RED	Control Measures Cannot be Implemented - Refer to Supervisor – Do Not Proceed
AMBER	Partial Control Measures Implemented - Further Controls Required- Refer to Supervisor – Do Not Proceed
GREEN	All Control Measures Implemented - Assessor to sign the risk assessment, Approver can then complete their sections once satisfied that the process/task etc. can proceed

COSHH/Risk Assessments Cross-Reference	
COSHH	
Risk Assessments	

Approval Process	
COSHH Assessors Signature:	

Assessors Name:	<i>GEORGINA HUDSON</i>
Date:	10/10/2016
Confirmation received that all actions have been completed and the required control measures are in place:	Yes / No
Confirmation that relevant MSDS are attached and have been read:	Yes / No
Process Supervisors Name: <i>e.g. Principal Investigator, Line Manager</i>	<i>KIRSTIE PARNELL</i>
Approval Date:	
Confirmation that a copy is stored locally with the Laboratory Manager:	Yes / No

NB: Keep a copy of this risk assessment for your own records

COSHH for LTES fabrication

Assessment Reference Number:	Soft (Lean) Tissue Mimicking x-ray Phantom			
Date of Assessment :	02/02/2017			
Review Date: <i>Annually as standard or more frequently if (see examples below):</i> <i>Change to process or substance</i> <i>Control measures are failing</i> <i>Changes in toxicity information/ revised MSDS</i>	<i>Changes in personnel (vulnerability)</i> <i>Following an incident/accident/case of ill health</i> <i>Changes in frequency/quantity used</i>			
Building / Laboratory / Work Area:	The Main Laboratory, University of Exeter Medical School St Luke's Campus			
COSHH Assessors Name:	Saeed Alqahtani			
Identify the persons carrying out the process / using this/these substance(s)	Saeed Alqahtani			
Who is likely to be exposed? (highlight as appropriate)	Staff and/or Student(s)	Visitors	Maintenance	Other Groups <i>Give details</i>
How many people are likely to be exposed? (highlight as appropriate)	0-5	6-9	>10	
Any vulnerable or high risks groups likely to be exposed? (highlight as appropriate)	Young Person (staff or student under 18)	Pregnant Workers (staff or student)	Other Groups <i>Give details</i>	
List relevant MSDS forms	caco3.pdf, PMC-121-SERIES.pdf,			
Process details:				
<i>NB: If you are working with micro-organism(s) or biological agents please refer to the <u>Microbiology Risk Assessment for information.</u></i>				
<i>If working with Nano-materials please refer to the <u>Working Safely with Nanomaterials in Research & Development</u></i>				

guidance document

For work with chemicals continue completing this form.

The materials noted in this document will be used to produce multiple sheets of urethane based rubber which is believed to mimic lean tissue in regard to x-ray attenuation coefficient. The aim of building these materials is to conduct an ionising radiation dose optimisation experiments.

PMC 121/30 dry will be used to mimic lean tissue density along with small quantity of calcium carbonate. Part A and B of the PMC will be mixed 1:1, then 2.8% of calcium carbonate will be added to achieve the desired density. The rubber will then be left to set for approximately 16 hours before the final use.

What products/substances are being used in the process?

Products / Substance(s) in process	Hazard or Risk phrases defined for this product in the Material Safety Data Sheet	Red, Amber, Green, (R,A,G,)	What form is this hazard?		Quantity Used / Stored?	Length of Time Used? (Duration)	How often is it used? (Frequency)	Is there a <u>Workplace Exposure Limit</u> for this product / substance?
PMC-121 Series (Polyurethane Elastomer)	H302/H312/H332/H315/H319/H335/H351/H360FD/ Harmful if swallowed/if in contact with skin/if inhaled/ causes skin irritation/ causes serious eye irritation/ suspected of causing cancer/ may damage fertility or the unborn child	R	Gas		3.5 kg	1hr	<10 times a year	Contains Toluene-2,6-diisocyanate and Toluene-2,4-diisocyanate TWA: 0.005 ppm 0.04 mg/m3
			Liquid	√				
			Vapour					
			Fume					
			Solid/ Powder/ Dust					

Calcium Carbonate	Not considered hazardous	G	Gas		70 g	1hr	<10 times a year	N/A
			Liquid					
			Vapour					
			Fume					
			Solid/ Powder/ Dust	√				
			Gas					
			Liquid					










			Vapour				
			Fume				
			Solid/ Powder/ Dust				
			Gas				
			Liquid				
			Vapour				
			Fume				
			Solid/ Powder/ Dust				
			Gas				
			Liquid				
			Vapour				
			Fume				
			Solid/ Powder/ Dust				

STOP CHECK AND CONSIDER THE NEXT QUESTION CAREFULLY					
Can product(s) / substance(s) be substituted?		Y/N	Describe the options and the elimination / substitution process		
Can you eliminate any of the substances?		N			
Can you substitute any of the substances with less hazardous products?		N			
Are any of the substances being mixed?					
Number of substances being mixed	2	Highest risk (RAG) of the substances to be mixed?		OVERALL RISK OF THE SUBSTANCE(S) (without control measures in place)	RED AMBER GREEN
NB: Treat overall assessment as highest risk (RAG)					
Is the process likely to create new hazards or enhance any existing hazards e.g. producing a violent or highly exothermic reaction, toxic fumes, by-products etc.?					Y / N
If Yes, detail any additional control measures that need to be in place					
What are the risks of fire and/or explosion etc.?					
Is there a risk of fire?					Y / N
Is there a risk of explosion?					Y / N
Is there a risk of toxic fumes?					Y / N
Is there any other associated fire related risk with this process?					Y / N
If Yes to any of the above, detail any additional control measures that need to be in place.					
NB: A separate risk assessment may be also required in accordance with the Dangerous Substances and Explosive Atmospheres Regulations (DSEAR).					

What are the health effects?		
Possible route of entry into the body?		<p>Detail the health effects? (refer to the Material Safety Data Sheet)</p> <p><i>Consider both short-term and long-term health effects where applicable</i></p>
Ingestion	Y / N	Polyurethane Elastomer may cause cancer. Organ specific damage: Respiratory. Polyurethane Elastomer may also affect fertility or an unborn child.
Inhalation	Y / N	Polyurethane Elastomer may cause asthma, lung edema, wheezing, shortness of breath, breathing difficulties and reduced lung function.
Contact e.g. skin	Y / N	Chemicals may cause irritation, allergic skin reactions, and can causes burns to the skin. Polyurethane Elastomer may also cause eczema
Absorption via skin and/or mucus membrane e.g. eyes, nose, mouth	Y / N	Can cause serious eye irritation and is harmful.
Other e.g. young persons, pregnancy	Y / N	
What are the first aid requirements: (consult the MSDS for details)		
Ingestion	<p>Get medical attention immediately. Wash out mouth with water. Move exposed person to fresh air. Do not induce vomiting unless directed to do so by medical personnel.</p> <p>Chemical burns must be treated promptly by a physician. Never give anything by mouth to an unconscious person.</p>	
Inhalation	<p>Move exposed person to fresh air. Get medical attention immediately, loosen tight clothing such as a collar, tie, belt or waistband. Symptoms may be delayed</p>	
Contact e.g. skin	<p>Get medical attention immediately. Remove contaminated clothing and shoes.</p> <p>Flush contaminated skin with plenty of water.</p> <p>Chemical burns must be treated promptly by a physician. Wash clothing before reuse. Clean shoes thoroughly before reuse</p>	
Absorption e.g. eyes, nose, mouth, skin	<p>Get medical attention immediately. Immediately flush eyes with plenty of water, occasionally lifting the upper and lower eyelids. Check for and remove any contact lenses. Continue to rinse for at least 15 minutes. Chemical burns must be treated promptly by a physician.</p>	
What are the required controls measures?		
Describe the arrangements		
Enclosed System e.g. glove box	Y / N	
Fume Cabinet	Y / N	<u>MUST be carried out in fume hood</u>

Extractor / Hood / Local Exhaust Ventilation	Y / N	
Ventilation / Air Change <i>(If unknown seek advice from EDS/Campus Services)</i>	Y / N	
Biological Safety Cabinet	Y / N	
Sensors and / or alarms	Y / N	
Personal Protective Equipment <i>(see details below)</i>	Y / N	
Other:	Y / N	Sensible shoes and emergency shower and eye wash stations recommended.

What are the PPE requirements (in addition to the standard issue laboratory coat)

									Other:
Eye Protection	Respiratory Protection	Face protection	Gloves	Hard Hat	Ear Defenders	Safety footwear	Outer layer	Apron	
Y / N	Y / N	Y / N	Y / N	Y / N	Y / N	Y / N	Y / N	Y / N	Y / N

Describe the type / make/ model of PPE to be used – refer to the Material Safety Data Sheet(s) for guidance

Not necessary if working in fumehood with sash as low down as possible	Not necessary if working in fumehood with sash as low down as possible		Nitrile			No open toed shoes			
-------------------------------------------------------------------------------	-------------------------------------------------------------------------------	--	----------------	--	--	---------------------------	--	--	--

STOP CHECK AND CONSIDER THE USE OF PERSONAL PROTECTIVE EQUIPMENT (PPE) CAREFULLY

Where Respirators (inc. FFP2 or 3 disposable masks) are required - face fit tests can be arranged for staff and students? Consult your Supervisor for advice or contact Safety@exeter.ac.uk to book an appointment.

Are there any Health Surveillance requirements to be considered?

Consult your Supervisor for advice and guidance or contact occupationalhealth@exeter.ac.uk to book an appointment

What actions to be taken in the event of spillage(s) and/or other emergency situations?	
NB: Refer to Material Safety Data Sheet(s) for guidance	
Small Quantity <500ml	PPE should be worn at all times. Absorbent material such as paper towels should be used to clean up the spillage. It should then be placed into an appropriate container (As supplied in the spill kit) and disposed of via an approved clinical waste contractor.
Large Quantity >500ml	PPE should be worn at all times. Only attempt to clean if it is safe to do so (i.e. the area is well ventilated and there is low volumes of dust and vapour). Approach released substance from upwind. Contain and collect spillage with non-combustible absorbent material i.e. sand, earth, vermiculite or diatomaceous earth. Place in an appropriate container (as supplied in spill kit) and dispose of via an approved clinical waste contractor. Prevent entry into sewers and water systems.
Do you have correct spill kit provisions to deal with spills (should they occur)?	
Y / N	
Are there any other emergency situations (not referenced above) to be considered?	
Y / N	
If Yes, detail any additional control measures that need to be in place	To make any spillage inside the fume hood more controllable, a plastic sheet will cover the entire ground surface of the fume hood. After finishing the experiment, the plastic sheet will be removed and disposed of in the chemical waste bin.
What are the storage requirements for substances used during this process?	
NB: Refer to Material Safety Data Sheet(s) for guidance	
Are there any specific storage requirements for substances?	
<i>(Is there a maximum recommended volume/quantity to be stored in one place or a specific temperature, type of cabinet, segregation etc.?) Also consider in laboratory and in holding areas for disposal</i>	
Y / N	
If Yes, detail the storage arrangements that need to be in place Refer to Material Safety Data Sheet(s) for guidance	<p>PMC-121 Series (Polyurethane Elastomer) : Keep container(s) tightly closed and properly labeled. Store in cool (65 – 105 °F), dry, well ventilated place away from heat, direct sunlight, strong oxidizers, bases and any incompatibles. Store in approved containers and protect against physical damage. Keep containers securely sealed when not in use.. Containers that have been opened must be carefully resealed to prevent leakage. Empty containers retain residue and may be dangerous. Avoid water contamination as CO2 forms and pressure builds up.</p> <p>Calcium Carbonate: Keep container tightly sealed, in a cool well ventilated area, hygroscopic.</p>

How should the substances used be disposed of?				
<i>(include environmental impacts and by-products in your explanation if appropriate)</i>				
NB: Refer to Material Safety Data Sheet(s) for guidance				
Dispose of as hazardous waste via approved chemical waste contractor. Do not dispose waste into drains or sinks. Inform lab manager of quantities for disposal				
What are the management arrangements i.e. Training, SOP's, Communication etc.?				
How will this risk assessment be communicated?				
<i>(i.e. how will staff/students be informed of this assessment?)</i>				
All individuals exposed will be directed to relevant COSHH forms, SOP's and MSDS available on the shared network (PCMD- UEMS Medical Imaging- UEMS MI Health and Safety). Paper copies available in the lab.				
Are Safe Systems of Work (SSoW) / Standard Operating Procedure (SOP) needed for this product/task/process in addition to this risk assessment?				Y / N
If Yes, detail / append the SSoW and/or the SOP if applicable			<u>Protocol for preparing a tissue mimicking x-ray phantom</u>	
Are training requirements necessary and who will provide this?				Y / N
If Yes, detail any specialist training required to undertake this process and who will provide said training				
Are there any remaining (residual) risks to be operationally managed?				Y / N
If Yes, detail any specific risks to be considered (e.g. pregnancy, vulnerable people, etc.)?				
Actions				
<i>Use the table below to record actions to be taken if additional control measures are needed to meet the requirements of this risk assessment (identified above)</i>				
No.	Action (describe)	By	Target	Date

		Who?	Date	Completed

OVERALL RISK RATING OF THIS PROCESS (with control measures in place)	
RED	Control Measures Cannot be Implemented - Refer to Supervisor – Do Not Proceed
AMBER	Partial Control Measures Implemented - Further Controls Required- Refer to Supervisor – Do Not Proceed
GREEN	All Control Measures Implemented - Assessor to sign the risk assessment, Approver can then complete their sections once satisfied that the process/task etc. can proceed

COSHH/Risk Assessments Cross-Reference	
COSHH	
Risk Assessments	

Approval Process	
COSHH Assessors Signature:	<i>Saeed</i>
Assessors Name:	<i>Saeed Alqahtani</i>
Date:	02/02/2017
Confirmation received that all	Yes / No

actions have been completed and the required control measures are in place:	
Confirmation that relevant MSDS are attached and have been read:	Yes / No
Process Supervisors Name: <i>e.g. Principal Investigator, Line Manager</i>	Dr Rachel M Palfrey
Approval Date:	07/03/2017
Confirmation that a copy is stored locally with the Laboratory Manager:	Yes / No

NB: Keep a copy of this risk assessment for your own records

COSHH for FTES fabrication

Assessment Reference Number:	Adipose (Fat) Tissue mimicking x-ray Phantom			
Date of Assessment :	02/02/2017			
Review Date:				
<i>Annually as standard or more frequently if (see examples below):</i>				
<i>Change to process or substance</i>		<i>Changes in personnel (vulnerability)</i>		
<i>Control measures are failing</i>		<i>Following an incident/accident/case of ill health</i>		
<i>Changes in toxicity information/revised MSDS</i>		<i>Changes in frequency/quantity used</i>		
Building / Laboratory / Work Area:	The Main Laboratory, University of Exeter Medical School St Luke's Campus			
COSHH Assessors Name:	Saeed Alqahtani			
Identify the persons carrying out the process / using this/these substance(s)	Saeed Alqahtani			
Who is likely to be exposed? (highlight as appropriate)	Staff and/or Student(s)	Visitors	Maintenance	Other Groups <i>Give details</i>
How many people are likely to be exposed? (highlight as appropriate)	0-5	6-9	>10	
Any vulnerable or high risks groups likely to be exposed? (highlight as appropriate)	Young Person (staff or student under 18)	Pregnant Workers (staff or student)	Other Groups <i>Give details</i>	
List relevant MSDS forms	PhenolicMicroBalloonsMSDS.pdf, PMC-121-SERIES.pdf,			
Process details:				
<i>NB: If you are working with micro-organism(s) or biological agents please refer to the <u>Microbiology Risk Assessment for information.</u></i>				
<i>If working with Nano-materials please refer to the <u>Working Safely with Nanomaterials in Research & Development</u></i>				

guidance document

For work with chemicals continue completing this form.

The materials noted in this document will be used to produce multiple sheets of urethane based rubber which is believed to mimic fat tissue in regard to x-ray attenuation coefficient. The aim of building these materials is to conduct an ionising radiation dose optimisation experiments.

PMC 121/30 dry will be used to mimic fat tissue density along with small quantity of phenolic microspheres. Part A and B of the PMC will be mixed 1:1, then 2% of phenolic micro-spheres will be added to achieve the desired density. The rubber will then be left to set for approximately 16 hours before the final use.

What products/substances are being used in the process?

Products / Substance(s) in process	Hazard or Risk phrases defined for this product in the Material Safety Data Sheet	Red, Amber, Green, (R,A,G,)	What form is this hazard?		Quantity Used / Stored?	Length of Time Used? (Duration)	How often is it used? (Frequency)	Is there a <u>Workplace Exposure Limit</u> for this product / substance?
PMC-121 Series (Polyurethane Elastomer)	H302/H312/H332/H315/H319/H335/H351/H360FD/ Harmful if swallowed/if in contact with skin/if inhaled/ causes skin irritation/ causes serious eye irritation/ suspected of causing cancer/ may damage fertility or the unborn child	R	Gas		3.5 kg	1hr	< 20 times a year	Contains Toluene-2,6-diisocyanate and Toluene-2,4-diisocyanate TWA: 0.005 ppm 0.04 mg/m3
			Liquid	√				
			Vapour					
			Fume					
			Solid/ Powder/ Dust					

Phenosest Microspheres	May cause eye irritation This material may contain trace amount (<0.001%) of free formaldehyde, which is listed by IARC, NTP and OSHA as a carcinogen.	G	Gas		98 g	1hr	< 20 times a year	N/A
			Liquid					
			Vapour					
			Fume					
			Solid/ Powder/ Dust	√				
			Gas					










			Liquid				
			Vapour				
			Fume				
			Solid/ Powder/ Dust				
			Gas				
			Liquid				
			Vapour				
			Fume				
			Solid/ Powder/ Dust				
			Gas				
			Liquid				
			Vapour				
			Fume				
			Solid/ Powder/ Dust				

STOP CHECK AND CONSIDER THE NEXT QUESTION CAREFULLY				
Can product(s) / substance(s) be substituted?	Y / N	Describe the options and the elimination / substitution process		
Can you eliminate any of the substances?	N			
Can you substitute any of the substances with less hazardous products?	N			
Are any of the substances being mixed?				
Number of substances being mixed	2	Highest risk (RAG) of the substances to be mixed?		OVERALL RISK OF THE SUBSTANCE(S) (without control measures in place)
				RED AMBER GREEN
NB: Treat overall assessment as highest risk (RAG)				
Is the process likely to create new hazards or enhance any existing hazards e.g. producing a violent or highly exothermic reaction, toxic fumes, by-products etc.?				Y / N
If Yes, detail any additional control measures that need to be in place				
What are the risks of fire and/or explosion etc.?				
Is there a risk of fire?				Y / N
Is there a risk of explosion?				Y / N
Is there a risk of toxic fumes?				Y / N
Is there any other associated fire related risk with this process?				Y / N
If Yes to any of the above, detail any additional control measures that need to be in place.				
NB: A separate risk assessment may be also required in accordance with the Dangerous Substances and Explosive Atmospheres Regulations (DSEAR).				

What are the health effects?		
Possible route of entry into the body?		Detail the health effects? (refer to the Material Safety Data Sheet) <i>Consider both short-term and long-term health effects where applicable</i>
Ingestion	Y / N	Polyurethane Elastomer may cause cancer. Organ specific damage: Respiratory. Polyurethane Elastomer may also affect fertility or an unborn child.
Inhalation	Y / N	Polyurethane Elastomer may cause asthma, lung edema, wheezing, shortness of breath, breathing difficulties and reduced lung function.
Contact e.g. skin	Y / N	Chemicals may cause irritation, allergic skin reactions, and can causes burns to the skin. Polyurethane Elastomer may also cause eczema
Absorption via skin and/or mucus membrane e.g. eyes, nose, mouth	Y / N	Can cause serious eye irritation and is harmful.
Other e.g. young persons, pregnancy	Y / N	
What are the first aid requirements: (consult the MSDS for details)		
Ingestion	Get medical attention immediately. Wash out mouth with water. Move exposed person to fresh air. Do not induce vomiting unless directed to do so by medical personnel. Chemical burns must be treated promptly by a physician. Never give anything by mouth to an unconscious person.	
Inhalation	Get medical attention immediately. Move exposed person to fresh air. If it is suspected that fumes are still present, the rescuer should wear an appropriate mask or self-contained breathing apparatus. Keep person warm and at rest. If not breathing, if breathing is irregular or if respiratory arrest occurs, provide artificial respiration or oxygen by trained personnel. It may be dangerous to the person providing aid to give mouth-to-mouth resuscitation. If unconscious, place in recovery position and get medical attention immediately. Maintain an open airway. Loosen tight clothing such as a collar, tie, belt or waistband. In case of inhalation of decomposition products in a fire, symptoms may be delayed. The exposed person may need to be kept under medical surveillance for 48 hours.	
Contact e.g. skin	Get medical attention immediately. Flush contaminated skin with plenty of water. Remove contaminated clothing and shoes. Wash contaminated clothing thoroughly with water before removing or wear gloves. Continue to rinse for at least 10 minutes. Chemical burns must be treated promptly by a physician. Wash clothing before reuse. Clean shoes thoroughly before reuse.	
Absorption e.g. eyes, nose, mouth, skin	Get medical attention immediately. Immediately flush eyes with plenty of water, occasionally lifting the upper and lower eyelids. Check for and remove any contact lenses. Continue to rinse for at least 15 minutes. Chemical burns must be treated promptly by a physician.	
What are the required controls measures?		
Describe the arrangements		

Enclosed System e.g. glove box	Y / N	
Fume Cabinet	Y / N	<u>MUST be carried out in a fume hood</u>
Extractor / Hood / Local Exhaust Ventilation	Y / N	
Ventilation / Air Change <i>(If unknown seek advice from EDS/Campus Services)</i>	Y / N	
Biological Safety Cabinet	Y / N	
Sensors and / or alarms	Y / N	
Personal Protective Equipment <i>(see details below)</i>	Y / N	
Other:	Y / N	Sensible shoes and emergency shower and eye wash stations recommended.

What are the PPE requirements (in addition to the standard issue laboratory coat)

 Eye Protection	 Respiratory Protection	 Face protection	 Gloves	 Hard Hat	 Ear Defenders	 Safety footwear	 Outer layer	 Apron	Other:
Y / N	Y / N	Y / N	Y / N	Y / N	Y / N	Y / N	Y / N	Y / N	Y / N

Describe the type / make/ model of PPE to be used – refer to the Material Safety Data Sheet(s) for guidance										
Not necessary if workin in fumehood with sash as low down as possible	Not necessary if workin in fumehood with sash as low down as possible		Nitrile			No open toed shoes				
STOP CHECK AND CONSIDER THE USE OF PERSONAL PROTECTIVE EQUIPMENT (PPE) CAREFULLY										
<p>Where Respirators (inc. FFP2 or 3 disposable masks) are required - face fit tests can be arranged for staff and students? Consult your Supervisor for advice or contact Safety@exeter.ac.uk to book an appointment.</p> <p>Are there any Health Surveillance requirements to be considered?</p> <p>Consult your Supervisor for advice and guidance or contact occupationalhealth@exeter.ac.uk to book an <u>appointment</u></p>										
What actions to be taken in the event of spillage(s) and/or other emergency situations?										
<i>NB: Refer to Material Safety Data Sheet(s) for guidance</i>										
Small Quantity <500ml					PPE should be worn at all times. Absorbent material such as paper towels should be used to clean up the spillage. It should then be placed into an appropriate container (As supplied in the spill kit) and disposed of via an approved clinical waste contractor. The spill area should then be washed in diluted ammonia solution.					
Large Quantity >500ml					PPE should be worn at all times. Only attempt to clean if it is safe to do so (i.e. the area is well ventilated and there is low volumes of dust and vapour). Contain and collect spillage with non-combustible absorbent material i.e. sand, earth, vermiculite or diatomaceous earth. Place in an appropriate container (as supplied in spill kit) and dispose of via an approved clinical waste contractor. Prevent entry into sewers and water systems. The spill area should then be washed in diluted ammonia solution.					
Do you have correct spill kit provisions to deal with spills (should they occur)?									Y / N	
Are there any other emergency situations (<i>not referenced above</i>) to be considered?									Y / N	
If Yes, detail any additional control measures that need to be in place					To make any spillage inside the fume hood more controllable, a plastic sheet will cover the entire ground surface of the fume hood. After finishing the experiment, the plastic sheet will be removed and disposed of in the chemical waste bin.					
What are the storage requirements for substances used during this process?										
<i>NB: Refer to Material Safety Data Sheet(s) for guidance</i>										

Are there any specific storage requirements for substances?		Y / N
<i>(Is there a maximum recommended volume/quantity to be stored in one place or a specific temperature, type of cabinet, segregation etc.?) Also consider in laboratory and in holding areas for disposal</i>		
If Yes, detail the storage arrangements that need to be in place Refer to Material Safety Data Sheet(s) for guidance	<p>PMC 121/30 Dry: Keep container(s) tightly closed and properly labeled. Store in cool (65 – 105 °F), dry, well ventilated place away from heat, direct sunlight, strong oxidizers, bases and any incompatibles. Store in approved containers and protect against physical damage. Keep containers securely sealed when not in use. Indoor storage should meet OSHA standards and appropriate fire codes. Containers that have been opened must be carefully resealed to prevent leakage. Empty containers retain residue and may be dangerous. Avoid water contamination as CO2 forms and pressure builds up.</p> <p>Phenosect Microspheres: May undergo spontaneous smouldering if stored in temperatures above 35 degrees. Store in a cool, well ventilated area.</p>	

NB: Refer to Material Safety Data Sheet(s) for guidance	
Dispose of as hazardous waste via approved chemical waste contractor. Do not dispose waste into drains or sinks. Inform lab manager of quantities for disposal	
What are the management arrangements i.e. Training, SOP's, Communication etc.?	
How will this risk assessment be communicated? <i>(i.e. how will staff/students be informed of this assessment?)</i>	
All individuals exposed will be directed to relevant COSHH forms, SOP's and MSDS available on the shared network (PCMD- UEMS Medical Imaging- UEMS MI Health and Safety). Paper copies available in the lab.	
Are Safe Systems of Work (SSoW) / Standard Operating Procedure (SOP) needed for this product/task/process in addition to this risk assessment?	Y / N
If Yes, detail / append the SSoW and/or the SOP if applicable	<u>Protocol for preparing a tissue mimicking x-ray phantom</u>
Are training requirements necessary and who will provide this?	Y / N

If Yes, detail any specialist training required to undertake this process and who will provide said training				
Are there any remaining (residual) risks to be operationally managed?				Y / N
If Yes, detail any specific risks to be considered (e.g. pregnancy, vulnerable people, etc.)?				
Actions				
<i>Use the table below to record actions to be taken if additional control measures are needed to meet the requirements of this risk assessment (identified above)</i>				
No.	Action (describe)	By Who?	Target Date	Date Completed

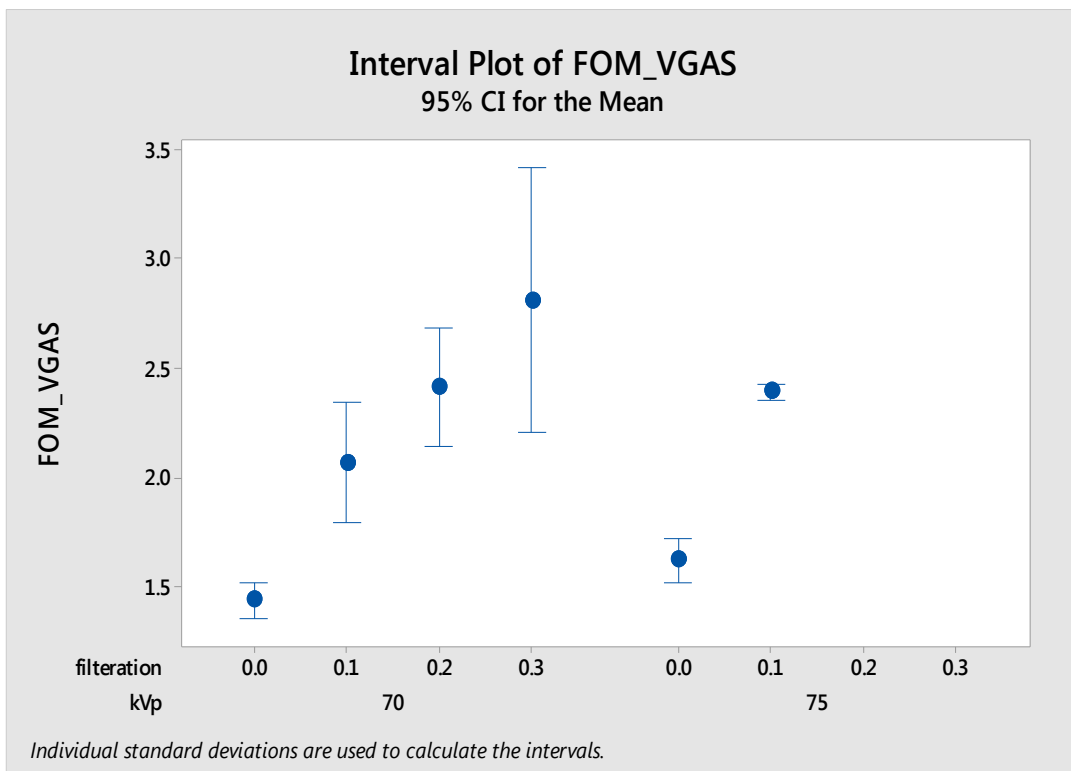
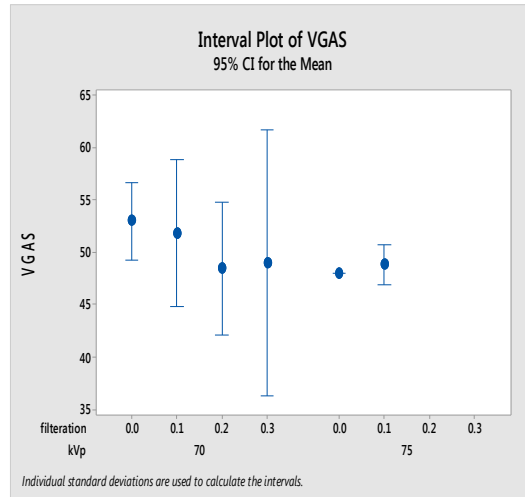
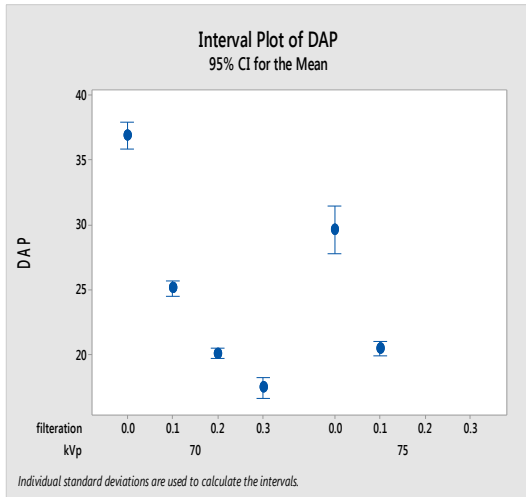
OVERALL RISK RATING OF THIS PROCESS (with control measures in place)	
RED	Control Measures Cannot be Implemented - Refer to Supervisor – Do Not Proceed
AMBER	Partial Control Measures Implemented - Further Controls Required- Refer to Supervisor – Do Not Proceed
GREEN	All Control Measures Implemented - Assessor to sign the risk assessment, Approver can then complete their sections once satisfied that the process/task etc. can proceed

COSHH/Risk Assessments Cross-Reference	
COSHH	
Risk Assessments	
SOP	Phantom

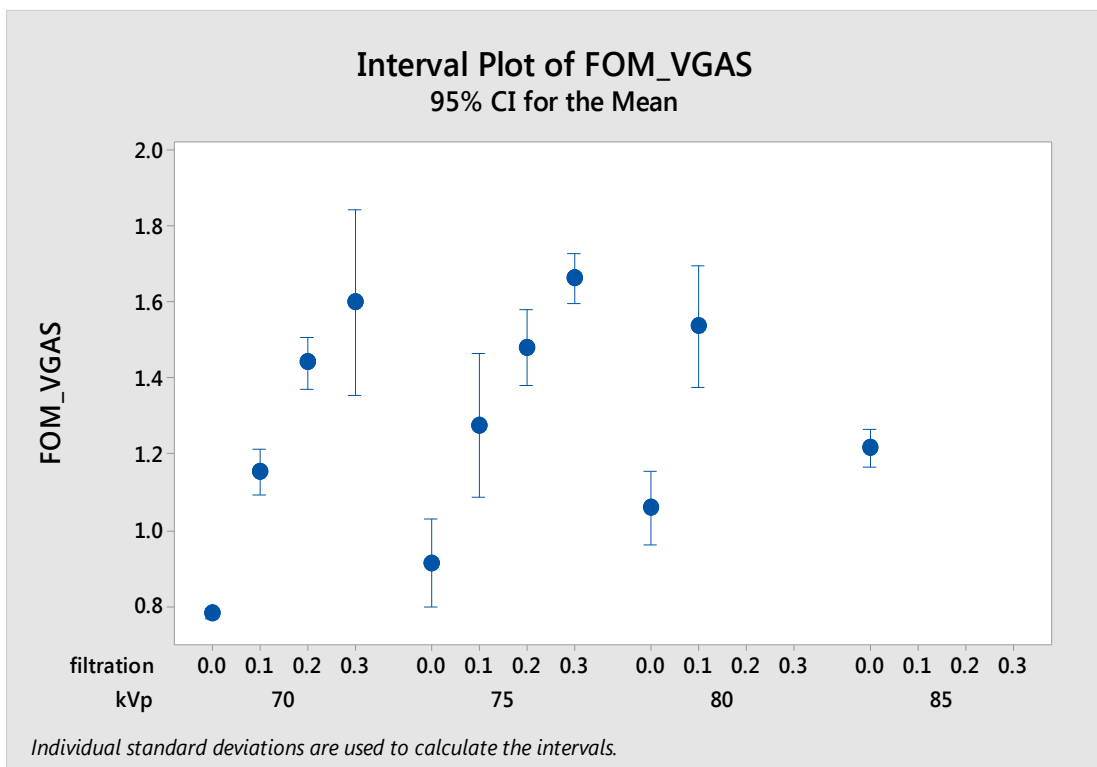
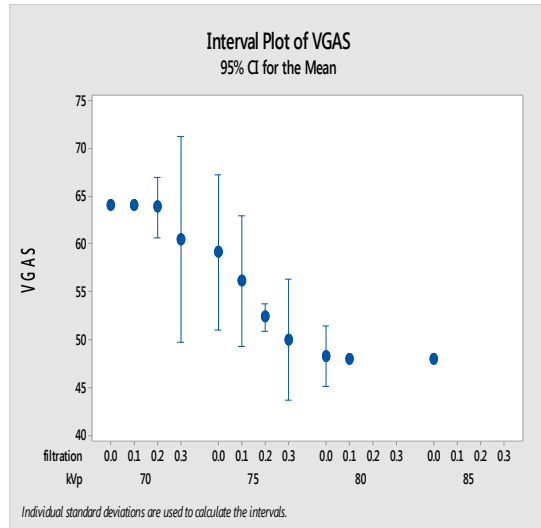
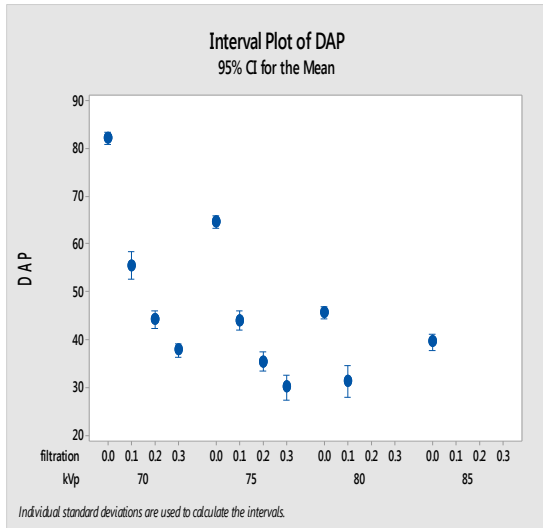
Approval Process	
COSHH Assessors Signature:	<i>Saeed</i>
Assessors Name:	Saeed Alqahtani
Date:	02/02/2017
Confirmation received that all actions have been completed and the required control measures are in place:	Yes / No
Confirmation that relevant MSDS are attached and have been read:	Yes / No
Process Supervisors Name: <i>e.g. Principal Investigator, Line Manager</i>	Dr Rachel M Palfrey
Approval Date:	07/03/2017
Confirmation that a copy is stored locally with the Laboratory Manager:	Yes / No

NB: Keep a copy of this risk assessment for your own records

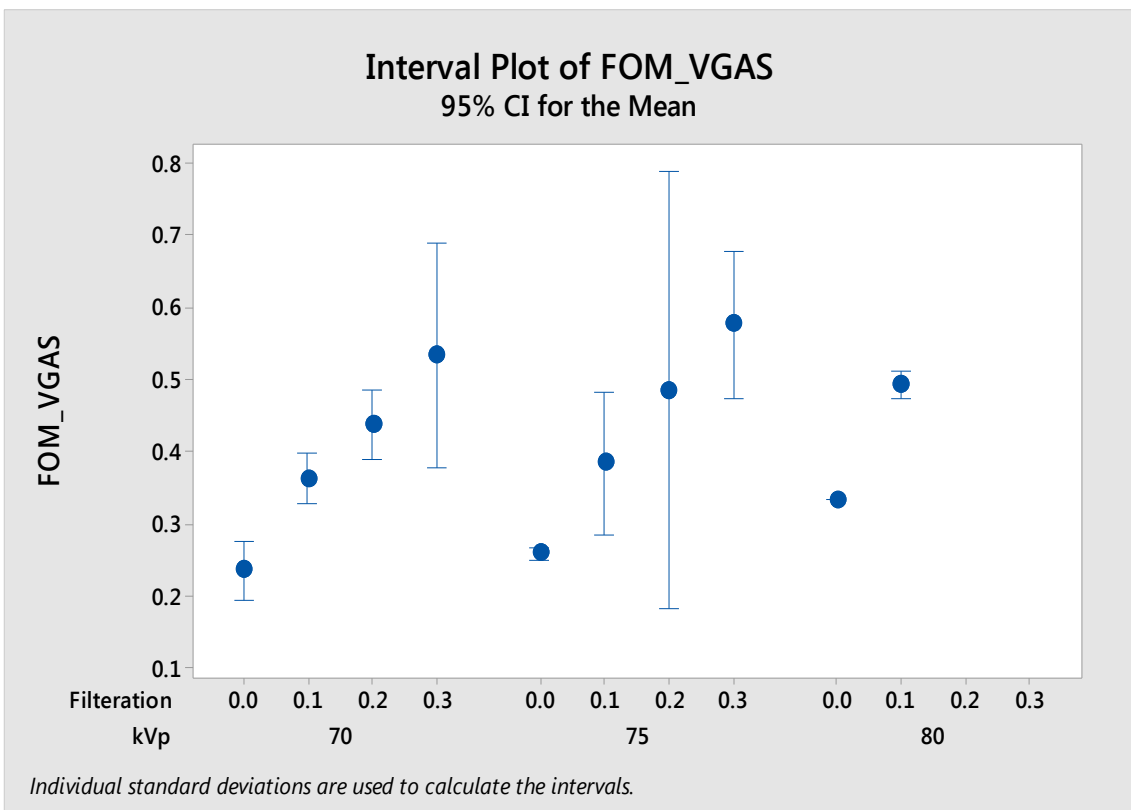
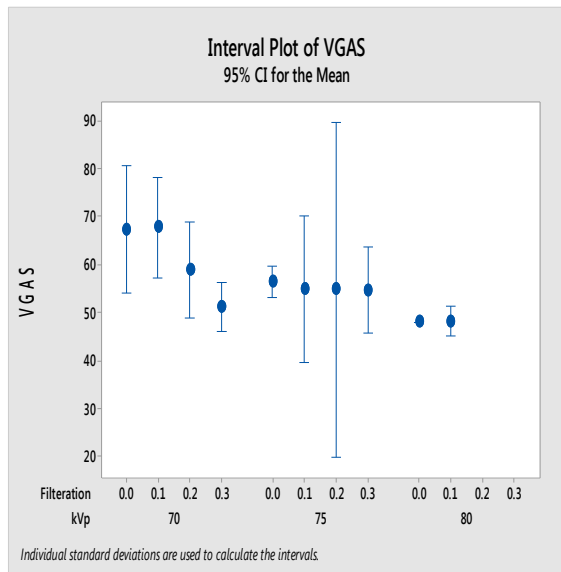
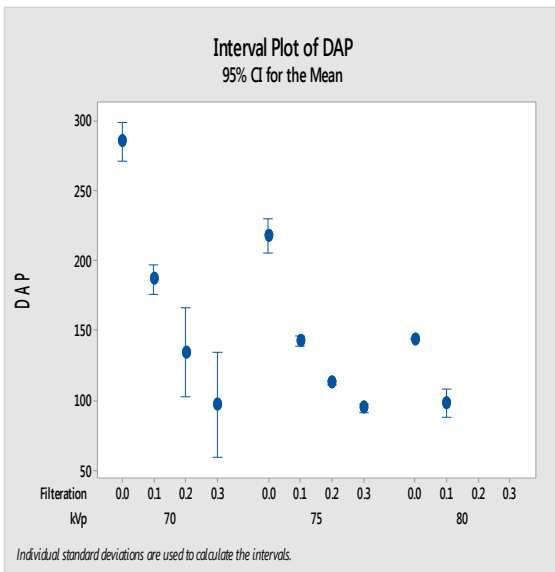
Appendix 7 Interval plots of DAP, VGAS and FOM_{VGAS} of experimental images that match VGAS of reference image and above for phantom (1)



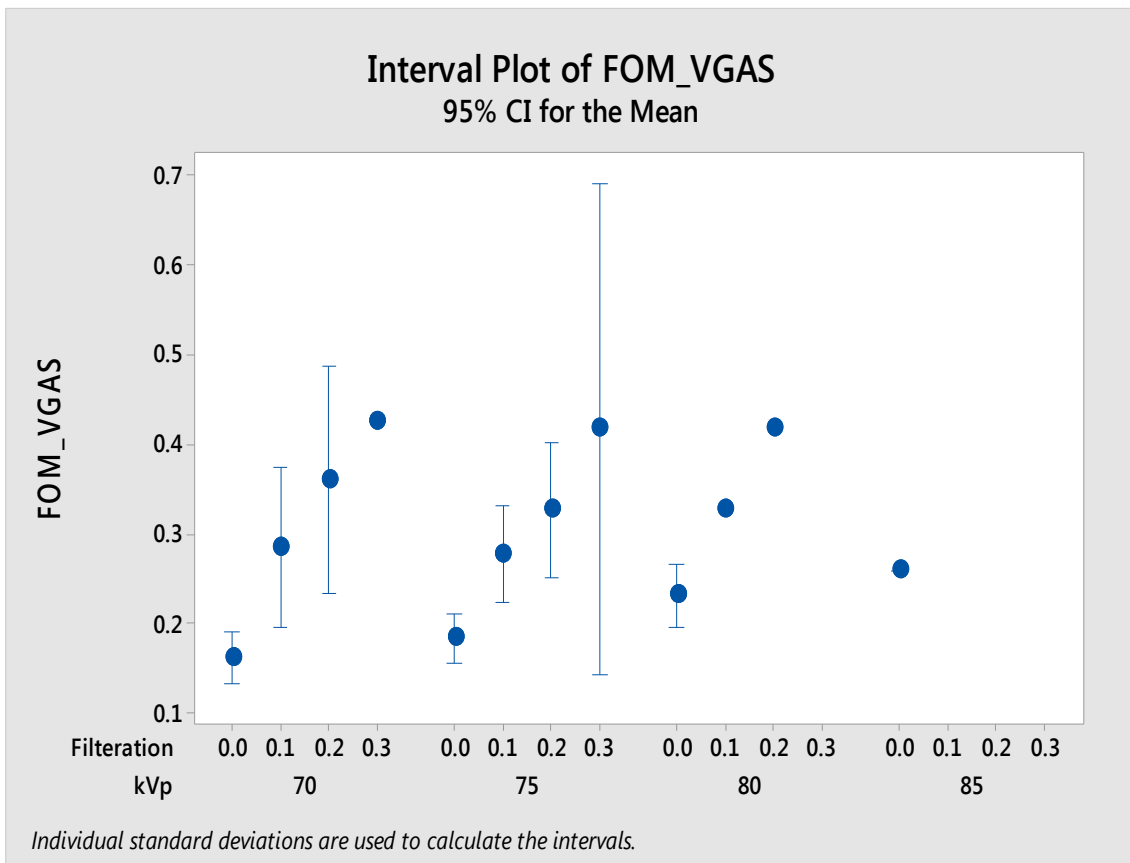
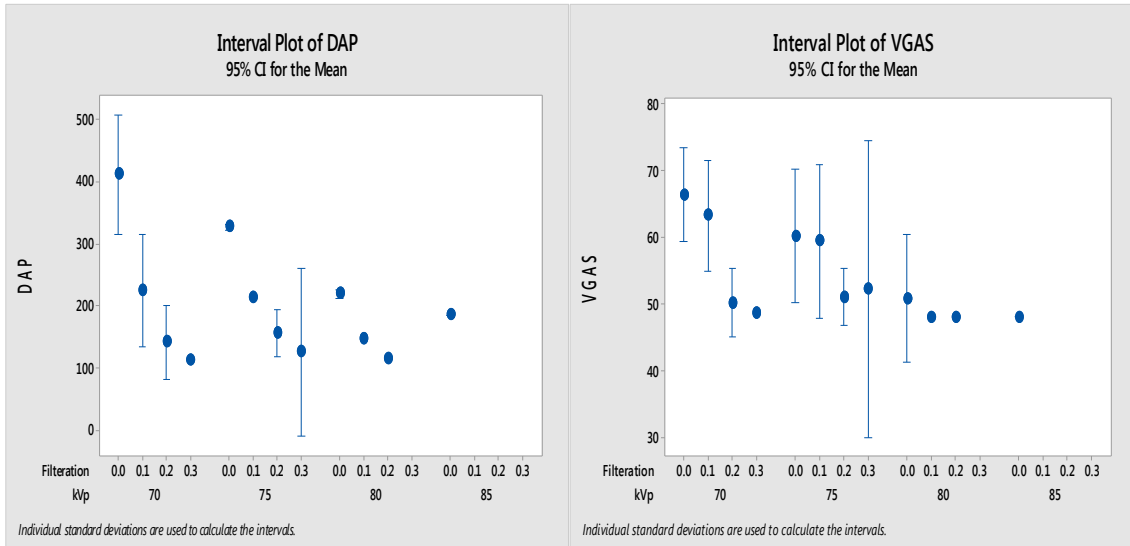
Appendix 8 Interval plots of DAP, VGAS and FOM_{VGAS} of experimental images that match VGAS of reference image and above for phantom (2)



Appendix 9 Interval plots of DAP, VGAS and FOMVGAS of experimental images that match VGAS of reference image and above for phantom (3)



Appendix 10 Interval plots of DAP, VGAS and FOMVGAS of experimental images that match VGAS of reference image and above for phantom (4)



9. References:

- RCR, NRPB, 1990. Patient dose reduction in diagnostic radiology. Documents of the NRPB, Vol. 1, No. 3. Chilton: NRPB.
- ABO, A., SHANNON, M., TAYLOR, G. & BACHUR, R. 2011. The influence of body mass index on the accuracy of ultrasound and computed tomography in diagnosing appendicitis in children. *Pediatric emergency care*, 27, 731-736.
- AICHINGER, H., DIERKER, J., JOITE-BARFUß, S. & SÄBEL, M. 2011. *Radiation exposure and image quality in X-ray diagnostic radiology: physical principles and clinical applications*, Springer Science & Business Media.
- AINSBURY, E., BOUFFLER, S., DÖRR, W., GRAW, J., MUIRHEAD, C., EDWARDS, A. & COOPER, J. 2009. Radiation cataractogenesis: a review of recent studies. *Radiation research*, 172, 1-9.
- AKPINAR, E., BASHAN, I., BOZDEMIR, N. & SAATCI, E. 2007. Which is the best anthropometric technique to identify obesity: body mass index, waist circumference or waist-hip ratio? *Collegium antropologicum*, 31, 387-393.
- AL-MURSHEDI, S., HOGG, P. & ENGLAND, A. 2018. An investigation into the validity of utilising the CDRAD 2.0 phantom for optimisation studies in digital radiography. *The British journal of radiology*, 91, 20180317.
- AL-MURSHEDI, S., HOGG, P. & ENGLAND, A. 2019. Relationship between body habitus and image quality and radiation dose in chest x-ray examinations: a phantom study. *Physica Medica*, 57, 65-71.
- AL QAROOT, B., HOGG, P., TWISTE, M. & HOWARD, D. 2014. A systematic procedure to optimise dose and image quality for the measurement of inter-vertebral angles from lateral spinal projections using Cobb and superimposition methods. *Journal of X-ray science and technology*, 22, 613-625.
- ALERS, H., BOS, L. & HEYNDERICKX, I. How the task of evaluating image quality influences viewing behavior. Quality of Multimedia Experience (QoMEX), 2011 Third International Workshop on, 2011. IEEE, 167-172.
- ALEXANDER, S. 2016. Image acquisition and quality in digital radiography. *Radiologic technology*, 88, 53-66.
- ALI, A. M., HOGG, P., JOHANSEN, S. & ENGLAND, A. 2018. Construction and validation of a low cost paediatric pelvis phantom. *European journal of radiology*, 108, 84-91.
- ALI, R. M., ENGLAND, A., MCENTEE, M. F. & HOGG, P. 2015. A method for calculating effective lifetime risk of radiation-induced cancer from screening mammography. *Radiography*, 21, 298-303.
- ALLEN, E., HOGG, P., MA, W. K. & SZCZEPURA, K. 2013. Fact or fiction: an analysis of the 10 kVp 'rule' in computed radiography. *Radiography*, 19, 223-227.
- ALMEIDA, D., OLIVEIRA, D., SOUZA, A., SILVA, A., ANJOS, M. & LOPES, R. 2019. Characterization of vegetable oils through scattered radiation and multivariate analysis. *Radiation Physics and Chemistry*, 156, 245-251.
- ALMÉN, A., TINGBERG, A., BESJAKOV, J. & MATTSSON, S. 2004. The use of reference image criteria in X-ray diagnostics: an application for the optimisation of lumbar spine radiographs. *European radiology*, 14, 1561-1567.
- ALSLEEM, H. & DAVIDSON, R. 2012. Quality parameters and assessment methods of digital radiography images. *Radiographer*, 59, 46-55.
- ALSLEEM, H. & DAVIDSON, R. 2015. Radiographers' Ability to Detect Low-Contrast Detail in Digital Radiography Systems. *Radiologic technology*, 87, 29-37.
- ALTMAN, D. G. 1991. *Practical Statistics For Medical Research*, London, Chapman & Hall/ CRC.
- ALUKIC, E., SKRK, D. & MEKIS, N. 2018. Comparison of anteroposterior and posteroanterior projection in lumbar spine radiography. *Radiology and Oncology*, 1.

- ALVAREZ, V. P., DIXON, J. B., STRAUSS, B. J., LAURIE, C. P., CHASTON, T. B. & O'BRIEN, P. E. 2007. Single frequency bioelectrical impedance is a poor method for determining fat mass in moderately obese women. *Obesity surgery*, 17, 211-221.
- ALZYOUD, K., HOGG, P., SNAITH, B., FLINTHAM, K. & ENGLAND, A. 2018. Impact of body part thickness on AP pelvis radiographic image quality and effective dose. *Radiography*.
- ALZYOUD, K., HOGG, P., SNAITH, B., FLINTHAM, K. & ENGLAND, A. 2019. Impact of body part thickness on AP pelvis radiographic image quality and effective dose. *Radiography*, 25, e11-e17.
- AMINI, I., AKHLAGHI, P. & SARBAKSHI, P. 2018. Construction and verification of a physical chest phantom from suitable tissue equivalent materials for computed tomography examinations. *Radiation Physics and Chemistry*, 150, 51-57.
- AMIS JR, E. S., BUTLER, P. F., APPLIGATE, K. E., BIRNBAUM, S. B., BRATEMAN, L. F., HEVEZI, J. M., METTLER, F. A., MORIN, R. L., PENTECOST, M. J. & SMITH, G. G. 2007. American College of Radiology white paper on radiation dose in medicine. *Journal of the american college of radiology*, 4, 272-284.
- ANDREOLI, A., GARACI, F., CAFARELLI, F. P. & GUGLIELMI, G. 2016. Body composition in clinical practice. *European journal of radiology*, 85, 1461-1468.
- ANDRIA, G., ATTIVISSIMO, F., GUGLIELMI, G., LANZOLLA, A., MAIORANA, A. & MANGIANTINI, M. 2016. Towards patient dose optimization in digital radiography. *Measurement*, 79, 331-338.
- ARNOLD, B. A. & SCHEIBE, P. 1984. Noise analysis of a digital radiography system. *American journal of roentgenology*, 142, 609-613.
- AWEIDAH, L., ROBINSON, J., CUMMING, S. & LEWIS, S. 2016. Australian diagnostic radiographers' attitudes and perceptions of imaging obese patients: A study of self, peers and students. *Radiography*, 22, e258-e263.
- BAKER, C. 2017. Obesity Statistics. House of Commons library briefing paper No 3336.
- BALIYAN, V., KORDBACHEH, H., SERRAO, J., SAHANI, D. V. & KAMBADAKONE, A. R. 2018. Dual-Source Dual-Energy CT Portal Venous Phase Abdominal CT Scans in Large Body Habitus Patients: Preliminary Observations on Image Quality and Material Decomposition. *Journal of computer assisted tomography*, 42, 932-936.
- BALL, J., MOORE, A. D. & BALL, J. 1997. *Essential physics for radiographers*, Blackwell Science London.
- BÅTH, M. 2010. Evaluating imaging systems: practical applications. *Radiation protection dosimetry*, 139, 26-36.
- BÅTH, M., HÅKANSSON, M., HANSSON, J. & MÅNSSON, L. G. 2005. A conceptual optimisation strategy for radiography in a digital environment. *Radiation protection dosimetry*, 114, 230-235.
- BATH, M. & MANSSON, L. 2007. Visual grading characteristics (VGC) analysis: a non-parametric rank-invariant statistical method for image quality evaluation. *The British journal of radiology*, 80, 169-176.
- BEECHY, L., GALPERN, J., PETRONE, A. & DAS, S. K. 2012. Assessment tools in obesity—Psychological measures, diet, activity, and body composition. *Physiology & behavior*, 107, 154-171.
- BEERES M, B. R., KERL JM, VOGL TJ, LEE C. 2015. Energy Limits in Second Generation High-pitch Dual Source CT - Comparison in an Upper Abdominal Phantom. *J Clin Imaging Sci*, 5:2.
- BEN-SHLOMO, A., BARTAL, G., MOSSERI, M., AVRAHAM, B., LEITNER, Y. & SHABAT, S. 2016. Effective dose reduction in spine radiographic imaging by choosing the less radiation-sensitive side of the body. *The Spine Journal*, 16, 558-563.
- BEN-SHLOMO, A., BARTAL, G., MOSSERI, M. & SHABAT, S. 2017. Effective Dose Reduction in Lateral Lumbar Spine Diagnostic Radiography Using X-Ray Tube Heel Effect. *Journal of Nuclear Engineering and Radiation Science*, 3, 030917.

- BEN-SHLOMO, A., BARTAL, G., SHABAT, S. & MOSSERI, M. 2013. Effective dose and breast dose reduction in paediatric scoliosis X-ray radiography by an optimal positioning. *Radiation protection dosimetry*, 156, 30-36.
- BERGER, M. J., COURSEY, J.S., ZUCKER, M.A., AND CHANG, J. 2005. ESTAR, PSTAR, and ASTAR: Computer Programs for Calculating Stopping-Power and Range Tables for Electrons, Protons, and Helium Ions 2005 ed. Gaithersburg, MD: National Institute of Standards and Technology.
- BHASIN, S., STORER, T. W., BERMAN, N., YARASHESKI, K. E., CLEVINGER, B., PHILLIPS, J., LEE, W. P., BUNNELL, T. J. & CASABURI, R. 1997. Testosterone replacement increases fat-free mass and muscle size in hypogonadal men. *The Journal of Clinical Endocrinology & Metabolism*, 82, 407-413.
- BLANC, D. 1998. European guidelines on quality criteria for diagnostic radiographic images.
- BOICE, J. D., MORIN, M. M., GLASS, A. G., FRIEDMAN, G. D., STOVALL, M., HOOVER, R. N. & FRAUMENI, J. F. 1991. Diagnostic x-ray procedures and risk of leukemia, lymphoma, and multiple myeloma. *Jama*, 265, 1290-1294.
- BOICE JR, J. D., PRESTON, D., DAVIS, F. G. & MONSON, R. R. 1991. Frequent chest X-ray fluoroscopy and breast cancer incidence among tuberculosis patients in Massachusetts. *Radiation research*, 125, 214-222.
- BONTRAGER, K. L. & LAMPIGNANO, J. 2013. *Textbook of radiographic positioning and related Anatomy-E-Book*, Elsevier Health Sciences.
- BOWTELL, J. L., JACKMAN, S. R., SCOTT, S., CONNOLLY, L. J., MOHR, M., ERMIDIS, G., JULIAN, R., YOUSEFIAN, F., HELGE, E. W. & JØRGENSEN, N. R. 2016. Short duration small sided football and to a lesser extent whole body vibration exercise induce acute changes in markers of bone turnover. *BioMed research international*, 2016.
- BRENNAN, P. & MADIGAN, E. 2000. Lumbar spine radiology: analysis of the posteroanterior projection. *European radiology*, 10, 1197-1201.
- BRENNAN, P. & NASH, M. 1998. Increasing FFD: an effective dose-reducing tool for lateral lumbar spine investigations. *Radiography*, 4, 251-259.
- BRENNAN, P. C., MCDONNELL, S. & O'LEARY, D. 2004. Increasing film-focus distance (FFD) reduces radiation dose for x-ray examinations. *Radiation protection dosimetry*, 108, 263-268.
- BRENNER, D. 2008. Effective dose: a flawed concept that could and should be replaced. *The British journal of radiology*, 81, 521-523.
- BRENNER, D. 2012. We can do better than effective dose for estimating or comparing low-dose radiation risks. *Annals of the ICRP*, 41, 124-128.
- BRENNER, D. 2014. Effective dose: a flawed concept that could and should be replaced. *The British journal of radiology*.
- BRINDHABAN, A., AL KHALIFAH, K., AL WATHIQI, G. & AL OSTATH, H. 2005. Effect of x-ray tube potential on image quality and patient dose for lumbar spine computed radiography examinations. *Australasian Physics & Engineering Sciences in Medicine*, 28, 216.
- BROGGIO, D., BEURRIER, J., BREMAUD, M., DESBRÉE, A., FARAH, J., HUET, C. & FRANCK, D. 2011. Construction of an extended library of adult male 3D models: rationale and results. *Physics in Medicine & Biology*, 56, 7659.
- BROSI, P., STUESSI, A., VERDUN, F. R., VOCK, P. & WOLF, R. 2011. Copper filtration in pediatric digital X-ray imaging: its impact on image quality and dose. *Radiological physics and technology*, 4, 148-155.
- BROYLES, S. T., BOUCHARD, C., BRAY, G. A., GREENWAY, F. L., JOHNSON, W. D., NEWTON, R. L., RAVUSSIN, E., RYAN, D. H., SMITH, S. R. & KATZMARZYK, P. T. 2011. Consistency of fat mass-fat-free mass relationship across ethnicity and sex groups. *British journal of nutrition*, 105, 1272-1276.

- BUCKLEY, O., WARD, E., RYAN, A., COLIN, W., SNOW, A. & TORREGGIANI, W. 2009. European obesity and the radiology department. What can we do to help? *European radiology*, 19, 298-309.
- BUISSINK, C., BOWDLER, M., ABDULLAH, A., AL-MURSHEDI, S., CUSTÓDIO, S., HUHN, A., JORGE, J., MOHAMMED ALI, A., PETERS, A. & REY, Y. 2016. IMPACT OF THE ANODE HEEL EFFECT ON IMAGE QUALITY AND EFFECTIVE DOSE FOR AP PELVIS: A PILOT STUDY. *OPTIMAX 2016*, 93.
- BURKHART, R. 1984. Nationwide Evaluation of X-Ray Trends (NEXT): Eight Years of Data (1974–1981). *National Technical Information Service, Springfield, VA*.
- BUSHBERG, J. T. & BOONE, J. M. 2011. *The essential physics of medical imaging*, Lippincott Williams & Wilkins.
- BUTLER, M., RAINFORD, L., LAST, J. & BRENNAN, P. 2010. Are exposure index values consistent in clinical practice? A multi-manufacturer investigation. *Radiation protection dosimetry*, 139, 371-374.
- CARACAPPA, P. F., CHAO, T. E. & XU, X. G. 2009. A study of predicted bone marrow distribution on calculated marrow dose from external radiation exposures using two sets of image data for the same individual. *Health physics*, 96, 661.
- CARLTON, R. R. & ADLER, A. M. 2012. *Principles of radiographic imaging: an art and a science*, Cengage Learning.
- CARROLL, Q. B. 2007. *Practical radiographic imaging*, Charles C Thomas Publisher.
- CARUCCI, L. R. 2013. Imaging obese patients: problems and solutions. *Abdominal imaging*, 38, 630-646.
- CARVER, E. & CARVER, B. 2012. *Medical Imaging-E-Book: Techniques, Reflection and Evaluation*, Elsevier Health Sciences.
- CASSOLA, V., MILIAN, F., KRAMER, R., DE OLIVEIRA LIRA, C. & KHOURY, H. 2011. Standing adult human phantoms based on 10th, 50th and 90th mass and height percentiles of male and female Caucasian populations. *Physics in Medicine & Biology*, 56, 3749.
- CEC 1996. European guidelines on quality criteria for diagnostic radiographic images: (EUR 16260 EN). . Brussels: CEC.
- CHAN, C. & FUNG, K. 2015a. Dose optimization in pelvic radiography by air gap method on CR and DR systems—A phantom study. *Radiography*, 21, 214-223.
- CHAN, C. T. & FUNG, K. K. 2015b. Dose optimization in lumbar spine radiographic examination by air gap method at CR and DR systems: A phantom study. *Journal of Medical Imaging and Radiation Sciences*, 46, 65-77.
- CHAPARIAN, A., KANANI, A. & BAGHBANIAN, M. 2014. Reduction of radiation risks in patients undergoing some X-ray examinations by using optimal projections: a Monte Carlo program-based mathematical calculation. *Journal of medical physics/Association of Medical Physicists of India*, 39, 32.
- CHERIF, R., VICO, L., LAROCHE, N., SAKLY, M., ATTIA, N. & LAVET, C. 2018. Dual-energy X-ray absorptiometry underestimates in vivo lumbar spine bone mineral density in overweight rats. *Journal of bone and mineral metabolism*, 36, 31-39.
- CHIN, K.-Y. 2017. A review on the performance of osteoporosis self-assessment tool for asians in determining osteoporosis and fracture risk. *Postgraduate medicine*, 129, 734-746.
- CHING, W., ROBINSON, J. & MCENTEE, M. 2014. Patient-based radiographic exposure factor selection: a systematic review. *Journal of medical radiation sciences*, 61, 176-190.
- CHING, W., ROBINSON, J. & MCENTEE, M. Comparing prediction models for radiographic exposures. *Medical Imaging 2015: Image Perception, Observer Performance, and Technology Assessment, 2015a*. International Society for Optics and Photonics, 94161J.
- CHING, W., ROBINSON, J. & MCENTEE, M. F. 2015b. DigiBit: A System for Adjusting Radiographic Exposure Factors in the Digital Era. *Radiologic technology*, 86, 614-622.

- CHUMLEA, W. C. 2006. Body composition assessment of obesity. In: BRAY GA, R. D. (ed.) *Overweight and metabolic syndrome: from bench to bedside*. New York (NY): Springer Science+Business Media, LLC.
- COCHRAN, W. G. & COX, G. M. 1950. Experimental designs.
- COMPAGNONE, G., BALENI, M. C., DI NICOLA, E., VALENTINO, M., BENATI, M., CALZOLAIO, L., OBERHOFER, N., FABBRI, E., DOMENICHELLI, S. & BAROZZI, L. 2013. Optimisation of radiological protocols for chest imaging using computed radiography and flat-panel X-ray detectors. *La radiologia medica*, 118, 540-554.
- CONNOLLY, L. J., SCOTT, S., MOHR, M., ERMIDIS, G., JULIAN, R., BANGSBO, J., JACKMAN, S. R., BOWTELL, J. L., DAVIES, R. C. & HOPKINS, S. J. 2014. Effects of small-volume soccer and vibration training on body composition, aerobic fitness, and muscular PCr kinetics for inactive women aged 20–45. *Journal of Sport and Health Science*, 3, 284-292.
- COWEN, A., KENGYELICS, S. & DAVIES, A. 2008. Solid-state, flat-panel, digital radiography detectors and their physical imaging characteristics. *Clinical radiology*, 63, 487-498.
- CRISTY, M. & ECKERMAN, K. 1987. Specific absorbed fractions of energy at various ages from internal photon sources. VI. Newborn. *ORNL/TM-8381*, 6.
- CUSHMAN, D. M., MATTIE, R., CLEMENTS, N. D. & MCCORMICK, Z. L. 2016. The effect of body mass index on fluoroscopic time and radiation dose during intra-articular hip injections. *PM&R*, 8, 876-882.
- DALE, B. M., BROWN, M. A. & SEMELKA, R. C. 2015. *MRI: basic principles and applications*, John Wiley & Sons.
- DANCE, D. 1990. Monte-Carlo calculation of conversion factors for the estimation of mean glandular breast dose. *Physics in Medicine & Biology*, 35, 1211.
- DARCY, S., RAINFORD, L., KELLY, B. & TOOMEY, R. 2015. Decision Making and Variation in Radiation Exposure Factor Selection by Radiologic Technologists. *Journal of Medical Imaging and Radiation Sciences*, 46, 372-379.
- DAS, S. K. 2005. Body composition measurement in severe obesity. *Current Opinion in Clinical Nutrition & Metabolic Care*, 8, 602-606.
- DAVEY, E. & ENGLAND, A. 2015. AP versus PA positioning in lumbar spine computed radiography: Image quality and individual organ doses. *Radiography*, 21, 188-196.
- DAVIS, A., SAFI, H. & MADDISON, S. 2014. The reduction of dose in paediatric panoramic radiography: the impact of collimator height and programme selection. *Dentomaxillofacial Radiology*, 44, 20140223.
- DE LORENZO, A., ANDREOLI, A., SERRANO, P., D’ORAZIO, N., CERVELLI, V. & VOLPE, S. L. 2003. Body cell mass measured by total body potassium in normal-weight and obese men and women. *Journal of the American College of Nutrition*, 22, 546-549.
- DE LORENZO, A., SORGE, R., CANDELORO, N., DI CAMPLI, C., SESTI, G. & LAURO, R. 1999. New insights into body composition assessment in obese women. *Canadian journal of physiology and pharmacology*, 77, 17-21.
- DE VRIES, G., HOEK, B. & BIJWAARD, H. 2015. Optimizing image quality at constant effective dose by adjusting tube voltage for lumbar spine radiography using a flat panel system. *European Congress of Radiology*. Vienna.
- DEGHAN, M. & MERCHANT, A. T. 2008. Is bioelectrical impedance accurate for use in large epidemiological studies? *Nutrition journal*, 7, 26.
- DENDY, P. P. & HEATON, B. 2011. *Physics for diagnostic radiology*, CRC press.
- DENTON, N. & KARPE, F. 2016. Measuring body composition and regional fat mass accurately. *Practical Diabetes*, 33, 224-226.
- DESPRES, J. P., ROSS, R., & LEMIEUX, S. 1996. Imaging techniques applied to the measurement of human body composition. In: A. F. ROCHE, S. B. H., AND T. G. LOHMAN. (ed.) *Human Body Composition*. Champaign, IL: Human Kinetics.

- DING, A., MILLE, M. M., LIU, T., CARACAPPA, P. F. & XU, X. G. 2012. Extension of RPI-adult male and female computational phantoms to obese patients and a Monte Carlo study of the effect on CT imaging dose. *Physics in Medicine & Biology*, 57, 2441.
- DOHERTY, P., O'LEARY, D. & BRENNAN, P. C. 2003. Do CEC guidelines under-utilise the full potential of increasing kVp as a dose-reducing tool? *European radiology*, 13, 1992-1999.
- DOWSETT, D. J., KENNY, P. A. & JOHNSTON, R. E. 2006. *The Physics of Diagnostic Imaging Second Edition*, CRC Press.
- DOYLE, P. 2009. *Assessment and optimisation of digital radiography systems for clinical use*. University of Glasgow.
- DOYLE, P., MARTIN, C. & GENTLE, D. 2005. Dose-image quality optimisation in digital chest radiography. *Radiation protection dosimetry*, 114, 269-272.
- DOYLE, P., MARTIN, C. & GENTLE, D. 2006. Application of contrast-to-noise ratio in optimizing beam quality for digital chest radiography: comparison of experimental measurements and theoretical simulations. *Physics in Medicine & Biology*, 51, 2953.
- DUREN, D. L., SHERWOOD, R. J., CZERWINSKI, S. A., LEE, M., CHOH, A. C., SIERVOGEL, R. M. & CHUMLEA, W. C. 2008. Body composition methods: comparisons and interpretation. *Journal of diabetes science and technology*, 2, 1139-1146.
- EATON, S. B. & EATON, S. B. 2017. Physical inactivity, obesity, and type 2 diabetes: an evolutionary perspective. *Research quarterly for exercise and sport*, 88, 1-8.
- EKPO, E. U., HOBAN, A. C. & MCENTEE, M. F. 2014. Optimisation of direct digital chest radiography using Cu filtration. *Radiography*, 20, 346-350.
- ELLIS, K. J. 2000. Human body composition: in vivo methods. *Physiological reviews*, 80, 649-680.
- ENGLAND, A., EVANS, P., HARDING, L., TAYLOR, E. M., CHARNOCK, P. & WILLIAMS, G. 2015. Increasing source-to-image distance to reduce radiation dose from digital radiography pelvic examinations. *Radiologic technology*, 86, 246-256.
- ENGLAND, N. 2016. Diagnostic Imaging Dataset: Annual statistical Release 2015-16.: Leeds: NHS England.
- EULER, A., HEYE, T., KEKELIDZE, M., BONGARTZ, G., SZUCS-FARKAS, Z., SOMMER, C., SCHMIDT, B. & SCHINDERA, S. T. 2015. Assessment of image quality and low-contrast detectability in abdominal CT of obese patients: comparison of a novel integrated circuit with a conventional discrete circuit detector at different tube voltages. *European radiology*, 25, 687-693.
- FARRELL, K. R. C., ABBOTT, C., ROUND, K., WILLIS, S., YALDEN, R. & KNAPP, K. 1615 Pelvic projection radiography: increasing the source image distance provides diagnostic images at a reduced dose. UK radiological congress, 2008.
- FAUBER, T. L. 2016. *Radiographic Imaging and Exposure-E-Book*, Elsevier Health Sciences.
- FAUBER, T. L. & DEMPSEY, M. C. 2013. X-ray field Size and patient dosimetry. *Radiologic technology*, 85, 155-161.
- FETTERLY, K. A. & SCHUELER, B. A. 2007. Experimental evaluation of fiber-interspaced antiscatter grids for large patient imaging with digital x-ray systems. *Physics in Medicine & Biology*, 52, 4863.
- FISHER, R. F. & HINTENLANG, D. E. 2014. Super-size me: adipose tissue-equivalent additions for anthropomorphic phantoms. *Journal of applied clinical medical physics*, 15, 306-312.
- FLEISS, J. L. 2011. *Design and analysis of clinical experiments*, John Wiley & Sons.
- FORBES, G. B. 1987. Lean body mass-body fat interrelationships in humans. *Nutrition reviews*, 45, 225-231.
- FRANKENFIELD, D. C., ROWE, W. A., COONEY, R. N., SMITH, J. S. & BECKER, D. 2001. Limits of body mass index to detect obesity and predict body composition. *Nutrition*, 17, 26-30.
- FRISARD, M. I., GREENWAY, F. L. & DELANY, J. P. 2005. Comparison of methods to assess body composition changes during a period of weight loss. *Obesity research*, 13, 845-854.

- FU, Q., FAN, G., WU, X., GU, G., GUAN, X., ZHANG, H., GU, X. & HE, S. 2016. Letter to the Editor: Impact of body habitus on fluoroscopic radiation to the surgeon. *Journal of Neurosurgery: Spine*, 24, 867-869.
- FUNG, K. & GILBOY, W. 2000. " Anode heel effect" on patient dose in lumbar spine radiography. *The British journal of radiology*, 73, 531-536.
- GALLAGHER, D., HEYMSFIELD, S. B., HEO, M., JEBB, S. A., MURGATROYD, P. R. & SAKAMOTO, Y. 2000. Healthy percentage body fat ranges: an approach for developing guidelines based on body mass index. *The American journal of clinical nutrition*, 72, 694-701.
- GEIJER, H., NORRMAN, E. & PERSLIDEN, J. 2009. Optimizing the tube potential for lumbar spine radiography with a flat-panel digital detector. *The British journal of radiology*, 82, 62-68.
- GEIJER, H. & PERSLIDEN, J. 2005. Varied tube potential with constant effective dose at lumbar spine radiography using a flat-panel digital detector. *Radiation protection dosimetry*, 114, 240-245.
- GHASEMI, A., ZAHEDIASL, S. & AZIZI, F. 2012. High serum nitric oxide metabolites and incident metabolic syndrome. *Scandinavian journal of clinical and laboratory investigation*, 72, 523-530.
- GINDE, S. R., GELIEBTER, A., RUBIANO, F., SILVA, A. M., WANG, J., HESHKA, S. & HEYMSFIELD, S. B. 2005. Air displacement plethysmography: validation in overweight and obese subjects. *Obesity research*, 13, 1232-1237.
- GISLASON-LEE, A. J., KUMCU, A., KENGYELICS, S. M., BRETTLE, D. S., TREADGOLD, L. A., SIVANANTHAN, M. & DAVIES, A. G. 2015. How much image noise can be added in cardiac x-ray imaging without loss in perceived image quality? *Journal of Electronic Imaging*, 24, 051006.
- GORHAM, S. & BRENNAN, P. C. 2010. Impact of focal spot size on radiologic image quality: a visual grading analysis. *Radiography*, 16, 304-313.
- GRAHAM, D., CLOKE, P. & VOSPER, M. 2012. *Principles and applications of radiological physics*, Churchill Livingstone.
- GRAY, D. S. & BAUER, M. 1991. The relationship between body fat mass and fat-free mass. *Journal of the American College of Nutrition*, 10, 63-68.
- GRAY, D. S., BRAY, G. A., BAUER, M., KAPLAN, K., GEMAYEL, N., WOOD, R., GREENWAY, F. & KIRK, S. 1990. Skinfold thickness measurements in obese subjects. *The American journal of clinical nutrition*, 51, 571-577.
- GRONDIN, Y., MATTHEWS, K., MCENTEE, M., RAINFORD, L., CASEY, M., TONRA, M., AL-QATTAN, E., MCCRUDDEN, T., FOLEY, M. & BRENNAN, P. 2004. Dose-reducing strategies in combination offers substantial potential benefits to females requiring X-ray examination. *Radiation protection dosimetry*, 108, 123-132.
- GUH, D. P., ZHANG, W., BANSBACK, N., AMARSI, Z., BIRMINGHAM, C. L. & ANIS, A. H. 2009. The incidence of co-morbidities related to obesity and overweight: a systematic review and meta-analysis. *BMC public health*, 9, 88.
- HALL, C. N. 2011. *Characterizing canine dose from external beam irradiation*. Colorado State University. Libraries.
- HAMER, O. W., SIRLIN, C. B., STROTZER, M., BORISCH, I., ZORGER, N., FEUERBACH, S. & VOLK, M. 2005. Chest radiography with a flat-panel detector: image quality with dose reduction after copper filtration. *Radiology*, 237, 691-700.
- HAMPEL, J. R. & PASCOAL, A. 2018. Comparison and optimization of imaging techniques in suspected physical abuse paediatric radiography. *The British journal of radiology*, 91, 20170650.
- HAN, S., LEE, B., SHIN, G., CHOI, J., KIM, J., PARK, C., PARK, H., LEE, K. & KIM, Y. 2011. Dose area product measurement for diagnostic reference levels and analysis of patient dose in dental radiography. *Radiation protection dosimetry*, 150, 523-531.

- HARBON, R. W. 2011. Deliberate Underexposure in Cases of Radiography of Suspected Ingested Highly Visible Foreign Bodies—A Preliminary Study. *Journal of Medical Imaging and Radiation Sciences*, 42, 175-178.
- HARDING, L., MANNING-STANLEY, A. S., EVANS, P., TAYLOR, E. M., CHARNOCK, P. & ENGLAND, A. 2014. Optimum patient orientation for pelvic and hip radiography: a randomised trial. *Radiography*, 20, 22-32.
- HART, D. & HILLIER, M. 2007. *Doses to patients from radiographic and fluoroscopic X-ray imaging procedures in the UK-2005 review*, Health Protection Agency, Radiation Protection Division.
- HART, D., HILLIER, M. & SHRIMPSON, P. 2012. Doses to patients from radiographic and fluoroscopic X-ray imaging procedures in the UK—2010 review. Health Protection Agency Report HPA-CRCE-034. Chilton, UK: Health Protection Agency.
- HART, D., WALL, B., HILLIER, M. & SHRIMPSON, P. 2010. Frequency and collective dose for medical and dental X-ray examinations in the UK, 2008. *Health Protection Agency*.
- HARTEMINK, N., BOSHUIZEN, H. C., NAGELKERKE, N. J., JACOBS, M. A. & VAN HOUWELINGEN, H. C. 2006. Combining risk estimates from observational studies with different exposure cutpoints: a meta-analysis on body mass index and diabetes type 2. *American journal of epidemiology*, 163, 1042-1052.
- HARTSTRA, A. V., BOUTER, K. E., BÄCKHED, F. & NIEUWDORP, M. 2015. Insights into the role of the microbiome in obesity and type 2 diabetes. *Diabetes care*, 38, 159-165.
- HAWKING, N. & ELMORE, A. 2009. Effects of AEC chamber selection on patient dose and image quality. *Radiologic technology*, 80, 411-419.
- HEATH, E. M., D ADAMS, T., DAINES, M. M. & HUNT, S. C. 1998. Bioelectric impedance and hydrostatic weighing with and without head submersion in persons who are morbidly obese. *Journal of the American Dietetic Association*, 98, 869-875.
- HEATH, R., ENGLAND, A., WARD, A., CHARNOCK, P., WARD, M., EVANS, P. & HARDING, L. 2011. Digital pelvic radiography: increasing distance to reduce dose. *Radiologic technology*, 83, 20-28.
- HERMANN, K., GEWORSKI, L., HATZKY, T., LIETZ, R. & HARDER, D. 1986. Muscle-and fat-equivalent polyethylene-based phantom materials for x-ray dosimetry at tube voltages below 100 kV. *Physics in Medicine & Biology*, 31, 1041.
- HERRMANN, C., SUND, P., TINGBERG, A., KEDDACHE, S., MANSSON, L. G., ALMEN, A. & MATTSSON, S. Comparison of two methods for evaluating image quality of chest radiographs. *Medical Imaging 2000: Image Perception and Performance*, 2000. International Society for Optics and Photonics, 251-259.
- HERRMANN, T. L., FAUBER, T. L., GILL, J., HOFFMAN, C., ORTH, D. K., PETERSON, P. A., PROUTY, R. R., WOODWARD, A. P. & ODLE, T. G. 2012. Best practices in digital radiography. *Radiologic technology*, 84, 83-89.
- HEYMSFIELD, S., LOHMAN, T., WANG, Z. & GOING, S. 2005. *Human body composition*, Human kinetics.
- HEYMSFIELD, S. B. 2009. Development of imaging methods to assess adiposity and metabolism. *International journal of obesity*, 32, S76.
- HEYWARD, V. H. & WAGNER, D. R. 2004. *Applied body composition assessment*, Human Kinetics.
- HILL, R., BROWN, S. & BALDOCK, C. 2008. Evaluation of the water equivalence of solid phantoms using gamma ray transmission measurements. *Radiation Measurements*, 43, 1258-1264.
- HOGG, P. & BLINDELL, P. Software for image quality evaluation using a forced choice method. United Kingdom Radiological Congress. Manchester, 2012. 139.
- HOLMES, K., ELKINGTON, M. & HARRIS, P. 2013. *Clark's Essential Physics in Imaging for Radiographers*, CRC Press.

- HOMOLKA, P., GAHLEITNER, A., PROKOP, M. & NOWOTNY, R. 2002. Optimization of the composition of phantom materials for computed tomography. *Physics in Medicine & Biology*, 47, 2907.
- HOPKINS, S., TOMS, A., BROWN, M., WELSMAN, J., UKOUMUNNE, O. & KNAPP, K. 2016. A study investigating short-and medium-term effects on function, bone mineral density and lean tissue mass post-total knee replacement in a Caucasian female post-menopausal population: implications for hip fracture risk. *Osteoporosis International*, 27, 2567-2576.
- HORIE, L. M., BARBOSA-SILVA, M. C. G., TORRINHAS, R. S., DE MELLO, M. T., CECCONELLO, I. & WAITZBERG, D. L. 2008. New body fat prediction equations for severely obese patients. *Clinical Nutrition*, 27, 350-356.
- HOWE, G. R. & MCLAUGHLIN, J. 1996. Breast cancer mortality between 1950 and 1987 after exposure to fractionated moderate-dose-rate ionizing radiation in the Canadian fluoroscopy cohort study and a comparison with breast cancer mortality in the atomic bomb survivors study. *Radiation research*, 145, 694-707.
- HSI, R. S., ZAMORA, D. A., KANAL, K. M. & HARPER, J. D. 2013. Severe Obesity is Associated With 3-Fold Higher Radiation Dose Rate During Ureteroscopy. *Urology*, 82, 780-785.
- HU, H. H., CHEN, J. & SHEN, W. 2016. Segmentation and quantification of adipose tissue by magnetic resonance imaging. *Magnetic Resonance Materials in Physics, Biology and Medicine*, 29, 259-276.
- HUDA, W. & GKANATSIOS, N. A. 1998. Radiation dosimetry for extremity radiographs. *Health Physics*, 75, 492-499.
- HUDA, W., OGDEN, K. M. & KHORASANI, M. 2008. Effect of dose metrics and radiation risk models when optimizing CT x-ray tube voltage. *Physics in Medicine & Biology*, 53, 4719.
- IAEA 2002. *Radiological protection for medical exposure to ionizing radiation*, International Atomic Energy Agency.
- ICRP 1977. Recommendations of the ICRP. *ICRP Publication 26. Ann. ICRP*, 1.
- ICRP 1991. 1990 Recommendations of the International Commission on Radiological Protection. *ICRP Publication 60. Ann. ICRP*, 21, (1-3).
- ICRP 1996. Radiological Protection and Safety in Medicine. *ICRP Publication 73. Ann. ICRP* 26 (2).
- ICRP 2006. The Optimisation of Radiological Protection - Broadening the Process. *ICRP Publication 101b. Ann. ICRP* 36 (3).
- ICRP 2007. The 2007 Recommendations of the International Commission on Radiological Protection. *ICRP Publication 103. Ann. ICRP* 37 (2-4).
- ICRP 2008. 2007 Recommendations of the International Commission on Radiological Protection. *ICRP Publication 103. Ann. ICRP*, 37, (2-4).
- ICRP 2017. Diagnostic reference levels in medical imaging. *ICRP Publication 135. Ann. ICRP* 46(1).
- ICRP. 1975. *Reference man: anatomical, physiological and metabolic characteristics*.
- ICRU, I. 1989. Tissue substitutes in radiation dosimetry and measurement. *International Commission on Radiation Units and Measurements*.
- ICRU, I. 1995. Report 54: Medical Imaging-The Assessment of Image Quality. *International Commission on Radiation Units and Measurements, Bethesda, Maryland*.
- IKEJIMBA, L. C., GRAFF, C. G., ROSENTHAL, S., BADAL, A., GHAMMRAOUI, B., LO, J. Y. & GLICK, S. J. 2017. A novel physical anthropomorphic breast phantom for 2D and 3D x-ray imaging. *Medical physics*, 44, 407-416.
- INSKIP, P. D., EKBOM, A., GALANTI, M. R., GRIMELIUS, L. & BOICE JR, J. D. 1995. Medical diagnostic x rays and thyroid cancer. *JNCI: Journal of the National Cancer Institute*, 87, 1613-1621.

- IPSM, N. 1992. CoR. National Protocol for Patient Dose Measurements in Diagnostic Radiology. *IPSM, London*.
- IR(ME)R. 2000. *The ionising radiation (medical exposure) regulations 2000. Statutory instrument*. [Online]. Available: <http://www.legislation.gov.uk/uksi/2000/1059/contents/made>. No. 1059. London:HMSO. [Accessed 03/01 2019].
- ISMAIL, A. A., MOHAMAD, M., AHMAD, R. & KADIR, A. B. A. 2017. Radiation Dose Obtained from Abdominal Computed Radiography: Comparison Between Supine and Prone Positions. *Jurnal Sains Kesihatan Malaysia (Malaysian Journal of Health Sciences)*, 15.
- ISMAILOS, E., MASTORAKOU, I., KELEKIS, N., PAPADOPOULOS, K., EFSTATHOPOULOS, E., PANAYIOTAKIS, G. & KELEKIS, D. 1996. Clinical evaluation of manual and automatic exposure control techniques in film-based chest radiography. *The British journal of radiology*, 69, 650-654.
- JANG, J. S., YANG, H. J., KOO, H. J., KIM, S. H., PARK, C. R., YOON, S. H., SHIN, S. Y. & DO, K.-H. 2018. Image quality assessment with dose reduction using high kVp and additional filtration for abdominal digital radiography. *Physica Medica*, 50, 46-51.
- JANSSEN, I. & ROSS, R. 1999. Effects of sex on the change in visceral, subcutaneous adipose tissue and skeletal muscle in response to weight loss. *International journal of obesity*, 23, 1035.
- JOHNSTON, J., KILLION, J. B., VEALÉ, B. & COMELLO, R. 2011. US technologists' radiation exposure perceptions and practices. *Radiologic Technology*, 82, 311-320.
- JONES, A., ANSELL, C., JERROM, C. & HONEY, I. 2015. Optimization of image quality and patient dose in radiographs of paediatric extremities using direct digital radiography. *The British journal of radiology*, 88, 20140660.
- JONES, A., HINTENLANG, D. & BOLCH, W. 2003. Tissue-equivalent materials for construction of tomographic dosimetry phantoms in pediatric radiology. *Medical physics*, 30, 2072-2081.
- JOYCE, M., MCENTEE, M., BRENNAN, P. C. & O'LEARY, D. 2013. Reducing dose for digital cranial radiography: The increased source to the image-receptor distance approach. *Journal of Medical Imaging and Radiation Sciences*, 44, 180-187.
- KALENDER, W. A. 2014. Dose in x-ray computed tomography. *Physics in Medicine & Biology*, 59, R129.
- KAM, J. & TAYLOR, D. M. 2010. Obesity significantly increases the difficulty of patient management in the emergency department. *Emergency Medicine Australasia*, 22, 316-323.
- KANG, S. M., YOON, J. W., AHN, H. Y., KIM, S. Y., LEE, K. H., SHIN, H., CHOI, S. H., PARK, K. S., JANG, H. C. & LIM, S. 2011. Android fat depot is more closely associated with metabolic syndrome than abdominal visceral fat in elderly people. *PloS one*, 6, e27694.
- KARAMI, V. & ZABIHZADEH, M. 2017. Beam collimation during lumbar spine radiography: A retrospective study. *Journal of biomedical physics & engineering*, 7, 101.
- KARAMI, V., ZABIHZADEH, M., SHAMS, N. & GILAVAND, A. 2017. Optimization of Radiological Protection in Pediatric Patients Undergoing Common Conventional Radiological Procedures: Effectiveness of Increasing the Film to Focus Distance (FFD). *International Journal of Pediatrics*, 5, 4771-4782.
- KARLSSON, A. K., KULLBERG, J., STOKLAND, E., ALLVIN, K., GRONOWITZ, E., SVENSSON, P. A. & DAHLGREN, J. 2013. Measurements of total and regional body composition in preschool children: a comparison of MRI, DXA, and anthropometric data. *Obesity*, 21, 1018-1024.
- KASRAIE, N., ROBINSON, A. & CHAN, S. 2018. Construction of an Anthropomorphic Phantom for Use in Evaluating Pediatric Airway Digital Tomosynthesis Protocols. *Radiology research and practice*, 2018.

- KEHAYIAS, R. R. J. J., DAWSON-HUGHES, B. & HEYMSFIELD, S. B. 1993. Use of dual-energy x-ray absorptiometry in body-composition studies: not yet a “gold standard”. *Am J Clin Nutr*, 58, 589-91.
- KEI, W., HOGG, P. & NORTON, S. 2014. Effects of kilovoltage, milliamperere seconds, and focal spot size on image quality. *Radiologic technology*, 85, 479-485.
- KEYES, A., ANDERSON, J. & BRO, E. 1955. J.: Weight gain from simple overeating. *Metabolism*, 4, 427.
- KEYS, A., ANDERSON, J. & BROZEK, J. 1955. Weight gain from simple overeating. 1. Character of the tissue gained. *Metabolism*, 4, 427-432.
- KEYS, A. & BROŽEK, J. 1953. Body fat in adult man. *Physiological reviews*, 33, 245-325.
- KIARASHI, N., NOLTE, A. C., STURGEON, G. M., SEGARS, W. P., GHATE, S. V., NOLTE, L. W., SAMEI, E. & LO, J. Y. 2015. Development of realistic physical breast phantoms matched to virtual breast phantoms based on human subject data. *Medical physics*, 42, 4116-4126.
- KIM, H., PARK, M., PARK, S., JEONG, H., KIM, J. & KIM, Y. 2012. Estimation of absorbed organ doses and effective dose based on body mass index in digital radiography. *Radiation protection dosimetry*, 153, 92-99.
- KIM, H. S., JEONG, J. H. & LEE, J. W. 2013. Research on Image Quality and Effective dose by Exposure Index Variation. *Journal of the Korean Society of Radiology*, 7, 63-69.
- KNAPP, K. M., WELSMAN, J. R., HOPKINS, S. J., FOGELMAN, I. & BLAKE, G. M. 2012. Obesity increases precision errors in dual-energy X-ray absorptiometry measurements. *Journal of clinical densitometry*, 15, 315-319.
- KONTIS, V., MATHERS, C. D., REHM, J., STEVENS, G. A., SHIELD, K. D., BONITA, R., RILEY, L. M., POZNYAK, V., BEAGLEHOLE, R. & EZZATI, M. 2014. Contribution of six risk factors to achieving the 25× 25 non-communicable disease mortality reduction target: a modelling study. *The Lancet*, 384, 427-437.
- KUCZMARSKI, R. J., FANELLI, M. T. & KOCH, G. G. 1987. Ultrasonic assessment of body composition in obese adults: overcoming the limitations of the skinfold caliper. *The American journal of clinical nutrition*, 45, 717-724.
- KYLE, U., GENTON, L., HANS, D., KARSEGARD, L., SLOSMAN, D. & PICHARD, C. 2001. Age-related differences in fat-free mass, skeletal muscle, body cell mass and fat mass between 18 and 94 years. *European journal of clinical nutrition*, 55, 663.
- KYLE, U. G., BOSAEUS, I., DE LORENZO, A. D., DEURENBERG, P., ELIA, M., GÓMEZ, J. M., HEITMANN, B. L., KENT-SMITH, L., MELCHIOR, J.-C. & PIRLICH, M. 2004. Bioelectrical impedance analysis—part I: review of principles and methods. *Clinical nutrition*, 23, 1226-1243.
- LADIA, A., MESSARIS, G., DELIS, H. & PANAYIOTAKIS, G. Organ dose and risk assessment in paediatric radiography using the PCXMC 2.0. *Journal of Physics: Conference Series*, 2015. IOP Publishing, 012014.
- LAMBERTS, S. W., VAN DEN BELD, A. W. & VAN DER LELY, A.-J. 1997. The endocrinology of aging. *Science*, 278, 419-424.
- LANÇA, L., BOWDLER, M., CREEDON, J., DAYER, V., STENSHOLT, N., STUIVENBERG, V., PINHÃO, S., VISSER, M. & JORGE, J. 2018. Paediatric phantom dose study using digital radiography with variation of exposure parameters and filtration. *European Congress of Radiology*. Vienna.
- LANÇA, L., FRANCO, L., AHMED, A., HARDERWIJK, M., MARTI, C., NASIR, S., NDLOVU, J., OLIVEIRA, M., SANTIAGO, A. R. & HOGG, P. 2014. 10 kVp rule—an anthropomorphic pelvis phantom imaging study using a CR system: impact on image quality and effective dose using AEC and manual mode. *Radiography*, 20, 333-338.
- LANCA, L. & SILVA, A. 2012. *Digital imaging systems for plain radiography*, Springer Science & Business Media.

- LANHEDE, B., BATH, M., KHEDDACHE, S., SUND, P., BJORNELD, L., WIDELL, M., ALMÉN, A., BESJAKOV, J., MATTSSON, S. & TINGBERG, A. 2002. The influence of different technique factors on image quality of chest radiographs as evaluated by modified CEC image quality criteria. *The British journal of radiology*, 75, 38-49.
- LASKEY, M. A. 1996. Dual-energy X-ray absorptiometry and body composition. *Nutrition*, 12, 45-51.
- LAUNDERS, J., COWEN, A., BURY, R. & HAWKRIDGE, P. 2001. Towards image quality, beam energy and effective dose optimisation in digital thoracic radiography. *European radiology*, 11, 870-875.
- LE CARVENNEC, M., FAGOUR, C., ADENIS-LAMARRE, E., PERLEMOINE, C., GIN, H. & RIGALLEAU, V. 2007. Body composition of obese subjects by air displacement plethysmography: the influence of hydration. *Obesity*, 15, 78-84.
- LE, N. T. T., ROBINSON, J. & LEWIS, S. J. 2015a. Obese patients and radiography literature: what do we know about a big issue? *Journal of medical radiation sciences*, 62, 132-141.
- LE, N. T. T., ROBINSON, J. & LEWIS, S. J. 2015b. A study of student radiographers' learning experiences in imaging obese patients. *Journal of Medical Imaging and Radiation Sciences*, 46, S61-S68. e1.
- LEE, C., LEE, S.-S., KIM, J.-E., SYMKHAMPHA, K., LEE, W.-J., HUH, K.-H., YI, W.-J., HEO, M.-S., CHOI, S.-C. & YEOM, H.-Y. 2016. A dose monitoring system for dental radiography. *Imaging science in dentistry*, 46, 103-108.
- LEE, J. J., PEDLEY, A., THERKELSEN, K. E., HOFFMANN, U., MASSARO, J. M., LEVY, D. & LONG, M. T. 2017. Upper body subcutaneous fat is associated with cardiometabolic risk factors. *The American journal of medicine*, 130, 958-966. e1.
- LEENDERS, M., VERDIJK, L. B., VAN DER HOEVEN, L., ADAM, J. J., VAN KRANENBURG, J., NILWIK, R. & VAN LOON, L. J. 2013. Patients with type 2 diabetes show a greater decline in muscle mass, muscle strength, and functional capacity with aging. *Journal of the American Medical Directors Association*, 14, 585-592.
- LINET, M. S., SLOVIS, T. L., MILLER, D. L., KLEINERMAN, R., LEE, C., RAJARAMAN, P. & BERRINGTON DE GONZALEZ, A. 2012. Cancer risks associated with external radiation from diagnostic imaging procedures. *CA: a cancer journal for clinicians*, 62, 75-100.
- LONGO, M., GENOVESE, E., DONATIELLO, S., CASSANO, B., INSERO, T., CAMPOLEONI, M., DEL VECCHIO, A., MAGISTRELLI, A., TOMÀ, P. & CANNATÀ, V. 2018. Quantification of scatter radiation from radiographic procedures in a neonatal intensive care unit. *Pediatric radiology*, 48, 715-721.
- LORUSSO, A., BRUNO, S. & L'ABBATE, N. 2007. Musculoskeletal complaints among Italian X-ray technologists. *Industrial health*, 45, 705-708.
- LOWE, D. G. 2004. Method and apparatus for identifying scale invariant features in an image and use of same for locating an object in an image. Google Patents.
- LUKASKI, H. C. 1987. Methods for the assessment of human body composition: traditional and new. *The American journal of clinical nutrition*, 46, 537-556.
- LYRA, M. E., KORDOLAIMI, S. D. & SALVARA, A.-L. N. 2010. Presentation of digital radiographic systems and the quality control procedures that currently followed by various organizations worldwide. *Recent Patents on Medical Imaging*, 2, 5-21.
- MA, W., HOGG, P., TOOTELL, A., MANNING, D., THOMAS, N., KANE, T., KELLY, J., MCKENZIE, M. & KITCHING, J. 2013. Anthropomorphic chest phantom imaging—the potential for dose creep in computed radiography. *Radiography*, 19, 207-211.
- MACKENZIE, A., WARREN, L. M., WALLIS, M. G., GIVEN-WILSON, R. M., COOKE, J., DANCE, D. R., CHAKRABORTY, D. P., HALLING-BROWN, M. D., LOONEY, P. T. & YOUNG, K. C. 2016. The relationship between cancer detection in mammography and image quality measurements. *Physica Medica*, 32, 568-574.
- MAHESH, M. 2001. Fluoroscopy: patient radiation exposure issues. *Radiographics*, 21, 1033-1045.

- MALONE, J., GULERIA, R., CRAVEN, C., HORTON, P., JÄRVINEN, H., MAYO, J., O'REILLY, G., PICANO, E., REMEDIOS, D. & LE HERON, J. 2012. Justification of diagnostic medical exposures: some practical issues. Report of an International Atomic Energy Agency Consultation. *The British journal of radiology*, 85, 523-538.
- MANINI, T. M., BUFORD, T. W., LOTT, D. J., VANDENBORNE, K., DANIELS, M. J., KNAGGS, J. D., PATEL, H., PAHOR, M., PERRI, M. G. & ANTON, S. D. 2013. Effect of dietary restriction and exercise on lower extremity tissue compartments in obese, older women: a pilot study. *Journals of Gerontology Series A: Biomedical Sciences and Medical Sciences*, 69, 101-108.
- MANNINEN, A.-L., KOTIAHO, A., NIKKINEN, J. & NIEMINEN, M. 2014. Validation of a MOSFET dosimeter system for determining the absorbed and effective radiation doses in diagnostic radiology. *Radiation protection dosimetry*, 164, 361-367.
- MANNING-STANLEY, A. S., WARD, A. J. & ENGLAND, A. 2012. Options for radiation dose optimisation in pelvic digital radiography: a phantom study. *Radiography*, 18, 256-263.
- MÅNSSON, L. 2000. Methods for the evaluation of image quality: a review. *Radiation protection dosimetry*, 90, 89-99.
- MANTIUK, R. K., TOMASZEWSKA, A. & MANTIUK, R. Comparison of four subjective methods for image quality assessment. Computer graphics forum, 2012. Wiley Online Library, 2478-2491.
- MARSHALL, N. 2009. An examination of automatic exposure control regimes for two digital radiography systems. *Physics in Medicine & Biology*, 54, 4645.
- MARTIN, C. 2007a. Optimisation in general radiography. *Biomedical imaging and intervention journal*, 3.
- MARTIN, C. J. 2007b. The application of effective dose to medical exposures. Oxford University Press.
- MASSANES, F. & BRANKOV, J. G. 2016. Full receiver operating characteristic curve estimation using two alternative forced choice studies. *Journal of Medical Imaging*, 3, 011010.
- MATANOSKI, G. M., BOICE JR, J. D., BROWN, S. L., GILBERT, E. S., PUSKIN, J. S. & O'TOOLE, T. 2001. Radiation exposure and cancer: case study. *American journal of epidemiology*, 154, S91-S98.
- MATTHEWS, K. & BRENNAN, P. C. 2009. Optimisation of x-ray examinations: General principles and an Irish perspective. *Radiography*, 15, 262-268.
- MATTSSON, S. & THOMAS, B. J. 2006. Development of methods for body composition studies. *Physics in Medicine & Biology*, 51, R203.
- MAYO, J. R. 2008. Radiation dose issues in longitudinal studies involving computed tomography. *Proceedings of the American Thoracic Society*, 5, 934-939.
- MCENTEE, M. F., BRENNAN, P. C. & CONNOR, G. O. 2004. The effect of X-ray tube potential on the image quality of PA chest radiographs when using digital image acquisition devices. *Radiography*, 10, 287-292.
- MEINEL, F. G., CANSTEIN, C., SCHOEPF, U. J., SEDLMAIER, M., SCHMIDT, B., HARRIS, B. S., FLOHR, T. G. & DE CECCO, C. N. 2014. Image quality and radiation dose of low tube voltage 3rd generation dual-source coronary CT angiography in obese patients: a phantom study. *European radiology*, 24, 1643-1650.
- MESSERLI, F. 1982. Cardiovascular effects of obesity and hypertension. *The Lancet*, 319, 1165-1168.
- METAXAS, V. I., MESSARIS, G. A., LEKATOU, A. N., PETSAS, T. G. & PANAYIOTAKIS, G. S. 2018. Patient Dose In Digital Radiography Utilising Bmi Classification. *Radiation protection dosimetry*.
- METTLER JR, F. A., HUDA, W., YOSHIZUMI, T. T. & MAHESH, M. 2008. Effective doses in radiology and diagnostic nuclear medicine: a catalog. *Radiology*, 248, 254-263.

- MIDGLEY, S. M., STELLA, D. L., CAMPBELL, B. C., LANGENBERG, F. & EINSIEDEL, P. F. 2017. CT brain perfusion: A static phantom study of contrast-to-noise ratio and radiation dose. *Journal of medical imaging and radiation oncology*, 61, 361-366.
- MILLER-KEANE 2003a. Encyclopedia and Dictionary of Medicine, Nursing, and Allied Health, Seventh Edition. (2003). Retrieved November 26 2018 from <https://medical-dictionary.thefreedictionary.com/collimation>.
- MILLER-KEANE 2003b. phantom. (n.d.) Miller-Keane Encyclopedia and Dictionary of Medicine, Nursing, and Allied Health, Seventh Edition. (2003). Retrieved August 17 2018 from <https://medical-dictionary.thefreedictionary.com/phantom>.
- MINGRONE, G., MARINO, S., DEGAETANO, A., CAPRISTO, E., HEYMSFIELD, S. B., GASBARRINI, G. & GRECO, A. V. 2001. Different limit to the body's ability of increasing fat-free mass. *Metabolism-Clinical and Experimental*, 50, 1004-1007.
- MODICA, M. J., KANAL, K. M. & GUNN, M. L. 2011. The obese emergency patient: imaging challenges and solutions. *Radiographics*, 31, 811-823.
- MOEY, S.-F. & SHAZLI, Z. 2018. Optimization of Dose and Image Quality in Full-field Computed Radiography Systems for Common Digital Radiographic Examinations. *Iranian Journal of Medical Physics*, 15, 28-38.
- MOLFINO, A., HEYMSFIELD, S. B., ZHU, F., KOTANKO, P., LEVIN, N. W., DWYER, T. & KAYSEN, G. A. 2013. Prealbumin is associated with visceral fat mass in patients receiving hemodialysis. *Journal of Renal Nutrition*, 23, 406-410.
- MONTGOMERY, D. C. 2017. *Design and analysis of experiments*, John Wiley & sons.
- MOONEY, R. & THOMAS, P. 1998. Dose reduction in a paediatric X-ray department following optimization of radiographic technique. *The British journal of radiology*, 71, 852-860.
- MOORE, C., WOOD, T., AVERY, G., BALCAM, S., NEEDLER, L., BEAVIS, A. & SAUNDERSON, J. 2014. An investigation of automatic exposure control calibration for chest imaging with a computed radiography system. *Physics in Medicine & Biology*, 59, 2307.
- MOORE, C., WOOD, T., AVERY, G., BALCAM, S., NEEDLER, L., JOSHI, H., SAUNDERSON, J. & BEAVIS, A. 2016. Automatic exposure control calibration and optimisation for abdomen, pelvis and lumbar spine imaging with an Agfa computed radiography system. *Physics in Medicine & Biology*, 61, N551.
- MOORE, C., WOOD, T., AVERY, G., BALCAM, S., NEEDLER, L., SMITH, A., SAUNDERSON, J. & BEAVIS, A. 2015. Investigating the use of an antiscatter grid in chest radiography for average adults with a computed radiography imaging system. *The British journal of radiology*, 88, 20140613.
- MOORE, C., WOOD, T., BEAVIS, A. & SAUNDERSON, J. 2013. Correlation of the clinical and physical image quality in chest radiography for average adults with a computed radiography imaging system. *The British journal of radiology*, 86, 20130077.
- MOORES, B. 2005. Radiation dose measurement and optimization. *The British journal of radiology*, 78, 866-868.
- MORISHIMA, Y., CHIDA, K. & WATANABE, H. 2016. Estimation of the dose of radiation received by patient and physician during a videofluoroscopic swallowing study. *Dysphagia*, 31, 574-578.
- MORSBACH, F., BICKELHAUPT, S., RÄTZER, S., SCHMIDT, B. & ALKADHI, H. 2014. Integrated circuit detector technology in abdominal CT: added value in obese patients. *American Journal of Roentgenology*, 202, 368-374.
- MOTT, J. W., WANG, J., THORNTON, J. C., ALLISON, D. B., HEYMSFIELD, S. B. & PIERSON JR, R. N. 1999. Relation between body fat and age in 4 ethnic groups-. *The American journal of clinical nutrition*, 69, 1007-1013.
- MRAITY, H. 2015. *Optimisation of radiation dose and image quality for AP pelvis radiographic examination*. University of Salford.

- MRAITY, H., ENGLAND, A. & HOGG, P. 2018. AP pelvis radiography: The impact of tube filtration on radiation dose and image quality. *EPOS presented at the European Congress of Radiology, Vienna, 28th February - 4th March*.
- MRAITY, H. A., ENGLAND, A., CASSIDY, S., EACHUS, P., DOMINGUEZ, A. & HOGG, P. 2016. Development and validation of a visual grading scale for assessing image quality of AP pelvis radiographic images. *The British journal of radiology*, 89, 20150430.
- MRAITY, H. A., ENGLAND, A. & HOGG, P. 2017. Gonad dose in AP pelvis radiography: impact of anode heel orientation. *Radiography*, 23, 14-18.
- MURAMATSU, C. 2018. Overview on subjective similarity of images for content-based medical image retrieval. *Radiological physics and technology*, 11, 109-124.
- MUSOLINO, S. V., DEFRANCO, J. & SCHLUECK, R. 2008. The ALARA principle in the context of a radiological or nuclear emergency. *Health physics*, 94, 109-111.
- NAEYE, R. L. & ROODE, P. 1970. The sizes and numbers of cells in visceral organs in human obesity. *American journal of clinical pathology*, 54, 251-253.
- NATIONAL RESEARCH COUNCIL 2006. Committee to Assess Health Risks from Exposure to Low Levels of Ionizing Radiation, Health Risks from Exposure to Low Levels of Ionizing Radiation (BEIR VII Phase 2). *Washington, DC: National Academies Press, Date*, 16, 406.
- NEELAND, I. J., AYERS, C. R., ROHATGI, A. K., TURER, A. T., BERRY, J. D., DAS, S. R., VEGA, G. L., KHERA, A., MCGUIRE, D. K. & GRUNDY, S. M. 2013. Associations of visceral and abdominal subcutaneous adipose tissue with markers of cardiac and metabolic risk in obese adults. *Obesity*, 21, E439-E447.
- NEOVIUS, M., HEMMINGSSON, E., FREYSCHUSS, B. & UDDÉN, J. 2006. Bioelectrical impedance underestimates total and truncal fatness in abdominally obese women. *Obesity*, 14, 1731-1738.
- NGUYEN, G. K., MELLNICK, V. M., YIM, A. K.-Y., SALTER, A. & IPPOLITO, J. E. 2018. Synergy of Sex Differences in Visceral Fat Measured with CT and Tumor Metabolism Helps Predict Overall Survival in Patients with Renal Cell Carcinoma. *Radiology*, 287, 884-892.
- NORRMAN, E. & PERSLIDEN, J. 2005. A factorial experiment on image quality and radiation dose. *Radiation protection dosimetry*, 114, 246-252.
- NOTOHAMIPRODJO, S., VERSTREEPEN, L., WANNINGER, F., HOBERG, B., RÖPER, K., MÜCK, F., TREITL, K., MAXIEN, D. & WIRTH, S. 2018. Dependence of low contrast detail on exposure dose and tube voltage in digital flat-panel detector radiography—a pre-clinical phantom study. *Biomedical Physics & Engineering Express*, 4, 025010.
- NUTE, J. L. 2015. CHARACTERIZATION OF LOW DENSITY INTRACRANIAL LESIONS USING DUAL-ENERGY COMPUTED TOMOGRAPHY.
- OBUCHOWSKI, N. A. 2004. How many observers are needed in clinical studies of medical imaging? *American journal of roentgenology*, 182, 867-869.
- OKORODUDU, D., JUMEAN, M., MONTORI, V., ROMERO-CORRAL, A., SOMERS, V., ERWIN, P. & LOPEZ-JIMENEZ, F. 2010. Diagnostic performance of body mass index to identify obesity as defined by body adiposity: a systematic review and meta-analysis. *International journal of obesity*, 34, 791.
- ORTEGA, F. B., LAVIE, C. J. & BLAIR, S. N. 2016. Obesity and cardiovascular disease. *Circulation research*, 118, 1752-1770.
- PADILLA, L., RADOSEVICH, D. & MILAD, M. 2005. Limitations of the pelvic examination for evaluation of the female pelvic organs. *International Journal of Gynecology & Obstetrics*, 88, 84-88.
- PETERS, S. E. & BRENNAN, P. C. 2002. Digital radiography: are the manufacturers' settings too high? Optimisation of the Kodak digital radiography system with aid of the computed radiography dose index. *European radiology*, 12, 2381-2387.
- PETRONI, M., BERTOLI, S., MAGGIONI, M., MORINI, P., BATTEZZATI, A., TAGLIAFERRI, M., LIUZZI, A. & TESTOLIN, G. 2003. Feasibility of air plethysmography (BOD POD) in morbid obesity: a pilot study. *Acta diabetologica*, 40, s59-s62.

- PIETROBELLI, A., FORMICA, C., WANG, Z. & HEYMSFIELD, S. B. 1996. Dual-energy X-ray absorptiometry body composition model: review of physical concepts. *American Journal of Physiology-Endocrinology And Metabolism*, 271, E941-E951.
- PIETROBELLI, A. & HEYMSFIELD, S. 2002. Establishing body composition in obesity. *Journal of endocrinological investigation*, 25, 884-892.
- PINA, D., DUARTE, S., NETTO, T. G. & MORCELLI, J. 2009. Phantom development for radiographic image optimization of chest, skull and pelvis examination for nonstandard patient. *Applied Radiation and Isotopes*, 67, 61-69.
- PINTO, A. & BRUNESE, L. 2010. Spectrum of diagnostic errors in radiology. *World journal of radiology*, 2, 377.
- PITTS, G. C. 1962. Density and composition of the lean body compartment and its relationship to fatness. *American Journal of Physiology-Legacy Content*, 202, 445-452.
- PLANK, L. D. 2005. Dual-energy X-ray absorptiometry and body composition. *Current Opinion in Clinical Nutrition & Metabolic Care*, 8, 305-309.
- PODGORSK, E. B. 2005. Radiation oncology physics. *Vienna: International Atomic Energy Agency*, 123-271.
- POLETTI, J. & MCLEAN, D. 2005. The effect of source to image-receptor distance on effective dose for some common X-ray projections. *The British journal of radiology*, 78, 810-815.
- POLUDNIOWSKI, G., LANDRY, G., DEBLOIS, F., EVANS, P. M. & VERHAEGEN, F. 2009. SpekCalc: a program to calculate photon spectra from tungsten anode x-ray tubes. *Physics in Medicine & Biology*, 54, N433.
- PRADO, C. M. & HEYMSFIELD, S. B. 2014. Lean tissue imaging: a new era for nutritional assessment and intervention. *Journal of Parenteral and Enteral Nutrition*, 38, 940-953.
- PRESTON, D., RON, E., TOKUOKA, S., FUNAMOTO, S., NISHI, N., SODA, M., MABUCHI, K. & KODAMA, K. 2007. Solid cancer incidence in atomic bomb survivors: 1958–1998. *Radiation research*, 168, 1-64.
- PUBLISHING, O. 2010. *Obesity and the Economics of Prevention: Fit Not Fat*, OECD Publishing.
- QURASHI, A., RAINFORD, L., AJLAN, A., KHASHOGGI, K., ASHKAR, L., AL-RADDADI, M., AL-GHAMDI, M., AL-THOBAITI, M. & FOLEY, S. 2018. Optimal abdominal CT protocol for obese patients. *Radiography*, 24, e1-e12.
- RANA, R., JAIN, A., SHANKAR, A., BEDNAREK, D. & RUDIN, S. Scatter estimation and removal of anti-scatter grid-line artifacts from anthropomorphic head phantom images taken with a high resolution image detector. *Medical Imaging 2016: Physics of Medical Imaging*, 2016. International Society for Optics and Photonics, 978364.
- RCR 2012. Picture archiving and communication systems (PACS) and guidelines on diagnostic display devices. *The Royal College of Radiologist London*.
- REEVES, T., MAH, P. & MCDONALD, W. 2012. Deriving Hounsfield units using grey levels in cone beam CT: a clinical application. *Dentomaxillofacial Radiology*, 41, 500-508.
- REIS, C., GONÇALVES, J., KLOMPMAKER, C., BÁRBARA, A. R., BLOOR, C., HEGARTY, R., LAGRANGE, T., TEMMING, N., SØNNESYN, M. & RØKENESS, H. 2014. Image quality and dose analysis for a PA chest X-ray: comparison between AEC mode acquisition and manual mode using the 10 kVp 'rule'. *Radiography*, 20, 339-345.
- RENEHAN, A. G., TYSON, M., EGGER, M., HELLER, R. F. & ZWAHLEN, M. 2008. Body-mass index and incidence of cancer: a systematic review and meta-analysis of prospective observational studies. *The Lancet*, 371, 569-578.
- REYNOLDS, A. 2011. Obesity and medical imaging challenges. *Radiologic technology*, 82, 219-239.
- RICE, B., JANSSEN, I., HUDSON, R. & ROSS, R. 1999. Effects of aerobic or resistance exercise and/or diet on glucose tolerance and plasma insulin levels in obese men. *Diabetes care*, 22, 684-691.
- ROBERTS, J., EVANS, S. & REES, M. 2006. Optimisation of imaging technique used in direct digital radiography. *Journal of Radiological Protection*, 26, 287.

- ROMERO-CORRAL, A., SOMERS, V. K., SIERRA-JOHNSON, J., THOMAS, R. J., COLLAZO-CLAVELL, M., KORINEK, J., ALLISON, T. G., BATSIS, J., SERT-KUNIYOSHI, F. & LOPEZ-JIMENEZ, F. 2008. Accuracy of body mass index in diagnosing obesity in the adult general population. *International journal of obesity*, 32, 959.
- ROSNER, B. 2015. *Fundamentals of biostatistics*, Nelson Education.
- RUTHERFORD, T. 2012. Population ageing: statistics. In: LIBRARY, H. O. C. (ed.).
- SA DOS REIS, C., BOWDLER, M., HOGG, P., HAUGE, I., JORGE, J., THOMPSON, J., O'CONNOR, M., REY, Y., SOARES, S. & AANDAHL, I. 2017. OPTIMAX 2017: radiation dose, image quality optimisation, the use of new technology in medical imaging. University of Salford.
- SAALFELD, S. 2008. Feature Extraction SIFT/MOPS (Fiji). Available from: https://imagej.net/Feature_Extraction [Accessed 09/01/2019 2019].
- SAMEI, E., DOBBINS III, J. T., LO, J. Y. & TORNAL, M. P. 2005. A framework for optimising the radiographic technique in digital X-ray imaging. *Radiation Protection Dosimetry*, 114, 220-229.
- SAMEI, E., JÄRVINEN, H., KORTESNIEMI, M., SIMANTIRAKIS, G., GOH, C., WALLACE, A., VANO, E., BEJAN, A., REHANI, M. & VASSILEVA, J. 2018. Medical imaging dose optimisation from ground up: expert opinion of an international summit. *Journal of Radiological Protection*, 38, 967.
- SANADA, S., KAWAHARA, K., YAMAMOTO, T. & TAKASHIMA, T. 1999. New tissue substitutes representing cortical bone and adipose tissue in quantitative radiology. *Physics in Medicine & Biology*, 44, N107.
- SANDBORG, M., ALM CARLSSON, G., PERSLIDEN, J. & DANCE, D. 1993. Comparison of different materials for test phantoms in diagnostic radiology. *Radiation Protection Dosimetry*, 49, 345-347.
- SATO, F., MAEDA, N., YAMADA, T., NAMAZUI, H., FUKUDA, S., NATSUKAWA, T., NAGAO, H., MURAI, J., MASUDA, S. & TANAKA, Y. 2018. Association of epicardial, visceral, and subcutaneous fat with cardiometabolic diseases. *Circulation Journal*, 82, 502-508.
- SCHAUDINN, A., LINDER, N., GARNOV, N., KERLIKOWSKY, F., BLÜHER, M., DIETRICH, A., SCHÜTZ, T., KARLAS, T., KAHN, T. & BUSSE, H. 2015. Predictive accuracy of single-and multi-slice MRI for the estimation of total visceral adipose tissue in overweight to severely obese patients. *NMR in Biomedicine*, 28, 583-590.
- SCHINDERA, S. T., NELSON, R. C., LEE, E. R., DELONG, D. M., NGYEN, G., TONCHEVA, G. & YOSHIZUMI, T. T. 2007. Abdominal multislice CT for obese patients: effect on image quality and radiation dose in a phantom study. *Academic radiology*, 14, 486-494.
- SCHINDERA, S. T., ODEDRA, D., MERCER, D., THIPPHAVONG, S., CHOU, P., SZUCS-FARKAS, Z. & ROGALLA, P. 2014. Hybrid iterative reconstruction technique for abdominal CT protocols in obese patients: assessment of image quality, radiation dose, and low-contrast detectability in a phantom. *American Journal of Roentgenology*, 202, W146-W152.
- SCHOELLER, D. A. & BUCHHOLZ, A. C. 2005. Energetics of obesity and weight control: does diet composition matter? *Journal of the American Dietetic Association*, 105, 24-28.
- SCHOENFELD, A. A., THIEBEN, M., HARDER, D., POPPE, B. & CHOFOR, N. 2017. Evaluation of water-mimicking solid phantom materials for use in HDR and LDR brachytherapy dosimetry. *Physics in Medicine & Biology*, 62, N561.
- SEERAM, E., DAVIDSON, R., BUSHONG, S. & SWAN, H. 2013. Radiation dose optimization research: exposure technique approaches in CR imaging—a literature review. *Radiography*, 19, 331-338.
- SEERAM, E., DAVIDSON, R., BUSHONG, S. & SWAN, H. 2014. Image quality assessment tools for radiation dose optimization in digital radiography: an overview. *Radiologic technology*, 85, 555-562.
- SEIBERT, J. A. 2004. Tradeoffs between image quality and dose. *Pediatric radiology*, 34, S183-S195.

- SEIBERT, J. A. 2008. Digital radiography: image quality and radiation dose. *Health physics*, 95, 586-598.
- SEIBERT, J. A. & MORIN, R. L. 2011. The standardized exposure index for digital radiography: an opportunity for optimization of radiation dose to the pediatric population. *Pediatric radiology*, 41, 573-581.
- SHAFER, K. J., SIDERS, W. A., JOHNSON, L. K. & LUKASKI, H. C. 2009. Validity of segmental multiple-frequency bioelectrical impedance analysis to estimate body composition of adults across a range of body mass indexes. *Nutrition*, 25, 25-32.
- SHAH, K., HILTON, T. N., MYERS, L., PINTO, J. F., LUQUE, A. E. & HALL, W. J. 2012. A new frailty syndrome: central obesity and frailty in older adults with the human immunodeficiency virus. *Journal of the American Geriatrics Society*, 60, 545-549.
- SHARMA, J., SARMA, J. & AGARWAL, S. 2018. Assessment of diagnostic reference level in radiography of neonatal chest anteroposterior examination: A hospital-based study. *Journal of medical physics*, 43, 200.
- SHAW, D., CRAWSHAW, I. & RIMMER, S. 2013. Effects of tube potential and scatter rejection on image quality and effective dose in digital chest X-ray examination: An anthropomorphic phantom study. *Radiography*, 19, 321-325.
- SHEN, J., BAUM, T., CORDES, C., OTT, B., SKURK, T., KOOIJMAN, H., RUMMENY, E. J., HAUNER, H., MENZE, B. H. & KARAMPINOS, D. C. 2016. Automatic segmentation of abdominal organs and adipose tissue compartments in water-fat MRI: application to weight-loss in obesity. *European journal of radiology*, 85, 1613-1621.
- SHIN, R. H., CABRERA, F. J., NGUYEN, G., WANG, C., YOUSSEF, R. F., SCALES, C. D., FERRANDINO, M. N., PREMINGER, G. M., YOSHIZUMI, T. T. & LIPKIN, M. E. 2016. Radiation dosimetry for ureteroscopy patients: a phantom study comparing the standard and obese patient models. *Journal of endourology*, 30, 57-62.
- SHRIMPTON, P., WALL, B., JONES, D., FISHER, E., HILLIER, M., KENDALL, G. & HARRISON, R. 1986. *A national survey of doses to patients undergoing a selection of routine X-ray examinations in English hospitals*, NRPB.
- SIEGEL, J. A., PENNINGTON, C. W. & SACKS, B. 2017. Subjecting radiologic imaging to the linear no-threshold hypothesis: a non sequitur of non-trivial proportion. *J Nucl Med*, 58, 1-6.
- SINNOTT, B., RON, E. & SCHNEIDER, A. B. 2010. Exposing the thyroid to radiation: a review of its current extent, risks, and implications. *Endocrine reviews*, 31, 756-773.
- SMANS, K., STRUELENS, L., SMET, M., BOSMANS, H. & VANHAVERE, F. 2010. Cu filtration for dose reduction in neonatal chest imaging. *Radiation protection dosimetry*, 139, 281-286.
- SMUCK, M., ZHENG, P., CHONG, T., KAO, M.-C. & GEISSER, M. E. 2013. Duration of fluoroscopic-guided spine interventions and radiation exposure is increased in overweight patients. *PM&R*, 5, 291-296.
- SOCIAL, N. & NEAVE, A. 2017. Health Survey for England 2016: Adult health trends. *Health and Social Care Information Centre*.
- SPALDING, K. L., ARNER, E., WESTERMARK, P. O., BERNARD, S., BUCHHOLZ, B. A., BERGMANN, O., BLOMQVIST, L., HOFFSTEDT, J., NÄSLUND, E. & BRITTON, T. 2008. Dynamics of fat cell turnover in humans. *Nature*, 453, 783.
- STENHOLM, S., HEAD, J., KIVIMÄKI, M., KAWACHI, I., AALTO, V., ZINS, M., GOLDBERG, M., ZANINOTTO, P., MAGNUSON HANSON, L. & WESTERLUND, H. 2016. Smoking, physical inactivity and obesity as predictors of healthy and disease-free life expectancy between ages 50 and 75: a multicohort study. *International journal of epidemiology*, 45, 1260-1270.
- STEWART, A., TAROLLO, M., MANDARANO, G. & LOMBARDI, C. 2018. Conventional Film-Screen Principles of Exposure Selection in the Digital Age. *Radiologic Technology*, 89, 488-494.

- STEWART, A., WEBB, J., GILES, D. & HEWITT, D. 1956. Malignant disease in childhood and diagnostic irradiation in utero. *The Lancet*, 268, 447.
- STEWART, F., AKLEYEV, A., HAUER-JENSEN, M., HENDRY, J., KLEIMAN, N., MACVITTIE, T., ALEMAN, B., EDGAR, A., MABUCHI, K. & MUIRHEAD, C. 2012. ICRP publication 118: ICRP statement on tissue reactions and early and late effects of radiation in normal tissues and organs—threshold doses for tissue reactions in a radiation protection context. *Annals of the ICRP*, 41, 1-322.
- STRAIN, G. W., WANG, J., GAGNER, M., POMP, A., INABNET, W. B. & HEYMSFIELD, S. B. 2008. Bioimpedance for severe obesity: comparing research methods for total body water and resting energy expenditure. *Obesity*, 16, 1953-1956.
- STULTS-KOLEHMAINEN, M., STANFORTH, P., BARTHOLOMEW, J., LU, T., ABOLT, C. & SINHA, R. 2013. DXA estimates of fat in abdominal, trunk and hip regions varies by ethnicity in men. *Nutrition & diabetes*, 3, e64.
- SUN, J.-W., ZHAO, L.-G., YANG, Y., MA, X., WANG, Y.-Y. & XIANG, Y.-B. 2015. Obesity and risk of bladder cancer: a dose-response meta-analysis of 15 cohort studies. *PloS one*, 10, e0119313.
- SUND, P., BÅTH, M., KHEDDACHE, S. & MÅNSSON, L. G. 2004. Comparison of visual grading analysis and determination of detective quantum efficiency for evaluating system performance in digital chest radiography. *European radiology*, 14, 48-58.
- SYKES, P. J. 2016. The ups and downs of low dose ionising radiobiology research. *Australasian physical & engineering sciences in medicine*, 39, 807-811.
- SZCZEPURA, K. & MANNING, D. Validated novel software to measure the conspicuity index of lesions in DICOM images. Medical imaging 2016: image perception, observer performance, and technology assessment, 2016. International Society for Optics and Photonics, 978703.
- TAPIOVAARA, M. 2008. Review of relationships between physical measurements and user evaluation of image quality. *Radiation protection dosimetry*, 129, 244-248.
- TAPIOVAARA, M. & SIISKONEN, T. 2008. PCXMC 2.0. User's Guide. Radiation and Nuclear Safety Authority STUK.
- TERLIZZI, R., D'ORONZO, M., ALEMANNI, A., SERRICCHIO, E., SIMEONE, A., CAPUTO, F., GUGLIELMI, G. & MAIORANA, A. Digital systems for chest imaging: Study on dose increase in patients of different size. Medical Measurements and Applications Proceedings (MeMeA), 2011 IEEE International Workshop on, 2011. IEEE, 404-407.
- THASANASUWAN, W., SRICHAN, W., KIJBOONCHOO, K., YAMBORISUT, U., WIMONPEERAPATTANA, W., ROJROONGWASINKUL, N., KHOUW, I. T. & DEURENBERG, P. 2016. Low Sleeping Time, High TV Viewing Time, and Physical Inactivity in School Are Risk Factors for Obesity in Pre-Adolescent Thai Children. *Journal of the Medical Association of Thailand= Chotmaihet thangphaet*, 99, 314-321.
- THEOCHAROPOULOS, N., PERISINAKIS, K., DAMILAKIS, J., VARVERIS, H. & GOURTSOYIANNIS, N. 2002. Comparison of four methods for assessing patient effective dose from radiological examinations. *Medical physics*, 29, 2070-2079.
- TINGBERG, A. 2000. *Quantifying the quality of medical x-ray images. An evaluation based on normal anatomy for lumbar spine and chest radiography*, Department of Radiation Physics, Lund university.
- TINGBERG, A. & SJÖSTRÖM, D. 2005. Optimisation of image plate radiography with respect to tube voltage. *Radiation protection dosimetry*, 114, 286-293.
- TOOMBS, R. J., DUCHER, G., SHEPHERD, J. A. & DE SOUZA, M. J. 2012. The impact of recent technological advances on the trueness and precision of DXA to assess body composition. *Obesity*, 20, 30-39.
- TOOTELL, A., SZCZEPURA, K. & HOGG, P. 2014. An overview of measuring and modelling dose and risk from ionising radiation for medical exposures. *Radiography*, 20, 323-332.

- TSALAFOUTAS, I. A. 2018. Electronic collimation of radiographic images: does it comprise an overexposure risk? *The British journal of radiology*, 91, 20170958.
- TUGWELL, J., EVERTON, C., KINGMA, A., OOMKENS, D., PEREIRA, G., PIMENTINHA, D., ROUILLER, C., STENSRUD, S., KJELLE, E. & JORGE, J. 2014. Increasing source to image distance for AP pelvis imaging—Impact on radiation dose and image quality. *Radiography*, 20, 351-355.
- TUNG, C., LEE, C., TSAI, H., TSAI, S. & CHEN, I. 2008. Body size-dependent patient effective dose for diagnostic radiography. *Radiation Measurements*, 43, 1008-1011.
- UFFMANN, M., NEITZEL, U., PROKOP, M., KABALAN, N., WEBER, M., HEROLD, C. J. & SCHAEFER-PROKOP, C. 2005. Flat-panel-detector chest radiography: effect of tube voltage on image quality. *Radiology*, 235, 642-650.
- UFFMANN, M. & SCHAEFER-PROKOP, C. 2009. Digital radiography: the balance between image quality and required radiation dose. *European journal of radiology*, 72, 202-208.
- UPPOT, R. N. 2007. Impact of obesity on radiology. *Radiologic Clinics of North America*, 45, 231-246.
- UPPOT, R. N., SAHANI, D. V., HAHN, P. F., KALRA, M. K., SAINI, S. S. & MUELLER, P. R. 2006. Effect of obesity on image quality: fifteen-year longitudinal study for evaluation of dictated radiology reports. *Radiology*, 240, 435-439.
- URSANI, A., ANWARI, V., LAI, A., SAJJA, S., REGO, K. & PAUL, N. 2018. Tissue Realistic Anthropomorphic Abdominal Phantom for Radiography—3D Printing. *CMBES Proceedings*, 41.
- VAN ASSELEN, B., WOLTHAUS, J., HACKETT, S., KOK, J., WOODINGS, S. & RAAYMAKERS, B. 2017. SP-0594: Pre-treatment phantom dosimetry: effects in different phantoms and detectors. *Radiotherapy and Oncology*, 123, S311-S312.
- VANDERSTRAETEN, B., CHIN, P. W., FIX, M., LEAL, A., MORA, G., REYNAERT, N., SECO, J., SOUKUP, M., SPEZI, E. & DE NEVE, W. 2007. Conversion of CT numbers into tissue parameters for Monte Carlo dose calculations: a multi-centre study. *Physics in Medicine & Biology*, 52, 539.
- VANDERWALL, C., CLARK, R. R., EICKHOFF, J. & CARREL, A. L. 2017. BMI is a poor predictor of adiposity in young overweight and obese children. *BMC pediatrics*, 17, 135.
- VASSILEVA, J. 2004. A phantom approach to find the optimal technical parameters for plain chest radiography. *The British journal of radiology*, 77, 648-653.
- VLADIMIROV, A. 2010. *Comparison of image quality test methods in computed radiography*.
- WALL, B., HAYLOCK, R., JANSEN, J., HILLIER, M., HART, D. & SHRIMPTON, P. 2011. Radiation risks from medical X-ray examinations as a function of the age and sex of the patient. *Health Protection Agency Centre for Radiation, Chemical and Environmental Hazards. HPA-CRCE-028*.
- WALLIMAN, N. 2017. *Research methods: The basics*, Routledge.
- WALLRAVEN, C. & CUNNINGHAM, D. W. 2011. *Experimental design: From user studies to psychophysics*, AK Peters/CRC Press.
- WALTER, H. & SLONE RICHARD, M. 2010. Review of radiologic physics. Lippincot Williams & Wilkins.
- WAMBERSIE, A., ZOETELIEF, J., MENZEL, H. & PARETZKE, H. 2005. The ICRU (International Commission on Radiation Units and Measurements): its contribution to dosimetry in diagnostic and interventional radiology. *Radiation protection dosimetry*, 117, 7-12.
- WANG, A. J., GOLDSMITH, Z. G., WANG, C., NGUYEN, G., ASTROZA, G. M., NEISIUS, A., IQBAL, M. W., NEVILLE, A. M., LOWRY, C. & TONCHEVA, G. 2013. Obesity triples the radiation dose of stone protocol computerized tomography. *The Journal of urology*, 189, 2142-2146.
- WANG, Z.-M., PIERSON JR, R. N. & HEYMSFIELD, S. B. 1992. The five-level model: a new approach to organizing body-composition research. *The American journal of clinical nutrition*, 56, 19-28.

- WATANABE, Y. & CONSTANTINOU, C. 2006. Phantom Materials in Radiology. *Encyclopedia of Medical Devices and Instrumentation*.
- WELLS, J. & FEWTRELL, M. 2006. Measuring body composition. *Archives of disease in childhood*, 91, 612-617.
- WHITE, D. 1978. Tissue substitutes in experimental radiation physics. *Medical physics*, 5, 467-479.
- WHITE, D. R., WILSON, I. J., BOOZ, J., SPOKAS, J. J. & GRIFFITH, R. V. 1989. Report 44. *Journal of the International Commission on Radiation Units and Measurements*, 23, NP-NP.
- WHO 1995. Physical status: the use and interpretation of anthropometry. *WHO Technical Report Series 854*. Geneva: World Health Organisation.
- WHO 2000. *Obesity: preventing and managing the global epidemic*, World Health Organization.
- WHO. 2016. *Obesity and overweight* [Online]. Available: <https://www.who.int/news-room/fact-sheets/detail/obesity-and-overweight> [Accessed 07/01/2019 2019].
- WILES, R., MEREDITH, S., MULLANY, J. & WILES, T. 2017. Are English CT departments and radiographers prepared for the morbidly obese patient? *Radiography*, 23, 187-190.
- WILLIAMS, M. B., KRUPINSKI, E. A., STRAUSS, K. J., BREEDEN III, W. K., RZESZOTARSKI, M. S., APPLGATE, K., WYATT, M., BJORK, S. & SEIBERT, J. A. 2007. Digital radiography image quality: image acquisition. *Journal of the American College of Radiology*, 4, 371-388.
- WINSLOW, J. F., HYER, D. E., FISHER, R. F., TIEN, C. J. & HINTENLANG, D. E. 2009. Construction of anthropomorphic phantoms for use in dosimetry studies. *Journal of applied clinical medical physics*, 10, 195-204.
- WISE, K., SANDBORG, M., PERSLIDEN, J. & CARLSSON, G. A. 1999. Sensitivity of coefficients for converting entrance surface dose and kerma-area product to effective dose and energy imparted to the patient. *Physics in Medicine & Biology*, 44, 1937.
- WONG, W. W., STRIZICH, G., HEO, M., HEYMSFIELD, S. B., HIMES, J. H., ROCK, C. L., GELLMAN, M. D., SIEGA-RIZ, A. M., SOTRES-ALVAREZ, D. & DAVIS, S. M. 2016. Relationship between body fat and BMI in a US Hispanic population-based cohort study: results from HCHS/SOL. *Obesity*, 24, 1561-1571.
- WOODS, A. L., MILLER, P. K. & SLOANE, C. 2016. Patient obesity and the practical experience of the plain radiography professional: On everyday ethics, patient positioning and infelicitous equipment. *Radiography*, 22, 118-123.
- YANCH, J. C., BEHRMAN, R. H., HENDRICKS, M. J. & MCCALL, J. H. 2009. Increased radiation dose to overweight and obese patients from radiographic examinations. *Radiology*, 252, 128-139.
- YIP, C., DINKEL, C., MAHAJAN, A., SIDDIQUE, M., COOK, G. J. & GOH, V. 2015. Imaging body composition in cancer patients: visceral obesity, sarcopenia and sarcopenic obesity may impact on clinical outcome. *Insights into imaging*, 6, 489-497.
- YOHANNES, I., KOLDITZ, D., LANGNER, O. & KALENDER, W. A. 2012. A formulation of tissue-and water-equivalent materials using the stoichiometric analysis method for CT-number calibration in radiotherapy treatment planning. *Physics in Medicine & Biology*, 57, 1173.
- ZANZONICO, P., DAUER, L. & STRAUSS, H. W. 2016. Radiobiology in cardiovascular imaging. *JACC: Cardiovascular Imaging*, 9, 1446-1461.
- ZARNOCH, K. P. & GUIDA, R. 1996. Anti-scatter X-ray grid device for medical diagnostic radiography. Google Patents.
- ZHENG, X. 2018. Body size and tube voltage-dependent guiding equations for optimal selection of image acquisition parameters in clinical X-ray imaging. *Radiological physics and technology*, 11, 212-218.
- ZHENG, X., NARDI, L. & MURRAY, M. 2017. Size effect on dose output in phantoms of X-ray tubes in medical X-ray imaging. *Biomedical Physics & Engineering Express*, 3, 065004.

- ZOETELIEF, J., BROERSE, J., DAVIES, R., OCTAVE-PRIGNOT, M., REZVANI, M., VERGARA, J. S. & TONI, M. 2001. Protocol for X-ray dosimetry in radiobiology. *International journal of radiation biology*, 77, 817-835.
- ZOICO, E., CORZATO, F., BAMBACE, C., ROSSI, A. P., MICCIOLO, R., CINTI, S., HARRIS, T. B. & ZAMBONI, M. 2013. Myosteatosi and myofibrosi: relationship with aging, inflammation and insulin resistance. *Archives of gerontology and geriatrics*, 57, 411-416.